MODULATION OF THE MDM2 SIGNALING AXIS SENSITIZES TRIPLE-NEGATIVE BREAST CANCER CELLS TO CARBOPLATIN

Eva Y. Tonsing-Carter

Submitted to the faculty of the University Graduate School
in partial fulfillment of the requirements
for the degree
Doctor of Philosophy
in the Department of Pharmacology and Toxicology,
Indiana University

December 2014

Accepted by the Graduate Faculty, Indiana University, in partial fulfillment of the requirements for the degree of Doctor of Philosophy.

Karen E. Pollok, Ph.D., Chair

Jian-Ting Zhang, Ph.D.

Doctoral Committee

Ahmad R. Safa, Ph.D.

October 27, 2014

Lindsey D. Mayo, Ph.D.

Jeffrey B. Travers, M.D., Ph.D.

DEDICATION

For my dad.

His passion for life will always direct me to do what makes me happy.

ACKNOWLEDGEMENTS

I would like to thank all members of the Pollok Lab for all of their continued support throughout my thesis project. They have become a second family and helped nurture my professional and scientific growth as well as personal growth. My mentor, Dr. Karen Pollok, has been instrumental throughout my thesis project. I am grateful to have been her first graduate student. I have learned so much not only scientifically, but personally, throughout our journey together. My other lab mates, Barb Bailey, Haiyan Wang, Shanbao Cai, Harlan Shannon, Larry Gelbert, Reza Saadatzadeh, Jixin Dong, and Mary Murray have helped me in so many ways through their shared knowledge and support over the years.

Dr. Harikrishna Nakshatri generously gifted the TMD231 cells used throughout my project. Dr. Paul Territo and the members of the Indiana Institute for Biomedical Imaging Sciences Core helped me tremendously with the validation and use of *in vivo* fluorescent imaging. Dr. Helmut Hanenberg designed and developed the lentiviral constructs used to transduce the fluorescent proteins and shp73 constructs. In collaboration with Dr. Christine Eischen and her laboratory, we conducted chromatin association assays. Her continued knowledge and discussion helped us to ask better scientific questions and enhance our scientific design. All the current and past members of the *In Vivo* Therapeutics Core helped with the planning and execution of all animal studies used throughout my thesis project. Our continued collaboration with Dr. George Sandusky has allowed for high-throughput pathology analysis as well as my increased understanding of pathology.

The members of the Thesis Committee, Drs. Zhang, Mayo, Safa, and Travers, have helped me become a better scientist through their continued support and scientific discussions. Dr. Jian-Ting Zhang served as Chair to my Thesis Committee, driving meetings with thoughtful leadership and scientific discussions. Dr. Lindsey Mayo has shared important scientific discussions as well as the use of cells and plasmid constructs that have been important for *in vitro* mechanism studies. Dr. Ahmad Safa has been greatly appreciated with his thoughtful discussions as well as serving as a student advocate through writing letters and critiquing my student seminars. Dr. Jeffrey Travers graciously allowed me to shadow him in the Dermatology Department at the VA Hospital in Indianapolis where I was able to gain further insight into the relationship between the clinic and laboratory.

The Herman B Wells Center for Pediatric Research with their support through personnel and core equipment allowed for increased productivity in the lab. I am thankful for the financial support awarded through the IUSCC Cancer Biology Training Program, NCI/NIH R01 CA138798, and the Riley Children's Foundation. Travel awards gifted from IUSCC, Department of Pharmacology, and Graduate Office allowed me to participate in several annual AACR meetings. The Department of Pharmacology and Toxicology has been truly supportive with members of staff, faculty, and students. My family and friends have always given me the love and support needed to complete this Ph.D. program and for that I am forever grateful.

Eva Y. Tonsing-Carter

MODULATION OF THE MDM2 SIGNALING AXIS SENSITIZES TRIPLE-NEGATIVE BREAST CANCER CELLS TO CARBOPLATIN

Triple-negative breast cancers (TNBCs) are highly refractive to current treatment strategies, and new multi-targeted treatments need to be elucidated. Combination therapy that includes targeting the murine double minute 2 (Mdm2) signaling axis offers a promising approach. Protein-protein interaction inhibitors such as Nutlin-3a block the binding of key signaling molecules such as p53, p73α, and E2F1 to the hydrophobic pocket of Mdm2 and can lead to activation of cell-death signaling pathways. Since clinical trials for TNBC are evaluating the DNA damaging agent carboplatin, the objective of this thesis was to evaluate the therapeutic potential and mechanism of action of combination carboplatin and Nutlin-3a to treat TNBC. In TNBC cell lines with a mutant p53 background, we determined if modulation of Mdm2 function in the context of carboplatin-mediated DNA damage resulted in a synergistic inhibition of cell growth. Several ratios of carboplatin:Nutlin-3a were strongly synergistic in increasing cell death, with combination indices of 0.5 and lower. Mechanistic studies indicated that drug sensitivity and Mdm2 expression were dependent on p73. Mdm2 localized to a larger degree in the chromatin fraction isolated from cells treated with the combination treatment consistent with observations by others that Mdm2 binds to the Mre11/Rad50/Nbs1 complex, inhibits the DNA damage response, and increases drug

sensitivity. *In vivo* efficacy experiments were conducted in the TMD231 orthotopic mammary fat pad model in NOD.Cg-Prkdc^{scid}Il2rg^{tm1Wjl}/SzJ (NSG) mice. For assessment of baseline tumor burden and randomization, fluorescent imaging of E2-Crimson expressing TMD231 cells was performed. Following Nutlin-3a and carboplatin combination treatment, there was a statistically significant reduction in primary tumor volume as well as lung metastases with significantly increased probability of survival compared to Vehicle and single drug treatments ($p<0.001$). While there was a decrease in bone-marrow cellularity, this did not lead to bone-marrow aplasia, and body weights recovered to normal levels within 7 days post-treatment. The present studies demonstrate the promise of Mdm2 as a therapeutic target in combination with conventional therapy, increase our understanding of how to potentiate DNA damage in cancers, and may lead to new clinical therapies for triple-negative primary and metastatic breast cancer.

Karen E. Pollok, Ph.D., Chair

TABLE OF CONTENTS

LIST OF TABLES

LIST OF FIGURES

LIST OF ABBREVIATIONS

2D	Two-dimensional
3D	Three-dimensional
7-AAD	7-aminoactinomycin D
10XTG	10X Tris-Glycine
Akt	Protein kinase B
AM	*Ante meridiem* (before noon)
ANOVA	Analysis of variance
Apaf-1	Apoptotic protease activating factor 1
Arf	Alternate reading frame protein
ATCC	American Tissue Culture Centre
ATM	Ataxia telangiectasia mutated
ATP	Adenosine triphosphate
Bax	Bcl2-associated protein X
BER	Base excision repair
BRCA1/2	BReast CAncer 1/2 gene
BSA	Bovine serum albumin
BLI	Bioluminescence
CBC	Complete blood count
CDK	Cyclin-dependent kinase
Cl/F	Apparent oral clearance
C_{max}	Maximum serum concentration

CO_2	Carbon dioxide
CR	E2-Crimson
CSK	Cytoskeleton buffer
CT	Computerized tomography
DI	De-ionized
DM	Double minute
DMEM	Dulbecco's Modified Eagle Medium
DMSO	Dimethyl sulfoxide
DNA	Deoxyribonucleic acid
DSB	Double strand break
EDTA	Ethylenediaminetetraacetic acid
eGFP	Enhanced green fluorescent protein
EGFR	Epidermal growth factor receptor
EGFRvIII	Epidermal growth factor receptor constitutively active variant
EGTA	Ethylene glycol tetraacetic acid
ELISA	Enzyme-linked immunosorbent assay
EMH	Extramedullary hematopoiesis
ER	Estrogen receptor
EtOH	Ethanol
FBS	Fetal bovine serum
FITC	Fluorescein isothiocyanate
GADD45	Growth Arrest and DNA Damage-inducible 45

GAPDH	Glyceraldehyde 3-phosphate dehydrogenase
GBM	Glioblastoma
GFP	Green fluorescent protein
H&E	Haematoxylin and eosin stain
H_2O	Water
HCl	Hydrochloric acid
HEPES	4-(2-hydroxyethyl)-1-piperazineethanesulfonic acid
HER2	Human epidermal growth factor receptor 2
Hif-1α	Hypoxia inducible factor-1α
HNO_3	Nitric acid
HR	Homologous repair
IC_{50}	Half maximal inhibitory concentration
ICP-MS	Inductively coupled plasma mass spectrometry
i.p.	Intraperitoneal injection
IR	Irradiation
IUSM	Indiana University School of Medicine
IV	Intravenous
kDa	Kilo Dalton
LARC	Laboratory Animal Resource Center
Leu	Leucine
MEM-α	Minimum Essential Medium α
Mdm2	Mouse double minute 2

MdmX	Mouse double minute 4
$MgCl_2$	Magnesium chloride
MMP9	Matrix metalloproteinase 9
MMR	Mismatch repair
MOI	Multiplicity of infection
MRI	Magnetic resonance imaging
MRN	Mre11/Rad51/Nbs1 complex
Mtp53	Mutant p53
NaCl	Sodium chloride
NC	Normalized counts
NER	Nucleotide excision repair
NES	Nuclear export signal
NHEJ	Non-homologous end joining
NK	Natural killer
NLS	Nuclear localization signal
NOD/scid	Nonobese diabetic/severe combined immunodeficiency
NSG	NOD.Cg-Prkdc^{scid}Il2rg^{tm1Wjl}/SzJ
PARP	Poly- (ADP) ribose polymerase
PBS	Phosphate buffered saline
PCNA	proliferating cell nuclear antigen
PD	Pharmacodynamic
PDX	Patient-derived xenograft

PET	Positron emission tomography
Phe	Phenylalanine
PI	Propidium iodide
PIPES	Piperazine-N,N-bis(2-ethanesulfonic acid)
PK	Pharmacokinetic
p.o.	*per os* (by mouth)
PM	*post mediem* (after noon)
PML	Probable transcription factor
PolH	DNA polymerase eta
PPI	Protein-protein inhibitor
PR	Progesterone receptor
Pt	Platinum
PUMA	p53 up-regulated modulator of apoptosis
RBC	Red blood cell
RIPA	Radioimmunoprecipitation assay buffer
Runx	Runt-related transcription factor
RNA	Ribonucleic acid
SD	Standard deviation
SDS	Sodium dodecyl sulfate
SEM	Standard error of the mean
SFFV	Spleen focus-forming virus
siRNA	Small interfering RNA

SSB	Single strand break
shRNA	small or short hairpin RNA
STAT	Signal Transducer and Activator of Transcription
$t_{½}$	Eliminated half-life
TBS	Tris-buffered saline
TBST	Tris-Buffered Saline and Tween 20
t_{max}	Time to reach maximum serum concentration
TNBC	Triple-negative breast cancer
Tris-HCl	Tris (hydroxymethyl)aminomethane hydrochloride
Trp	Tryptophan
UV	Ultraviolet light
VEGF	Vascular endothelial growth factor
WBC	White blood cell
Wtp53	Wild-type p53
XPC	xeroderma pigmentosum complementation group C
Y	Tyrosine
Yap1	Yes-associated protein

SECTION I: INTRODUCTION AND LITERATURE REVIEW

Chapter 1. Breast Cancer Background

Cancer describes a group of diseases in which cells abnormally grow forming tumors within the body. The hallmarks of cancer are described as dysregulation of proliferative signaling, evading growth suppressive signaling, resisting cell death signaling, replicative immortality, pro-angiogenesis signaling, and enabling invasion and metastasis [1]. Cancer is classified into different stages that can be helpful in deciding courses of treatment and prognosis. Stage 0 is defined by carcinoma *in situ* in which there is an abnormal cluster of cells that has not begun spreading to any surrounding tissues. Stages I-III are described as more extensive disease in which the size and grade of the tumor increases with increasing stage number. Additionally, the spread of cancer beyond the organ of origin into nearby lymph nodes and tissues increases with stage. Stage IV classifies cancer tumors that have spread to distant tissues or organs through the process of metastasis. There are different types of medical tests that can be used to determine the stage of cancer including physical exams, imaging tests, lab tests, pathology findings, and surgical observations (cancer.gov). The stage of cancer will also determine the treatment schema.

Breast cancer is the second leading cause of cancer related deaths in women after lung cancer. It is estimated that in 2014, there will be over 200,000 new cases with about 40,000 women succumbing to the disease. Breast cancer is a multi-faceted

disease with many different subtypes. There are numerous risks including genetic factors, family history, age, age at first menstrual cycle as well as pregnancy. It is estimated that 5-10% of all women harbor mutations in the BReast CAncer 1 and 2 (*BRCA1* and *BRCA2*) DNA repair genes, which has been shown to lead to increased risk of breast cancer [2]. In cases where there is a family history of breast cancer, specific screening strategies are developed, which may include regular breast exams and an earlier onset of mammograms. Breast cancer is a highly metastatic disease with estimations that 20-30% of all breast cancers will become metastatic [3]. It is also estimated that upon initial diagnosis, 6-10% of patients already have metastatic lesions [4]. Breast cancers commonly metastasize to the bone, brain, liver, and lungs. There is a critical need to research and develop treatment modalities that will not only treat the primary tumor but also treat metastatic sites.

There are four different breast cancer subtypes with different gene expression patterns, which is used to determine the best treatment strategy. Breast cancer can be divided into triple-negative/basal-like, human epidermal growth factor receptor 2 (*HER2*) positive, luminal A, and luminal B subtypes. Common molecular testing involves estrogen receptor (ER), progesterone receptor (PR), and HER2/neu receptor status testing. There are specific drug treatments for cancers that express ER, PR, and HER2 receptors involving antibodies against the receptors; however, these targeted therapies are only useful if the target is present.

Luminal breast cancers present with high levels of hormone receptors and comprise about 70% of invasive breast cancers. Luminal breast cancers respond to

endocrine therapy due to the high levels of hormone receptors [5]. With further gene level profiling, Luminal B cancer subtypes express the ER; however, they do not express estrogen-regulated genes suggesting that ER signaling is not a major factor in how these cancers grow [6]. The HER2+ subtype has high levels of HER2 and associated downstream gene levels and comprises about 15% of invasive cancers [5]. *HER2* cancer subtypes respond to trastuzumab, which is a monoclonal antibody to the HER2 receptor, but generally are associated with poor prognosis [5]. Basal breast cancers have high levels of basal epithelial genes and have low levels of ER and HER2. Basal breast cancers consist of about 15% of invasive cancer with most being triple-negative (ER^-, PR^-, and *HER2* non-overexpressing) [5]. Triple-negative breast cancers (TNBCs) do not respond to endocrine therapy due to the lack of hormone receptors. Based on new data analysis, triple-negative breast cancers are sensitive to platinum-based therapies in conjunction with Poly- (ADP) ribose polymerase (PARP) inhibitors especially in cases with *BRCA1/2* mutations [7]. PARP is involved in DNA repair, which when inhibited, leads to decreased DNA repair leading to increased cell death following treatment with DNA damaging chemotherapeutic drugs [7]. TNBCs are regarded as more aggressive types of cancer due to their lack of targeted therapies as well as the aggressive nature of the cancer cells [8].

Breast cancer is treated with a combination of surgery, radiation, and chemotherapy. Surgery is used to remove the bulk of the tumor from the breast through lumpectomy or partial/full mastectomy depending of the invasiveness of the tumor. Nearby lymph nodes are also removed as a biopsy to examine if there are any cancer cells present to examine the invasiveness of the tumor. Neoadjuvant therapy, or

chemotherapy prior to surgery, is used to shrink primary tumors before surgery. Radiation therapy can be given internally or externally. Internal radiation therapy delivers radioactive substances directly to the cancerous tissue through needles, wires or catheters. Chemotherapy is often given throughout the body through intravenous (IV) infusion; however, chemotherapy can also be given in a localized area. The type of treatment greatly depends on the stage of the tumor. Hormone therapy can be used in breast cancers that express hormone receptors, which ablates the naturally occurring hormones in the body. Without these hormones circulating in the body, the cancers that are dependent on hormone signaling are basically starved causing those cancer cells to die.

Targeted therapies include treatments that affect cells with specific molecular characteristics. For example, monoclonal antibodies have been developed against the HER2 receptor. This antibody binds to the receptor and blocks the growth signaling used by the cancer cells to continue proliferating. A new approach utilizes the concept of synthetic lethality to treat cancers. Synthetic lethality is described as the concept that mutations in two different genes may not have an effect in cells when only gene is mutated, but when both are mutated at the same time, leads cells to cell cycle arrest or death [9]. It has been described in the literature that the *BRCA1/2* genes act as tumor suppressors, and people with heterozygous mutations in *BRCA1/2* genes have an increased risk in breast, ovarian, pancreatic, prostate, and male breast cancer [9]. When patients have mutations in the DNA repair *BRCA1/2* genes, DNA repair is affected, and cells with *BRCA1/2* mutations are more sensitive to ionizing radiation and

chemotherapeutic drugs that induce DNA double strand breaks (DSBs) [9]. In the clinic, patients are screened for *BRCA1/2* mutations, and studies have shown that combination treatment with PARP inhibitors will lead to synthetic lethality when coupled with a DNA damaging drug, such as platinum drugs [7,9]. Both BRCA1/2 and PARP are involved in DNA repair pathways and when mutated singly, there is an increased risk of genomic instability. However, when *BRCA1/2* is mutated and PARP is inhibited together, coupled with increased DNA damage induced by chemotherapeutic drugs, the cells are unable to cope with the DNA damage and leads to increased cell death [9]. The use of genetic testing continues to be important as we increase our understanding of cancers and how expression profiles affect therapeutic strategies.

As mentioned earlier, targeted therapies are used including endocrine therapy for those types of cancers that express the hormone receptors. There are numerous types of treatments for non-endocrine therapies including signal transduction inhibitors, gene expression modulators, apoptosis inducers, mitotic inhibitors, angiogenesis inhibitors, and immunotherapies. Some of these treatments are FDA approved for treating cancer while others are still in development or clinical trials. The first line treatment for early stage TNBC include combination cytotoxic chemotherapies [10]. Taxanes are commonly used in breast cancer treatments and act as a mitotic inhibitor. The mechanism of action for the taxanes is the stabilization of microtubules leading to interference with normal microtubule deconstruction during cell division. As with any drug treatment, there are numerous side effects; however, the most notable is neurotoxicity leading to peripheral neuropathy. There has been recent data to suggest

that platinum agents used in combination with standard of care drugs offer enhanced tumor effects [11,12]. This is especially true in those patients who have mutations in *BRCA1/2* since there is defective DNA repair making the DNA-damaging drugs more effective in those patient tumors [13]. There are numerous ongoing clinical trials using carboplatin specifically treating TNBCs with metastases: NCT01881230, NCT00691379, and NCT01281150 (clinicaltrials.gov). Platinum agents are effective by forming DNA-platinum adducts resulting in intra- and interstrand crosslinks in the DNA leading to double strand breaks, which ultimately leads to cell death [14]. Later platinum generation drugs from cisplatin are often used in clinical settings due to the decreased side effects. The toxicity associated with cisplatin is most profound in the kidney whereas carboplatin causes little to no nephrotoxicity [15]. New treatment modalities need to be developed to decrease toxicity and increase efficacy.

Chapter 2. Models for Studying Breast Cancer

There are numerous *in vitro* and *in vivo* methods to study breast cancer. Many researchers begin initial studies utilizing human breast cancer cell lines grown in culture due to the quick experiment time and data generation. This method is commonly known as 2D monolayer cell growth in which cells are grown on plastic. These methods are inexpensive and high throughput with a wide range of experiments that can be derived from cells. However, some would argue that cells grown in 2D do not fully represent the tumor microenvironment due to the lack of stroma and that cell sensitivity to drugs is increased compared to sensitivity *in vivo* [16]. It has been reported by numerous laboratories that up to 80% of the breast tissue and the tumor microenvironment is comprised of stroma, suggesting that the stroma may play an important role in promoting growth of breast cancer cells. To circumvent these limitations, many investigators use 3D cultures in which the cells are grown in a matrix allowing the cells to grown in 3-dimensional space. With the addition of support cells, there are cell-cell and cell-matrix interactions that are able to occur naturally [16]. In these 3D settings, structure-function responses to drugs can be evaluated more accurately. There are numerous methods to study cancers in 3D including scaffold-based, spontaneous cell aggregation, and liquid overlay culture [16]. There are advantages and disadvantages to each of these methods. Briefly, scaffold-based methods can be very costly due to purchasing the extracellular matrix scaffold. Spontaneous aggregation only occurs in some types of cells, and these aggregates of cells do not form spheroids but only

clusters of cells. Also, spontaneous aggregation is an inexpensive and quick assay. Liquid overlay methods are also quick and relatively inexpensive. However, this method is a static method and only produces a small number of spheroids. It can be difficult to then collect these spheroid cells and examine further with Western blot, for example. The specific scientific question will determine ultimately which model would be best to use.

In this project, TNBC cell lines developed from patients were used as a model to study human breast cancer *in vitro* and *in vivo* to examine the effects of combination Nutlin-3a and carboplatin treatment. MDA-MB-231 and MDA-MB-468 cells were purchased from American Type Tissue Culture (ATCC). Both of these adenocarcinoma cell lines were developed from metastatic pleural effusions. Due to their highly tumorigenic ability, the MDA-MB-231 cells have been used by many laboratories to study TNBC primary tumors. For the in vivo studies in this thesis, we utilized the TMD231 cell line, which was derived from the parental MDA-MB-231 cell line [17]. The TMD231 cell line was a kind gift of Harikrishna Nakshatri (IUSM) and was established in his laboratory as a cell line that grows consistently in the appropriate microenvironment (i.e. mammary fat pad) and has a propensity to metastasize to the lung. The TMD231 cell line is more aggressive and has increased growth rates in culture compared to the parental MDA-MB-231 cells. To generate the TMD231 cells, MDA-MB-231 cells were implanted into the mammary fat pad of Nude mice, and the tumors were allowed to grow for a period of 6 weeks. The tumors were resected, dissociated, and grown in culture. The surviving cells became known as the TMD231 for 'tumor' MDA-MB-231 cells (Figure 1). *In vivo* models of metastasis to lungs, bone, and brain have been studied

using either tail vein injections or intracardiac injections of the cells into mice. The MDA-MB-468 cells are less invasive *in vivo* compared to the TMD231 cells, and typically metastasize to the lymph nodes following mammary fat pad implant [18]. Both the MDA-MB-231 (mtp53 R280K) and MDA-MB-468 (mtp53 R273H) cells have missense mutations within p53 in the DNA binding domain leading to abnormally functioning p53 [19]. The MDA-MB-231 cells have heterozygous mutations in BRAF and KRAS and homozygous mutations in TP53, CDKN2A, and NF2 [20]. The MDA-MB-468 cells express homozygous mutations in PTEN, RB1, SMAD4, and TP53 [20]. A summary of the cellular model systems can be found in Table 1. These cell lines were used to explore to what extent nutlin3a could decrease resistance to carboplatin and to evaluate potential mechanisms of action associated with this promising combination therapy.

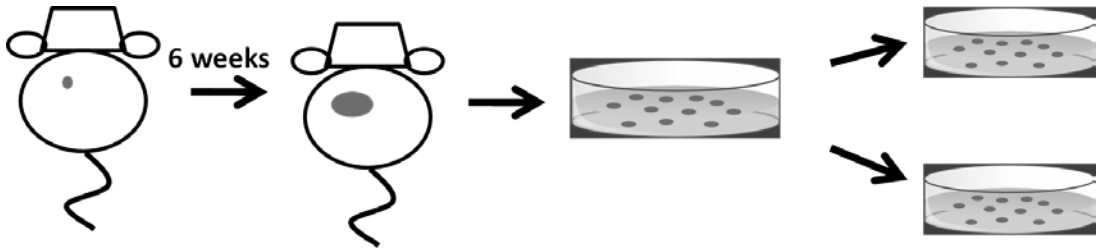

Figure 1. TMD231 triple-negative cell line is derived from MDA-MB-231 parental cells. Nude mice were implanted with $1x10^6$ parental MDA-MB-231 cells into the mammary fat pad, and the tumors were allowed to grow for 6 weeks. Tumors were surgically resected and grown in culture and expanded forming the TMD231 cell line after the 'tumor' MDA-MB-231 cells.

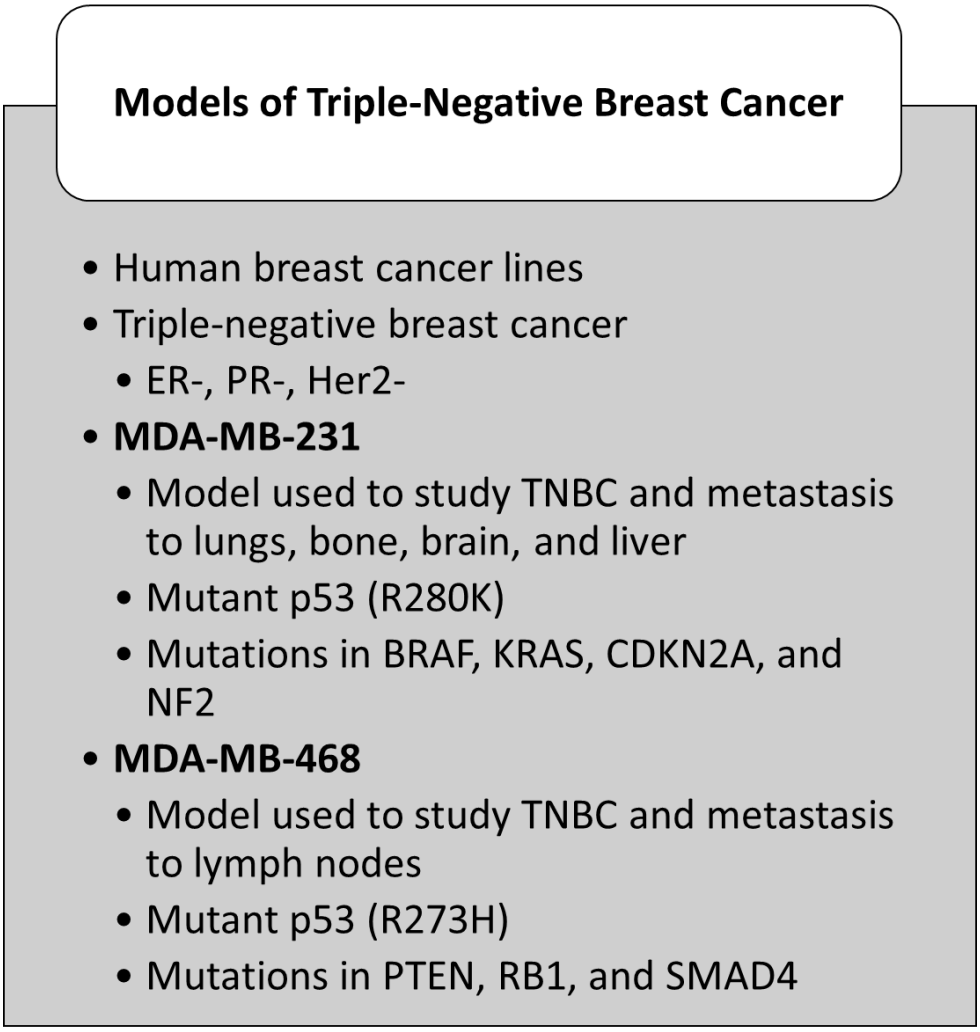

Table 1. Cellular models of triple-negative breast cancer. Both MDA-MB-231 and MDA-MB-468 cell lines were derived from human triple-negative breast cancer samples. Both cell lines have mutations in the DNA binding domain of p53 as well as other mutations that may play a role in dysregulation of signaling pathways required for growth, survival, and metastasis.

While *in vitro* experiments are clearly important for screening novel therapies and for interrogating potential therapy-mediated mechanisms, the need for further exploration using animal models is also very important for studying pharmacokinetic and pharmacodynamic relationships, efficacy, biomarker development, and off-target toxicity. With the generation of highly immune-compromised mouse models, xenograft animal models in which human cancers are implanted in mice have improved greatly over the years. Ectopic tumors describe tumors that are implanted and propagated in an anatomical location of the animal that does not represent the original microenvironment of the primary tumor tissue type. For example, a flank tumor of breast cancer cells would be considered to be an ectopic tumor. Conversely, if the tumor were located within the tissue of origin such as the mammary fat pad for breast cancer, the tumor would be considered to be an orthotopic tumor. Initial human cancer mouse models utilized Nude athymic mice. These mice are somewhat immune compromised compared to other mouse strains. However, Nude mice still have an intact innate immune system with circulating natural killer (NK) cells [21]. Another downside is hematopoietic cancer cells do not engraft efficiently in Nude mice. Nod/scid mice were developed following the development of Nude mice to provide an enhanced immune-compromised mouse strain better equipped to study human cancers. Nod/scid mice produce defective NK cells; however, these mice have a high incidence of thymic lymphoma and ultimately a short lifespan [22]. While the Nod/scid mice produce defective NK cells, there are still some functioning NK cells [23]. NOD.Cg-Prkdc^{scid}Il2rg^{tm1Wjl}/SzJ (NSG) mice were developed more recently in an effort to create a mouse strain that would be

suitable to study human hematopoietic stem cells. NSG mice allow for the engraftment of human peripheral blood and bone marrow [23]. NSG mice do not develop NK cells and have a very low incidence of thymic lymphoma with increased life expectancy compared to Nod/scid mice [23]. With these changes in immune system functions, the NSG mouse strain has been an ideal mouse model to study human cancers since there are less immune cells able to inhibit the human tumor engraftment. While mouse models allow for a more clinically relevant model, there are still disadvantages to using mouse models. While there is a tumor microenvironment *in vivo*, it is not a complete tumor microenvironment that one would find in humans due to the lack of immune and inflammatory cells as well as the fact that it is a mouse cell microenvironment. The immune system of mice must be suppressed in order for the human tumors to grow and there have been numerous studies to show the effects of the immune system on cancers. There are ongoing efforts to provide animal models with a humanized immune system [24].

The use of animal models allows for tumor growth and metastasis to be evaluated as well as the efficacy of drug treatment strategies. While there continues to be great discussion on the predictive value of mouse models in regards to clinical treatment, it is clear these models offer an opportunity to gain an understanding of pharmacokinetics (PK) and pharmacodynamics (PD), assess off target effects, and demonstrate the therapeutic potential and promise of new treatment strategies for cancer. However, animal studies are costly and therefore, appropriate preliminary data is needed before moving forward with *in vivo* animal models. Also, the personnel with

the appropriate training need to be utilized so that the animal study is completed in the most ethical manner possible. Pharmacokinetic studies of the drugs of interest need to be performed as well as animal model validation. The tumor growth kinetics need to be evaluated in order to properly assess tumor take rate and variability of base line tumor sizes, which ultimately dictate numbers of animals that must be included on a given study. The use of animal studies also allows for the drug dosing treatment strategy to be evaluated for drug efficacy, normal tissue toxicity in the mice as well as the evaluation of the pharmacokinetic properties of the compound in the mice and pharmacodynamic effects on the tumor. Additionally, with the use of *in vivo* models, there exists a tumor-extracellular matrix interaction that is lacking with traditional *in vitro* models, as well as the appropriate cell-matrix interactions and fluidics with the circulatory system. The tumor cells are able to shed naturally into the circulatory system and seed in near and distant locations, which better represents what occurs in human disease.

There are several types of clinical imaging used to visualize tumors including X-rays, CT scans, MRI, and PET scans. X-ray images are produced due to differential absorption of x-rays by different tissues. X-rays can be used to in chest radiographs and mammograms. Mammograms use X-rays to look for tumors in the breast area. Tumors in the lungs can be visualized easily due to the fact that air absorbs the least amount of X-rays, and therefore, the chest often looks black. However, tumors would appear shadowy on the films. Computed tomography (CT) scans are computer-controlled X-rays forming 2D mages. Multiple scans can be collected forming a 3D picture allowing for the size and depth of a tumor to be evaluated. Magnetic Resonance Imaging (MRI) utilizes

radio waves in combination with a strong magnetic field. Tissues differentially emit radio waves allowing for 3-dimensional images to be visualized. Positron emission tomography (PET) scans utilizes nuclear imaging. Low amounts of radioactive sugar substances are taken into the body, and when these radioactive substances collect in areas of the body and the sugar is metabolized, these collections can be visualized in the images. PET scans are more beneficial to detecting larger tumors than small tumors due to the nature of the sugar metabolism.

With the use of animal models, there needs to be sensitive and non-invasive methods to determine tumor burden. With *in vivo* studies, it is more challenging to image mice not only due to their small size but difficulty for high throughput imaging so that sufficient sample numbers can be generated. Additionally, the cost of small animal imaging is quite high per animal. To this end, the need for non-invasive small animal imaging that is feasible and cost effective is needed. Bioluminescent imaging (BLI) is a sensitive manner in which to measure tumor burden. Tumor cells, which stably express luciferase via lentiviral vectors, would be implanted into mice. At the time of imaging, mice are injected with the enzyme substrate, luciferin, to be catalyzed by luciferase present in the tumor cells. The tumor cells express luciferase, which when exposed to luciferin, use ATP and oxygen and catalyze two chemical reactions resulting in light being emitted. The light can then be detected by *in vivo* imaging. The peak of light emission can be used to determine the amount of tumor burden. Bioluminescent imaging is quite sensitive with signal detected from very small tumor burdens [25]. However, there are some drawbacks to this method of *in vivo* animal imaging. The basis

of bioluminescent imaging is that the substrate, luciferin, reaches the tumor at maximal capacity and while this may be true for tumors at baseline, once therapy ensues, the blood supply to the tumors could vary greatly mouse to mouse. Differences in blood flow could limit uptake of luciferin and produce confounding data. The blood supply to tumors is often leaky and the blood pressure going to the tumor could be a lot different than that of the rest of the mouse. There is no way of knowing if the whole tumor is exposed to the substrate. Also, bioluminescent imaging can be lengthy and stressful to the mouse due to the fact that every tumor will reach the peak of bioluminescence emission at a different rate; therefore, multiple snapshots over a predetermined time frame (typically 20-45 minutes) need to be taken to evaluate bioluminescent signal. With bioluminescent imaging, the imaging times can be quite lengthy compared to other imaging modalities, which is an increased stressor to the mice due to long periods of time that they are exposed to anesthesia.

Fluorescent imaging improves upon some of the drawbacks of BLI. A fluorescent protein of choice is stably expressed in cancer cells. The excitation and emission spectra would be evaluated for optimal use with the optical imaging platform. The use of optical imaging would allow for the substrate injection to be removed. In optical imaging, the imager has a laser component that acts to excite the fluorescent protein out of the resting state into the excited state. As the excited protein moves back to the resting state, the protein emits energy, which can be captured and measured. The fluorescent intensity would be the read out value for the *in vivo* imaging. This method would be non-invasive and more time saving as a single fluorescent imaging scan can take around

5-10 minutes, which is significantly less time than bioluminescent imaging (20-45 minutes) and ultimately less time under anesthesia for the mice. Fluorescent proteins that are in the near-infrared (NIR) spectra would be the best choice for fluorescent protein as there is less fluorescent signal lost to surrounding tissues as well as reduced autofluorescence [26]. However, several fluorescent proteins in the red spectra including E2-Crimson [27], mCherry [28], and mPlum [28] have been successfully used for *in vivo* imaging. A disadvantage to fluorescent imaging is the limiting factor of the depth of signal. It is unclear at this time the depths to which fluorescent signal can be measured. In some animal models, windows are created in the skin to image organs within the mice. Also, the sensitivity of the optical imaging apparatus will also need to be validated for each fluorescent protein used. Additionally, we have seen some instances in which the fluorescent protein levels leads to cellular toxicity. There are clearly advantages and disadvantages to both types of *in vivo* imaging. However, some of these are model dependent and validation is necessary for any type of animal model and imaging approach.

Chapter 3. Targeting the Mdm2 Signaling Network

Targeting the mouse double minute 2 (Mdm2) signaling axis is a novel therapeutic approach in cancer since Mdm2 is a multi-faceted protein involved in determining cell fate. The *mdm2* gene was first described as the gene responsible for transforming 3T3 cells [29]. In the spontaneously transformed 3T3 cells, it was found that the cells expressed 25-30 copies of paired, acentric chromatin bodies, which are known as double minutes (DMs). The cell line became known as 3T3-DM for the increased levels of double minutes [29]. The genes responsible for the production of the double minutes was determined to be *mdm1* and *mdm2* [29]. Overexpression of *mdm2* in cell lines led to tumor development in Nude mice showing the growth advantage of *mdm2* overexpressing cells [30]. *mdm2* knockout mice are embryonic lethal; however, dual knockout of p53 results in viable offspring [31,32]. Over a third of sarcoma tumors have overexpression of Mdm2 while maintaining wild-type p53, which would lead to decreased functionality of p53 due to the high levels of Mdm2 [33,34]. Mdm2 is often overexpressed in tumors and in a p53-independent manner can lead to increased genome instability by inhibiting Nbs1 function required for repair of DNA double-strand breaks [35]. There is mounting evidence demonstrating the important role Mdm2 has in cell growth regulation and cancer.

Mdm2 has been described as an oncogene since increased levels of *mdm2* led to tumor development in nude mice [30]. Mdm2 has been found to be overexpressed in a number of tumor types [36]. Specifically in breast cancers, studies have shown Mdm2

protein levels and *mdm2* gene amplifications ranging from 10-60% with some studies indicating a worse prognosis with overexpression of Mdm2 or gene amplification [36]. There are also numerous studies suggesting that overexpression of Mdm2 leads to increased distant metastasis *in vivo* [36]. A proposed mechanism by which Mdm2 upregulated metastasis was through a vascular endothelial growth factor (VEGF) dependent manner in which increased Mdm2 led to increased VEGF production, which led to increased metastatic potential [36]. Additionally, it was shown in breast cancer patients that Mdm2 levels correlated with disease-free survival with Mdm2 overexpression leading to decreased survival [37]. Chen and colleagues also showed a direct relationship between Mdm2 levels and matrix metalloproteinase 9 (MMP9) levels in which increased Mdm2 led to increased MMP9 and increased cell migration and invasion *in vitro* [37]. Mdm2 plays an important role in cell regulation; however, when Mdm2 is dysregulated, the oncogenic functions of Mdm2 can lead to increased tumorigenesis.

The *mdm2* gene is located on chromosome 12 and encodes for a 491 amino acid-protein with several different domains (Figure 2). Mdm2 has two different promoters, P1 and P2, which encode for a shorter, 75kDa, and full-length, 90kDa, proteins, respectively. The P1 promoter encodes for a housekeeping version of the protein while the P2 promoter leads to full-length protein, which is regulated by p53-mediated signaling [38,39] The p53 binding domain of Mdm2 is located at the N-terminal of the Mdm2 protein within a deep hydrophobic pocket. This hydrophobic pocket is where Mdm2 antagonist Nutlin-3a was designed to bind thus inhibiting the binding of Mdm2 to

p53 [40,41]. Mdm2 is regulated by numerous post-translational modifications, which help to determine different cellular processes [42]. Mdm2 also has nuclear localization signal (NLS) and nuclear export signal (NES) domains, which are posttranslationally modified to signal the movement of Mdm2 in and out of the nucleus. It has been shown that phosphorylation of S166 and S186 located near the NLS and NES domains of Mdm2 by Protein kinase B (Akt) leads to Mdm2 localization to the nucleus [43,44]. Mdm2 is able to monoubiquitinate p53 while p300 is necessary for polyubiquitination of p53.The C-terminal RING domain is important for Mdm2 E3 ubiquitin ligase activity to negatively regulate p53 due to the interaction of zinc with the RING finger domain [45-48]. Within the Acidic domain, there is a cluster of phosphorylation sites (Serines 240, 242, 246, 253, 256, 260, 262), which under normal conditions are phosphorylated. However, following DNA damage, these sites become hypophosphorylated leading to decreased p53 degradation but does not affect the ability of Mdm2 to ubiquitinate p53 [49]. There are upstream effectors that modulate Mdm2 activity including alternate reading frame protein (Arf) and Ataxia telangiectasia mutated (ATM), which are important for Mdm2 localization from the nucleus and phosphorylation-mediated inhibition of p53 degradation, respectively [50]. ATM also indirectly leads to the phosphorylation of two tyrosine residues through c-abl, which is also necessary to allow levels of p53 to rise following DNA damage [51]. The c-abl-mediated phosphorylation of Y394 leads to inhibition of ubiquitination of p53 by Mdm2 as well as inhibition of p53 nuclear exports [52]. Also, phosphorylation of Y276 increases interactions with Arf leading to increased Mdm2 in the nucleus and decreased p53 turnover [53]. Mdm2 plays a role in a large

signaling network mediated by numerous effectors and binding partners, which can determine certain cell fates [42].

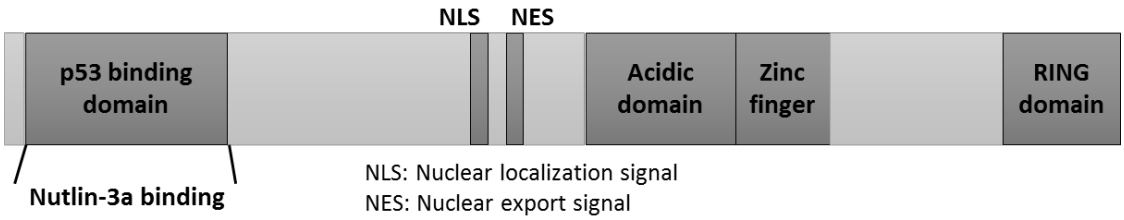

Figure 2. Mdm2 protein has several domains and posttranslational modification sites.

Mdm2 is an important protein involved determining cell through its interaction with numerous protein-binding partners. One of the main roles of Mdm2 is acting as an E3 ubiquitin ligase that negatively regulates p53 in cells. Interestingly, Mdm2 binds p73, which is a family member of p53; however, Mdm2 interaction does not lead to the degradation of p73. It appears as though Mdm2 binding to p73 leads to sequestration of p73 inhibiting normal functions of p73. Mdm2 has both a nuclear localization signal and nuclear export signal so that Mdm2 can localize to both the cytoplasm and nucleus. The N-terminal has the p53-binding domain in which Mdm2 can bind to the N-terminal of p53 and p73. Nutlin-3a binds to the hydrophobic pocket of Mdm2 in which p53 normally binds, thus inhibiting p53 binding as well as p73α, E2F1, and Hif-1 α. The inhibition of the interaction of Mdm2 and Hif-1α leads to decreased VEGF levels, which is important in angiogenesis signaling. Studies have shown that in p53 null cells, Mdm2 inhibits E2F-mediated apoptosis through regulating distribution of DP-1 within the cell. The RING domain is important for Mdm2 for the E3 ubiquitin ligase activity. Within the Acidic domain, there is a cluster of phosphorylation sites (Serines 240, 242, 246, 253, 256, 260, 262), which under normal conditions are phosphorylated. However, following DNA damage, these sites become hypophosphorylated, which leads to decreased p53 degradation but does not affect the ability of Mdm2 to ubiquitinate p53.

Mdm2 is a multi-functional protein and was first described to physically interact with the tumor suppressor p53 [54]. Mdm2 is an E3 ubiquitin ligase that acts as a negative regulator of p53. Under normal conditions p53 levels are relatively low in the cell. When the cells are stressed, p53 levels rapidly rise allowing for p53-mediated signaling. Once the stress is removed, Mdm2 acts to negatively regulate p53 by ubiquitination of p53 and targeting it for degradation by the proteasome [54]. Following DNA damage, ATM is able to phosphorylate Mdm2 at S395, which leads to the inhibition of p53 export from the nucleus as well as decreased degradation of p53 [42,55-57]. Additionally, p53 plays a role in this negative feedback loop by activating the transcription of Mdm2 and thus negatively regulates itself [58]. Mdm2 can also ubiquitinate itself leading to the reduction of Mdm2 levels in the cell [50]. Interestingly, Mdm2 binds p73, which is a family member of p53; however, Mdm2-p73 interaction does not lead to the degradation of p73 [59-61]. It appears as though Mdm2 binding to p73 leads to sequestration of p73 inhibiting normal functions of p73. The inhibition of the interaction of Mdm2 and Hif-1α via Mdm2 protein-protein interaction inhibitors such as Nutlin-3a, ultimately leads to decreased VEGF levels, which is important for angiogenesis [62]. Studies have shown that in p53 null cells, Mdm2 inhibits E2F-mediated apoptosis through regulating distribution of DP-1 within the cell. Additionally, Mdm2 can be regulated by the adapter protein, 14-3-3σ, where decreased levels of 14-3-3σ leads to increases in Mdm2 protein levels [63]. Interestingly, in the MDA-MB-231 breast cancer cell line, it has been shown that 14-3-3σ is highly downregulated [64], which may explain the increased basal Mdm2 protein levels in the TMD231 cells (Figure 17). The interaction of Mdm2 and protein binding partners

is tightly regulated and dysregulation can lead to inhibition of several signaling pathways including apoptosis, metastasis, and invasion, which can have great implications within cancers. Targeting the Mdm2 signaling axis, as a possible therapeutic approach, would lead to a multi-targeted approach due to the fact that Mdm2 is involved in several different signaling pathways.

Vassilev and colleagues designed a small molecule inhibitor, Nutlin-3a, which was initially characterized as blocking protein-protein interactions (PPIs) between Mdm2 and p53 [40]. There are three chemical moieties of Nutlin-3a that were designed to be similar to three key residues of p53 (Phe^{19}, Trp^{23}, and Leu^{26}), which binds into the hydrophobic pocket of Mdm2 [40]. Nutlin-3 exists as a chiral enantiomer with enantiomer-a and enantiomer-b [40]. Enantiomer-a was the active compound, whereas, enantiomer-b was about 150 times less active [40]. Therefore, throughout our studies, we elected to continue our studies using purified Nutlin-3a instead of a racemic mixture of Nutlin-3a/b. Mdm2 also interacts with p73, E2F1, and hypoxia inducible factor-1α (Hif-1α) and modulates their downstream effector functions. The interactions of Mdm2 with p73, E2F1, and Hif-1α are also inhibited by Nutlin-3a binding [62,65,66]. p73, E2F1, and Hif-1α share sequence homology with p53 in the region that binds to Mdm2 and thus, Nutlin-3a would inhibit the binding of Mdm2 from these binding partners [62]. Due to the numerous binding partners of Mdm2 resulting in a multi-targeted approach, we elected to use Nutlin-3a as a research tool to better understand how modulation of the Mdm2 signaling axis in combination with chemotherapeutic drug, carboplatin, may lead increased cell death in triple-negative breast cancers in a mutant p53 background.

It is estimated that p53 is mutated in about 30% of all cancers with 60% of basal TNBCs bearing mutations in p53 [67,68]. Approximately 90% of mutations in p53 occur in the DNA binding domain with 'hotspot' areas; whereas, p73 is rarely mutated in cancers [69,70] (Figure 3). Additionally, p53 also has been shown to exhibit gain-of-function mutations, which further antagonize other tumor suppressing capabilities of cells. Specifically, Xu and colleagues showed that some forms of mutant p53 (mtp53) (R282W and R110P) led to increased aggregation of mtp53 with p73 in perinuclear aggregates causing inhibition of p73 function [71]. This gain of function ability of mutant p53 would be interesting to study in our model system to see if the p53 mutation in the MDA-MB-231 (R280K) cells plays a similar role in co-aggregation with p73. Since it has been shown that Nutlin-3a inhibits the binding of Mdm2 from p73, E2F1, and Hif-1α, we elected to examine the p53-independent functions of Nutlin-3a in combination with clinically relevant chemotherapeutic, carboplatin.

Both p53 and p73 share sequence homology in key domains including the transactivation (30%), DNA binding (60%), and oligomerization (38%) domains (Figure 3) [72]. The N-terminal transactivation (TA) domain of p53 and p73 contain the region that binds to Mdm2 [41]. The DNA binding domain is important in the activation of genes important in pro-apoptotic signaling. The oligomerization domain is important for protein dimerization allowing for proper protein function [73,74]. Lau and colleagues showed that when cells treated with Nutlin-3a, the binding of Mdm2 from p73 was inhibited leading to p73-mediated induction of pro-apoptotic downstream targets and increased apoptosis in cells lacking wild-type p53 [66]. It has also been shown that Mdm2

binding to p73 leads to antagonism of p73 signaling but does not result in the degradation of p73 [59-61]. Since Mdm2 does not act as an ubiquitin ligase of p73, others have shown that p73 is regulated by Hect ubiquitin-protein ligase, Itch, which results in p73 degradation by the proteasome [75]. Runt-related transcription factor (Runx) and Yes-associated protein (Yap1) form a complex that is able to bind to the promoter of Itch and increase protein levels resulting in decreased levels of p73 [76]. Following DNA damage, the levels of Itch are reduced through c-abl phosphorylation of Y357 of Yap1 leading to the inhibition of Yap1 and Runx interaction, which inhibits their activity at the promoter of Itch, allowing the levels of p73 to rise enabling pro-apoptotic gene upregulation [75,76]. Additionally, following DNA damage, Yap1 has been shown to act as a transcription co-activator by forming a complex with p73 and Probable transcription factor (PML) and helps to stabilize p73 and promotes binding to pro-apoptotic gene promoters including Bcl2-associated protein X (Bax) [77]. Yap1 plays dual roles in the cell by mediating the inhibition of Itch upregulation as well as stabilizing p73 and increasing upregulation of pro-apoptotic gene levels.

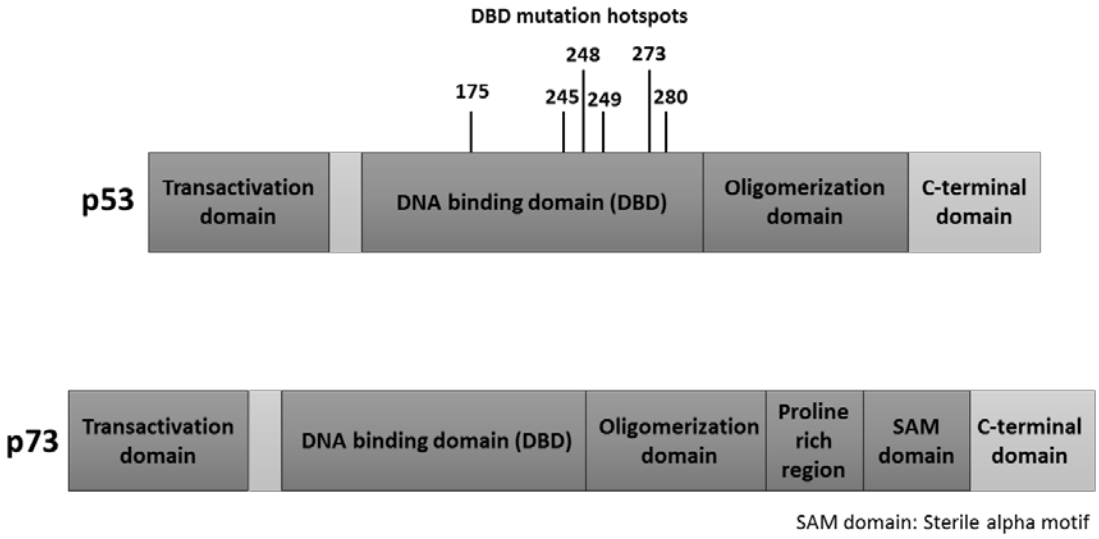

Figure 3. p53 and p73 have similar protein structure. Family members, p53 and p73, share sequence homology in many key domains including the transactivation (30%), DNA binding (60%), and oligomerization (38%) domains. The N-terminal transactivation domain contains the protein region that binds to Mdm2. The DNA binding domain is important in the activation of genes important in pro-apoptotic signaling. The oligomerization domain is important for protein dimerization, which allows for proper protein function. 90% of mutations in p53 occur in the DNA binding domain; whereas, p73 is rarely mutated in cancers.

p73 is a family member of p53 and has similar functions relating to the induction of pro-apoptotic genes in response to cellular stress [78,79]. p73 has several different N-terminal splice variants in which isoforms lacking the transactivation domain (ΔNp73) act as negative regulators of the transactivation domain containing p73 C-terminal isoforms (TAp73) [72]. The TAp73 isoforms have similar functions to p53 [72]. The ΔNp73 isoforms act as negative regulators of transactivating p73 isoforms by inhibiting p73 and by competing for DNA binding sites [80,81]. Mice lacking all p73 isoforms exhibited profound neurological deficiencies indicating the importance of p73 during development [80]. Jost *et al.* showed that the p73α isoform has pro-apoptotic functions [78], and Melino *et al.* showed that the p73α isoform has functional transactivation function leading to the induction of pro-apoptotic genes. [79]. Since the p73α isoform has been shown by numerous laboratories to be important for pro-apoptotic signaling, we elected to specifically focus on this isoform throughout our studies. When overexpressed, p73α has been shown to induce apoptosis and cell cycle arrest as well as having similar p53-target genes in relation to apoptosis and cell cycle arrest including the cyclin-dependent kinase (CDK) inhibitor, *p21*, Growth Arrest and DNA Damage-inducible 45, *gadd45*, p53 up-regulated modulator of apoptosis (*PUMA*), and Bcl2-associated protein X (*Bax*) through direct and indirect methods [78,79,82]. Following both genotoxic and non-genotoxic stress signals, GADD45 is quickly activated and mediates pro-apoptotic, cell cycle arrest, and DNA repair pathways [83]. Melino and colleagues showed that p73-mediated apoptosis occurred through upregulation of PUMA, which in turn led to the mitochondrial translocation of Bax and subsequent cytochrome C release

[79]. Bax is a pro-apoptotic Bcl-2 family member involved in the intrinsic apoptotic pathway, and stress signals can lead to oligomerization of Bax monomers and translocation to the mitochondria leading to the release of cytochrome C [84]. Free cytochrome C binds to Apoptotic protease activating factor 1 (Apaf-1) leading to the formation of the apoptosome and activation of pro-caspase-9 [84]. This activation of pro-caspase 9 to active caspase-9 leads to a caspase signaling cascade in which caspase-3, -6, and -7 are activated leading to apoptotic cell death [84].

It was also shown that p73 is phosphorylated at Y99 by c-abl following DNA damage, which leads to increased p73 protein stabilization as well as increased protein levels in some cell systems [85-87]. Specifically in cells where p53 is not functioning normally, there have been links between the lack of p53 and levels of p73. In cells where p53 was mutant or reduced with siRNA, p73 levels were increased, which was regulated at the transcription level by binding of E2F1 at the promoter region of TAp73 [88]. In the context of DNA damage, there are several proteins that mediate the upregulation of p73. It has been shown that Chk1 and Chk2 kinases are important drivers of p73 upregulation, which in turn are also important for driving E2F1-mediated signaling followed by E2F1-mediated upregulation of p73 [89].

The cyclin-dependent kinase inhibitor, p21 also known as p21 $^{WAF1/Cip1}$, is an important signaling mediator in cell cycle signaling by promoting cell cycle arrest following stress signals. p21 inhibits the activity of the cyclin-dependent kinases CDK1 and CDK2, which leads cell cycle arrest in S and G2 phases of the cell cycle [90]. p21 also acts to inhibit cell proliferation by competing for the DNA polymerase-δ binding site of

proliferating cell nuclear antigen, PCNA, which ultimately leads to inhibition of DNA synthesis [90]. p21 can also bind to E2F1 and inhibit the ability of E2F1 to upregulate cell proliferation transcription targets [90]. While there are several p53-dependent mediators of p21 upregulation including the HRAS-Raf-MapK pathway, there are several p53-independent drivers of p21 upregulation [90]. Since our model system is utilizing cells with mutant p53, the p53-indepenent upregulation of p21 is of particular importance. *p21* gene levels can be upregulated through retinoid and vitamin D receptors as well as several transcription factors including p73, specificity factor 1 and 3 (SP1 and Sp3), and Signal Transducers and Activators of Transcription (STATs) [90]. There are several links between major players p73, E2F1, and mutant p53 following DNA damage. These proteins may drive p21 levels and activity leading to cell cycle arrest and ultimately apoptosis in our model system if the levels of DNA damage and stress surpass DNA damage stress thresholds set by the cell.

Ambrosini and colleagues showed that the use of Nutlin-3a inhibited Mdm2 from binding to E2F1 and combined with DNA damaging drug, cisplatin, there was increased cytotoxicity through E2F1-mediated signaling [65]. The use of E2F1 siRNA led to decreased amounts of apoptosis in combination Nutlin-3a and cisplatin treated cells [65]. E2F1 is a transcription factor that plays an important role in cell proliferation, cell cycle, and apoptosis depending differential cell signaling [91]. Following DNA damage, E2F1 is activated and can lead to the transactivation of pro-apoptotic genes including Apaf1 and p73 [91]. It has been shown that Mdm2 inhibits the pro-apoptotic functions of E2F1 through interplay between Mdm2, E2F1 and DP-1 in the absence of p53 [92]. Some studies

have shown that when E2F1 is knocked out, mice form spontaneous tumors suggesting that E2F1 may play a role as a tumor suppressor [93]. LaRusch and colleagues also showed that Nutlin-3a inhibits Mdm2 from binding to Hif-1α and thus led to decreases in VEGF [62]. Decreased VEGF production would be important in an *in vivo* setting due to the necessity for tumors to form new blood vessels to support prolonged tumor growth [94].

The combined protein-protein interactions with Mdm2, p53, p73, E2F1, and Hif-1α that are inhibited by the small molecule inhibitor, Nutlin-3a, may lead to a multi-targeted approach to treating cancer especially when coupled with clinically relevant DNA damaging drugs like carboplatin since many of these binding partners are involved in DNA damage responses. There are five major types of DNA repair mechanisms including nucleotide excision repair (NER), base excision repair (BER), mismatch repair (MMR), non-homologous end joining (NHEJ), and homologous recombination (HR). Briefly, NER repairs large, bulky lesions, which cause distortions in the DNA helical structure caused by agents like platinums or photoadducts from UV damage [95]. NER is primarily the DNA repair pathway utilized by cells to repair platinum induced damage. BER repairs single strand breaks (SSBs), chemically altered bases as a result of oxidative stress, and abasic sites [95]. MMR removes incorrect nucleotides on the opposite DNA strand often caused by error prone polymerases, which is also utilized in repairing platinum based DNA damage [95,96]. NHEJ occurs when there are DSBs induced by ionizing radiation, oxidative free radicals, and mechanical stress [95]. HR also repairs DSBs when there is strong sequence homology. HR occurs during late S-G2 phases of the cell cycle since sister chromatids can be used as a template [95]. HR can also repair damage caused

by platinum agents when double strand breaks occur [96].

The role of Mdm2 in DNA damage and repair in relation to tumorigenesis is an emerging area of study. Mdm2 may play a role in NER through Arf mediated signaling. Arf is necessary in the absence of p53 to stimulate xeroderma pigmentosum, complementation group C (XPC) levels, and XPC is involved in a multi-protein complex that is needed for recognition of the DNA damage [95]. Arf can bind and inhibit Mdm2; however, the mechanism of by which Mdm2 may play a role in NER is not well defined [95]. Also, DNA polymerase eta (PolH) is a Y-type polymerase and is an important protein involved in NER. Jung and colleagues showed that Mdm2 acts as an E3 ubiquitin ligase leading to polyubiquitination of PolH, which results in degradation through the proteasome [97]. It was also shown that Mdm2 acts to decrease PolH levels both at basal and UV-induced DNA damage conditions [97]. Interestingly, there has been recent data to suggest that Mdm2 plays a role in HR DNA repair by antagonizing the Mre11, Rad50, and Nbs1 (MRN) complex [35]. Mdm2 binds directly to Nbs1 and inhibits its function in the MRN complex [35]. DNA damage persists due the fact that the initial sensing mechanism of the MRN complex is unable to continue signaling at sites of DNA damage [35]. Carboplatin is effective at killing cancer cells by causing DNA damage imparted by platinum (Pt) adduct formation in DNA. Platinum agents lead to Pt adducts covalently bonding to N^7 position of purine bases resulting in intrastrand and interstrand DNA crosslinks. DNA repair resulting from platinum-induced DNA damage could be inhibited in cells where levels of Mdm2 are increased [35].

The role of MdmX (Mdm4) has been increasingly studied in the context of cancer

in recent years. The p53- and Mdm2-independent functions of MdmX have only recently been studied. Like Mdm2, MdmX can be upregulated in cancers, though this upregulation is independent of p53. Gilkes and colleagues showed that MdmX levels can be upregulated through mitogenic signaling mediated by K-Ras and insulin-like growth factor 1 (IGF-1) [98]. Since it was shown that Mdm2 increases genomic instability by Bouska and colleagues, the authors also studied the effects of MdmX on genomic stability in the context of Mdm2- and p53-independence [35]. Carillo and colleagues showed that following irradiation- (IR) induced DNA DSBs, MdmX inhibited the repair of DSBs independent of p53, Arf, and Mdm2 [99]. Carrillo and colleagues also showed that MdmX associated with Nbs1 independent of both p53 and Mdm2 using co-immunoprecipitation experiments showing a direct connection between MdmX and the repair machinery in the MRN complex [99]. Based on data from Carrillo et al.[99], MdmX also plays a similarly important role in genomic instability as Mdm2 and may be important to increase our understanding of how MdmX affects cancer growth and survival. It has been described that in breast cancers, 27% overexpress MdmX with concurrent p53 inactivation as well as 30% of aggressive breast cancers also have increased MdmX levels with mutant p53 [99]. It is possible there may be certain subtypes of cancers that have MdmX overexpression, which may affect how tumors respond to treatments.

The overall objective of this thesis was to evaluate the therapeutic potential of a new combination therapy to treat TNBC. Based on front-line therapies currently being tested in clinical trials for TNBC, the platinum agent, carboplatin was selected for study. Novel drug targets need to be elucidated to improve treatment modalities especially in

treating aggressive cancers like TNBC. Mdm2 is an unexplored target in breast cancers. Histological studies have indicated that up to 56% of breast cancer biopsies contain high levels of Mdm2 [36]. In this thesis, the potentiation of carboplatin-mediated DNA damage in the context of blocking some aspects of Mdm2 function was investigated. Pharmacodynamic studies were designed to gain insight into and validate molecular mechanisms that based on the literature could be operative following treatment. In our correlative PD studies, we also sought to identify targets that could potentially serve as biomarkers of treatment response and efficacy for future clinical trials of TNBC.

Nutlin-3a binds to the hydrophobic pocket of Mdm2 and inhibits the interaction of binding partners of Mdm2 including p53, p73, E2F1, and Hif-1α. In our model, we are utilizing triple-negative breast cancer cells that harbor a p53 mutation (R280K and R273H) in the DNA binding domain. These cancers are considered to be more aggressive due since there are limited targeted therapies and that mutant p53 drives cell survival and metastasis [100,101]. Due to the interest of platinum agents in metastatic breast cancer trials (NCT01881230, NCT00691379, and NCT01281150) (clinicaltrials.gov), carboplatin was selected as the chemotherapeutic drug in which to interrogate the effect of the small molecule inhibitor, Nutlin-3a. Carboplatin causes DNA damage by the binding of Pt to DNA and leading to intra- and interstrand DNA crosslinks and indirectly DNA strand breaks. The hypothesis is modulation of Mdm2 signaling through inhibition of protein-protein interactions with Nutlin-3a in combination with carboplatin-mediated DNA damage will lead to increased cell death. The proposed mechanism of action is that once Nutlin-3a is bound to Mdm2, the binding between Mdm2 and p73, E2F1, and Hif-1α is

inhibited allowing p73 and E2F1 to activate target genes leading to an increase in pro-apoptotic gene expression and cell death. Mdm2 levels would increase following Nutlin-3a treatment through p73-mediated upregulation, and the amount of Mdm2 associating at the chromatin could increase following combination treatment. Increased Mdm2 at the chromatin can lead to increased Mdm2-Nbs1 interaction, which could inhibit the sensing of DNA damage once DNA strand breaks have occurred. This delay in sensing of DNA damage could lead to decreased DNA repair, which would result in an increased DNA damage window. As the DNA damage window increases, cell signaling mechanisms could lead to the determination of cell fate, and ultimately leading to cell death. The signaling pathways that could be modulated in our model system can be seen in detail in Figure 4. There is a growing consensus in the literature that the levels of Mdm2 and the localization of Mdm2 in the cell may dictate in part how a cell senses and responds to DNA damage, and whether the outcome of DNA damage will be survival or death.

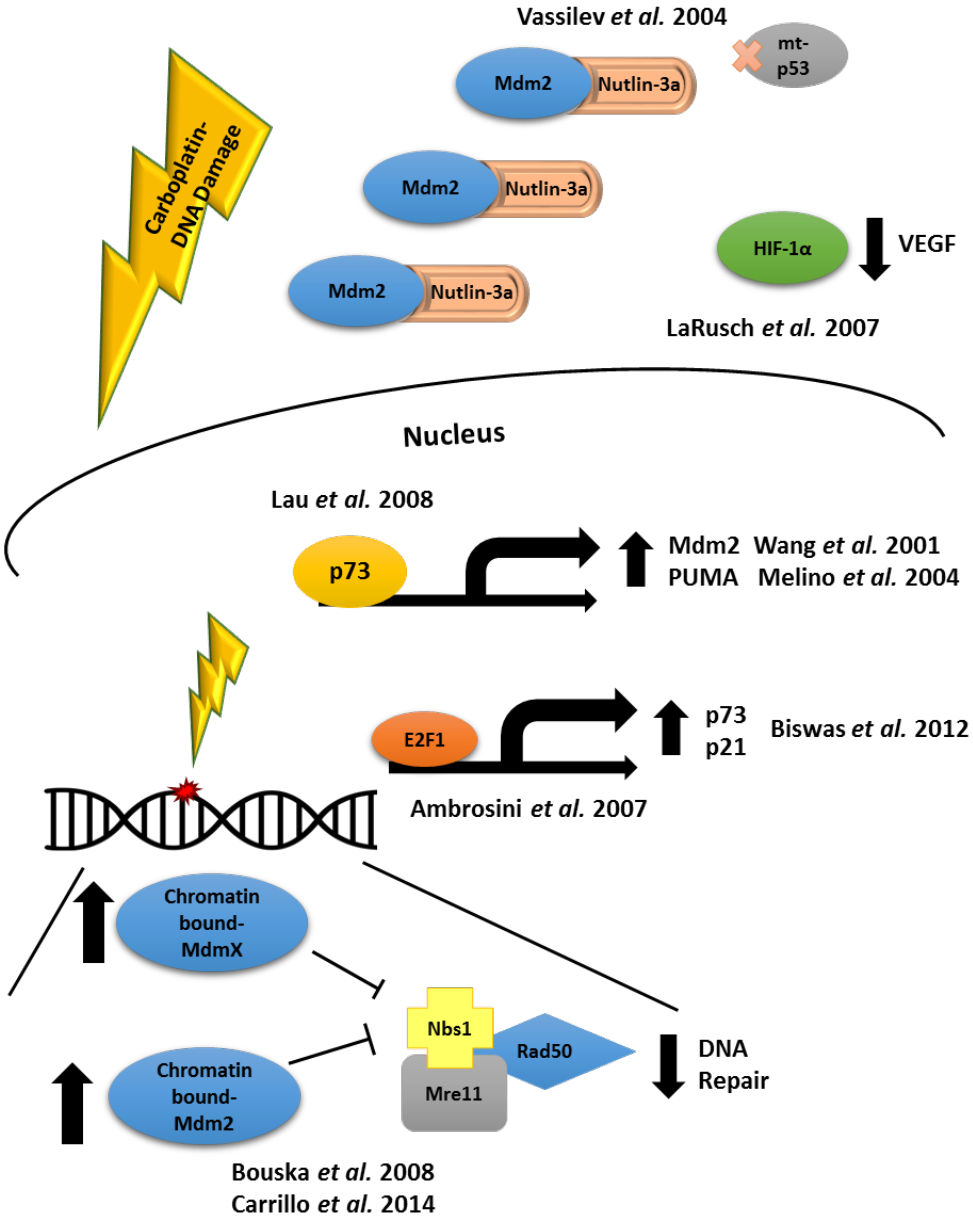

Figure 4. Nutlin-3a and carboplatin combination treatment increases cell death by upregulating pro-apoptotic gene levels and inhibits DNA repair. Nutlin-3a binds to the p53 binding pocket of Mdm2 and inhibits the binding of p73, E2F1, and HIF1-α, which can enable these proteins to upregulate the transcription of pro-apoptotic genes, cell cycle genes, and decrease the levels of VEGF. Carboplatin causes DNA damage by creating intra- and interstrand crosslinks in the DNA leading to cell death. Nutlin-3a

potentiates carboplatin-mediated DNA damage leading to increased cell death through delayed DNA repair. This delayed DNA repair may be mediated by Mdm2 binding at the chromatin and based on studies by Dr. Christine Eischen and colleagues showing that Mdm2 antagonizes Nbs1, a member of the MRN complex. The MRN complex is important in initial DNA damage sensing and recruitment of other DNA damage response proteins to sites of DNA damage. Carboplatin mediated-DNA damage leads to activation of p73α pro-apoptotic signaling. p73-mediated signaling can lead to increased Mdm2 levels since p73 has been shown to bind to the Mdm2 promoter. With increased levels of Mdm2, there is more Mdm2 present in the cells that could bind the MRN complex at the chromatin. Increased binding of Mdm2 to the MRN complex leads to delays in DNA damage detection and thus lead to delays in DNA repair. This delay in repair, may allow DNA damage response elements to commit to cell death pathways allowing more cells to be affected by the combination treatment than by single drug treatments alone.

In future studies increased clinically relevant patient-derived xenograft (PDX) models and small molecule inhibitors used in clinical trials would be used to expand on these efficacy studies. Primary patient tumor samples could be used in mouse models to better understand the efficacy of the combination platinum and Mdm2 inhibitor treatment. Jackson Laboratories in collaboration with UC Davis Cancer Hospital are providing mice that harbor primary patient tumors from women with triple-negative breast cancer (http://jaxservices.jax.org/invivo/pdx.html). These tumors have undergone extensive genetic screening with gene expression profiles as well as copy number variation testing. These tumors would have increased clinical relevance since the molecular signatures are fully validated with the primary patient breast cancer tissue. Additionally, there are numerous Mdm2 inhibitors, which are in early phase clinical trials. There is a second-generation compound to Nutlin-3a, RG7112 (RO5045337 Roche) that is in Phase I clinical trials. Additionally, there are several other Mdm2 antagonists being studied including SD-3032b (Baiichi Sankyo Inc.), SAR4058338 (Sanofi), CGM-097 (Novartis), and AMG-232 (Amgen) that are currently being investigated. We utilized Nutlin-3a as a tool to study the mechanism at which Nutlin-3a synergizes with carboplatin to cause increased cell death in TNBC with mutant p53 as there is a critical need to find new treatments for metastatic TNBC harboring mtp53 due to the aggressiveness of the disease and lack of targeted therapies [100,101]. The TMD231 orthotopic NSG model used here provides a feasible pre-clinical approach to further determine and validate the best set of biomarkers that can be used to assess biological effect of the combination carboplatin and Nutlin-3a treatment. In this research, as we

continue to delineate the underlying mechanisms leading to cell death, incorporation of PDX models, and clinically utilized Mdm2 inhibitors can be used to increase the understanding of the benefit of using dual carboplatin and Mdm2 protein-protein inhibition. Additionally, it will be important to perform detailed PK/PD studies to further validate targets that are modulated by the dual carboplatin and Nutlin-3a treatment. Understanding how long and to what extent the blocking of Mdm2–p73 protein-protein interactions must be modulated to observe therapeutic effects will be critical for development of clinical trials in the future.

SECTION II. MATERIALS AND METHODS

Chapter 1. *In Vitro* Studies

A. **Cell Culture and Reagents**

1. **Cells and Cell Culture.** MDA-MB-231 (ATCC® HTB-26™) and MDA-MB-468 (ATCC® HTB-132™) were purchased from ATCC. TMD231 cells were a kind gift of Dr. Harikrishna Nakshatri and were developed as described in Helbig *et al.* [17]. TMD231 cells were grown in MEM-α medium (Gibco®) containing 10% FBS (Atlanta Biologicals) and 1% HEPES (Gibco®). MDA-MB-231 and MDA-MB-468 cells were grown in DMEM medium (Gibco®) containing 10% FBS (Atlanta Biologicals). Cells were cultured at 37°C with 5% CO_2.
2. **Mycoplasma Detection.** Cells were tested for mycoplasma using MycoAlert™ Mycoplasma Detection Kit (Lonza). Cell culture medium was collected from cultured cell lines and if mycoplasma was present, the addition of MycoAlert™ Substrate, catalyzed the conversion of ADP to ATP. The levels of ATP were detected following the addition of the MycoAlert™ Reagent. The before (read A) and after the addition of the MycoAlert™ Substrate (read B) reads allowed for a ratio to be determined (B/A). If the ratio was above 1, the sample was contaminated with mycoplasma. Cell lines were tested regularly for the presence of mycoplasma and were negative.
3. **Drugs and Small Molecules.** Nutlin-3a was synthesized at the IUPUI Chemical Synthesis and Organic Drug Lead Development Core and confirmed through HPLC-

MS analysis. Nutlin-3a was dissolved in DMSO up to 100mM stock solutions. Carboplatin was purchased from Sigma and dissolved in H_2O at 10mM stock solution. RG7112 was dissolved in DMSO with stock concentrations up to 50mM (ApexBio and ChemScene).

B. **Proliferation Assays**

a. **Methylene Blue Proliferation Assay.** The methylene blue proliferation assay was derived from Oliver *et al.* which utilized 5% methylene blue stain to stain cells in microplate assay [102]. The assay was high throughput with sensitive measures of cells present and fixed to the plate. The methylene blue stain bound to negatively charged moieties within cells including DNA and negatively charged portions of proteins. In all methylene blue assays, the outermost wells of 96-well plates were filled with 200µL PBS to diminish the effects of plate evaporation. To determine the optimal cell number to seed in 96-well plates for a 5-day proliferation assay, plating efficiencies were completed. All cell lines were plated in 96-well plates in increasing cell number starting from 500 cells/well and ranging up to $4.0x10^3$ cells/well. Cells were mock treated with media and allowed to grow for 5 days as a drug treatment would have been given. At the end of treatment, the media was aspirated and the cells were fixed with methanol. Then, cells were stained with 5% methylene blue stain, washed in DI H_2O, and air dried. Plates were destained with 100-150µL 0.5M HCl, and absorbances were read at 610nm. Optimal absorbance values were between 0.7-0.9. TMD231 cells were seeded with 500 cells/well in 96-well plates. MDA-MB-231 and MDA-MB-468 cells were seeded with $2x10^3$ cells/well. Cells were

seeded on Day -1 and treated 24 hours later on Day 0. For drug treatments, each plate had a vehicle control, which consisted of DMSO for Nutlin-3a and H_2O for carboplatin. Cells were treated with increasing concentrations of Nutlin-3a (0-120μM), carboplatin (0-100μM), or 1:1 combination (0-100μM). For the combination treatments, the highest concentration used was 100μM, which was comprised of 50μM Nutlin-3a and 50μM carboplatin. For shorter treatments, cell number was adjusted accordingly. Each plate contained untreated media controls and Vehicle controls. The Vehicle controls contained the amount of vehicle in each of the highest drug concentrations.

b. **Clonogenic Proliferation Assay.** TMD231 cells were plated at low cell density with 50 cells per 10cm dish on Day -1. On Day 0, TMD231 cells were treated with 0-60μM Nutlin-3a, 0-10μM carboplatin, or 0-6μM 1:1 combination. Colonies were allowed to grow for 14 days. The media was removed, cells were washed with PBS, and fixed with methanol. Colonies were stained with 5% methylene blue stain, washed in DI H_2O, and air dried. Visible colonies were numerated using a digital counting pen to ensure accurate counts.

c. **Cell Counting Proliferation Assay.** TMD231 cells were seeded with on 12-well plates on Day -1 with $6.5x10^3$ cells per well. On Day 0, cells were treated with 15μM Nutlin-3a, 15μM carboplatin, or 15μM Nutlin-3a+15μM carboplatin combination, or appropriate dilutions of DMSO in H_2O as a Vehicle control. DMSO concentrations were kept below 0.1% in all experiments. Later experiments also used 7.5μM Nutlin-3a, 7.5μM carboplatin, or 7.5μM Nutlin-3a+7.5μM carboplatin combination. Each

treatment was completed in triplicate to ensure accurate cell counts. Each day following treatment, cells were photographed to visualize changes in cell number and cell morphology. On the day of harvest, growth medium was removed, cells were washed with PBS, and trypsinized with 0.05% trypsin-EDTA (Life technologies). Trypsinized cells were resuspended in an appropriate volume of cell culture medium, mixed with trypan blue, and live cells were counted via hemocytometer. Total cell counts were calculated.

d. **Annexin V and 7-AAD Apoptosis Assay.** Annexin V readily binds to phosphatidylserine, which is expressed the exterior of cells when undergoing early apoptotic signaling. Annexin V tagged with FITC (BD Biosciences) enabled its use with flow cytometry. 7-AAD (BD Biosciences) was used since it is a fluorescent DNA marker that intercalates into DNA in GC rich areas and is indicative of cell membrane leakage. When cells were positive for Annexin V alone, those cells were considered to be undergoing early apoptosis. When cells were positive for both Annexin V and 7-AAD, those cells were considered to be undergoing late apoptosis or necrosis. To measure apoptosis, Annexin V-FITC and 7-AAD was used to determine the number of apoptotic cells following drug treatment. TMD231 cells were seeded on 10cm dishes on Day -1 in normal growth medium at an appropriate cell density for the treatment length to ensure proper cell numbers at the end of the study. On Day 0, the TMD231 cells were treated with 1:1, 3:1, or 1:3 combination and corresponding single drug IC_{50} value concentrations as derived from the 5-day methylene blue proliferation assays. TMD231 cells were treated with 0.8µM Nutlin-3a, 0.8µM

carboplatin, or 0.8µM Nutlin-3a+0.8µM carboplatin 1:1 combination, 3.75µM Nutlin-3a, 1.25µM carboplatin, or 3.75µM Nutlin-3a+1.25µM carboplatin 3:1 combination or 0.7µM Nutlin-3a, 2.1µM carboplatin, or 0.7µM Nutlin-3a+2.1µM carboplatin 1:3 combination in normal growth medium for a total of 96 hours. The Vehicle control was DMSO +H_2O. On Day 4, cells were harvested. The medium was removed and saved in collection tubes. Cells were washed with PBS, and the PBS was also saved to ensure proper analysis of all cells present in the cultures. Accumax Cell Dissociation Solution (Innovative Cell Technologies) was used to free adherent cells. The dissociated cells were added to the appropriate collection tubes and spun down to pellet cells. Cells were washed with PBS and spun down again. Pellets were then resuspended in 1X Annexin V Binding Buffer (BD Biosciences). Each sample was stained using 5µL Annexin V-FITC (BD Pharmigen) and 5µL 7-AAD (BD Pharmigen). Single and double stained cells treated with carboplatin were used as controls to set the gating parameters of the flow cytometer to distinguish between negative and positive staining.

e. **Cell Cycle.** Propidium iodide (PI) staining was used to determine cell cycle analysis. PI intercalates into DNA allowing the DNA content in cells to be measurable by flow cytometry. PI cannot pass through an intact cellular membrane and therefore cells must be permeable during PI staining solution incubation as described below. TMD231 cells were seeded on 10cm dishes on Day -1 in normal growth medium at an appropriate cell density for the treatment length to ensure proper cell numbers at the end of the study. On Day 0, the TMD231 cells were treated with 3.75µM,

7.5µM, or 15µM Nutlin-3a, carboplatin, and 1:1 combination in normal growth medium. The Vehicle control contained DMSO+H_2O. For the combination treatments, 3.75µM combination was comprised of 3.75µM Nutlin-3a+3.75µM carboplatin so that the combination treatments have equal amounts of each drug as the single drug treated cells. On Day 3, cells were harvested. The medium was removed and saved in collection tubes. Cells were washed with PBS, and the PBS was also saved to ensure proper analysis of all cells present in the cultures. Accumax Cell Dissociation Solution (Innovative Cell Technologies) was used to free adherent cells. The dissociated cells were added to the appropriate collection tubes and spun down to pellet cells. Supernatant was removed, and cells were washed with PBS before spinning down again. Pellets were resuspended in PBS and mixed with PI staining solution: 0.1% (v/v) Triton X-100, 10 µg/mL PI, 100 µg/mL DNase-free RNaseA. Cells were incubated for 1 hour at room temperature before analysis with flow cytometry.

C. **Molecular Biology Assays**

1. **Lentiviral Transduction.** Cells were typically transduced with a multiplicity of infection (MOI) of 50. That is, there were 50 viral particles to each cell, and the total amount of viral supernatant was calculated and used in the transduction. When using highly concentrated (>10^7) lentiviral supernatants, cells were transduced for 4 hours. Lentiviral supernatant containing media was removed and replaced with fresh media. Retronectin-coated plates were used to enhance transduction efficiency [103]. Flow cytometry was used to validate the presence of fluorescent

proteins. Appropriate settings were used for optimal detection of the fluorescent protein of choice (eGFP, mCherry, E2-Crimson). Unmarked parental cells were used as background controls.

a. **Lentiviral Supernatant Production.** Lentiviral supernatants were produced as described in Leurs *et al.* [104]. Briefly, lentiviral supernatants were produced following co-transfection of 293T cells with vector plasmids and *env* expression plasmids, using FuGENE 6 (Roche, Basel, Switzer- land) or Polyfect (Qiagen, Valencia, CA) transfection reagents according to the manufacturer's recommendations. Twenty-four hours after transfection, gene expression from the human spleen focus forming virus (SFFV) immediate-early gene enhancer/promoter was used for E2-Crimson levels. Forty-eight hours after transfection, supernatants were collected, filtered through a 0.45µm filter, and stored at -80°C. Lentiviral stocks were concentrated by centrifugation (10,000 x *g*; 45 min; 4°C), and the lentiviral titers were determined using HT1080 cells.

2. **Western Blot.** Cells were lysed with 1% SDS lysis buffer containing 1%SDS, 1 Complete-EDTA free mini tablet (Roche), and 1% phosphatase inhibitor 3 (Sigma). Growth medium was removed from cells and washed with PBS. An appropriate volume of 1% SDS lysis buffer was added directly to cells on the culture plates, and lysates were scraped with a cell scraper. Lysates were collected and placed in microcentrifuge tubes. The lysates were boiled at 95°C for 8-10 minutes. Lysates were sonicated to dissociate any DNA. Protein quantification was determined using the DC™ Protein Assay (Bio-Rad) as per manufacturer's instructions. Standard curves

were determined using BSA standards. Samples were stored at -80°C until ready for use. Westerns were run using Criterion™ TGX™ Precast 4-20% Gels (Bio-Rad). Running buffer was comprised of 10% 10XTG buffer (Bio-Rad) and 0.1% SDS. Transfer buffer contained 10% 10XTG buffer (Bio-Rad) and 20% methanol. Nitrocellulose membranes were blocked with 5% BSA. Antibodies were diluted in 5% BSA and incubated with membranes overnight. Membranes were washed with 1X TBS containing 0.02% Tween-20 (TBST) for a total of three 12 minute washes. All antibodies were diluted 1:1,000 except GAPDH, which was 1:10,000. Mdm2 (90kDa band) antibody cocktail included SMP14 (sc-965, Santa Cruz), 2A9 (OP155T, Calbiochem), 4B11 (OP143, Calbiochem). E2F1 (55kDa, KH-95, Santa Cruz), p73 (~80kDa, A300-126A, Bethyl Laboratories) PUMA (21kDa, #4976, Cell Signaling), p21 (21kDa, DCS60, Cell Signaling), MdmX (55kDa, ab154324, abcam) and GAPDH (37kDa, 14C10, #2118, Cell Signaling) were also used. Secondary HRP-conjugated anti-mouse and anti-rabbit antibodies were diluted 1:5,000 in 1X TBST for 1-1½ hours. SuperSignal West Femto Chemiluminescent Substrate (Thermo Scientific) was used to activate secondary antibodies and membranes were exposed with autoradiography film.

a. **Densitometry Measurements.** Western blot densitometry was evaluated using ImageJ software (http://imagej.nih.gov/ij/). Blots were scanned and evaluated by ImageJ. All proteins of interest were normalized to appropriate loading control lanes and untreated controls.

3. **Invasion Assay.** Cell invasion was determined using CytoSelect™ Cell Invasion Assay Kit (Cell BioLabs). TMD231 cells were seeded into polycarbonate inserts with $3.5x10^3$ cells per insert on Day -2. Cells were serum starved overnight on Day -1. On Day 0, cells were treated with 7.5µM Nutlin-3a, carboplatin, 1:1 combination, or Vehicle for 24 hours. Cytochalasin D was used as a negative control, which inhibited invasion by interfering with microtubule formation. The bottom chamber contained 10% FBS containing medium, which served as a chemoattractant. The cells that were able to invade through the dried basement membrane matrix layer and pore layer were stained and quantified using a plate reader. Concurrent cell survival assays were conducted with $3.5x10^3$ TMD231 cells seeded in a 24-well plate. Cells were serum starved and treated in the same drug conditions as the invasion assay. To confirm that treatments did not cause cell death, total number of cells and cell viability via trypan blue staining were determined.
4. **Stable Knockdown of Mdm2.** TMD231-shcontrol and TMD231-shMdm2 were a kind gift of Dr. Lindsey Mayo. TMD231-shcontrol and TMD231-shMdm2 cells were first evaluated for Mdm2 protein levels using Western blot. TMD231-shcontrol or TMD231-shMdm2 were grown in medium containing 2.5µg/mL puromycin to keep selective pressure on the cells throughout the experiments. Cells were lysed with 1% SDS lysis buffer and examined by Western blot. For methylene blue proliferation assays, the TMD231-shcontrol and TMD231-shMdm2 cells were plated with 500 cells per well in 96-well plates and treated with 0-120µM Nutlin-3a, 0-100µM carboplatin, or 0-100µM 1:1 combination for 5 days. Cells were grown in medium

with 2.5µg/mL puromycin to keep selective pressure throughout the experiment. Cells were fixed and stained with methylene blue and cell proliferation was examined. For shMdm2 cell counting assays, the experimental design was the same as the TMD231 cell counting experiment as described above.

5. **Transient knockdown of p73 with siRNA.** ON-TARGETplus siRNAs were purchased from Dharmacon (GE Healthcare). p73 siRNA constructs included:

   1. GAGACGAGGACACGUACUA

   2. GCAAUAAUCUCUCGCAGUA

   3. GAACUUUGAGAUCCUGAUG

   4. CCACCAUCCUGUACAACUU.

   Since p73 has several N-terminal and C-terminal isoforms, we BLAST searched the p73 siRNA sequences to ensure that proper coverage of the mRNA would be accomplished leading to a reduction in total p73 levels. These p73 siRNA constructs target p73 within the DNA binding and oligomerization domain to ensure knockdown of the numerous isoforms of p73. On Day -1, $5x10^5$ TMD231 cells were seeded into 6-well plates, which yielded an appropriate cellular confluency on the day of transfection. Liprofectamine® RNAiMAX (Life Technologies) was used to transfect 9pmol control ON-TARGETplus Non-Targeting Pool siRNA or ON-TARGETplus SMARTpool p73 siRNA into TMD231 cells on Day 0. The siRNA effectiveness was evaluated on Day 1-3 post transfection by Western blot. For proliferation assays, TMD231 cells were transfected on Day 0 with either control siRNA or p73 siRNA. On Day 1 post transfection, cells were counted and $2.5x10^3$ cells

were seeded into 96-well plates. The cells were treated with 0-120µM Nutlin-3a, 0-100µM carboplatin, or 1-100µM 1:1 combination treatments later that same day to increase the time that the treatment would be present in cells with reduced p73. Plates were incubated for a total of 3 days. DMSO and H_2O were used as Vehicle controls. Methylene blue proliferation assay procedure was used and IC_{50} values were determined.

6. **Stable Knockdown of p73.** We purchased a panel of p73 shRNA constructs from Sigma Mission shRNA, and they were expressed in a pLKO (Sigma) lentiviral backbone.

   1. TRCN0000284787
   2. TRCN0000006511
   3. TRCN0000272587
   4. TRCN0000006508
   5. TRCN0000006509
   6. TRCN0000272526
   7. TRCN0000272525

   TMD231 cells were transduced with the lentiviral vectors and positive cells expressing either the scrambled control or shp73 constructs were selected with 2.5µg/mL puromycin. p73 protein levels were evaluated by Western blot. Throughout the shp73 experiments, cells were grown in puromycin containing medium to ensure usage of positive cells only. Two shp73 constructs (shp73-3-500 and shp73-4-500) produced the highest level of reduction in p73 protein levels as

measured by Western blot. We also utilized a scrambled control (Scr-500). TMD231-Scr-500, TMD231-shp73-3-500, and TMD231-shp73-4-500 were seeded in 96-well plates and treated with 0-120µM Nutlin-3a, 0-100µM carboplatin, or 1-100µM 1:1 combination for 5 days. DMSO and H_2O were used as Vehicle controls. Methylene blue proliferation assay procedure was used and IC_{50} values were determined.

7. **Stable Knockdown of shE2F1.** shRNA lentiviral constructs were purchased from Mission shRNA (Sigma). TMD231 cells were transduced with either shGFP or shE2F1 constructs as described above:

   1. TRCN0000010327
   2. TRCN0000010328
   3. TRCN0000039658
   4. TRCN0000039659
   5. TRCN0000039660

   Knockdown was evaluated by Western blot. shRNA positive cells were selected using 2.5µg/mL puromycin in the growth culture medium. TMD231-shGFP and TMD231-shE2F1 cells were seeded in 96-well plates and treated with 0-120µM Nutlin-3a, 0-100µM carboplatin, or 1-100µM 1:1 combination for 5 days. DMSO and H_2O were used as Vehicle controls. Methylene blue proliferation assay procedure was used and IC_{50} values were determined

   a. **shE2F1 Clonal Selection.** Clones were developed using serial dilution methods. $4.0x10^3$ TMD231-shGFP, TMD231-327, and TMD231-328 cells were added into one well in a 96-well plate. In the first dilution, the cells were diluted 1:2 down

the first column. The first column was diluted it 1:2 across the whole plate to completed the second dilution. Wells with single cell colonies were then expanded to form clonal populations. Knockdown of E2F1 was evaluated by Western blot. shRNA positive cells were selected using 2.5µg/mL puromycin in the growth culture medium.

8. **Chromatin Association Assay.** Chromatin association assays were performed in collaboration with Dr. Christine Eischen. We sent the TMD231 cells, FBS, drug aliquots, and detailed instructions in relation to cell culture and treatment conditions. In discussions with Dr. Eischen, we concluded this was the best way to inhibit as many differences between laboratories as possible. TMD231 cells were left untreated or were treated with 15µM Nutlin-3a, 15µM Carboplatin, 15µM Nutlin-3a and 15µM Carboplatin, or DMSO Vehicle control for 6 hours. Cells were harvested and soluble and chromatin bound proteins were separated with CSK buffer (10mM PIPES pH6.8, 100mM NaCl, 300mM sucrose, 1mM $MgCl_2$, 1mM EGTA, 0.1% Triton X-100) as previously described [105]. The chromatin bound proteins were extracted with RIPA buffer containing protease inhibitors (1mM PMSF, 10mM BGP, 38µg/mL Aprotinin, 5µg/mL Leupeptin, 5µg/mL Pepstatin, 1mM NaF, 0.1mM $NaVO_4$). Whole cell lysates were prepared as previously reported [106]. Equal amounts of protein lysates (130µg whole cell and 170µg of chromatin-bound) were subjected to SDS-PAGE. Proteins were transferred to nitrocellulose membranes and examined with Western blot. Antibodies were used as follows with anti-Mdm2 (3G9, 1:2000,

Millipore), anti-H2AX (A300-082A, 1:15,000, Bethyl), and anti-β-Actin (AC-15, 1:5,000, Sigma), as previously reported [35].

9. **Inductively Coupled Plasma Mass Spectrometry (ICP-MS).** Cells were seeded on 10cm dishes and treated with 15µM Nutlin-3a, 15µM carboplatin, or 15µM Nutlin-3a+15µM carboplatin combination, or DMSO+H_2O as a Vehicle control. Each treatment was completed in triplicate. Following appropriate time point, cells were lysed with modified Laird buffer (100mM Tris-HCl, pH 7.5, 5mM EDTA, 0.2% SDS, 200nM NaCl, 100µg/mL Proteinase K) at 37°C [107]. Total DNA was precipitated using one part isopropanol on a shaker. DNA was spooled and rinsed in 70% EtOH. DNA was dissolved in H_2O and DNA concentration was determined via nanodrop. 50µg DNA was hydrolyzed overnight in 2.5% HNO_3 at 70°C. Samples were diluted in 1% HNO_3 and total platinum content was analyzed via ICP-MS. Standard curves using Platinum (Pt) were used, and Yttrium was used as an internal control.

D. **Statistical Analyses.** IC_{50} values were calculated according to the linearization method of Chou and Talalay [108] and were used to construct isobologram graphs as previously described [109]. Data were analyzed by one- or two-way ANOVA and Student's T-test, as appropriate, with repeated measures across varying time points using SigmaPlot 11.2 (Systat Software, Inc.). Differences among individual pairs of means were determined by the Holm-Sidak post-hoc test. Kaplan-Meier survival plots were generated to determine any effect of treatment regimen on survival using SigmaPlot. Data were considered significant at $p<0.05$.

Chapter 2. *In vivo* Experiments

A. **Animal Studies.** All studies were carried out in accordance with, and approval of, the Institutional Animal Care and Use Committee of Indiana University School of Medicine (Study #10463), and the Guide for the Care and Use of Laboratory Animals. Female NOD/scid and NOD.Cg-*Prkdc*^{scid}Il2rg^{tm1Wjl}/SzJ (NSG) mice were obtained from the *In Vivo* Therapeutics Core of the Indiana University Simon Cancer Center and acclimated at least one week prior to commencement of the study. Animals were maintained under pathogen-free conditions and maintained on Irradiated Global 2018 (Uniprim® 4100 ppm) (TD.06596, Harlan Laboratories USA) food pellets with *ad libitum* access to autoclaved, acidified tap water under a 12-hour light-dark cycle at 22-24°C. Uniprim® food contains 275 ppm trimethoprim and 1,365 ppm of the sulfonamide sulfadiazine which helped to inhibit infections.

B. **Animal Strain Comparisons.** NOD/scid and NSG mice were implanted with 1x10^6 TMD231 cells into the mammary fat pad. Tumors were allowed to grow and caliper measurements were collected twice weekly to evaluate tumor growth of the primary tumors. Mice were sacrificed throughout the study to better understand longitudinal metastasis formation in the lungs. Lung metastases were examined following H&E staining.

C. **Fluorescent Imaging Validation Studies**

1. ***In vitro* Imaging.** TMD231-CR and TMD231 cells were counted and placed into 96-well plates. The TMD231 parental cells were used as a control for any

autofluorescence. The cells were plated in PBS to reduce any noise that we may have encountered with fluorescence from components in the growth medium. In 96-well plates, $4x10^6$ TMD231 or TMD231-CR cells were plated and serial diluted 1:2 across the plate resulting in 0.03125, 0.0625, 0.125, 0.5, 1, 2, and $4x10^6$ cells. Each cell number was plated in triplicate. Imaging analysis was completed and fluorescent intensity was calculated.

2. ***In vivo* Imaging.** Typical optical imaging for small animals consisted of animal being anesthetized in polycarbonate box with isoflurane (1-2% with 100% oxygen mix). Mice were shaved and depilatory cream was used to remove any remaining fur surrounding the primary tumor site. The mice were anesthetized using isoflurane gas during depilatory cream use and imaging. The mice were placed on the warmed imaging bed inside the Optix MX3 (ART Technologies). The muzzle was placed inside the built in nose cone of the imaging bed where constant isoflurane gas mixture was administered throughout the imaging process. Imaging proceeded with average scan times lasting from 5-10 minutes. Once imaging was complete, the mice were removed from the MX3 and placed back in their cages lying on their side until fully conscious. The cages were placed on heating pads to minimize hypothermia. While under anesthesia, it was unlikely the animal will not move so constraints were not necessary; however, medical tape could have been used to secure the legs of the animal while being imaged if necessary.
3. ***In vivo* Cell Number Imaging.** Mice were implanted in the lower half of the mammary fat pad at 4 different nipple regions. Each mouse was implanted with

0.125, 0.25, 0.5, and $1x10^6$ TMD231 or TMD231-CR cells. There were 3 mice imaged for each cell line. Following analysis, fluorescent intensity for each cell number was calculated. TMD231 parental implanted mice were used as a control for any background fluorescence.

4. **Longitudinal Animal Imaging.** NSG mice were implanted with either $1x10^6$ TMD231 or TMD231-CR cells on Day 0. The TMD231 parental cell implanted mice were used as imaging controls to subtract background fluorescence. Throughout the study, the primary tumor was measured via caliper twice weekly. On Day 7 post implant, the mice were imaged with the Optix MX3 (ART Technologies). Mice were imaged three mice per scan. The mice were imaged once weekly for a total of 5 weeks. Imaging analysis yielded the fluorescent intensity of tumors for comparison to measured tumor volume via caliper.
5. ***Ex-vivo* E2-Crimson Levels.** Mice from the longitudinal animal imaging study were used to examine the maintenance of E2-Crimson fluorescent protein in excised TMD231-CR tumors. The excised tumors were dissociated with a scalpel and grown *ex-vivo* in cell culture. Growth medium was changed frequently and contained 0.5% Gentamicin antibiotics. After stable lines were generated, the TMD231 parental and TMD231-CR tumors were examined with flow cytometry to determine the percentage of E2-Crimson positive cells.

D. **Efficacy Studies**

1. **Drug Treatments.** Carboplatin was dissolved in PBS. Nutlin-3a was mixed in 0.5% methylcellulose and 0.05% Tween80 solution. Proper drug mixture was ensured following sonication in a sonicating water bath and mixing via vortex.
2. **Carboplatin Dose Finding Study.** NSG mice were implanted with $1x10^6$ TMD231 or TMD231-CR cells on Day 0. On Day 7, the mice were imaged to collect initial tumor fluorescent intensity for randomization purposes. The mice received carboplatin (Carb) or Vehicle (Veh) (PBS) through intraperitoneal (i.p.) injections once MWF for a total of 6 doses. Mice received 1m/kg, 3mg/kg, or 30mg/kg carboplatin. Throughout the study, mice were examined for overt toxicity. We continued to monitor primary tumor growth with caliper measurements twice weekly as well as collecting weekly body weights. The study endpoint was when the primary tumor reached $\geq 1000mm^3$. At the time of sacrifice, the primary tumor and lungs were collected for histology purposes and fixed in 10% buffered formalin.
3. **Combination Study 1.** As in other studies, NSG mice were implanted with $1x10^6$ TMD231 or TMD231-CR cells in the mammary fat pad. Mice were imaged on Day 7 with optical imaging. Primary tumor fluorescent intensity was used to randomize the mice into the treatment groups: Vehicle (PBS+methylcellulose) (Veh), 25mg/kg carboplatin (Carb), 200mg/kg Nutlin-3a (Nut), and 25mg/kg carboplatin+200mg/kg Nutlin-3a (Combo). There were 7-9 mice per group. Mice were dosed three times weekly for a total of 6 doses. Based on pharmacokinetic (PK) data from other animal studies in the lab, the dosing of carboplatin and Nutlin-3a were separated by at least

4 hours. We chose to dose with carboplatin first in the morning so that the drug could act on the primary tumor and lead to DNA damage in tumor cells, which in turn could activate DNA damage responses and lead to increased cell stress. When Nutlin-3a is dosed later in the afternoon, Mdm2 could be bound by Nutlin-3a allowing for proteins involved in the DNA damage response including p73 and E2F1 to be free and lead to target gene activation. Carboplatin was dosed i.p. in the morning while Nutlin-3a was dosed orally (p.o.) in the afternoon. The combination and Vehicle groups were dosed twice a day on treatment days with the appropriate drug or Vehicle at the appropriate time, AM or PM. Throughout the study, the mice were examined for any overt toxicity. Body weights were collected weekly throughout the course of the study and primary tumors were measured via caliper twice weekly throughout the study. The endpoint for the study was when the first primary tumors reached ≥1000mm^3. Mice were sacrificed on Day 47 post implant. At the time of sacrifice, the primary tumors and lungs were collected and fixed in 10% buffered formalin. Fixed tissues were set in paraffin blocks, cut and sectioned, and stained with H&E to evaluate primary tumor health and lung metastases.

4. **Combination Study 2.** As in other studies, NSG mice were implanted with 1x10^6 TMD231 or TMD231-CR cells in the mammary fat pad. Mice were imaged on Day 7 with optical imaging. Mice were randomized into two groups of mice, repeat study mice (n=4 per group) and survival (n=8 per group). Within each group, the mice were randomized into the treatment arms: Vehicle (PBS+methylcellulose) (Veh), 20mg/kg carboplatin (Carb), 200mg/kg Nutlin-3a (Nut), and 20mg/kg carboplatin+200mg/kg

Nutlin-3a combination (Combo). Carboplatin was dosed i.p. in the morning while Nutlin-3a was dosed orally (p.o.) in the afternoon. The combination and Vehicle groups were dosed twice a day on treatment days with the appropriate drug or Vehicle at the appropriate time, AM or PM. The mice were dosed twice weekly (Tuesdays and Fridays) for a total of 8 doses. Throughout the study, the mice were examined for any overt toxicity. Body weights were collected weekly throughout the course of the study and primary tumors were measured via caliper twice weekly throughout the study. The endpoint for the repeat study mice was when the first primary tumors reached ≥1000mm^3, which was 5 days following the completion of drug treatment. At the time of sacrifice, the primary tumors and lungs were collected and fixed in 10% buffered formalin. Fixed tissues were set in paraffin blocks, cut and sectioned, and stained with H&E to evaluate primary tumor health and lung metastases. Femurs were collected to determine bone marrow cellularity. The survival group of mice was sacrificed when primary tumor volume reached 800mm^3. When the mice reached the tumor volume endpoint, the mice were sacrificed and femurs were collected for total bone marrow cell counts. In the survival mice, they were sacrificed with about a 2-week recovery period following the completion of drug treatment.

a. **Bone Marrow Flow Cytometry.** Mice from Combination study 2 were evaluated for the presence of bone metastases by examining isolated bone marrow cells from crushed femur bones for the presence of TMD231-CR cells using flow cytometry (See Histological analysis: Bone marrow cellularity).

5. **Combination Study 3.** NSG mice were implanted with $1x10^6$ TMD231 or TMD231-CR cells in the mammary fat pad. We were unable to image the mice on Day 7 for randomization purposes due to failure of the motherboard on the MX3 Optix. Our previous imaging data, however, has demonstrated that we get a 100% tumor take in the NSG model and that tumor volumes are consistent amongst the animals. Therefore, we elected to randomize the mice based on body weights on Day 7 into the treatment groups: Vehicle (PBS+methylcellulose) (Veh), 20mg/kg carboplatin (Carb), 200mg/kg Nutlin-3a (Nut), and 20mg/kg carboplatin+200mg/kg Nutlin-3a (Combo). Carboplatin was dosed i.p. in the morning while Nutlin-3a was dosed orally (p.o.) in the afternoon. The combination and Vehicle groups were dosed twice per day on treatment days with the appropriate drug or Vehicle at the appropriate time, AM or PM. The mice were dosed twice weekly (Tuesdays and Fridays) for a total of 8 doses. Mice were sacrificed when initial mice reached ≥$1000mm^3$ tumor volume. Following necropsy, lungs, primary tumors, livers, spleens and femurs were collected. We performed H&E staining of the lungs, primary tumors, livers, spleens, and femurs. We repeated bone marrow cellularity and also evaluated the effects of the drug treatments on complete blood counts (CBCs) and progenitor assays.
6. ***In vivo* Pharmacodynamic Study.** NSG mice were implanted with $1x10^6$ TMD231-CR cells, and tumors were allowed to grow. Caliper measurements were taken twice weekly to monitor tumor volume. When tumors reached ~$500mm^3$, mice were randomized based on tumor volume into treatment groups. Mice were dosed with Vehicle (PBS+methylcellulose) (Veh), 20mg/kg carboplatin (Carb), 200mg/kg Nutlin-

3a (Nut), or 20mg/kg carboplatin+200mg/kg Nutlin-3a (Combo) for 3 consecutive days. Two house after the last drug dose, the mice were sacrificed and primary tumors were weighed and collected. Primary tumors were cut in half for human VEGF ELISA analysis and the other half for Western blot analysis and snap frozen in liquid nitrogen.

a. **Human VEGF ELISA.** Tumors were lysed in an appropriate volume of 1X Lysis Buffer (Cell Signaling) on ice using the Omni Tissue Homogenizer (TH) (Omni International, Kennesaw, GA). Protein concentration was determined as described previously. Equal protein for each tumor sample was added to the VEGF ELISA plate and Human VEGF Quantikine ELISA Kit (R&D Systems) was completed per manufacturer's instructions. Total VEGF levels were normalized to protein levels and average VEGF presence was graphed.

b. **Tumor Lysates for Western.** Snap frozen tumors were lysed with 1% SDS lysis buffer using the Omni Tissue Homogenizer (TH) (Omni International, Kennesaw, GA). Samples were boiled and protein concentration was determined as described previously. Samples were examined by Western blot for protein levels as described previously.

E. **Histological Analyses**

1. **Tissue Specimens.** All mice tissue samples were collected following a detailed LARC approved lab animal protocol.
2. **Tissue Processing.** Tissues were fixed in 10% neutral buffered formalin at 4°C for 24 hours followed by tissue processing, and then embedded in paraffin. Five-micron

sections were cut and stained for routine H&E and Ki67 staining.

3. **Immunostaining.** The slides were deparaffinized in xylene and rehydrated through graded alcohols ending in water. Antigen retrieval was performed by immersing the slides in Target Retrieval Solution (Dako) for 20 minutes at 90°C, cooling at room temperature for 10 minutes, washing in water and then proceeding with immunostaining. Slides were blocked with protein blocking solution (Dako) for 30 minutes. All subsequent staining steps were performed using the Dako FLEX SYSTEM on an automated Immunostainer; incubations were done at room temperature and Tris buffered saline plus 0.05% Tween 20, pH 7.4 (TBS - Dako Corp.) was used for all washes and diluents. Thorough washing was performed after each incubation period.
    a. **H&E Staining.** Sections were stained with haemotoxylin and eosin (DAKO).
    b. **Ki67 Staining.** The primary antibody was anti-human Ki67 (Dako). Control sections were treated with an isotype control using the same concentration as primary antibodies to verify the staining specificity. For the Ki67 positive nuclei, (tumor areas) nuclei were measured in one section per xenograft tumor and expressed as the number of positive cells per 16X power field (160X) in the cross-sectional area. For the immunohistochemical quantification, three randomly selected images (16X power fields) each (total area, 7.3 mm^2) were analyzed by a pathologist hand count and averaged for each lung.
    c. **Whole Slide Digital Imaging.** The Aperio whole slide digital imaging system was used for whole slide imaging. The Aperio Scan Scope CS system (Leica

Biosystems) was used. The system imaged all slides at 20X. The scan time ranged from 1.5-2.25 minutes. The whole images were housed and stored in the Spectrum software system, and images were taken from the whole slides.

d. **Automatic Image Quantitation.** Computer-assisted morphometric analysis of digital images was done using the Aperio software that came with the Aperio Imaging system (Leica Biosystems). An optimized algorithm for the positive pixel algorithm that was designed for H&E staining was used for imaging of the H&E lung tumor metastases. The positive pixel algorithm was modified to distinguish between the red and blue colors. The tumors were blue and it was easy to discern the difference between normal lung tissue and the tumors that filled the lung lobes using this algorithm. The total nuclear labeling index (Ki67) was generated using the Aperio Image Scope standard positive pixel algorithm. This Image Analysis software was used engraft and the software package (positive pixel algorithm) calculated the percent of positive pixels (brown staining) in one large cross section area from one lung lobe in the control and each drug treated group.

F. **Measures of Drug Toxicity**

1. **Bone Marrow Cellularity.** Mice were sacrificed at the end of the study and both femurs were collected. Bones were crushed with mortar and pestle and passed through a 70µm cells strainer. Red blood cells were lysed with RBC Lysis Buffer (Qiagen). Total cell counts were counted using a Beckman Coulter Counter.

2. **Bone Marrow Smears.** Femur bones were excised during necropsy. Bones were fixed in 10% buffered formalin and decalcified with Decal®. Bones were set in paraffin blocks, sectioned, stained with H&E, and evaluated by pathologist.
3. **Total Complete Blood Counts (CBCs).** Tumor-bearing mice were treated with Vehicle control (Veh), carboplatin (Carb), Nutlin-3a (Nut) or carboplatin+Nutlin-3a combination (Combo). After a 2-week recovery period, an aliquot of peripheral blood was analyzed via hemavet for red blood cells, thrombocytes, and white blood cells.
4. **Progenitor Assay.** After completing total bone marrow cell counts, $2x10^4$ bone marrow cells were plated in triplicate in MethoCult™ GF M3434 (StemCell™ Technologies). Cells were allowed to grow for 2 weeks. Hematopoietic progenitor cells were counted for each plate and averages were taken for each of the mouse samples. Progenitor assays were conducted as described in Cai *et al.* [110].

SECTION III. RESULTS

Chapter 1. Aim 1: Determination of cellular sensitivity to Nutlin-3a and carboplatin in triple-negative breast cancer cells *in vitro*

A. Background and Rationale

The overall objective of this thesis was to evaluate the therapeutic potential of a new combination therapy to treat TNBC. Based on front-line therapies currently being tested in clinical trials for TNBC, the platinum agent, carboplatin was selected for study. New molecular targets need to be elucidated to enhance treatment efficacy. Mdm2 is an unexplored target in breast cancers and Mdm2-mediated signaling can be altered using Nutlin-3a. Our first objective of this thesis was to determine the effects of combination carboplatin and Nutlin-3a treatment on TNBC cell proliferation, cell death, and cell cycle *in vitro*. To address this objective, drug sensitivity studies were conducted using Nutlin-3a and carboplatin alone and in combination. A panel of mutant p53 TNBC lines (MD-MB-231, MDA-MB-468, and TMD231) were utilized to determine to what extent modulation of Mdm2 via the protein-protein inhibitor, Nutlin-3a, can potentiate carboplatin-mediated cell death. Both the MDA-MB-231 and MDA-MB-468 cells are adenocarcinoma lines that were developed from metastatic pleural effusions. We also utilized the TMD231 cells, which were derived from the parental MDA-MB-231 cells [17] and were a kind gift of Dr. Harikrishna Nakshatri (IUSM). Both the MDA-MB-231 (R280K) and MDA-MB-468 (R273H) cells have missense mutations within p53 in the DNA binding

domain resulting in the inactivation of normal p53 function and abnormally increases proliferation, invasion, and metastasis [19,47,101,111,112].

Initially, cellular sensitivity to Nutlin-3a and carboplatin was determined using methylene blue proliferation assay so that relevant drug concentrations for future experiments could be utilized. Single drug sensitivities were needed for later design of combination treatments. Also, we were interested in determining if a broad or narrow range of dose ratios would result in decreased proliferation. The methylene blue proliferation assay is a reliable measure of cell growth over time. This assay measures the number of adherent cells, and there is a direct relationship between numbers of adherent cells to the optical absorbance. Methylene blue stain electrostatically binds to negatively charged particles in cells such as negatively charged phosphate groups in DNA and moieties of proteins [102]. The methylene blue proliferation assay is not a metabolic assay, which is important if any drugs used alter metabolism. The methylene blue proliferation assay is a quick and easily replicated experiment to experiment with little variance between similarly treated wells.

We also evaluated the effects of the single and dual treatment on the ability of the cells to form colonies in a 2D colony formation assay. The cells were seeded at low density and treated with single or combination treatments and allowed to grow for 2 weeks. Following the initial drug sensitivity determination of Nutlin-3a and carboplatin in the MDA-MB-231, TMD231, and MDA-MB-468 cells, we also wanted to determine the effects of single and combination drug treatment on cell proliferation through cell counting assays. Longitudinal cell counting experiments allowed us to examine the

effects of the single and dual treatments on the cells ability to proliferate as well as determine if the cells are dying throughout the treatment window. To better understand how the single and combination carboplatin and Nutlin-3a treatment may affect cell viability, we also utilized flow cytometry to evaluate the impact of single and dual treatment on cell cycle and apoptosis. These assays allowed for a better understanding of whether apoptosis and/or cell cycle arrest might account for decreased cell growth.

Cell cycle kinetics can play a major role in how normal and cancerous cells respond to therapy. When cells are treated with chemotherapeutic drugs, there is significant damage to DNA. The DNA damage will accumulate and as a survival mechanism, cells will undergo cell cycle arrest in either G0/G1, S, or G2 phase to determine if the damage can be repaired [113]. If the damage is too great and cannot be sufficiently repaired, the cells can signal for pro-apoptotic and other cell-death mediators to be activated. Apoptosis and cell cycle analysis via flow cytometry uses dyes, like 7-AAD and PI with that stain DNA allowing for the amounts of DNA to be quantitated [114]. In determining the populations of cells undergoing early and late apoptosis, DNA stains like 7-AAD can be used with minimal overlap with other conjugated antibodies like Annexin V-FITC that binds to phosphatidylserine, which is a sensitive marker of early apoptosis. In cell cycle analysis, cells are permeabilized and mixed with a DNA staining solution, and the stained DNA present will show which phase of the cell cycle the cells are accumulating. When cells are in the G0/G1 phase, the DNA content is 2N since each cell has 2 copies of DNA. The G2/M phase has double the

amount of DNA as the G1 phase since the cells are getting ready to divide into two daughter cells [115]. The DNA content measure in the S phase is between 2N and 4N as the DNA is being synthesized for separation into the daughter cells. There are several signaling mediators involved in successful cell division and can be aberrant in cancers allowing for genetically unstable cells to continue proliferating [115]. Most normal mammalian cells are diploid in nature in that they carry two copies of each chromosome. However, in cancers, cells often become aneuploidy in that they have chromosomal aberrations such as alterations in total copies of chromosomes as well as chromosomal rearrangements with amplifications, deletions and translocations [116]. These genetic abnormalities result in changes to multiple signaling pathways and promote survival and proliferation of cancer cells.

Interestingly, Le *et al.* showed that in the MDA-MB-231 cells, the potential for metastases was enhanced in the MDA-MB-231 cells when the cells underwent hypertetraploidy which is a type of aneuploidy [117]. It has been shown that in breast adenocarcinoma, patients with tumors exhibiting aneuploidy tumors had a worse prognosis and hypertetraploid tumors were the most aggressive tumor types [118,119]. As the parental MDA-MB-231 cells were cultured over long periods of time, some of the cells developed spontaneous a hypertetraploidy state with DNA peaks just smaller than 4N and 8N [117]. More interestingly, the hypertetraploid cells showed an increased metastatic potential to the lungs and brain but not bone when compared to the parental cells [117] which may help to explain the increased aggressiveness of the hypertetraploidy cells.

B. **Combination treatment had increased potency in cell proliferation, apoptosis, and cell cycle assays**

Initially, we tested the cellular sensitivity of the parental MDA-MB-231 cells to Nutlin-3a and carboplatin alone using methylene blue proliferation assays. The IC_{50} value for Nutlin-3a was 40.2μM±0.6, carboplatin was 28.6μM±1.2, and 1:1 combination was 5.3μM±0.3 (Figure 5A). It is noteworthy that the IC_{50} values for Nutlin-3a are quite high relative to what is generally used for selective targeting of the Mdm2-p53 interactions, and it is possible that off-target effects do come into play at high micromolar concentrations. Lau and colleagues showed IC_{50} values for Nutlin-3a to be around 30μM in $p53^{-/-}$ cells which is comparable to our mutant p53 cell system [66]. However, as shown below, once Nutlin-3a is combined with carboplatin, the IC_{50} values for Nutlin-3a are in the low micromolar range, which is what is typically used in cells with wild-type p53 [40]. The MDA-MB-231 cellular proliferation assay was examined using isobologram analysis. Isobologram analysis was described by Tallarida to determine synergy between two different drugs [109]. Briefly, the IC_{50} value for each single drug is plotted on a graph, and a line is drawn connecting the two points. In our studies, we plotted the IC_{50} of carboplatin on the x-axis while the IC_{50} of Nutlin-3a was plotted on the y-axis. A line was drawn connecting these two points, which becomes known as the 'line of additivity'. The line of additivity helps determine the interaction between the two different drugs. Following combination treatment, the IC_{50} values for the different drug combinations also known as the 'isoboles' are plotted on the graph. If the isoboles fall along the line of additivity, the interaction between the two drugs is considered to

be additive. If the isoboles fall below the line of additivity, the two drugs are determined to have a synergistic relationship while if the isoboles fall above the line of additivity, the interaction is considered antagonistic. These data indicate the Nutlin-3a decreased cellular resistance to carboplatin. When the IC_{50} value for a 1:1 Nutlin-3a:carboplatin combination treatment was determined, the isobole fell below the line of additivity, suggesting a synergistic effect (Figure 5B).

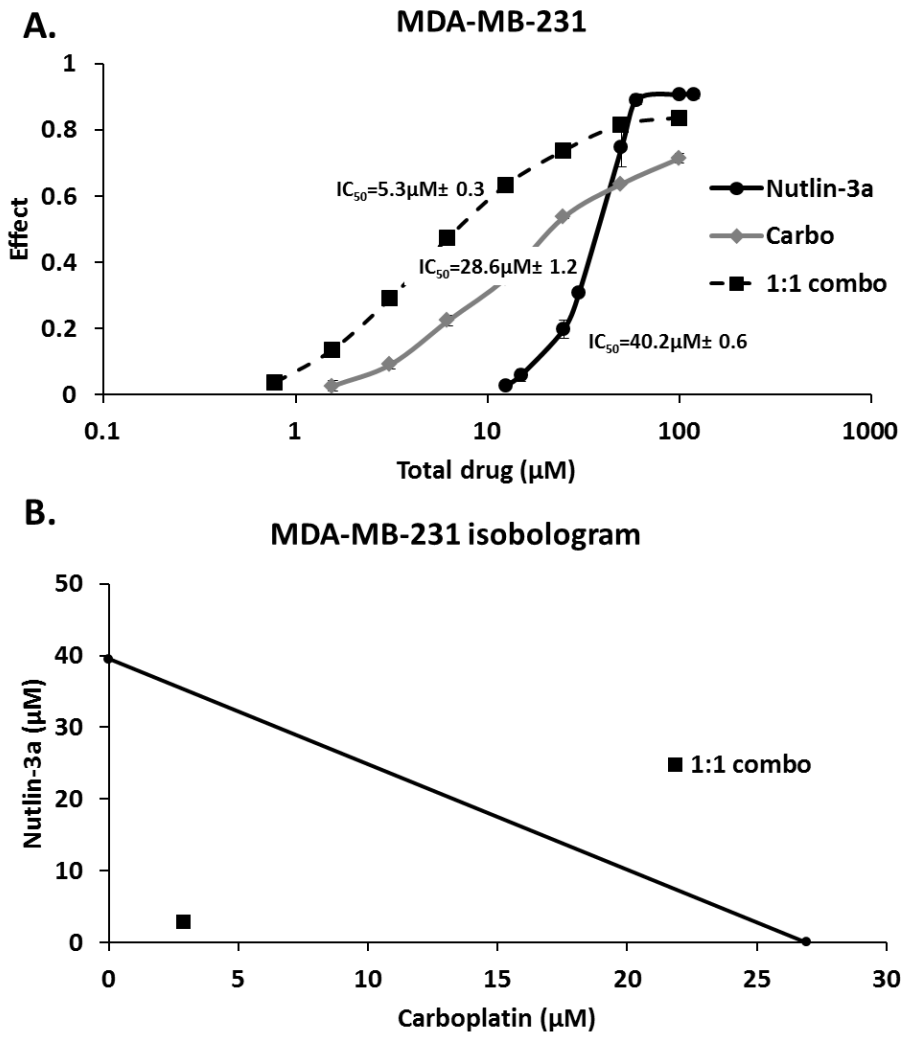

Figure 5. Combination treatment increases potency and synergistic effects in MDA-MB-231 cells. MDA-MB-231 cells were seeded in 96-well plates and treated with increasing concentrations of Nutlin-3a, carboplatin (Carbo), or combination (1:1 combo) for 5 days. Cells were fixed and stained with methylene blue. Cell proliferation was determined for each treatment. (A) Combination treatment had an increased potency in MDA-MB-231 cells compared to Nutlin-3a and carboplatin alone treated cells. (B) Following isobologram analysis, the 1:1 combination was examined with the isobole falling below the line of additivity, which indicated a synergistic effect.

Since the highly metastatic TMD231 cells were derived from the parental MDA-MB-231 cells, we next investigated if the two cell lines had similar cellular sensitivity to Nutlin-3a, carboplatin and 1:1 combination treatment. Nutlin-3a, carboplatin, and 1:1 combination inhibited cell proliferation in a dose-dependent manner, similar to the parental cells. Treatment of Nutlin-3a, carboplatin, and 1:1 combination inhibited cellular proliferation in a dose dependent manner with IC_{50} values of 19.4μM±3 for Nutlin-3a, 6.3μM±1.9 for carboplatin, and less than 0.7μM±0.5 for combination treated TMD231 cells (Figure 6A). Isobologram analysis was used to determine the type of drug interaction involved in the combination treatment. Several drug ratios of Nutlin-3a:carboplatin were examined including 1:1, 3:1, 9:1, 1:3, and 1:9. The 1:1 combination had the most potent effect with the lowest IC_{50} values, which fell the furthest away from the line of additivity (Figure 6B). The 3:1 Nutlin-3a:carboplatin ratio had next lowest IC_{50} value. Since the 1:1 ratio had the biggest effect, we elected to continue the experiments using the 1:1 combination in future experiments focused on mechanism of action (Figure 6B). Individual IC_{50} values were determined as shown in inset table (Figure 6B). There was some variability in cellular sensitivity to the drugs between different experiments especially with Nutlin-3a (IC_{50} values ranged from 20-40μM) as seen in Figure 6. However in all cases, Nutlin-3a concentrations required to inhibit 50% growth were in the low micromolar range in the presence of carboplatin-mediated DNA damage.

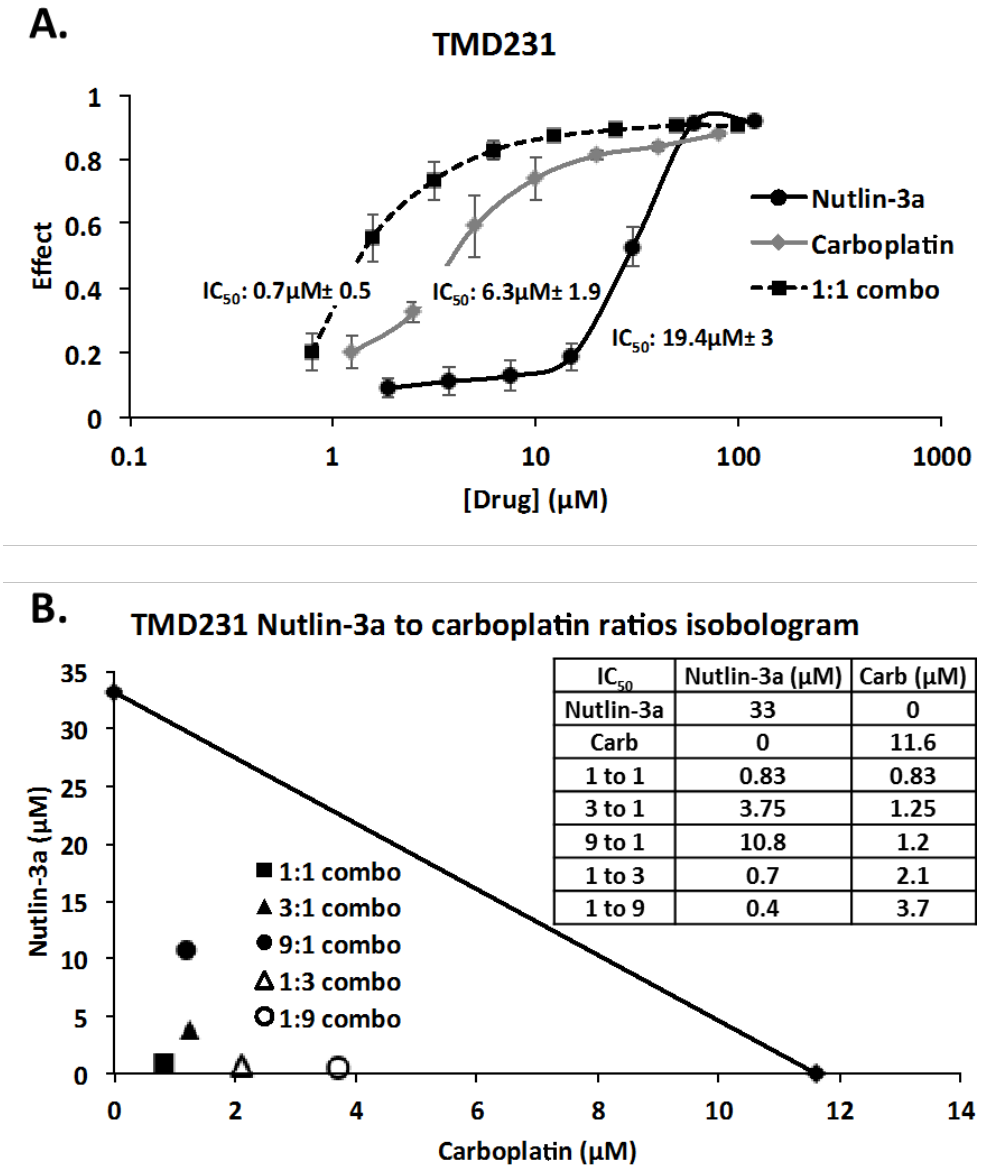

Figure 6. Combination treatment increases potency and synergistic effects in TMD231 cells. TMD231 cells were seeded in 96-well plates and treated with increasing concentrations of Nutlin-3a, carboplatin, or combination for 5 days. Cells were fixed and stained with methylene blue. Cell proliferation was determined for each treatment. (A) A 1:1 combination treatment showed an increased potency in TMD231 cells compared to Nutlin-3a and carboplatin alone treated cells with IC_{50} values compared to each single drug alone. (B) Several drug ratios of Nutlin-3a:carboplatin (1:1, 3:1, 9:1, 1:3, and 1:9)

were examined using isobologram analysis. All isoboles from the different combination treatments fell below the line of additivity indicating a synergistic effect. The 1:1 combination had the smallest combined IC_{50} value. The IC_{50} values for each of the combinations were represented in the inset table.

To further confirm the effectiveness of the dual carboplatin-Nutlin-3a combination and also to determine if this approach is applicable to other TNBC cells with mutant p53, a secondary TNBC cell line was also evaluated. The MDA-MB-468 cells are another triple-negative breast cancer cell line that harbors a different p53 mutation (R273H) within the DNA binding domain. The MDA-MB-468 cells exhibited similar sensitivity to Nutlin-3a, carboplatin, and 1:1 combination treatment as seen with the TMD231 cells. The IC_{50} values for the MDA-MB-468 cells were 23.8μM±7 for Nutlin-3a, 5μM±1.8 for carboplatin alone, and 1.3μM±0.3 for the 1:1 combination (Figure 7A). A broad range of dose ratios resulted in a synergistic inhibition of MDA-MB-468 cell growth; Nutlin-3a:carboplatin ratios including 1:1, 3:1, 9:1, 1:3, and 1:9 were evaluated and results were similar to those obtained with the TMD231 cells (Figure 7B).

To assess the effect of Nutlin-3a, carboplatin, and 1:1 combination treatment on clonogenicity, 2D clonogenic assays were completed. Nutlin-3a, carboplatin, and combination treatments inhibited colony formation in a dose-dependent manner (Figure 8). Clonogenic assays were attempted with the MDA-MB-468 cells; however, these cells did not form measurable colonies and therefore could not be evaluated by this assay.

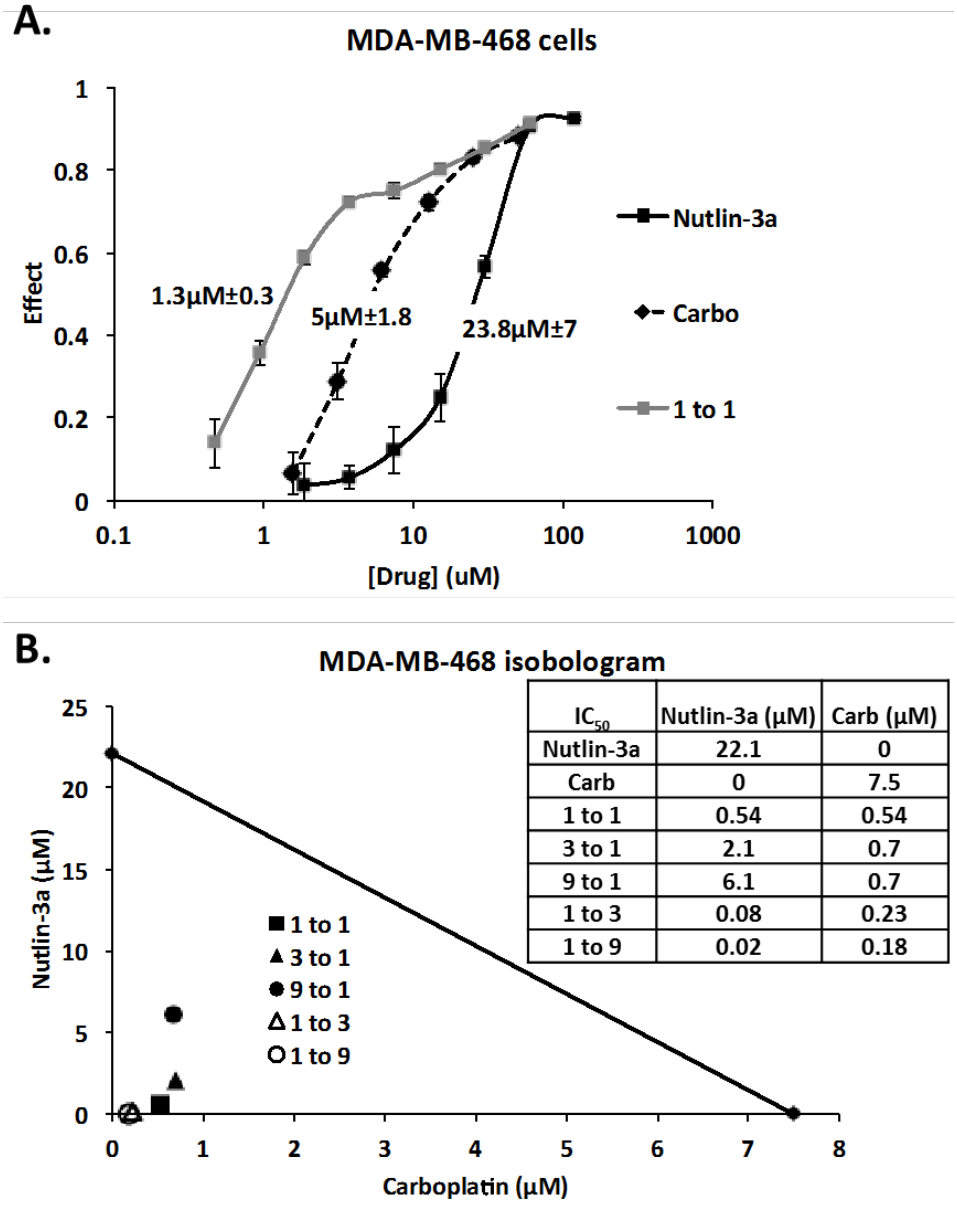

IC_{50}	Nutlin-3a (µM)	Carb (µM)
Nutlin-3a	22.1	0
Carb	0	7.5
1 to 1	0.54	0.54
3 to 1	2.1	0.7
9 to 1	6.1	0.7
1 to 3	0.08	0.23
1 to 9	0.02	0.18

Figure 7. Combination treatment increased potency and synergistic effects in MDA-MB-468 cells. MDA-MB-468 cells were seeded in 96-well plates and treated with increasing concentrations of Nutlin-3a, carboplatin (carbo), or combination (1:1) for 5 days. Cells were fixed and stained with methylene blue. Cell proliferation was determined for each treatment. (A) Combination treatment had an increased potency in MDA-MB-468 cells compared to Nutlin-3a and carboplatin alone treated cells. (B)

Following isobologram analysis, several drug ratios of Nutlin-3a:carboplatin (1:1, 3:1, 9:1, 1:3, and 1:9) were examined with isoboles falling below the line of additivity, which indicates a synergistic effect. The 1:3 and 1:9 combinations had the smallest combined IC_{50} value. The IC_{50} values for each of the combinations were represented in the inset table.

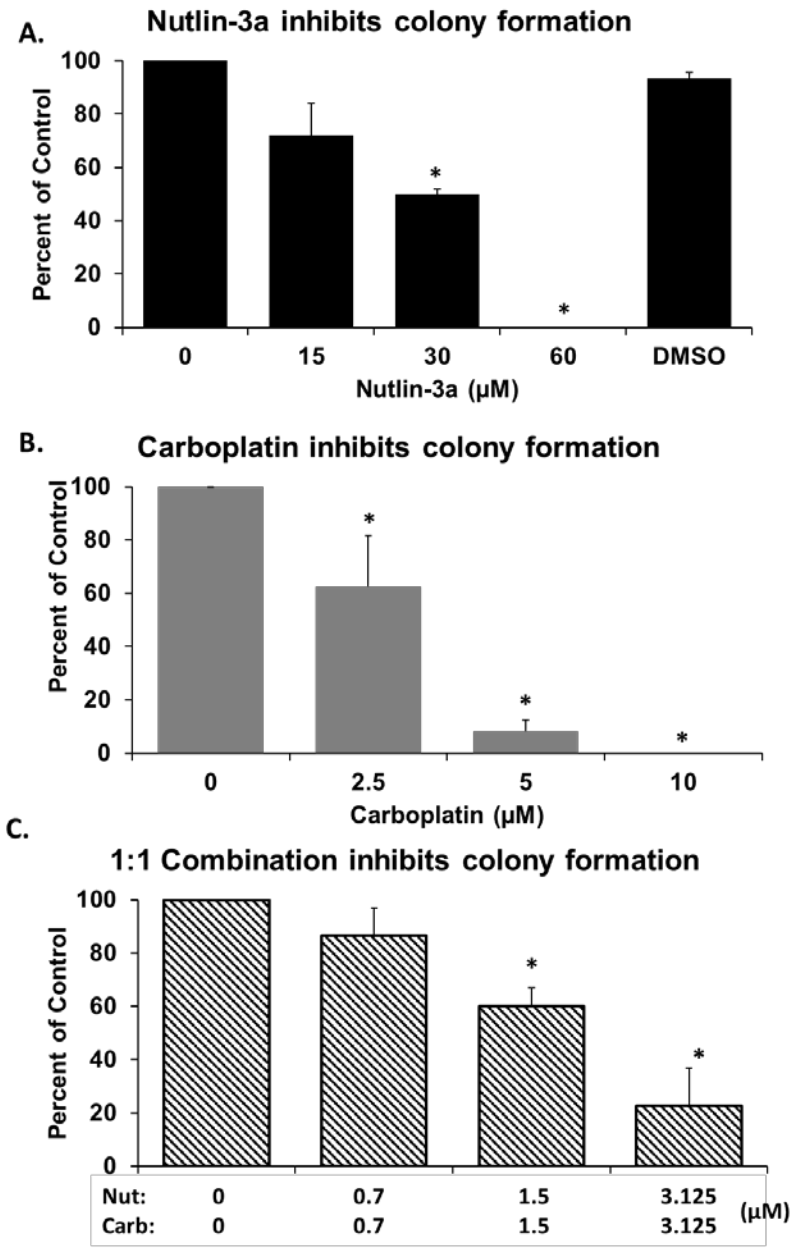

Figure 8. Combination treatment inhibits clonogenic cell growth. TMD231 cells were seeded at low density (50 cells per 10cm dish) to assess the effects of Nutlin-3a, carboplatin, and combination treatment on clonogenicity. Cells were treated with drug and allowed to grow for 2 weeks. Colonies were stained with methylene blue and counted using a cell counting pen. (A) Nutlin-3a significantly inhibited colony formation

in a dose dependent manner (n=3, *p<0.05 compared to untreated, mean±SD). (B) Carboplatin inhibited colony formation in a dose-dependent manner (n=3, *p<0.05 compared to untreated, mean±SD). (C) Combination treatment inhibited colony formation with decreased amounts Nutlin-3a (Nut) and carboplatin (Carb) compared to single drug treatments (n=3, *p<0.05 compared to untreated, mean±SD).

To better understand potential cytotoxic versus cytostatic effects of Nutlin-3a, carboplatin, or 1:1 combination treatment on cell proliferation, we performed longitudinal cell counting assays. TMD231 cells exposed to Vehicle continued to grow and reached confluence around Day 5. The Vehicle treatment did not alter cell growth throughout the study (Figure 9). Based on the isobologram results, we elected to evaluate compound effects at a dose ratio of Nutlin-3a:carboplatin that resulted in a synergistic inhibition of cell growth. The ratio of 1:1 was selected and drug treatments were performed at 7.5-15µM of each compound. These values centered on the IC_{50} value of carboplatin and about half of the IC_{50} of Nutlin-3a for TMD231 cells. We found that this dose ratio allowed us sufficient cells to be able to determine differences in combination treated cells versus each single drug in cell counting experiments and in the analysis of target modulation by Western blots. Low concentrations of Nutlin-3a alone do not affect cell proliferation to any significant degree (Figure 10). When TMD231 cells are exposed to 15µM carboplatin, this concentration only inhibits about 50% of cells allowing for further reductions in cell proliferation when combined with Nutlin-3a.

When TMD231 cells were exposed to 15µM Nutlin-3a, there was no effect on cell proliferation throughout the 5-day time course (Figure 10). Growth kinetics of cultures exposed to vehicle and Nutlin-3a were similar. Carboplatin induced a significant inhibitory effect on the growth of TMD231 cells compared to the Vehicle- and Nutlin-3a-treated cells (Figure 13). By Day 3, carboplatin-treated cells were stressed exhibiting a more rounded and swollen appearance, and this correlated with a significant reduction

in cell number (Figure 11 and 13). When evaluating Day 3 cultures, a noticeable change in cell number was observed; the 1:1 combination showed a significant reduction in total cell number compared to all groups (Figure 13). The 1:1 combination cells were very stressed by Day 3 with morphological changes showing large flattened cells with elongated spindle formation (Figure 12). There was a significant reduction in total cell number between Day 3 and 4 for both the carboplatin alone and 1:1 combination treated cells with further decreases in total cell number by Day 5 in the combination treated cells compared to other groups (Figure 11 and 12). The cell counting experiment was also repeated using lower drug concentrations, (1:1, carboplatin, and Nutlin-3a at 7.5µM of each drug). At the7.5µM concentrations of carboplatin and Nutlin-3a, cell proliferation was inhibited in a similar manner as the 15µM drug treatments. As would be expected, total cell counts were ~50% higher in the 7.5µM treated compared to the 15µM treated cells (Figure 14).

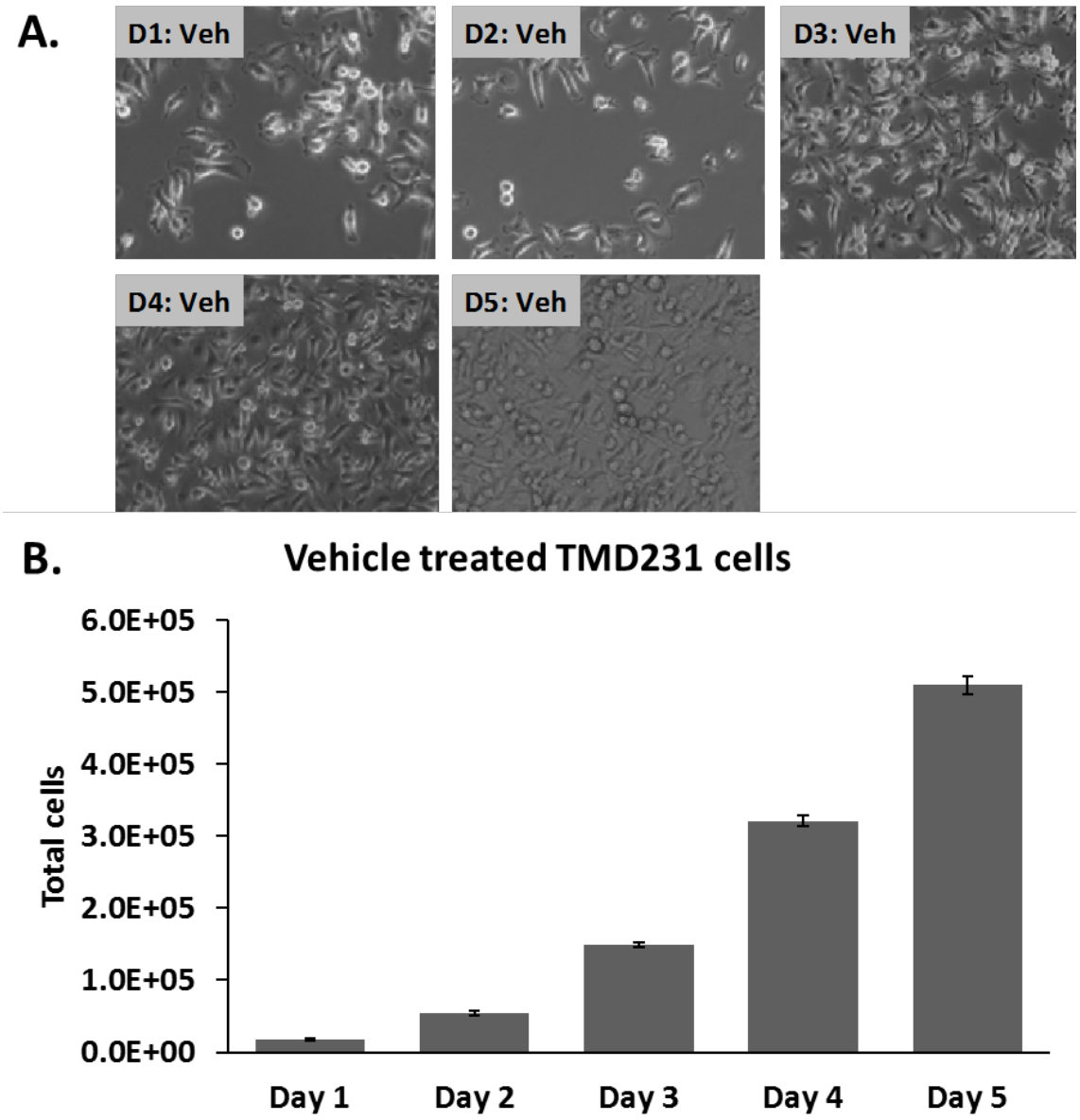

Figure 9. Vehicle treated TMD231 cell proliferation is not inhibited over time. TMD231 cells were seeded in 12-well plates with 6,500 cells on Day -1. Cells were treated with Vehicle on Day 0, and cell number was evaluated daily for a total of 5 days. (A) Pictorial representation of Vehicle (Veh) treated TMD231 cells over time. (B) Graphical representation of Vehicle treated TMD231 cells over time showed an increase in cell proliferation.

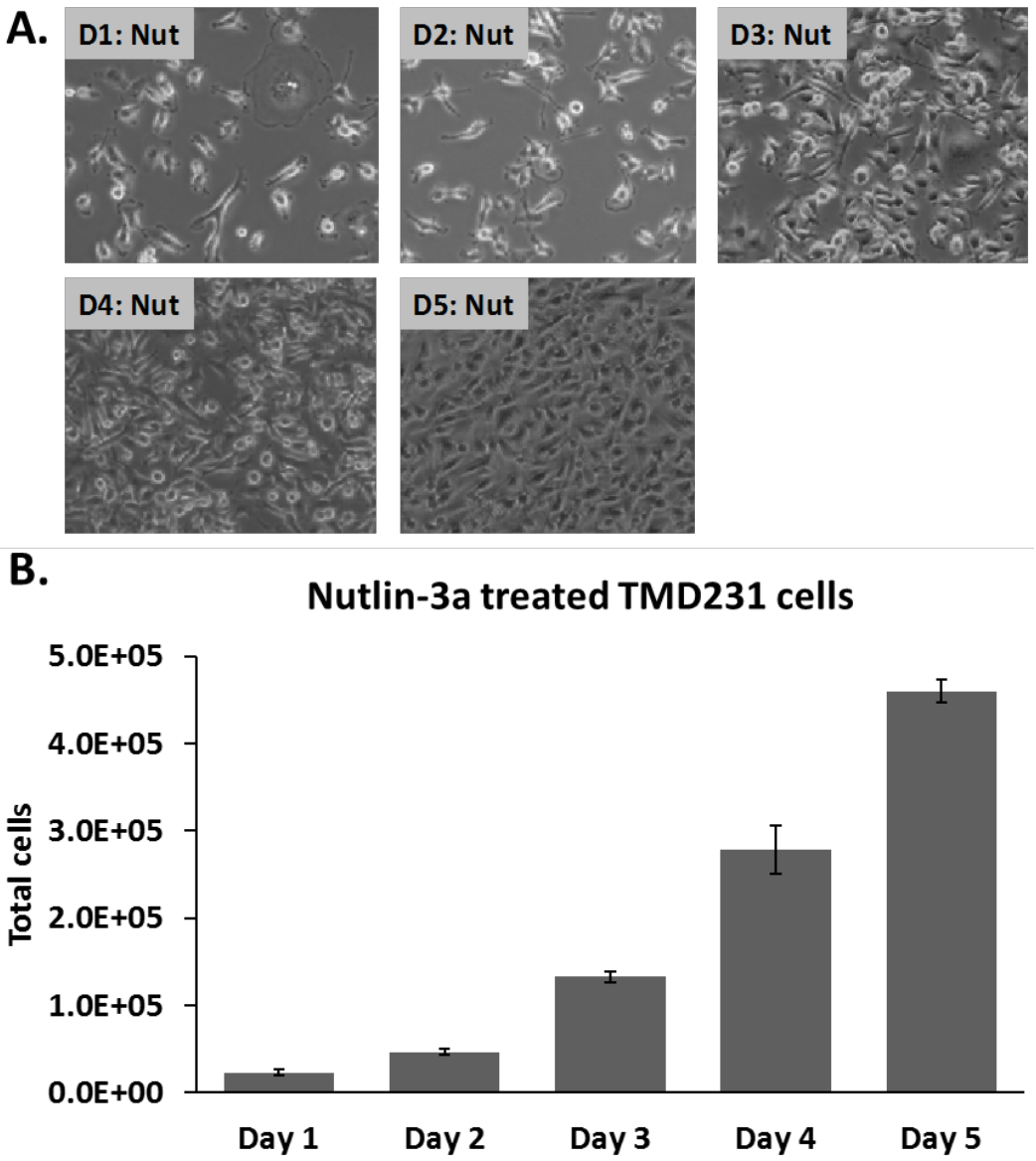

Figure 10. Nutlin-3a treated TMD231 cell proliferation is not inhibited over time. TMD231 cells were seeded in 12-well plates with 6,500 cells on Day -1. Cells were treated with Nutlin-3a, and cell number was evaluated daily for a total of 5 days. (A) Pictorial representation of 15µM Nutlin-3a (Nut) treated TMD231 cells over time. (B) Graphical representation of 15µM Nutlin-3a treated TMD231 cells over time showed an increase in cell proliferation.

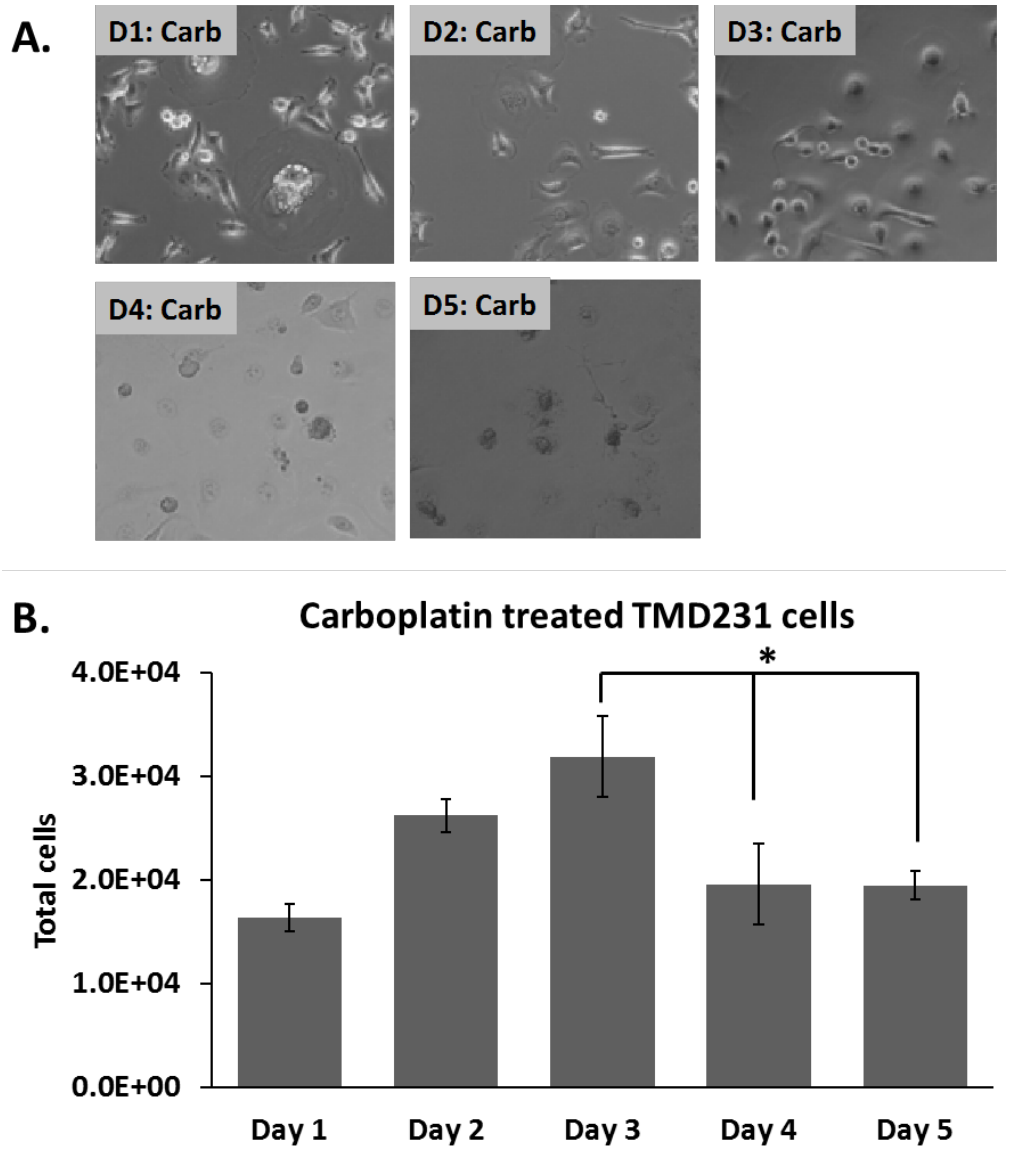

Figure 11. Carboplatin inhibits TMD231 cell proliferation after Day 3. TMD231 cells were seeded in 12-well plates with 6,500 cells on Day -1. Cells were treated with carboplatin, and cell number was evaluated daily for a total of 5 days. (A) Pictorial representation of 15µM carboplatin (Carb)-treated TMD231 cells over time. (B) Graphical representation of 15µM carboplatin-treated TMD231 cells over time showed an increase in cell proliferation until Day 3 after which cell number significantly decreased (One-Way ANOVA, *$p<0.05$, n=3, mean±SD).

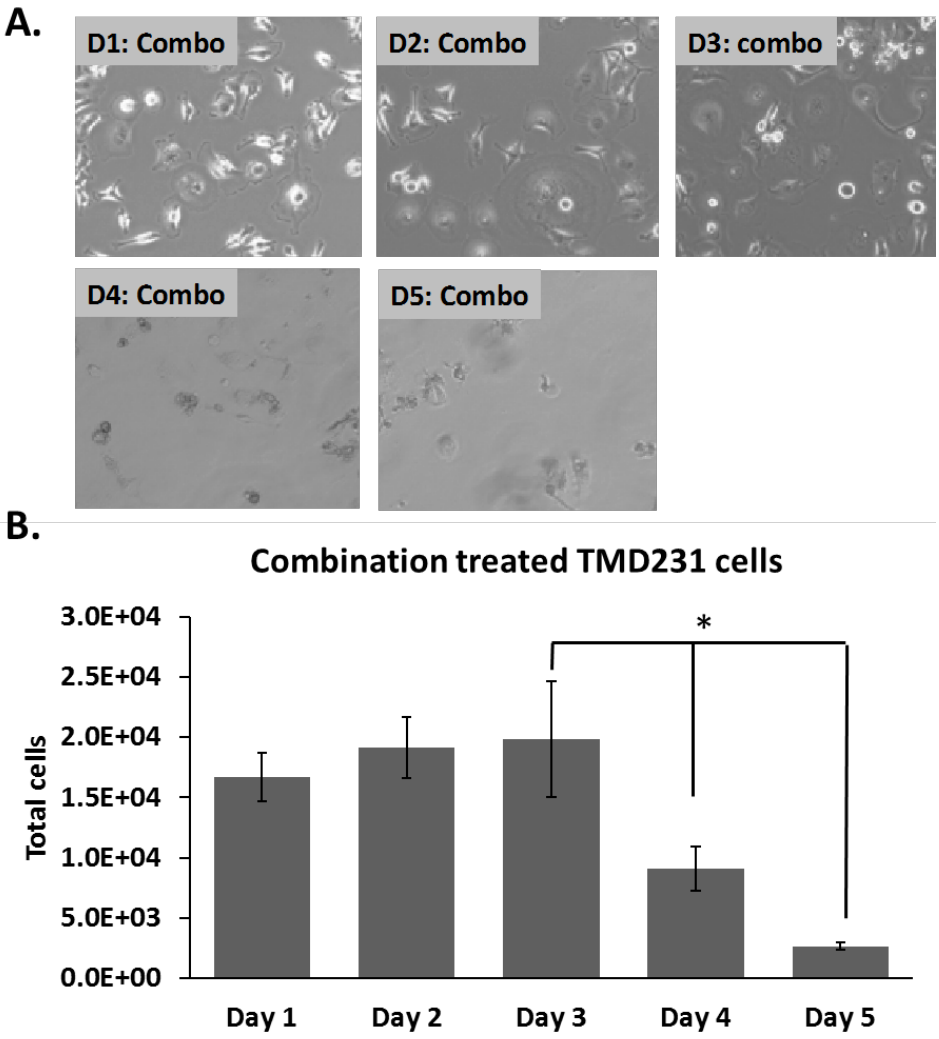

Figure 12. Combination treatment inhibits TMD231 cell proliferation after Day 3. TMD231 cells were seeded in 12-well plates with 6,500 cells on Day -1. Cells were treated with 1:1 combination, and cell number was evaluated daily for a total of 5 days. (A) Pictorial representation of 15µM Nutlin-3a + 15µM carboplatin combination (Combo) treated TMD231 cells over time. (B) Graphical representation of 15µM Nutlin-3a + 15µM carboplatin combination treated TMD231 cells over time showed a significant inhibition of cell proliferation after 3 days drug treatment (One-Way ANOVA, *$p<0.05$, n=3, mean±SD)..

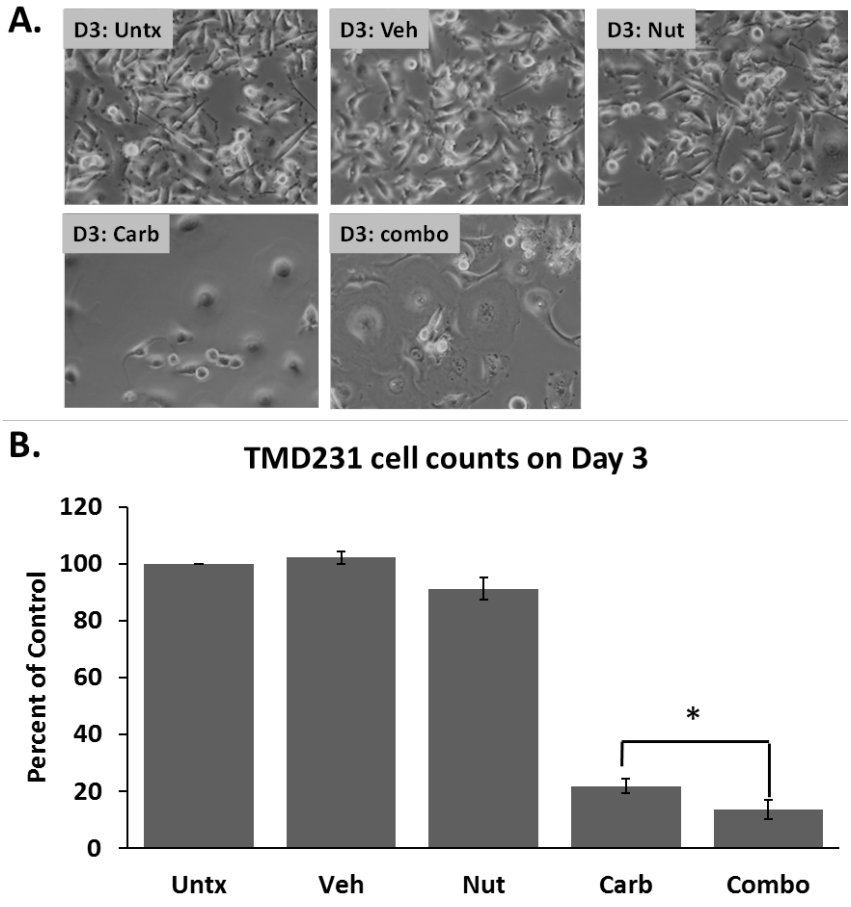

Figure 13. Carboplatin and combination treatment significantly inhibits cell proliferation by Day 3 post treatment. TMD231 cells were seeded in 12-well plates with 6,500 cells on Day -1. Cells were treated with Vehicle (Veh), Nutlin-3a (Nut), carboplatin (Carb), and 1:1 combination (Combo). There was also an untreated control (Untx), and cell number was evaluated daily for a total of 5 days. (A) Pictorial representation of TMD231 cells on Day 3 post treatment showed stressed and dying cells in carboplatin (Carb) and combination (Combo) treatments. (B) The cell counts for the carboplatin and combination treated TMD231 cells showed significant reductions in total cell number at Day 3. There was a statistically significant reduction in the combination treated cells compared to the carboplatin alone cells (Student's t-test, *$p<0.05$, n=3, mean±SD).

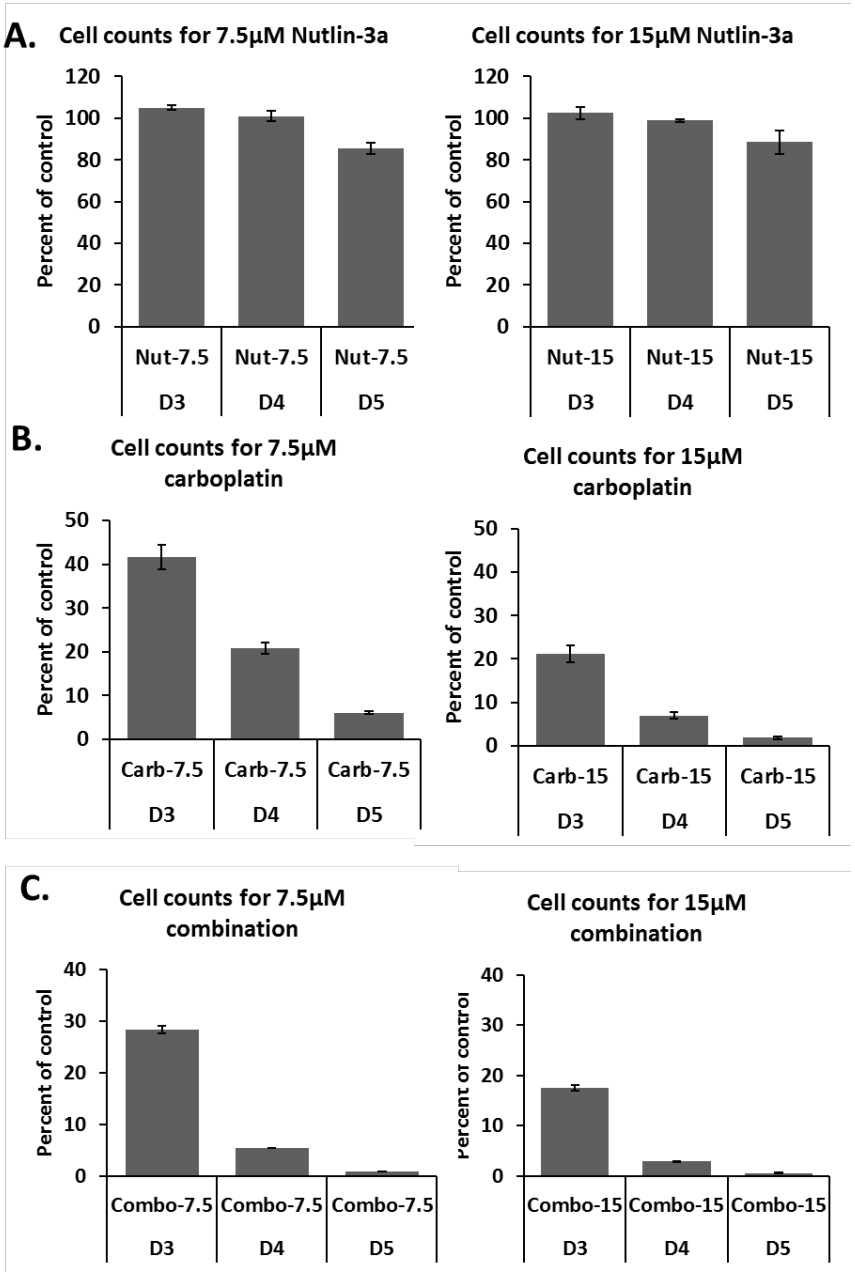

Figure 14. Dose-dependent decreases in number of TNBC cells exposed to combination carboplatin and Nutlin-3a. TMD231 cells were seeded in 12-well plates at 6,500 cells per well, and treated with 7.5µM or 15µM Vehicle, Nutlin-3a, carboplatin, or 1:1 combination. Total cell counts were evaluated Day 3-5 post treatment to examine the effects of drug treatment on cell proliferation. (A) Nutlin-3a in both treatments had

similar effects with slight decreases in both the 7.5µM and 15µM treated cells on Day 5. (B-C) Both the 7.5µM and 15µM carboplatin and 1:1 combination drug treatments inhibited cell proliferation and resulted in a decline in total cell number. The effects were about half in the 7.5µM treated cells compared to the 15µM treated cells which would be expected.

We next examined how the combination carboplatin and Nutlin-3a leads to decreased cell growth. Utilizing flow cytometry, we compared single and combination treatments and determined the frequency of early and late apoptotic cells. We began by using Annexin V-FITC and 7-AAD to determine if Nutlin-3a, carboplatin, and three different Nutlin-3a:carboplatin combination ratios (1:1, 3:1, and 1:3) promote apoptosis and/or necrosis. The drug concentrations used for these single and combinations were derived from TMD231 methylene blue proliferation data. TMD231 cells were treated for 4 days, which was determined based on cell counting assays as the cells reach a critical point between Day 3 and Day 4 (Figure 11 and 12). Following Annexin V-FITC and 7-AAD staining, flow cytometry indicated that at Day 4 post treatment, low levels of Nutlin-3a and carboplatin lead to moderate increases in both early and late apoptosis (Figure 15A), while the 1:1, 3:1 and 1:3 Nutlin-3a:carboplatin combinations lead to further increases in total apoptosis/necrosis when compared to each single drug alone (Student's T-test, $p<0.05$, $n=3$, ±SEM) (Figure 15B). Flow cytometry experiments show that TMD231 cells are undergoing apoptosis following low level combination treatment for all ratios (1:1, 3:1, and 1:3) (Figure 15B) while single drug treatments did not significantly increase the number of apoptotic cells compared to Vehicle treated cells.

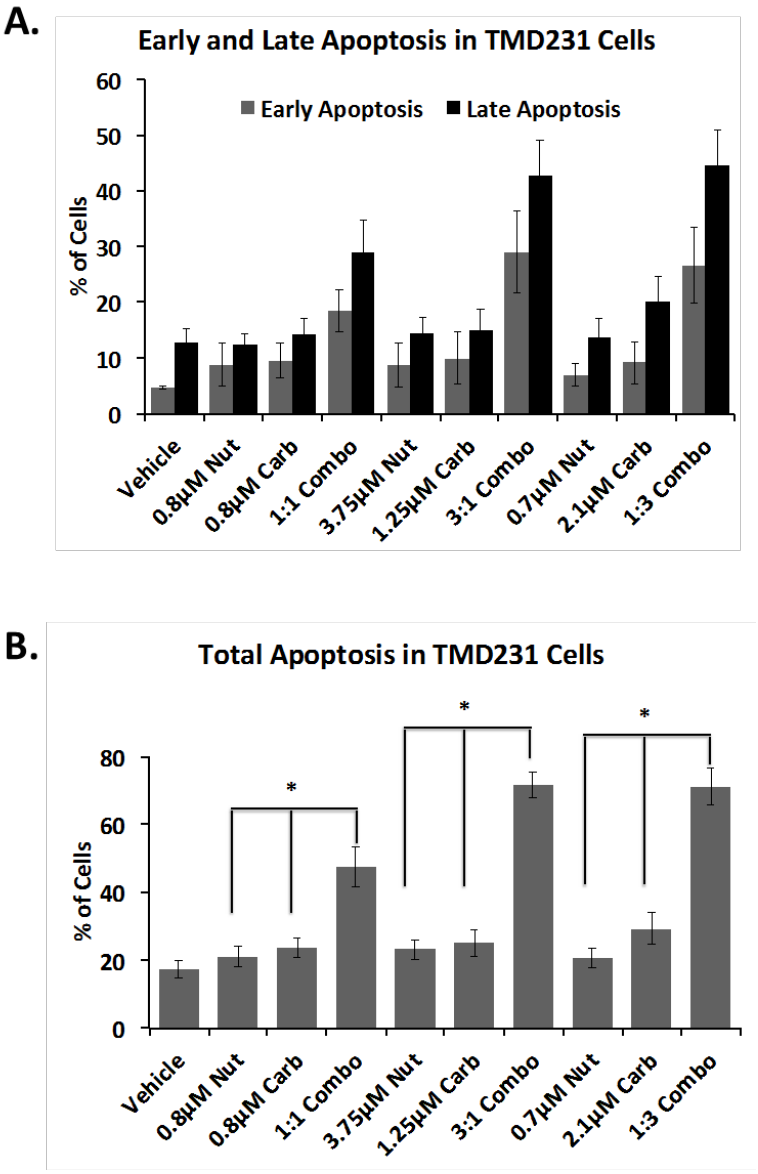

Figure 15. Combination treatment enhances apoptosis in TMD231 cells. TMD231 cells were treated with three different Nutlin-3a:carboplatin dose ratios (1:1, 3:1, and 1:3) and corresponding single drug treatment concentrations, which were the IC_{50} values determined from isobologram analysis in Figure 6B. (A) Flow cytometry analysis showed that Nutlin-3a, carboplatin, and combination caused increases in early and late apoptotic TMD231 cells following Annexin V and 7-AAD staining. (B) Combination

treatment caused significantly increased total apoptotic TMD231 cells compared to carboplatin and Nutlin-3a alone treated cells following flow cytometry Annexin V and 7-AAD staining (Student's T-test, *$p<0.05$, $n=3$, ±SEM).

To gain insight into treatment effects on cell cycle in the context of a mutant p53 background, we treated the TMD231 cells with increasing concentrations of Nutlin-3a, carboplatin, or 1:1 combination. Numerous cancer cell lines have aneuploid subpopulations, and in our model, the TMD231 cells have about 50% diploid and 50% aneuploid cellular subpopulations. In both the diploid and aneuploid populations, Nutlin-3a as a single agent did not induce cell cycle arrest in G1 or G2/M (Figure 16). In carboplatin and combination treated TMD231 cells, there was a dose-dependent increase in diploid and aneuploid cells in the S-phase compared to vehicle control which is consistent with previously published reports [120] (Figure 16). During this accumulation in the S-phase, cell could be undergoing an intra-S-phase checkpoint in which replication is reduced following DNA damage allowing cells more time to determine cell fate [121]. Cell cycle arrest may play a small role in the big picture; however, based on the cell counting experiments, the total cell number in the carboplatin and combination treated cells continued to decline after 3 days of treatment indicating that the cells were dying (Figures 11-12).

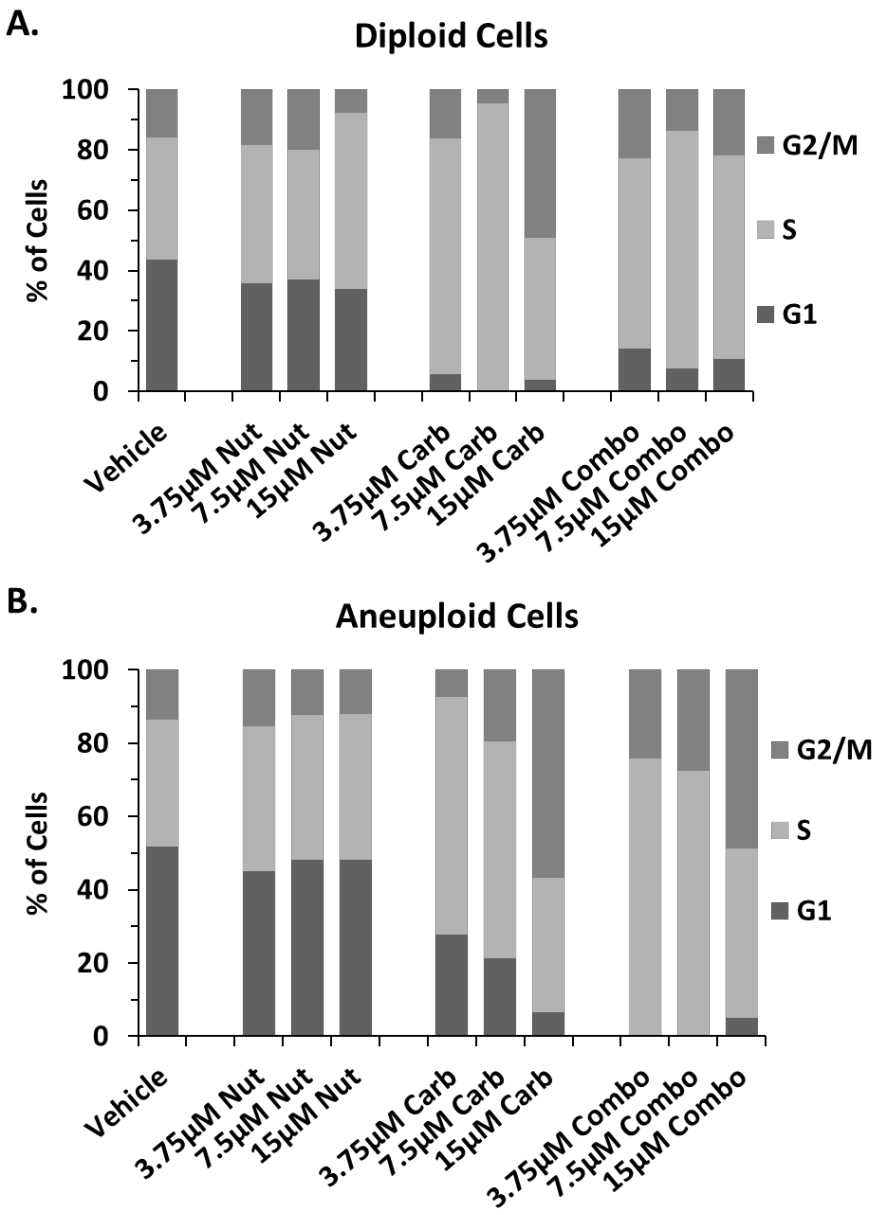

Figure 16. Carboplatin and combination treatment leads to S and G2/M accumulation while Nutlin3-a does not affect cell cycle. TMD231 cells were seeded on 10cm dishes and treated with 3.75, 7.5, and 15μM Nutlin-3a, carboplatin or 1:1 combination for 3 days. Cells were harvested and stained with a PI staining solution to examine DNA content in cell cycle analysis via flow cytometry. (A-B) Nutlin-3a had no effect on cell cycle in both diploid and aneuploid cells. In both diploid and aneuploid cells, carboplatin

treatment led to cell accumulation in S-phase. The percentage of cells accumulating in the G2/M phase increased in a carboplatin-dose-dependent manner in both cell types. The combination treatment lead most cells to accumulate in S-phase in both diploid and aneuploid cells.

C. **Discussion and Future Directions**

In summary, Nutlin-3a and carboplatin inhibited cell proliferation in methylene blue proliferation assays in the MDA-MB-231, TMD231, and MDA-MB-468 cell lines. The combination treatment led to an enhanced inhibition of cell proliferation as measured by methylene blue proliferation assays. Using isobologram analysis as described by Tallarida [109], the combination Nutlin-3a:carboplatin treatment led to a synergistic effect in all combinations tested. Nutlin-3a, carboplatin, and 1:1 combination treatment inhibited colony formation in a dose-dependent manner in the highly aggressive TMD231 cells while the MDA-MB-468 cells did not readily form colonies *in vitro*. In the colony formation assay, the number of colonies was significantly inhibited with increased amounts of each drug when compared to number of colonies in the single drug treated plates. For example, there was about a 50% decrease in number of colonies following 2.5µM carboplatin treatment while combined 1.5µM Nutlin-3a+1.5µM carboplatin also inhibited about 50% of colonies. To better understand how the single and combination treatment inhibited cell proliferation, cell counting assays were used to examine the total number of cells present over a 5-day period. The TMD231 cells were treated with 7.5µM or 15µM Nutlin-3a, carboplatin or 1:1 combination, and carboplatin and combination treated cells were greatly inhibited with significant reductions in total cell number after Day 3. The inhibition of total cell number was concentration-dependent with increased inhibition in cells treated with 15µM drug compared to 7.5µM drug treatments. There were significant differences in total cell number between the combination and carboplatin alone treated with the most effect

seen in the combination treated cells adding further support to the enhanced effect of dual Nutlin-3a and carboplatin treatment. In contrast to single agent, there was a potentiation in total apoptosis (early and late) following low concentrations of Nutlin-3a:carboplatin combination (1:1, 3:1, and 1:3) treatments in TMD231 cells. Low concentrations of Nutlin-3a and carboplatin alone did not increase apoptosis and/or necrosis compared to Vehicle treated cells. Additionally, carboplatin alone and combination treatment lead to increased cell cycle arrest in the S and G2/M phases compared to Vehicle or Nutlin-3a. Nutlin-3a alone did not lead to increased cell cycle arrest.

In our model, we utilized TNBC cell lines that do not have *Brca1/2* mutations. However, the dual treatment of Nutlin-3a and carboplatin may have further efficacy in TNBC cell lines that also have mutations in the *Brca1/2* gene. Recent studies have shown improved complete response rates of patients with germline mutations in *Brca1/2* when standard of care paclitaxel or paclitaxel plus doxorubicin was combined with carboplatin [122]. Additionally, if drug treatment was combined with the PARP inhibitor, iniparib, there was an improved complete response rate in those patients who had *Brca1/2* mutations compared to *Brca1/2* wild-type patients [122]. Synthetic lethality is an emerging area of research since TNBCs with mutant *Brca1/2* in combination with a DNA damaging drug like carboplatin and PARP inhibitors can lead to increased cell death due to inhibition of key DNA repair pathways. Combination Nutlin-3a and carboplatin treatment coupled with a PARP inhibitor may lead to further efficacy in TNBCs that have concomitant *Brca1/2* mutations.

In these cellular models of TNBC, there was increased sensitivity to Nutlin-3a in combination with carboplatin. Dr. Martin Smith showed that Mdm2 overexpression increased sensitivity to platinum agents by inhibition of wild-type 53 and thus inhibition of the NER pathway and removal of platinum adducts [123]. Mdm2-mediated inhibition of wild-type p53 resembled similar cellular responses to platinum agents in mutant p53 cancer cells in which platinum treatments led to a strong S-phase cell cycle arrest[123], which was similar to our results. While cell cycle arrest was evident in treated cells, the arrest in G2/M or S phase was not sufficient to allow for repair and cell survival of combination treatment since we saw significant reductions in total cell numbers between Days 3 and 4 post treatment in cell counting assays. It has been shown that Mdm2 affects $p21^{WAF1/Cip1}$ by acting to decrease the half-life of $p21^{WAF1/Cip1}$ and by increasing proteasomal turnover of the $p21^{WAF1/Cip1}$ protein independent of ubiquitylation [124]. Jin and colleagues also showed that in p53 null cells, Mdm2 inhibits $p21^{WAF1/Cip1}$-mediated cell cycle arrest, which could play a role in the analysis of cell cycle following drug treatment [124]. Additionally, based on flow cytometry experiments, there was increased cell death (apoptosis and/or necrosis) in the combination treated TMD231 cells compared to single drug treated cells. This was particularly evident when cells were exposed to low concentrations of Nutlin-3a and carboplatin (0.8µM Nutlin-3a:carboplatin used in apoptosis flow assay versus 15µM Nutlin-3a:carboplatin used in cell counting assays) with >50% cells undergoing apoptosis. Future studies would include further analysis of apoptotic markers including activated Caspases-3, -7 and -9 to better understand the role of apoptosis at the molecular level in our model system.

Additionally, the role of senescence should be examined following combination carboplatin and Nutlin-3a treatment to see if senescence also plays a role in the effects observed following combination treatment [125,126]. Senescence staining could be completed using β-galactosidase staining. The effects of the combination carboplatin and Nutlin-3a treatment on isolated cancer stem cells should also be evaluated to see if these cell are also sensitive to the combination treatment since these cells could give rise to recurrent tumors. The role of combination treatment could also be examined on normal tissue toxicity. MCF10A, which are a non-transformed mammary epithelial cell line, could be used in proliferation assays to examine the effects of dual treatment on normal human cells as well.

Cell cycle analysis showed that carboplatin and combination treatment lead to increased populations in S-phase and some increases in G2/M. There has also been evidence for cancer cells to undergo mitotic catastrophe in which during the cell cycle, the cells undergo aberrant chromosome segregation [127], and this area of study is an emerging area of interest in our laboratory. Aberrant chromosome segregation leads to the generation of aneuploid cells as the cells [127]. In the TMD231 cells, Vehicle treated cells contained about 50% aneuploid cells, whereas following some carboplatin and combination treatments, there were small increases in the aneuploid populations (>60%). As the TMD231 cells accumulate in S-phase, cell could be undergoing an intra-S-phase checkpoint in which replication is reduced following DNA damage, which could allow cells more time to determine cell fate [121]. During accumulation in the S-phase, there may be some cells undergoing mitotic catastrophe as a means of survival, which

could possibly explain the slight increases in aneuploid cells in the DNA damage treated groups. There has been much discussion in the literature to describe the phenotype of mitotic catastrophe. Some reports describe that the mitotic catastrophe phenotype is similar to apoptosis since there are instances where the cells have condensed chromatin aggregates [127]. The formation of micronuclei have also been implicated in the mitotic catastrophe phenotype [127]. Treated cells could be stained with acridine orange, which is fluorescent dye that is specific for nucleic acids allowing for specific staining rather than non-specific Giemsa-stains, which can lead to overestimation of nuclear abnormalities [128,129].

Based on our results, the combination of Nultin-3a and DNA damaging drug carboplatin could be used in other cancer models. In our laboratory, we are also investigating the combination of Nutlin-3a with standard of care, temozolomide, in primary gliobalstoma (GBM) models with both mutant and wild-type p53. We have observed Nutlin-3a mediated sensitization to temozolomide *in vitro* and *in vivo* in GBM. Other standard of care chemotherapeutic drugs could be combined with Mdm2 inhibition in other cancer models especially in those cancers where Mdm2 is overexpressed.

Chapter 2. Aim 2: Determination of signaling mechanisms operative in response to combination carboplatin and Nutlin-3a treatment *in vitro*

A. Background and Rationale

Several studies have demonstrated that Nutlin-3a can affect cells in a p53-independent manner. Nutlin-3a effectively inhibited the binding of p73α, E2F1, and HIF-1a to the hydrophobic pocket of Mdm2 in cancer cells [62,65,66]. In this next series of experiments, our objective was to gain insight into the p53-independent effects of Nutlin-3a in combination with carboplatin in the TMD231 mtp53 TNBC cells. We have shown that the combination treatment has enhanced effects in inhibiting cell proliferation in methylene blue, clonogenic, and cell counting assays as well as increased apoptosis and cell cycle arrest. To better understand the signaling mechanisms active in our model system following dual carboplatin and Nutlin-3a treatment *in vitro*, we used a series of experiments to understand changes in protein levels, effects of target protein knockdown, as well as intracellular localization of Mdm2 following single and dual treatment.

In a p53 mutant background, we reasoned that Mdm2, p73α, and E2F1 could be key players in promotion of cell death in the context of carboplatin-mediated DNA damage. To gain information on the potential role of these proteins and if they are involved in carboplatin/Nutlin-3a-mediated cell death, we tested a series of cell lines with stable or transient knockdown of Mdm2, p73 and E2F1. Additionally, carboplatin is a DNA damaging drug which leads to the incorporation of Pt adducts leading to bulky

lesions in the DNA [14]. These Pt adducts can lead to intra and interstrand DNA crosslinks and can also lead to DSBs if left unrepaired and ultimately cell death [14].

As background, Mdm2 has been shown to lead to genomic instability by binding to Nbs1, a member of the DNA damage sensing MRN complex [35]. Mdm2 binds to Nbs1 and inhibits its function at recruitment of DNA repair machinery to sites of double strand breaks [35]. This delay in DNA damage sensing, leads to a delay in DNA repair and thus leads to increased genomic instability. With Mdm2 able to antagonize Nbs1 and inhibit DNA repair, the increased DNA damage window may allow the threshold of the cells to undergo stress to be reached leading ultimately cell death. We wanted to test the effects of Mdm2 protein reduction using cells stably expressing shRNA to Mdm2. If Mdm2 was a major player in the system, reductions in Mdm2 levels should lessen the effects of Mdm2-mediated inactivation of the MRN complex. This would allow the MRN complex to sense the DNA double strand breaks and if DNA repair (NHEJ and HR) is adequate in the cell, the DNA breaks would be repaired and the cell would survive. We found that while a 70% reduction in Mdm2 could be achieved with stable shRNA knockdown, this did not change cellular sensitivity to combination treatment. The remaining Mdm2 may have been sufficient to block the function of the MRN complex and thereby inhibiting repair of DNA double-strand breaks. It appears that there is a very small threshold at which Mdm2 can still antagonize DNA repair (personal correspondence with Dr. Christine Eischen). As mentioned previously, 27% of breast cancers overexpress MdmX with concurrent p53 inactivation as well as 30% of aggressive breast cancers also have increased MdmX levels with mutant p53 [99]. These

findings are particularly important since MdmX has also been implicated in genomic stability as it plays a role in DNA repair by binding to Nbs1 and inhibiting DNA repair independent of p53 and Mdm2 which would be an interesting avenue to follow up in this system [99].

Additionally, since it has been shown that p73 can upregulate Mdm2 levels by binding to the Mdm2 promoter as well as E2F1-mediated upregulation of p73 following DNA damage, we wanted to explore the dependency of p73 or E2F1 in our signaling mechanism [130,131]. E2F1 is a transcription factor that is also important in cell proliferation as well pro-apoptotic signaling depending on the cellular context. E2F1 is tightly regulated by the retinoblastoma (RB) protein. Following DNA damage, RB is phosphorylated by the Chk1/2 kinases leading to decreased association of E2F1 and RB, which allows E2F1 to increase its transcriptional activity [131]. Following DNA damage, E2F1 is involved in pro-apoptotic signaling through upregulation of pro-apoptotic genes including *p73* and *caspase-7* as well as the downregulation of cell cycle progression genes including *cyclin A2* [131]. p73 is a family member of p53 and has similar effects following DNA damage by increasing PUMA, p21, and Mdm2 [78,79,82,130,132,133]. We utilized lentiviral constructs to stably express shRNA for either p73 or E2F1. Our rationale was that if Mdm2, p73, or E2F1 were major signaling mediators in our model system then the reduction in protein levels would lead to decreased drug sensitivity. In cells with p73 and E2F1 transient or stable knockdowns, exposure to carboplatin and Nutlin-3a would not lead to enhanced cells death since there would little to no p73 or E2F1 available to upregulate pro-apoptotic gene levels. This lack of gene upregulation would lead to

increased resistance to treatment due to the lack of apoptosis. While incomplete knockdown of the target RNA can preclude one from obtaining interpretable data, the levels of shRNAs from stably integrated lentiviral vectors can have a downside and yield variable results. Lentiviral vectors randomly integrate into the genome and this can result in nonspecific effects on levels of other genes.[134]. For example, we found that some but not all cell lines generated with control vectors that express a GFP shRNA (shGFP) could lead to significant changes in drug sensitivity. One shGFP clone used in the shE2F1 experiments caused the cells have the highest drug resistance compared the shE2F1. The control shRNA vectors made the results difficult to interpret. Because of these issues with the stable shRNA transductions, we elected to evaluate p73 dependency using transient transfections of siRNA specific for p73. In the TMD231 cells, the non-targeting control siRNA did not affect cellular sensitivity to drug treatment when compared to parental cells in our experiments.

Nutlin-3a was selected for this project since it was the only Mdm2 inhibitor available at the time this project was initiated. It has served as a reliable research tool to probe how inhibition of Mdm2 mediated signaling in combination with carboplatin mediated-DNA damage affects the growth and survival of TNBC cells with mutant p53. Since the advent of Nutlin-3a, there have been several second generation molecules to Nutlin-3a (RG7112, Roche/Genentech) as well as numerous Mdm2 inhibitors from competing companies: SD-3032b (Baiichi Sankyo Inc.), SAR4058338 (Sanofi), CGM-097 (Novartis), and AMG-232 (Amgen). Because there are more clinically relevant small

molecules being used, we also tested more recently the Nutlin-3a derivative RG7112 in combination with carboplatin in our model system.

B. **Combination treatment affects Mdm2 cellular localization and cellular sensitivity is altered following transient transfection of p73 siRNA**

After examining the effects of Nutlin-3a, carboplatin, and combination treatment at the cellular level, we wanted to examine the effects of the drug treatments at the molecular level. We first used Western blot experiments to evaluate changes in protein levels in the treated TNBC cells. Following Nutlin-3a treatment, there were increases in Mdm2 protein levels, which has been consistent through my studies (Figure 17) as well as the literature [65,66]. There were also concentration-dependent increases in p21 following Nutlin-3a treatment. The 1:1 combination treatment resulted in modest increases in Mdm2 protein levels and this correlated with slight decreases in MdmX. Mdm2 levels in the combination treated cells were not as high as protein levels in the Nutlin-3a alone treated cells though the combination still showed an increase in Mdm2 levels compared to untreated cells. Interestingly, in the combination treatment, there were reductions in MdmX levels whereas the other treatments showed high baseline levels that did not change in the single Nutlin-3a or carboplatin treated cells. In wtp53 cells, it has been shown that following ionizing radiation, MdmX is degraded by Mdm2, which allows the levels of p53 to increase leading to DNA repair and/or apoptosis [135,136]. MdmX is degraded following posttranslational modifications in which ATM is activated following DNA damage, which allows for phosphorylation at S403 [137]. This phosphorylation site allows for Mdm2 to target MdmX for degradation by the proteasome [137]. In our model system, we hypothesize that p73 would induce Mdm2

levels and following DNA damage, may then lead to decreased MdmX levels in the combination treated TMD231 cells.

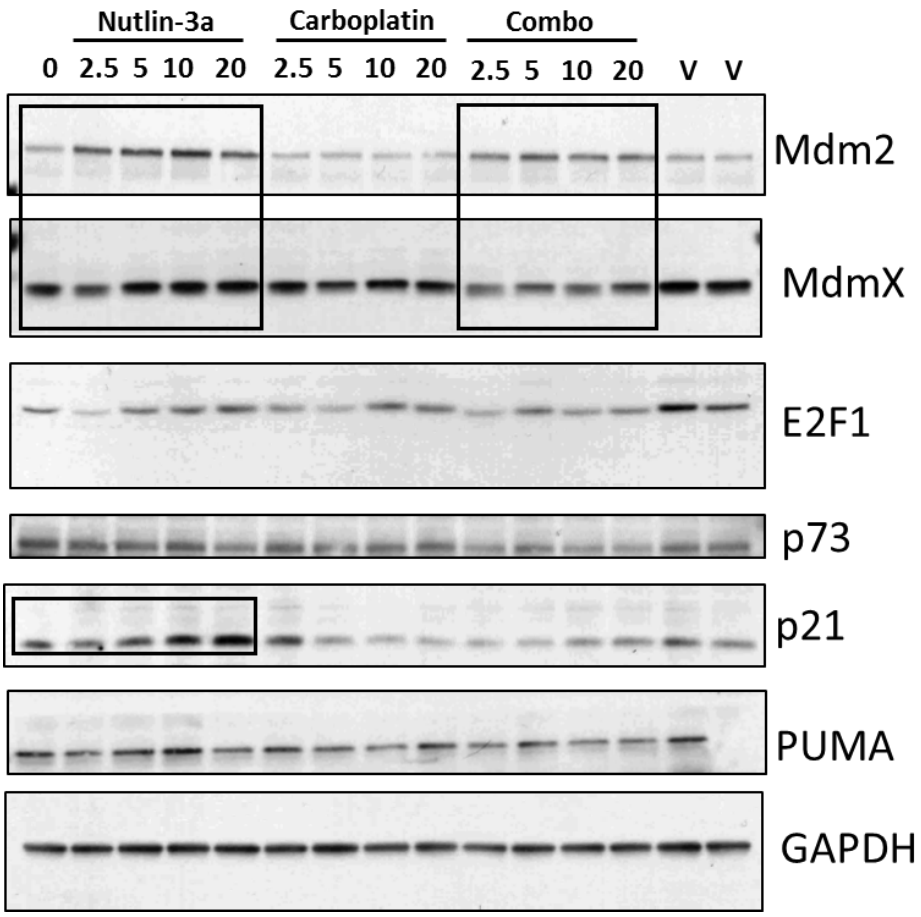

Figure 17. Nutlin-3a upregulates Mdm2 protein levels with dose-dependent increases in p21 while combination treatment downregulates MdmX. TMD231 cells were seeded in 10cm dishes and treated with increasing concentrations of Nutlin-3a, carboplatin, or 1:1 combination for 24 hours. Cells were treated with vehicle controls (V). Cells were lysed with 1% SDS lysis buffer. Following Nutlin-3a and combination treatment, levels of Mdm2 were increased with the highest levels of Mdm2 in the Nutlin-3a alone treated cells when compared to the untreated control cells. There were dose-dependent increases in p21 following Nutlin-3a treatment. Interestingly, Mdm2 levels were slightly increased in the combination treated cells while there was a downregulation of MdmX in the combination treated cells.

There are several studies indicating the increased capacity of mutant p53 cancer cells to have increased invasion [112]. There are also studies showing that Mdm2 overexpression drives invasion through upregulation of MMP9 [37]. Following Nutlin-3a and combination treatments, we observed increases in Mdm2 levels following Western blot analysis (Figure 17). We therefore, wanted to test the effects of single Nutlin-3a and carboplatin as well as combination treatment on TMD231 cell invasion. The invasion assay was designed to measure the amount of cells that are able to pass through a dried basement membrane matrix solution and subsequently pass through an 8µm pore-filled layer towards a chemoattractant (FBS) containing medium. The cells must be able to secrete enough enzymes to be able to pass through the basement membrane matrix. This assay not only tests the ability of the cells to migrate into the bottom layer but also the ability for the cells to invade through the basement membrane matrix. Following 24-hour 7.5µM treatment of Nutlin-3a, carboplatin, or combination, there was no difference in TMD231 cell invasion between treatment groups compared to Vehicle treated cells (Figure 18A). Cytochalasin D was used as a negative control and inhibited about 50% of cell invasion compared to Vehicle controls (Figure 18A). Cytochalasin D is a mycotoxin that inhibits actin filaments important in cell invasion and migration by inhibiting the addition of actin monomers to the end of actin filaments [138]. A concurrent cell survival experiment was conducted to ensure that the drug treatment did not affect total cell survival, which may have made the invasion data difficult to interpret. There was no difference in cell survival based on cell counting experiments between single drug and combination treatments when compared to Vehicle treated cells at the 24-

hour time point (Figure 18B). Cytochalasin D itself led to some inhibition of cell viability due to its mechanism of action by inhibition of actin filaments, which would be critical for normal cell division. This modest inhibition of TMD231 cell viability following Cytochalasin D treatment was similar to results as described by Fronczak and colleagues using MDA-MB-231 cells (Platypus Technologies, 2011 AACR Abstract #4897).

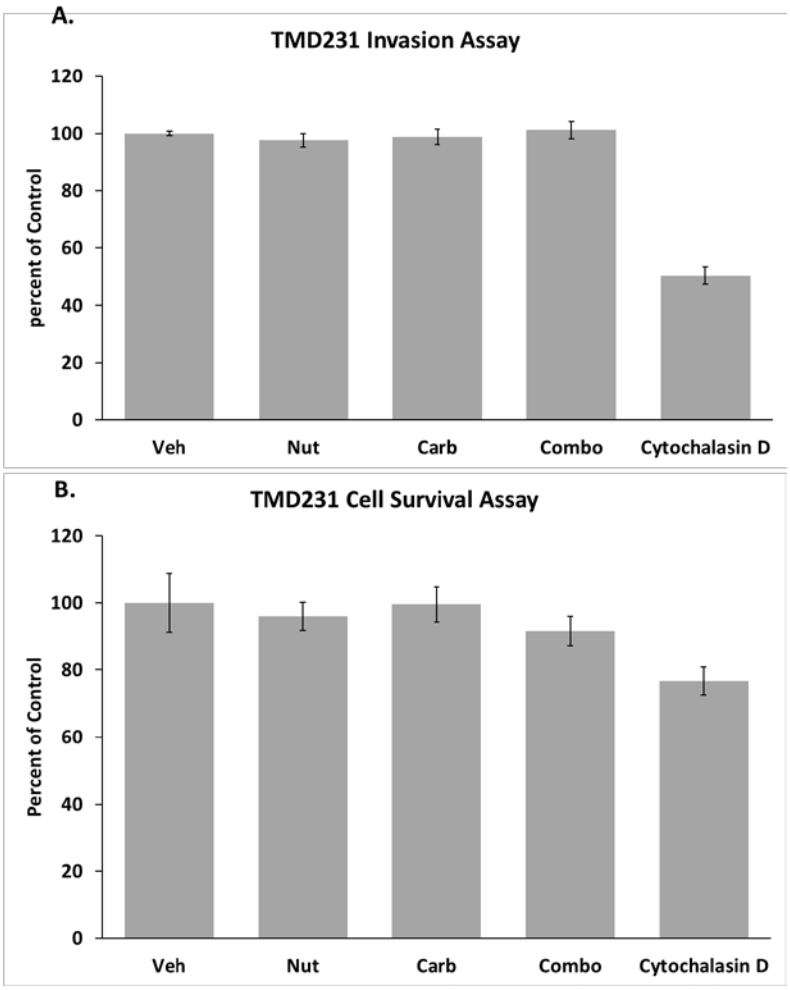

Figure 18. Single and combination treatment does not affect cell invasion. TMD231 cells were seeded in cell culture invasion inserts and corresponding 24-well plate with 3,500 cells per well. Cells were serum starved overnight and treated with 7.5µM Nutlin-3a, carboplatin, 1:1 combination, or Vehicle for 24 hours. (A) Single drug and combination treatment did not affect cell invasion. Cytochalasin D inhibited about 50% of cellular invasion. (B) Concurrent cell survival assays showed that the drug treatments did not affect total cell number. Cytochalasin D treatment lead to decreased cell survival, however this result is expected as inhibition of actin monomers is critical for normal cell division.

There is a growing body of evidence that Mdm2 has numerous p53-independent functions and plays a role in genome stability by binding to Nbs1, which is part of the MRN complex, at sites of DNA damage [35]. The MRN complex acts as an initial sensing mechanism at sites of double strands breaks in the DNA. When the MRN complex recognizes these sites, a series of phosphorylation events occur with ATM leading to downstream DNA repair signaling. Since we observed increased levels of Mdm2 following Nutlin-3a and 1:1 combination treatment, we investigated if Mdm2 could be differentially localizing in the chromatin fraction where it would presumably inhibit DNA repair as described above. In collaboration with Dr. Christine Eischen's laboratory, chromatin association assays were conducted. Following 24-hour treatments, the chromatin fraction was isolated and evaluated for Mdm2 protein via Western blot. Following a 6-hour drug treatment, Mdm2 levels associated with the chromatin fraction in the combination treated cells were higher compared to the single drug treated cells or vehicle control (Figure 19A). Whole cell lysates indicated that there were about equal amounts of Mdm2 in the Nutlin-3a and combination treated cells (Figure 19B). Therefore, in the combination treated cells, more Mdm2 associated with the chromatin fraction compared to the single drug-treated cells. It is possible that the increased level of Mdm2 at the chromatin could be inhibiting DNA repair by Mdm2 binding to Nbs1 within the MRN complex. This delay in DNA repair could allow an increased amount of DNA damage to accrue causing cells to be pushed towards increased cell death when exposed to carboplatin and Nutlin-3a in combination.

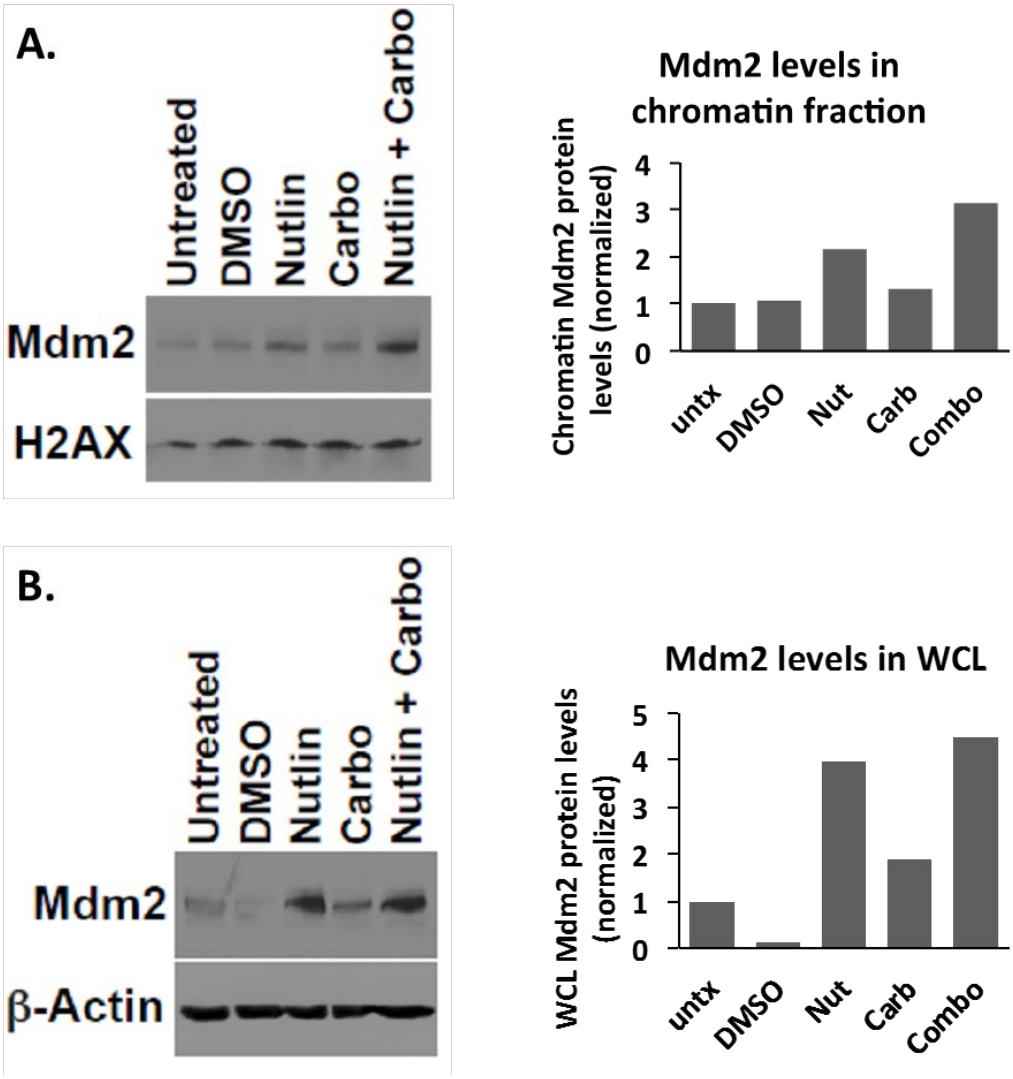

Figure 19. Mdm2 protein levels were increased in the chromatin bound fraction in combination treated cells. TMD231 cells were treated with Vehicle (DMSO), Nutlin-3a, carboplatin (Carbo), or 1:1 combination (Nutlin+Carbo) for 6 hours. Cells were lysed and the soluble protein fraction was collected. (A) The chromatin bound fraction was then collected and evaluated for Mdm2 levels. H2AX was used as a loading control for the chromatin fraction. Graphical representation of densitometry following ImageJ protein quantification showed increased levels of Mdm2 in the combination treated chromatin fraction compared to the single drug treated Mdm2 levels. (B) Western blot of whole

cells lysates showed similar amounts of Mdm2 protein in both the Nutlin-3a and combination treated TMD231 cells. β-actin was used as a loading control for whole cell lysates. ImageJ densitometry analysis showed a subtle increase in Mdm2 levels in combination treated cells compared to Nutlin-3a alone. This was repeated 2 times with similar results.

Since there were increased amounts of Mdm2 at the chromatin, we used a shRNA knockdown approach to evaluate if Mdm2 dependency of drug effect could be assessed. We utilized lentiviral transduced TMD231 cells expressing shcontrol or shMdm2 that were a kind gift of Dr. Lindsey Mayo. Western blot analysis showed that TMD231-shMdm2 had about 70% reduction in Mdm2 compared to the TMD231-shcontrol cells as evaluated by densitometry using ImageJ software (Figure 20A). All densitometry measurements were normalized to GAPDH loading control for each lane. Next, we evaluated the effects of Nutlin-3a, carboplatin, or combination treatment on cell proliferation in the TMD231-shcontrol and TMD231-shMdm2 cells using methylene blue staining. When TMD231-shcontrol and TMD231-shMdm2 cells were compared, there were no differences in cell proliferation following Nutlin-3a, carboplatin, and combination treatment. No differences in IC_{50} values between the two cell lines (Figure 20B) were observed. Based on the methylene blue cell growth assay, knockdown of Mdm2 levels by 70% was not sufficient to demonstrate Mdm2-dependency of drug effect. In discussions with Dr. Christine Eischen (Vanderbilt University), only small amounts of Mdm2 can still block DNA repair. Additionally, partial or complete knock-down of Mdm2 experiments are difficult to interpret due to potential redundancies of Mdm2 and MdmX in blocking the DNA damage response [35,99]. As shown in Figure 17, while the combination treatment led to a downregulation of MdmX protein levels, MdmX was still detected.

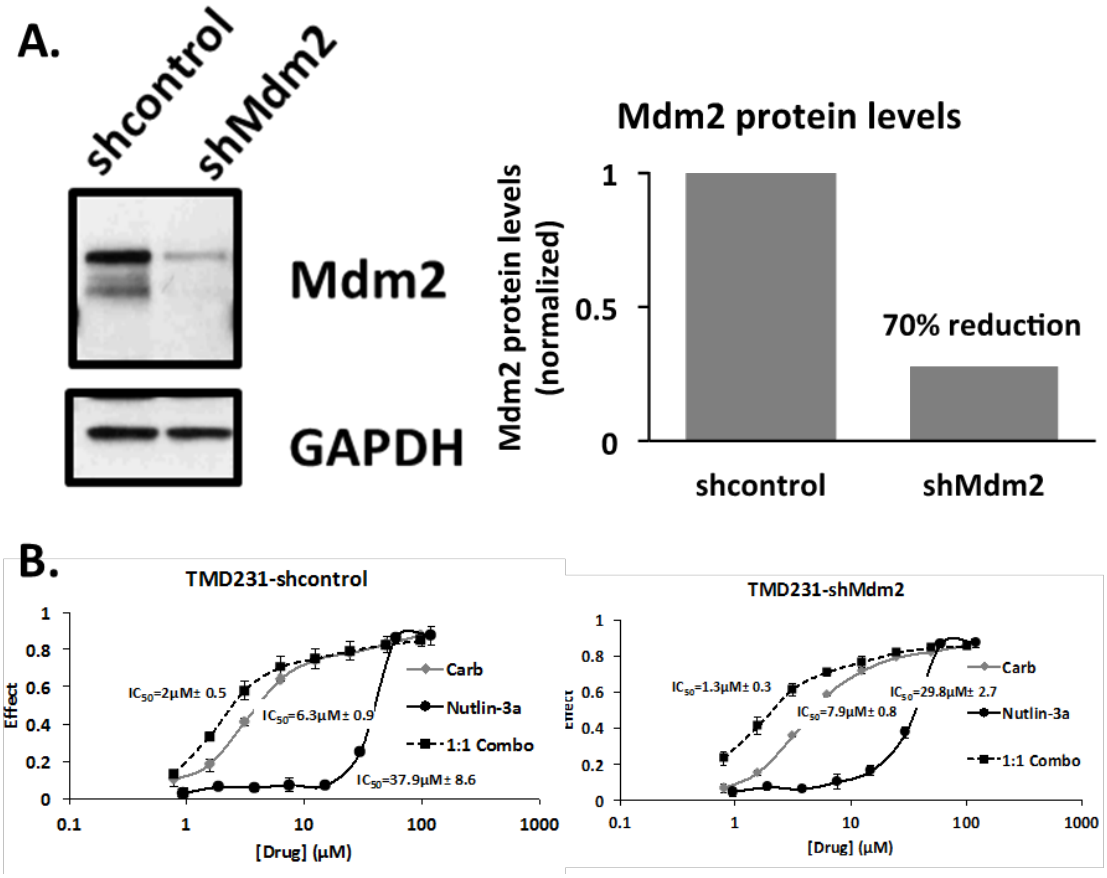

Figure 20. Mdm2 protein levels are reduced in TMD231-shMdm2 cells, but this does not confer cellular resistance to drug treatment. TMD231 cells were transduced with a lentiviral vector either expressing shMdm2 or shcontrol. (A) Western blot analysis showed decreased levels of Mdm2 in shMdm2 cells compared to the shcontrol cells. ImageJ analysis was used to determine that there was a 72% reduction in Mdm2 protein levels in the shMdm2 cells compared to the shcontrol cells. Protein levels were normalized to GAPDH loading control. (B) TMD231-shMdm2 and TMD231-shcontrol cells were treated with increasing concentrations of Nutlin-3a, carboplatin, or 1:1 combination for 5 days. Cells were fixed and stained with methylene blue, and cellular proliferation was evaluated. shMdm2 and shcontrol cells showed no difference in cell

proliferation following increasing Nutlin-3a, carboplatin or combination drug treatments. (C) Isobologram analysis for 1:1 combination treatment showed similar cellular sensitivity in both TMD231-shcontrol and TMD231-shMdm2 cells.

To confirm the effects on growth inhibition we observed using the methylene blue proliferation assay, we also used cell counting methods to examine changes in cell proliferation in the TMD231-shcontrol and TMD231-shMdm2 cells. TMD231-shcontrol and TMD231-shMdm2 cells were treated with DMSO, 15µM Nutlin-3a, 15µM carboplatin, and 15µM combination. Total cell counts were determined at Day 3-5 post treatment. Pictures of the TMD231-shcontrol and TMD231-shMdm2 cells on Day 3 of treatment showed morphological changes in the carboplatin and combination treated cells (Figure 21A). Interestingly, according to total cell counts, the shMdm2 cells were slightly more sensitive to Nutlin-3a treatment compared to TMD231-shcontrol cells on Day 3 and 4 (Figure 21B-C). However, there were no differences in total cell numbers in the TMD231-shcontrol and TMD231-shMdm2 cells for all treatments by Day 4 and 5 (Figure 21C), which is consistent with data from the methylene blue proliferation assay.

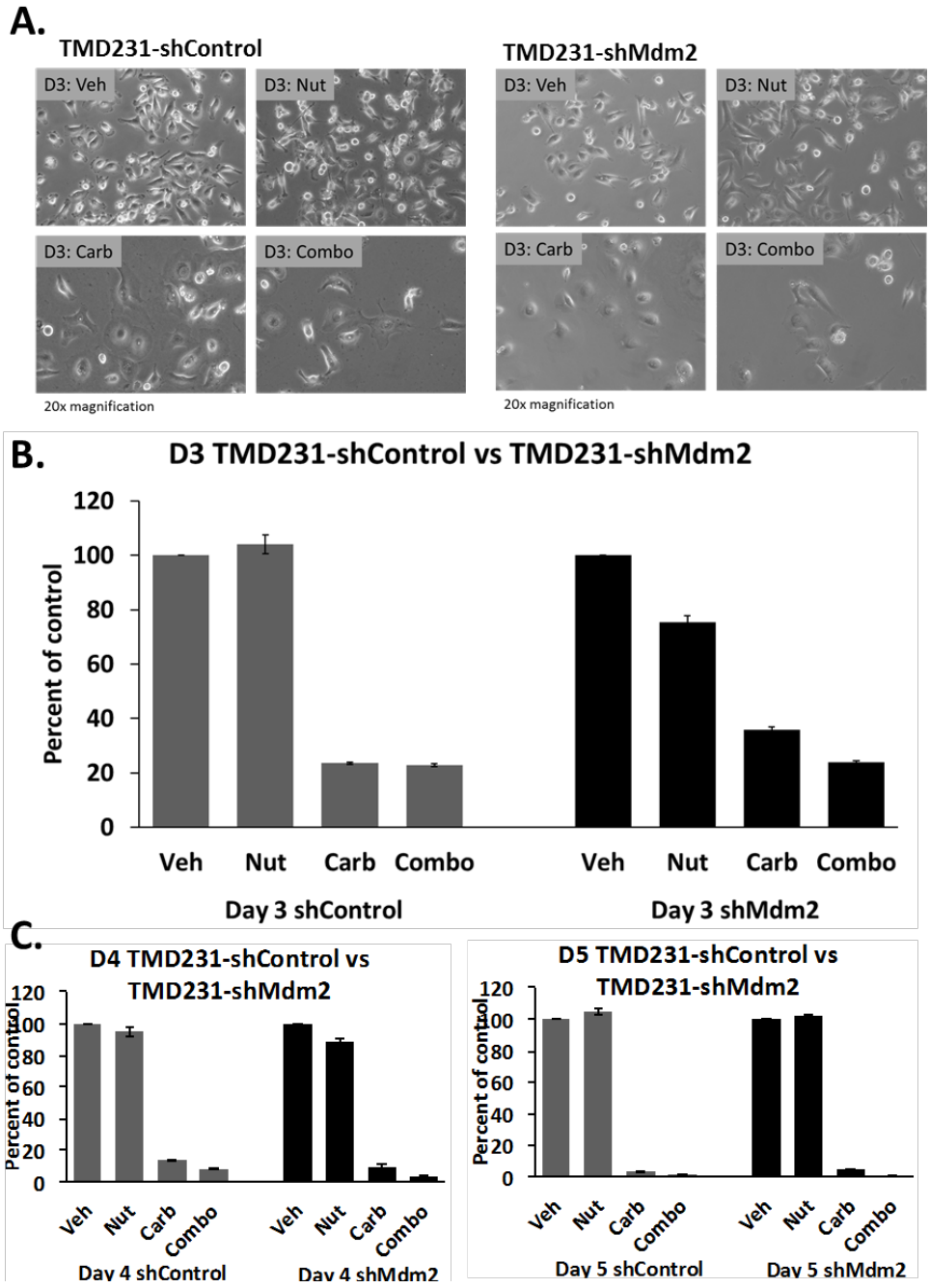

Figure 21. Decreased Mdm2 levels do not affect cell growth in the presence of Nutlin-3a, carboplatin, or combination treatment. TMD231 cells were seeded at 6.5 x 10^3 per well in 12-well plates on Day 0 and treated with 15µM Vehicle (Veh), Nutlin-3a (Nut), carboplatin (Carb), or 1:1 combination (Combo). (A) Pictorial representation of TMD231-

shControl and TMD231-shMdm2 cells on Day 3 post treatment. Magnification was 20X. (B) Graphical representation of cell counts on Day 3 from 15μM Nutlin-3a, 15μM carboplatin, or 15μM Nutlin-3a + 15μM carboplatin treated TMD231-shControl and TMD231-shMdm2 cells. In TMD231-shControl cells, there was no difference in cell number between 15μM carboplatin and 15μM Nutlin-3a + 15μM carboplatin combination treated cells. In the TMD231-shMdm2 cells, there was a significant reduction in total cells in the combination treated cells compared to the carboplatin alone treated cells (Student's t-test, $n=3$, $p<0.05$). (C) By Day 4 and 5, the TMD231-shControl cell counts closely resembled TMD231-shMdm2 and parental TMD231 cells with differences in cell numbers between the carboplatin and combination treated cells.

In this thesis, our objective was to investigate the p53-independent therapeutic potential of Nutlin-3a in combination with carboplatin. To this end, we elected to evaluate the role of the p53 family member, p73. Both p73 and p53 function similarly in the presence of DNA damage, and can activate the transcription of key target proteins involved in apoptosis [78,79,82,132]. We first determined to what extent the inhibition of cell growth was dependent p73 levels. Two approaches, transient and stable knockdown strategies, were utilized to knockdown p73 in TMD231 cells.

We opted to test the effect of a transient p73 siRNA knockdown approach. We utilized the SMARTpool: ON-TARGETplus siRNA for p73 and the ON-TARGETplus non-targeting pool as a control from Dharmacon (GE Healthcare). The SMARTpool: ON-TARGETplus siRNA is comprised of 4 different siRNA constructs pooled together for the gene of choice. There was significant p73 knockdown in the cells collected on Day 1 and 2-post transfection with reductions of p73 by 79% as measured by densitometry (Figure 22A). By Day 3 post transfection, the levels of p73 started to increase with knockdown of p73 less than 50% (data not shown). Wang *et al.* have demonstrated that Mdm2 can be a downstream transcription target of p73 and our data are consistent with their observations (Figure 22BA) [130]. Western analysis confirmed that decreased p73 levels correlated with decreased Mdm2 levels. (Figure 22B). The reductions in Mdm2 were about 71% and 65% at Day 1 and Day 2 post transfection, respectively. In the transient siRNA approach Mdm2 was knocked down to a larger degree (65-75% reduction) than in cells with the stable shp73 approach (30-37% reduction) (Figure 23B and Figure 24C). All densitometry measurements were normalized to GAPDH loading control for each lane.

We also probed sip73 cell lysates for MdmX, which has also been shown in the literature to bind to Mdm2 as well as have similar effects at the chromatin (Figure 22B) but did not observe any changes in MdmX levels [99].

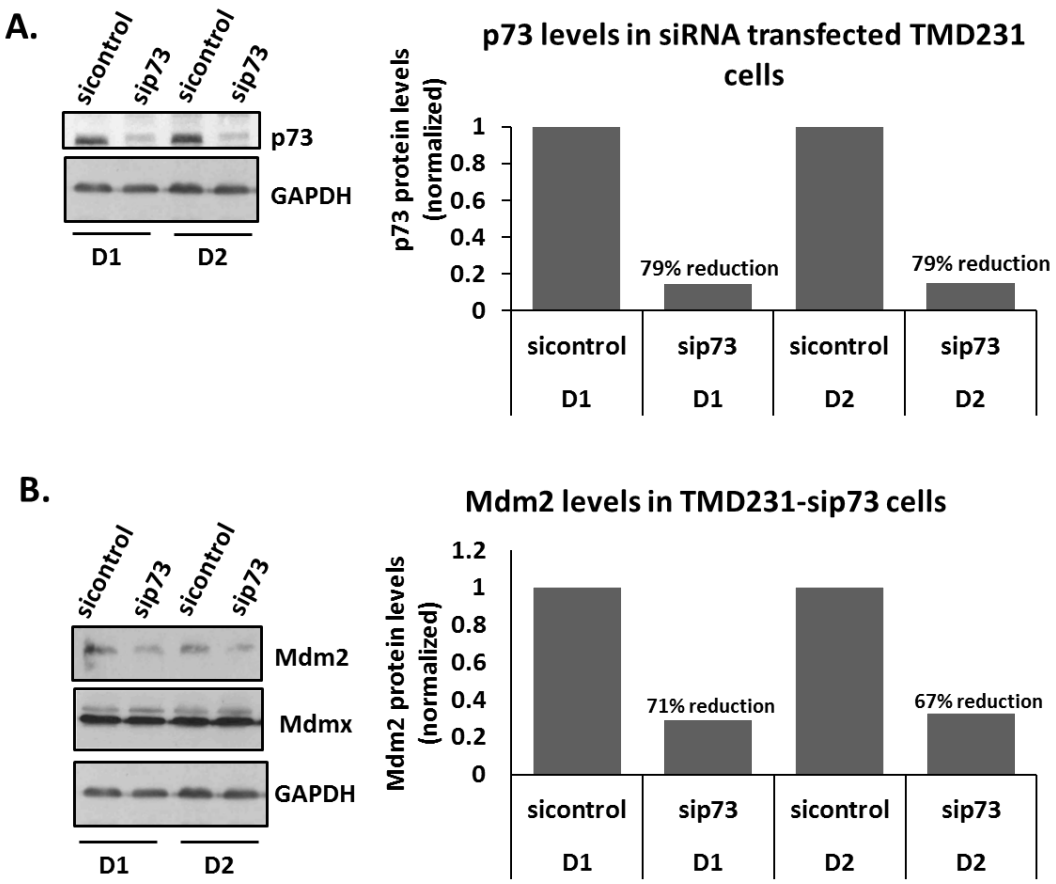

Figure 22. Transient transfection inhibited p73 levels for 2 days post transfection and this correlated with decreased Mdm2 levels. p73 knockdown increases resistance to carboplatin mediated-DNA damage. TMD231 cells were transfected with SMARTpool: ON-TARGETplus TP73 siRNA or ON-TARGETplus Non-targeting Pool. (A) Western blot analysis of p73 levels TMD231-sicontrol and TMD231-sip73 cells showed decreases in p73 in the TMD231-sip73 cells compared to TMD231-sicontrol cells. Graphical representation of p73 protein levels showed 79% reduction in p73 protein levels the TMD231-sip73 compared to TMD231-sicontrol cells on both 1 and 2 Days post transfection. Blot densitometry was evaluated using ImageJ. Protein levels were normalized to GAPDH loading control. (B) Interestingly, the levels of Mdm2 were

decreased in the TMD231-sip73 cells compared to the TMD231-sicontrol cells. Reduced p73 levels did not affect the levels of MDMX. Graphical representation of Mdm2 densitometry as determined using ImageJ showed 71% and 67% decreases in Mdm2 levels in the TMD231-sip73 on Days 1 and 2-post transfection, respectively. Protein levels were normalized to GAPDH loading control.

Next, we evaluated treatment sensitivity of p73 siRNA transfected cells compared to a non-targeting siRNA control cells using methylene blue proliferation assays. There were no differences in the IC_{50} values for the Nutlin-3a treated TMD231-sicontrol and TMD231-sip73 treated cells (Figure 23). However, in both the carboplatin alone and combination treated cells, there was a significant increase in IC_{50} values for the TMD231-sip73 cells compared to the TMD231-sicontrol cells (Figure 23). These results support our hypothesis that reduced p73 levels would decrease sensitivity to drug treatment. p73 signaling is important following DNA damage, which is caused by carboplatin. When p73 levels are reduced, there is less protein available to signal for pro-apoptotic proteins to be produced. Additionally, with less p73 present, there is also less Mdm2 present. It is not clear at this time why we did not see decreased sensitivity in the shp73 model but this could be related to differences in Mdm2 reduction seen in the stable versus transient knockdown approaches.

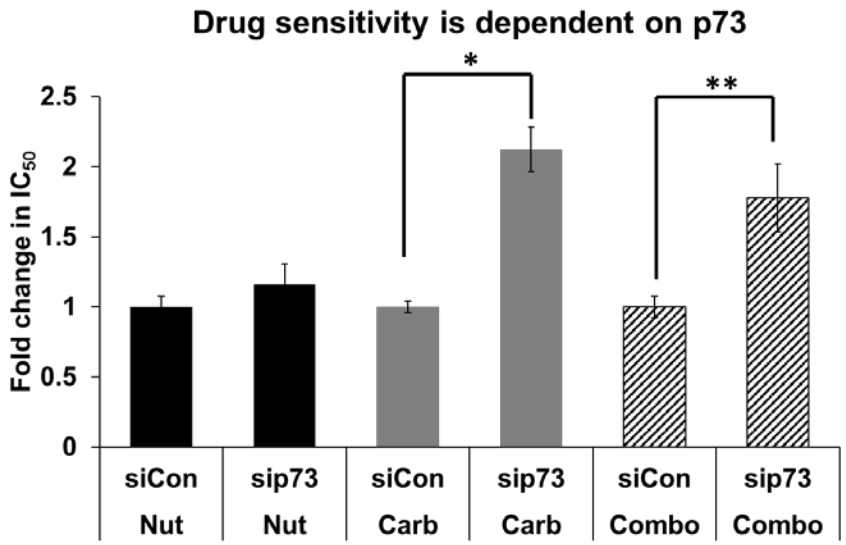

Figure 23. Sensitivity to carboplatin mediated-DNA damage is dependent on p73 levels in mtp53 TMD231 cells. TMD231 cells were transfected with SMARTpool: ON-TARGETplus TP73 siRNA or ON-TARGETplus Non-targeting Pool siRNA. On Day 1 post transfection, cells were seeded and treated with increasing concentrations of Nutlin-3a, carboplatin, and 1:1 combination for 3 days. Cell proliferation was evaluated using methylene blue staining. IC_{50} values were determined using Calcusyn. Cellular sensitivity to Nutlin-3a treatment was not inhibited by p73 knockdown. p73 inhibition led to decreased sensitivity to carboplatin treatment compared to non-targeting control cells. There was a significant increase in IC_{50} value for the carboplatin treated sip73 cells (80.1±13.4µM) compared to the control cells (37.7±3.3µM) (Student's t-test, *$p<0.05$, Carb siCon vs sip73, n=5, ±SD). Similar effects were seen with the 1:1 combination treated cells with the p73 knockdown cells being less sensitive to drug treatment. There was a significant increase in IC_{50} value for the 1:1 combination treated sip73 cells (20.8±6.3µM) compared to the control cells (11.7±2µM siCon) (Student's t-test, **$p<0.05$, Combo siCon vs sip73, n=5, ±SD).

For stable p73 knockdown, TMD231 cells were first transduced with 7 different lentiviral constructs to generate stable lines, and positively transduced cells were selected with puromycin. p73 levels were evaluated by Western blot. Two of the clones shp73-3-500 and shp73-4-500 exhibited the most knockdown and were selected for further study. We examined the levels of p73 and both of the shp73 constructs resulted in >90% knockdown of p73 (Figure 24A-B). Since we observed decreased levels of Mdm2 in the sip73 cells, we also examined the effects of shRNA to p73 on Mdm2 protein levels. In non-treated TMD231 cells with the shp73 constructs, there was about 30-40% reduction in Mdm2 levels as determined by densitometry using ImageJ software (Figure 24C). All densitometry measurements were normalized to GAPDH loading control for each lane. It has been shown in the literature that p73 can bind to the promoter of Mdm2 in increase its levels. Therefore, with less p73 present in the cells, there is a reduction in Mdm2 being produced by p73 activation [130].

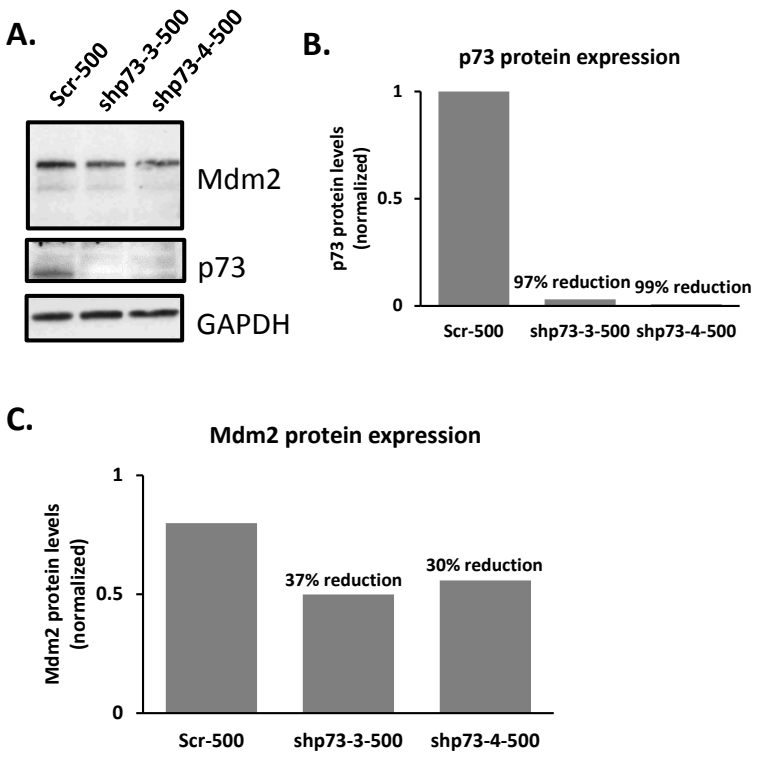

Figure 24. p73 protein levels are reduced in TMD231 cells stably transduced with shp73 lentiviral vectors and p73 decreases correspond to decreases in basal Mdm2 protein levels. TMD231 cells were transduced with lentiviral vectors expressing Scrambled control (Scr-500) and two constructs for shp73 (3-500 and 4-500). Transduced cells were selected using 2.5µg/mL puromycin for 2 days. All experiments were conducted under selective pressure. (A) Western blot analysis of p73 and Mdm2 in two different TMD231-shp73 cell lines. (B) p73 levels were greatly reduced in two shp73 (3-500 and 4-500) lines compared to the scrambled (Scr-500) control using ImageJ analysis. Protein levels were normalized to GAPDH loading control. (C) Interestingly, the two TMD231-shp73 cells lines also showed decreased levels of Mdm2. The Mdm2 protein levels were quantified using ImageJ. Protein levels were normalized to GAPDH loading control.

Next, we evaluated the effects of reduced p73 protein levels on cellular sensitivity to Nutlin-3a, carboplatin, or combination treatment using methylene blue proliferation assays. We expected that if p73 protein levels were reduced, the cells would less sensitive to drug treatment since there would be less p73 available to be involved with pro-apoptotic signaling. Also, with less p73 present, there would be less Mdm2 present. With less Mdm2 present, there would be less Mdm2 available to go to the nucleus and inactivate Nbs1 in the MRN complex. However, through discussions with Dr. Christine Eischen, very small amounts of Mdm2 can still locate to the chromatin and antagonize DNA repair through interactions with Nbs1. Knockdown of Mdm2 may lead to confounding data especially with the Mdm2/MdmX interplay and both of their roles on genomic instability. In the shp73 experiments, there was no difference on cell proliferation without any changes in IC_{50} values between the scrambled control and shp73 cells for Nutlin-3a, carboplatin, and combination treatments (Figure 25).

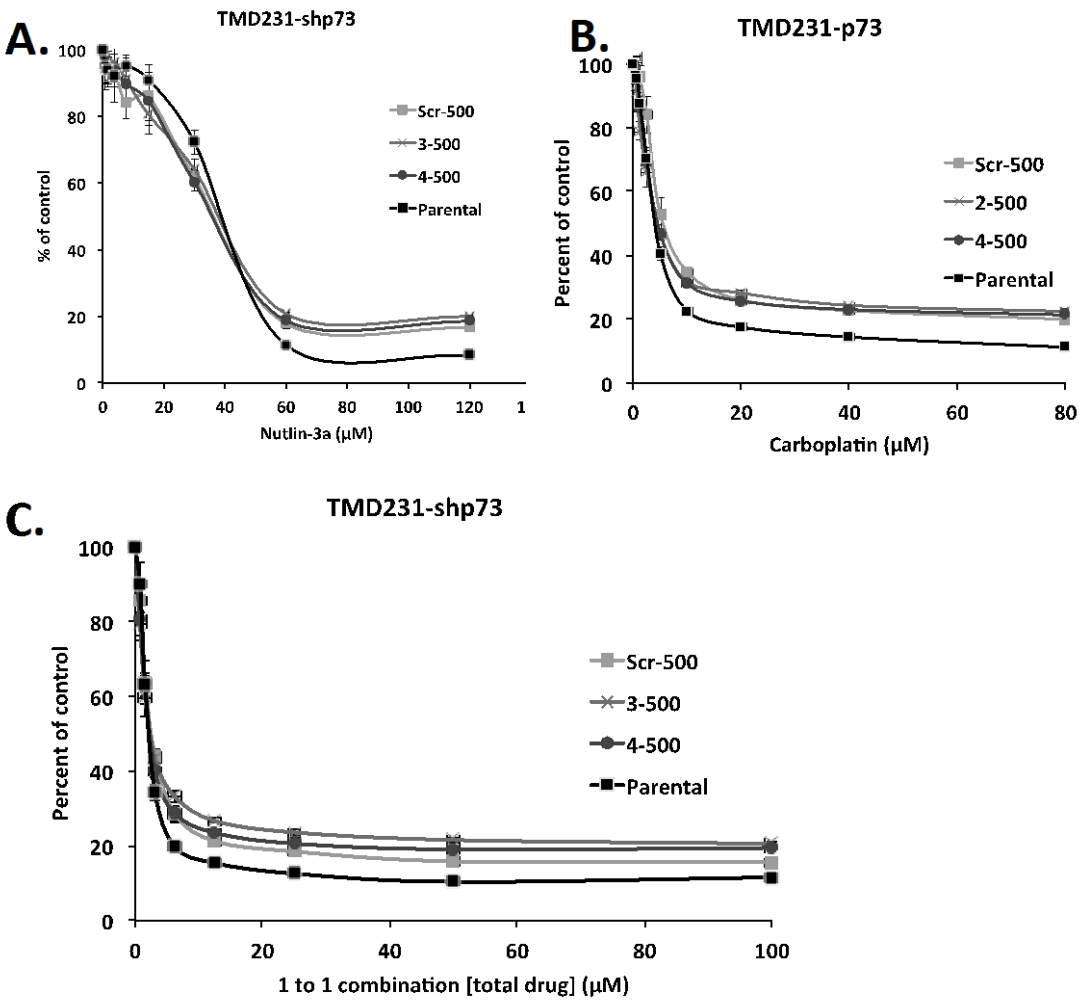

Figure 25. Possible off-target effects of stable lentiviral vector integration in TMD231 cells (shp73 versus shGFP control) impact ability to determine cellular sensitivity to single or dual drug treatment. TMD231-Scr and two TMD231-shp73 (3-500 and 4-500) cell lines were seeded in 96-well plates and treated with increasing concentration of Nutlin-3a, carboplatin, and 1:1 combination for 5 days. Cells were under selective pressure throughout the experiment with the presence of 2.5μg/mL puromycin. Cells were fixed and stained with methylene blue. Cell proliferation was examined, and both

TMD231-shp73 lines showed that cell proliferation was not different from TMD231-Scr cells following Nutlin-3a (A), carboplatin (B), or 1:1 combination (C) drug treatment.

In the literature, it has been shown that Mdm2 can also bind E2F1. The binding of E2F1 to Mdm2 can be inhibited with Nutlin-3a [65]. We wanted to evaluate the effects of E2F1 in our cellular mode by utilizing shRNA for E2F1. Several constructs were transduced into TMD231 cells, and following initial Western blot screening, constructs 327 and 328 showed the best knockdown of E2F1 (data not shown). However, the knockdown was about 50% and 30% for constructs 327 and 328 respectively, we opted to select TMD231 clones of the shGFP and shE2F1 327 and 328 to see if we could get clonal populations with a high efficiency of E2F1 knockdown. A series of clones were screened for E2F1 protein levels by Western blot (Figure 26A). One clone in particular, 328-6, had >90% knockdown of E2F1 (Figure 26B). Proliferation assays were completed with the shE2F1 clone 328-6 and two shGFP clones, GFP-3 and GFP-6, to evaluate the effects of E2F1 knockdown on cell sensitivity to Nutlin-3a, carboplatin, and combination treatment using methylene blue proliferation assays. Following analysis, the effects of drug treatments were difficult to interpret due to the shGFP control clones being similarly resistant to treatment or more resistant than shE2F1 clones (Figure 27). Since we have had trouble with the shcontrol vectors in the p73 model, it would be of great interest to repeat these experiments using siRNA to E2F1 and examine the effects of Nutlin-3a, carboplatin, and 1:1 combination treatment.

A.

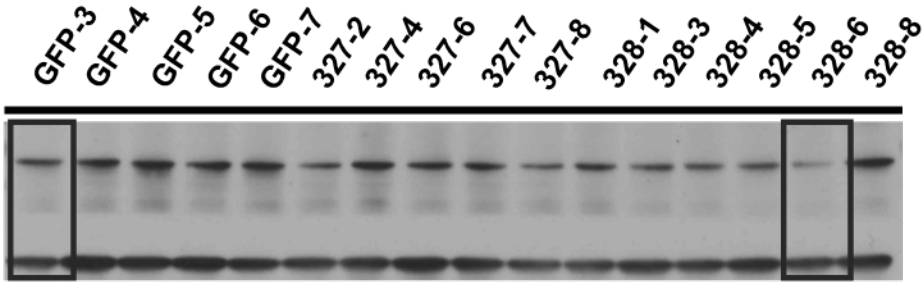

B.

Clone	% reduction in expression
GFP-3	-0.32
GFP-6	0.32
327-2	-24.33
327-8	21.06
328-4	34.78
328-6	97.35

Figure 26. TMD231-shE2F1 clone 328-6 had a significant reduction in E2F1 protein levels. TMD231 cells were transduced with lentiviral vectors expressing shGFP or shE2F1. (A) Clones were derived from the shGFP and shE2F1-327, and -328 constructs. Western blot analysis for several different clones showed one clone with significant reductions in levels of E2F1 (328-6). Protein levels were normalized to GAPDH loading control. (B) E2F1 levels were greatly reduced in one clone, shE2F1-328-6 compared to shGFP-3 using densitometry analysis with ImageJ software.

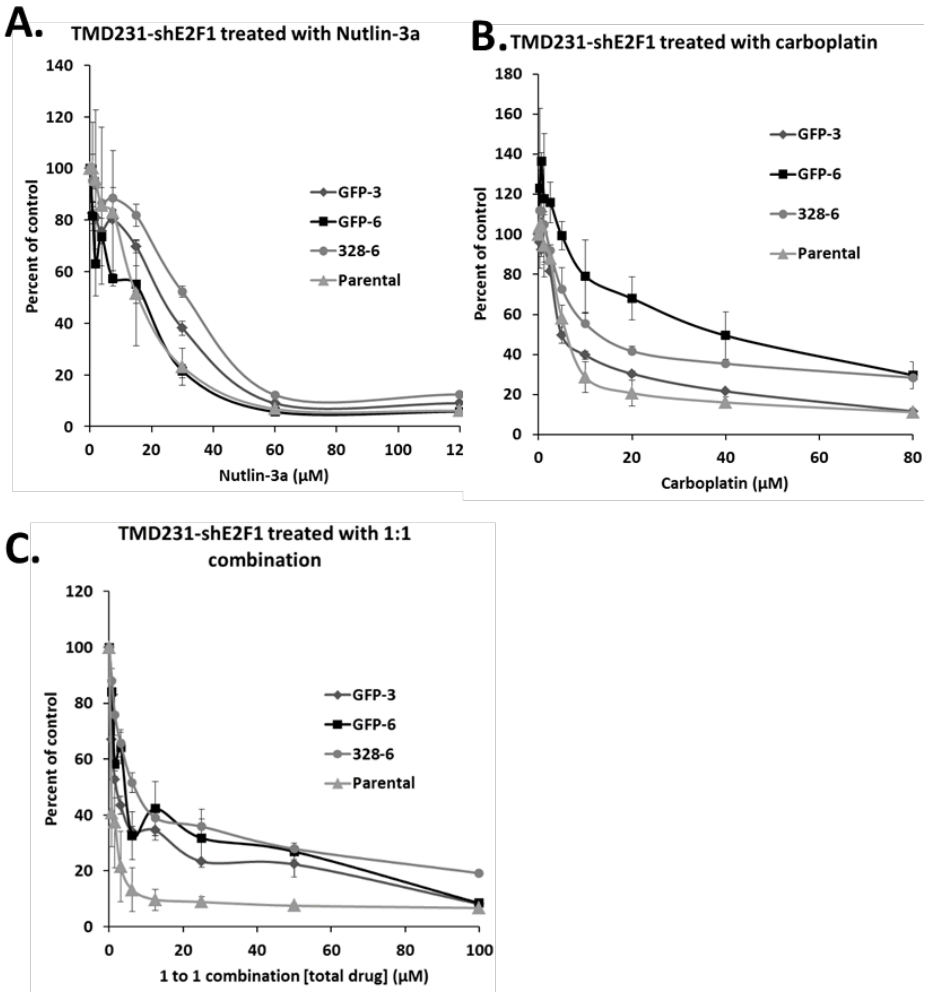

Figure 27. Lentiviral transduction of shRNA to E2F1 results in confounding data due to cellular drug resistance in shGFP control cells. TMD231 parental, TMD231-shGFP-3, TMD231-shGFP-6, and TMD231-shE2F1 (328-6) cells were evaluated for cellular sensitivity to Nutlin-3a, carboplatin, and 1:1 combination treatment using methylene blue proliferation assays. Cells were seeded in 96-well plates and treated with increasing concentrations of Nutlin-3a, carboplatin, and 1:1 combination for 5 days. (A-B) TMD231-shE2F1-328-6 cell proliferation was not different from TMD231-GFP-3 cells following Nutlin-3a and carboplatin. (C) shGFP cells were not different from shE2F1 cells following combination treatment.

As mentioned previously, Nutlin-3a was the first generation Mdm2 PPI to be studied in detail by Vassilev and colleagues [40] and has been used by many laboratories as a pre-clinical tool to study the effects of inhibiting protein-protein interactions with Mdm2 and its binding partners. As of 2014, there are now numerous second and third generation inhibitors some of which are currently being tested in clinical trials (www.clinicaltrials.gov). One these second generation molecules is a Nutlin-3a derivative compound, RG7112, which has increased potency (about 2X more potent than Nutlin-3a) and also has improved bioavailability and PK parameters *in vivo*. RG7112 has been used in Phase I clinical trials treating solid tumors and hematological neoplasms. In the past year, the RG7112 has become available to the research community. Therefore we elected to compare effects of RG7112 in combination with carboplatin. In TMD231 cells, RG7112 was approximately 2X more potent than Nutlin-3a as indicated by IC_{50} values (Figure 28A). However, the 1:1 combination of RG7112 and carboplatin was not as robust as Nutlin-3a+carboplatin and tended to produce an additive effect instead of a synergistic effect (Figure 28B). Additionally, RG7112- and Nutlin-3a-mediated effects on Mdm2 levels were compared via Western blot. RG7112 and Nutlin-3a treatment both induced Mdm2 levels, with RG7112 and Nutlin-3a inducing Mdm2 levels following 5µM and 10µM drug treatment (Figure 28C). At 20µM of RG7112 there was decreased levels of Mdm2, however, the cells were highly stressed and beginning to break down which may have affected the protein levels observed (Figure 28C).

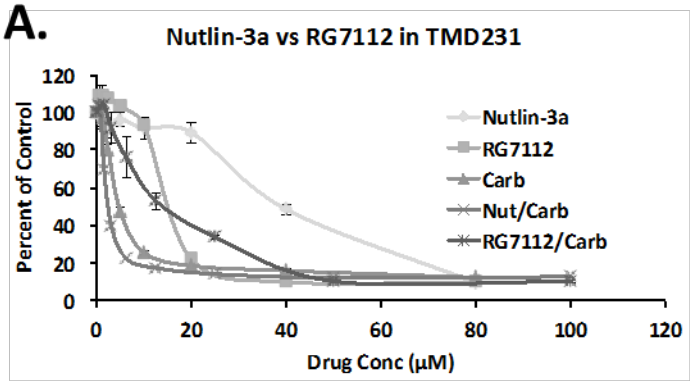

Drug Treatment	IC_{50}
Nutlin-3a	42.8µM±1.8
RG7112	16.5µM±3.5
Carboplatin	12.6µM±4.3
Nutlin-3a+carboplatin	1.2µM±0.3
RG7112+carboplatin	7.1µM±0.4

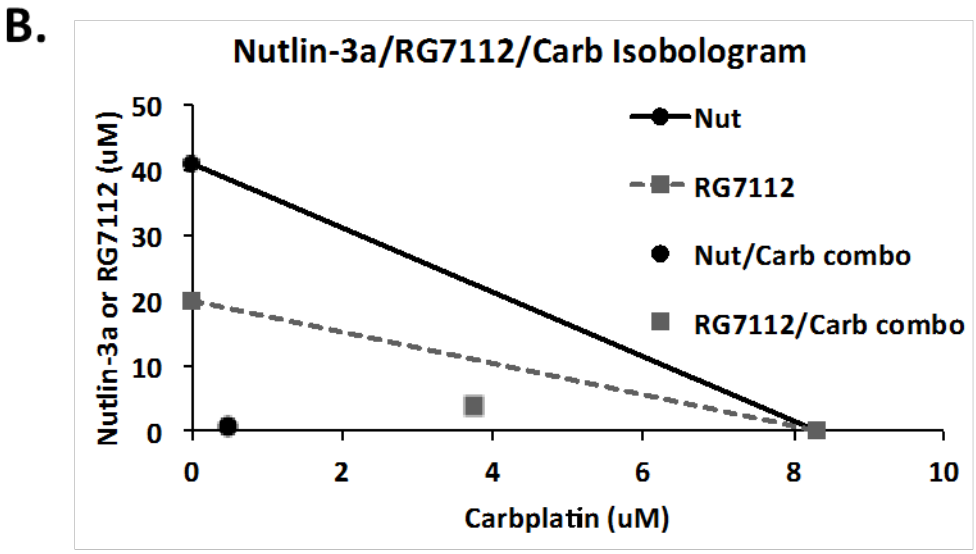

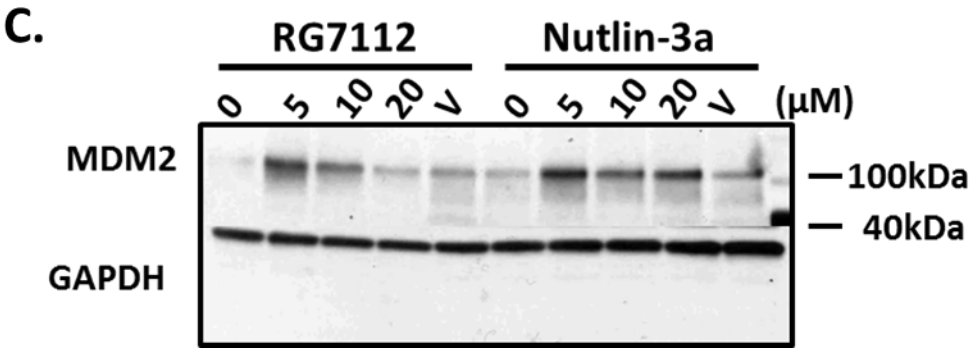

Figure 28. Nutlin-3a analogue, RG7112 alone, is more potent in TMD231 cells. TMD231 cells were treated with Nutlin-3a and second generation, RG7112, alone and in combination with carboplatin. TMD231 cells were seeded in 96-well plates and treated

with increasing concentrations of Nutlin-3a, RG7112, carboplatin, and combination treatments for 5 days. Cell proliferation was evaluated using methylene blue staining. (A) RG7112 alone is about twice as potent as Nutlin-3a alone with IC_{50} values half that of Nutlin-3a. However, RG7112 in combination with carboplatin is not as potent as Nutlin-3a in combination with carboplatin. (B) Isobologram analysis for 1:1 Nutlin-3a+carboplatin and 1:1 RG7112+carboplatin was evaluated. Nutlin-3a in combination with carboplatin had lower IC_{50} values compared to the combination of RG7112 and carboplatin. (C) RG7112 and Nutlin-3a treatment both induced Mdm2 levels, with RG7112 and Nutlin-3a inducing Mdm2 levels following 5µM and 10µM drug treatment.

C. **Discussion and Future Directions**

Nutlin-3a treatment increased Mdm2 levels with a corresponding dose-dependent increase in p21. Lau and colleagues showed that in p53 null cells, Nutlin-3a treatment led to increases in Mdm2; however, the mechanism by which Mdm2 increased was not determined [66]. Wang *et al*. demonstrated that p73α can bind to the promoter of Mdm2 and increase Mdm2 levels using luciferase constructs [130], which may explain why levels of Mdm2 increase following Nutlin-3a treatment and why when p73 is knocked down, there are decreases in basal levels of Mdm2. Through collaborations with Dr. Lindsey Mayo, we have luciferase constructs bearing the Mdm2 promoter in which we can test if p73 plays a role in promoting Mdm2 levels. We can also utilize the siRNA to p73 with co-transfection with the Mdm2 promoter luciferase constructs to visualize the dependency of p73 in this system. Additionally, we have p21 and PUMA-promoter-luciferase constructs to examine the effects on down targets in our model system. These experiments are ongoing in the laboratory. We did not observe notable changes in p73 or E2F1 protein levels following Western blot following increasing Nutlin-3a, carboplatin, or 1:1 combination treatment at 24 hours. While we did not observe increases in protein levels, increased protein stabilization, post-translational modifications, and/or subcellular relocalization of the protein may lead to downstream molecular changes in the cell. The protein-protein interactions between Mdm2 and E2F1 and Mdm2 and p73 should be examined following Nutlin-3a to ensure that in our system, Nutlin-3a inhibits the binding of Mdm2 from both E2F1 and p73. Preliminary results show decreased Mdm2 and p73 association following Nutlin-3a treatment in co-

immunoprecipitation experiments. Additionally, Dr. Mayo has generously provided dominant negative p73 and control constructs (p73DD and p73DD (L371P)) which can oligomerize with wild-type p73 and inhibits downstream p73-mediated effects by blocking the p73 DNA-binding [132,139]. The use of the dominant negative p73 construct could be used to confirm our siRNA p73 experiments showing that p73-mediated signaling is important following carboplatin-induced DNA damage. Also, there may be small changes in protein levels that cannot be detected by Western blot that may lead to important protein signaling events. Our next step is to utilize quantitative RT-PCR to examine the effects of single and dual treatment on mRNA levels changes in Mdm2, p73, E2F1, and PUMA. These data may be a more sensitive measure of the activity of mRNA upregulation in our system. The role of ΔNp73 should also be evaluated since it acts to negatively regulate Tap73 isoforms [140]. The ΔNp73 isoform also can act to negatively regulate wild-type p53, which would be important in that molecular context if ΔNp73 is signaling aberrantly [140]. Additionally, ΔNp73 can inhibit TAp73 and p53 by competing for binding sites at the chromatin and thus inhibiting target gene expression [141]. More studies would need to be completed to more fully understand the role of ΔNp73 in our model system.

While we did not see increases in PUMA protein levels (Figure 17), expanded time course studies and cell synchronization studies may help to discern if PUMA is a major player in our model system. Through collaborations with Dr. Lindsey Mayo, we also have luciferase constructs for the p21 and PUMA promoters, which may help to understand the effects of dual Nutlin-3a and carboplatin treatment on gene levels.

Expanded time courses may show increased protein levels, however, as mentioned above, some of these drug effects may mediate increased protein activity and/or re-localization of proteins rather than increases in protein levels. These studies are ongoing in the laboratory. In the TMD231 model, some experiments have shown increases in p73 protein levels following carboplatin or combination treatment while other experiments exhibited very high levels of basal p73α. It has also been shown in the literature, that the epidermal growth factor receptor (EGFR) and a constitutively active variant (EGFRvIII) can play a role in inhibition of apoptosis by inhibiting PUMA. In some instances, EGFR is able to evade lysosomal-mediated degradation and can traffic to other organelles within in the cell including the mitochondria [142]. When EGFR is located at the mitochondria, it was shown to bind to PUMA inhibiting pro-apoptotic signaling [143]. Constitutively and while under stress conditions, EGFR and EGFRvIII can bind to PUMA, sequester PUMA in the cytoplasm, and inhibit its translocation into the nucleus [143]. In our model system, >95% of the TMD231 cells express the EGFR on the cell surface (data not shown) and whether PUMA interacts with EGFR in TMD231 cells has not been studied. More work would need to be completed to better understand the interplay between EGFR and PUMA interactions within our model system.

It has also been shown in the literature that Yap1 plays dual roles in the cell by blocking upregulation of Itch (ligase that can ubiquitinate p73α) as well as stabilizing p73α and increasing upregulation of pro-apoptotic gene levels [75-77]. Enhancement of Yap1 interaction with p73 in the context of DNA damage may lead to an enhanced cellular response when combined with Nulin-3a and carboplatin in our model system. It

has been shown that the inhibition of Akt-mediated phosphorylation of Yap1 led to increased nuclear localization of Yap1 to bind to p73 and induce apoptosis [144]. Studies by Mayo and Donner showed that Mdm2 is phosphorylated at Serine 166 and 186 by Akt, resulting in the relocation of Mdm2 to the nucleus [43]. If Akt signaling is aberrant in our model, there could be increased Akt activity leading to more Mdm2 in the nucleus. Mass spectrometry could be used to examine the phosphorylation status of Serines 166 and 186 in our model. There are also commercially available antibodies for both phospho- serine 166 and 186 to examine these phosphorylation sites by Western blot. These changes in Mdm2 localization could influence the fine balance between life and death. Several Akt inhibitors are currently being used in clinical trials specifically treating breast cancers including MK2206 [145], GSK2141795 (GSK), and AZD5363 (AstraZeneca) (clinicaltrials.gov). Inhibition of Akt signaling may increase the multi-targeted effect of combination Nutlin-3a and carboplatin in TNBC cells with mutant p53. Ongoing studies in the laboratory have indicated that combination second-generation Mdm2 antagonists and AKT inhibitors are synergistic in inhibiting growth of primary patient-derived GBM cells *in vitro* (unpublished observations, Ding, Saadatzadeh, and Pollok).

Following combination treatment, chromatin association assays revealed increased Mdm2 in the chromatin fraction compared to single drug alone. Increased association of Mdm2 with the chromatin fraction may account for why cells are more sensitive to combination treatment. As described earlier, Eischen and colleagues previously demonstrated that localization of Mdm2 in the chromatin fraction correlated with Mdm2 specifically binding to Nbs1 leading to inactivation of the MRN complex and

inhibition of DNA repair due to a block in the cell's ability to signal that DNA damage has occurred [35]. This delay in repair may be essential in deciding cell fate and pushing the treated cells towards cell death. To provide further information on the outcome of increased localization of Mdm2 in the chromatin following combination treatment, future studies could focus on determining to what extent Mdm2 specifically binds to Nbs1 in the MRN complex following treatment. Co-immunoprecipitation experiments could be conducted from lysates isolated from the chromatin fraction to examine the binding of Mdm2 and Nbs1. This is especially important as Mdm2 can also bind to the promoter of genes to upregulate transcription as well binding to other transcriptional factors at the chromatin [92,146,147]. Additionally, it would be informative to follow up on determining the effects of combination treatment on MdmX levels at the chromatin since it has been shown that MdmX can act similarly as Mdm2 and inhibit Nbs1 in the MRN complex following DNA damage 5. The knockdown of Mdm2 by shRNA were not interpretable due to the fact that Mdm2 levels could not be completely knocked down. As described in detail earlier, Mdm2 is a multi-functional protein that plays a role in numerous aspects of growth and survival; therefore, complete knockdown of Mdm2 is unlikely.

Increasing our understanding of the DNA damage/repair kinetics following carboplatin and Nutlin-3a combination treatment will also be important in future studies. We explored technologies that would help us gain a better understanding of the DNA damage/repair kinetics in model systems used within our laboratory. In the TMD231 cells, inductively-coupled plasma mass spectrometry (ICP-MS) was used to

quantitatively ascertain the amount of platinum adducts bound to DNA from extracted DNA samples from single and combination treated cells overtime. However, while there were trends showing increased levels of Pt adducts bound to DNA in combination treated cells, the assay was highly variable and we elected to re-prioritize our approach. The role of combination carboplatin and Nutlin-3a treatment on the NER pathway should also be examined to see if Nutlin-3a leads to any inhibition in the NER pathway. Additionally, as DNA damage continues to accumulate in cells, the role of HR will also become important as DNA double strand breaks form and the role of Mdm2-mediated inhibition of Nbs1 should be examined in this context.

Stable levels of shRNA that target p73 and E2F1 via lentiviral vectors led to decreased levels of target proteins. However this did not confer altered cellular sensitivity to any of the drug treatments. These data are difficult to interpret due to the off target effects of the control vectors used. Based on our data, transient transfection of p73 lead to decreased cellular sensitivity to carboplatin and combination treatments with significant increases in IC_{50} values in the p73 knockdown cells compared to control knockdown cells. Experiments are ongoing in the lab utilizing siRNA to E2F1 to determine if the effects of reduced E2F1 in our system following combined Nutlin-3a and carboplatin treatment. Our hypothesis is that when E2F1 levels are reduced, the cells should be less sensitive to DNA damaging treatment since there will be less E2F1 present to upregulate pro-apoptotic genes.

While the clinical grade Mdm2 antagonist RG7112 and carboplatin are synergistic in inhibiting growth of TMD231 cells, it is interesting to note that the growth-

inhibition effect was less potent than the Nutlin-3a:carboplatin combination. The IC_{50} for the RG7112:carboplatin combination was 7.1±0.4μM compared to 1.2±0.3μM for the Nutlin-3a:carboplatin combination. More studies would need to be completed with RG7112 or other Mdm2 inhibitors to better understand the differences in these compounds and the subsequent effects in cancer. This difference in potency when RG7112 is combined with carboplatin compared to Nutlin-3a/carboplatin combination treatments, may have to do with increased selectivity of the RG7112 for the Mdm2 binding pocket in the context of p53 and not with other Mdm2 binding partners. While it is well documented that p73α interacts with N-terminal hydrophobic pocket, it is possible that binding in the pocket is slightly different. It is not known as this time to what degree RG7112 can block binding of p73α to the hydrophobic pocket of Mdm2 and this is currently being investigated in the laboratory. We have also seen similar differences in RG7112 and Nutlin-3a combinations with DNA damaging drug, temozolomide in wtp53 GBM and neuroblastoma cells suggesting that either selectivity for the Mdm2 binding site or other off-target effects could be the underlying reason for the difference in potency of effect between RG7112 and Nutlin-3a.

RG7112 is currently being used in several Phase I clinical trials treating hematologic neoplasms (NCT00623870) and advanced solid tumors (NCT00559533) (clinicaltrials.gov). Results from clinical trials showed that the major dose-limiting factor toxicity was thrombocytopenia. Iancu-Rubin *et al.* reported that RG7112 leads to thrombocytopenia through two distinct mechanisms: the RG7112-mediated p53 activation affected megakaryocytopoiesis and impaired platelet production [148]. The

effects were reversible following cessation of treatment indicating that optimization of dosing schedules will be key for future trials. Higgins and colleagues showed dosing with another second generation Nutlin-3a compound, RG7388, that a 50mg/kg weekly dose was equivalent in efficacy to 10mg/kg daily dosing in an osteosarcoma model showing that intermittent dosing schedules may be better in the clinic since RG7112 did not have high patient tolerability [149]. Drug dosing optimization will be important in the design of both animal and clinical studies utilizing these new therapeutic agents.

Chapter 3. Aim 3: Development and validation of *in vivo* animal model of human triple-negative breast cancer

A. Background and Rationale

The use of *in vitro* cell culture continues to be the initial screen for assessing the potential of new therapeutic approaches. *In vitro* cell culture allows the investigator to evaluate cellular sensitivity to drugs and delve into in signaling mechanisms altered by anti-cancer agents. However, to fully evaluate the promise of a new therapy, *in vivo* models that can assess drug efficacy and toxicity need to be included. In this thesis project, we focused on TNBC that forms metastatic lesions in the lung and first elected to determine if we could improve upon the current *in vivo* models that utilized Nude mice. While there are murine models of breast cancer, these models only study mouse cellular sensitivity to the drugs and are not as clinically relevant human models. To study human breast cancer in mouse models, we must utilize mouse models in which the immune system is not intact so that the human cells are not the targets of the murine immune system. As described previously, there have been numerous types of immunocompromised mouse models used to study human cancers through the years. However, based on available mouse models, we chose to examine the tumor growth and metastasis kinetics of the TMD231 human breast cancer cells in two different mouse strains, NOD/scid and NOD.Cg-Prkdc^{scid}Il2rg^{tm1Wjl}/SzJ (NSG) mice. Both of these mouse strains have severely compromised immune systems.

Nod/scid mice were developed following the development of nude mice to provide an enhanced immune compromised mouse strain better equipped to study human hematopoietic cells and human cancers. While Nod/scid mice produce defective natural killer (NK) cells, there is still some residual NK activity, and the mice have a high incidence of thymic lymphoma. NSG mice were developed in an effort to create mice suitable to study human blood diseases. NSG mice allow for the engraftment of human peripheral blood and bone marrow. In NSG mice, there is increased engraftment of malignant and nonmalignant human hematopoietic cells. NSG mice do not produce NK cells due to the lack of normal interleukin 2 (IL-2) receptor expression, which prevents normal NK-cell development. NSG mice also have a very low incidence of thymic lymphoma with increased life expectancy [23]. NK cells are involved in recognizing cells that are in stressed states in which stress ligands are expressed on the exterior of the cell [150]. Additionally, NK cells recognize 'non-self' ligands expressed on the cell surface and especially detecting circulating tumor cells. It was shown mouse NK cells can be involved in the rejection of tumors *in vivo*, and this was dependent on the tumor cells expressing NK ligands [151]. The absence of NK cells in the NSG mice would allow for better tumor engraftment especially with the use of human cancer cells. The comparison of mouse strain allowed for the optimal mouse strain to be used to ensure consistent tumor take as well as validate the metastasis from the primary tumor to the lung.

The need for a sensitive measure of tumor burden in a non-invasive manner is needed when using animal models to study human cancers. Measurements of primary

tumor volume by caliper have been an accepted way to determine tumor volume; however, the tumor must be palpable to ensure accurate measurements. When studying aggressive cancer models, the need to begin drug therapy at an early time point in tumor development is highly critical especially since in many tumors, there is a size threshold in which efficacy and length of treatment of window is impacted. To this end, our objective was to design an animal model in which the tumor cells could be visualized and accurately measured in non-palpable tumors growing under the mammary fat pad. There are numerous imaging modalities that would allow for the sensitive detection of tumors *in vivo*. Bioluminescent imaging is very sensitive but there are some disadvantages. The substrate for bioluminescent imaging must be injected into mice in which delivery can be impacted depending on tumor location. Additionally, the mice must be in general good health and well-hydrated otherwise blood flow can be altered and this could easily alter delivery of the luciferin substrate to the site of the tumor cells. Scans are typically 20-45 minutes for BLI. While bioluminescent imaging is very sensitive, the disadvantages outlined here would need to be evaluated in the design of animal studies and the questions posed.

Using fluorescent imaging, the tumor cells express a fluorescent protein. Using an optical imager, the fluorescent protein can be excited using a laser and the emission can be captured using a camera. Fluorescent imaging allows for a snapshot of the fluorescent intensity to be collected in less than 10 minutes. The biggest advantage of fluorescent imaging is that it excludes problems associated with delivery of a substrate due to compromised blood flow to the tumor. There does need to be careful planning

when choosing a fluorescent protein to use for *in vivo* imaging. The excitation and emission spectra should be optimized for the specific laser/filter set in the optical imager. Also, some fluorescent proteins overlap with other proteins that auto-fluoresce. For example, the excitation/emission spectra for the green fluorescent protein (GFP) is also within the range of auto-fluorescence of hemoglobin as well as chlorophyll which is often added to murine food sources [152]. The use of near-infrared (NIR) proteins eliminates much of the signal loss due to surrounding tissues as well as auto-fluorescent proteins [152]. In our system, we opted to use the far-red fluorescent protein, E2-Crimson, which was optimal for the laser/filter set of the optical imager, Optix MX3 (ART Technologies). Following implant, the TMD231 cells expressing the E2-Crimson fluorescent protein (TMD231-CR) could be visualized as early as two hours following implant. We used the TMD231-CR cells to visualize and measure fluorescent intensity as a measure of tumor volume which could be used to randomize the mice into treatment groups at a very early time point (Day 7).

Throughout the fluorescent protein *in vivo* imaging validation process, a series of studies were used to determine the relationship between fluorescent intensities measured by *in vitro* and *in vivo* imaging and cell number. We tested the imaging sensitivity of the Optix MX3 (ART Technologies) with our TMD231-CR cells both *in vitro* and *in vivo* to better understand the fluorescent intensity measurements as they related to cell number. We also validated if fluorescent intensity correlated to tumor volume *in vivo* to determine if fluorescent imaging would be a feasible way to measure tumor volume in non-palpable tumors. Initial tumor burden could be accurately assessed by

this methodology and mice randomized into treatment groups based on the photon emission. However, we also discovered that evaluation of treatment effects by fluorescent imaging was not possible due to tissue attenuation of signal, lack of depth sensitivity, and possible presence of residual E2-Crimson protein in the tumor mass.

B. ***In vivo* animal model optimization and validation of fluorescent imaging**

The types of immunodeficient mouse strains have vastly improved over the past decade and offer an opportunity to explore and optimize the use of the metastatic breast cancer cell line TMD231. Our laboratory as well as others has found that NOD/scid and NSG mice provide a tumor microenvironment that increases tumor take frequency and consistently provides mice with similar baseline tumor sizes. The MDA-MB-231 cells were originally passed through Nude mice, and tumors were resected and grown in culture forming the TMD231 cell line [17]. We compared two different immunodeficient mouse strains, NOD/scid and NSG to evaluate the kinetics of tumor growth and metastasis to the lung. Over time, the primary tumors in the NSG mice grew larger and at a faster rate compared to the tumors implanted in the NOD/scid mice (Figure 29A). During the study, groups of mice were also sacrificed starting at 28 days post-implantation of TMD231 cells. In NSG mice, metastases in the lungs were evident as early as 28 days post implant and the number of metastatic foci increased over time at Days 35 and 49 days post implant. However, in the NOD/scid mice, metastases in the lungs were not detected until 72 days post implant (Figure 29A inset graph). H&E staining of excised lungs confirmed metastases in the lungs of NSG mice implanted with TMD231 cells in the mammary fat pad (Figure 29B; compare normal mouse lung (i) to multiple metastatic foci (ii) in the lungs). Many of the lung foci were large and coalescing into one another (iii). Tumor emboli were observed in some mice blocking blood flow within in the lungs (iv). Circulating tumor cells were also observed within the blood vessels of the lungs (v). The mitotic index was high with about 4+ mitotic figures per

high power field (vi). Based on the increased tumor growth kinetics and improved metastasis to the lungs in the NSG mice, we chose to continue our future animal studies using NSG mice.

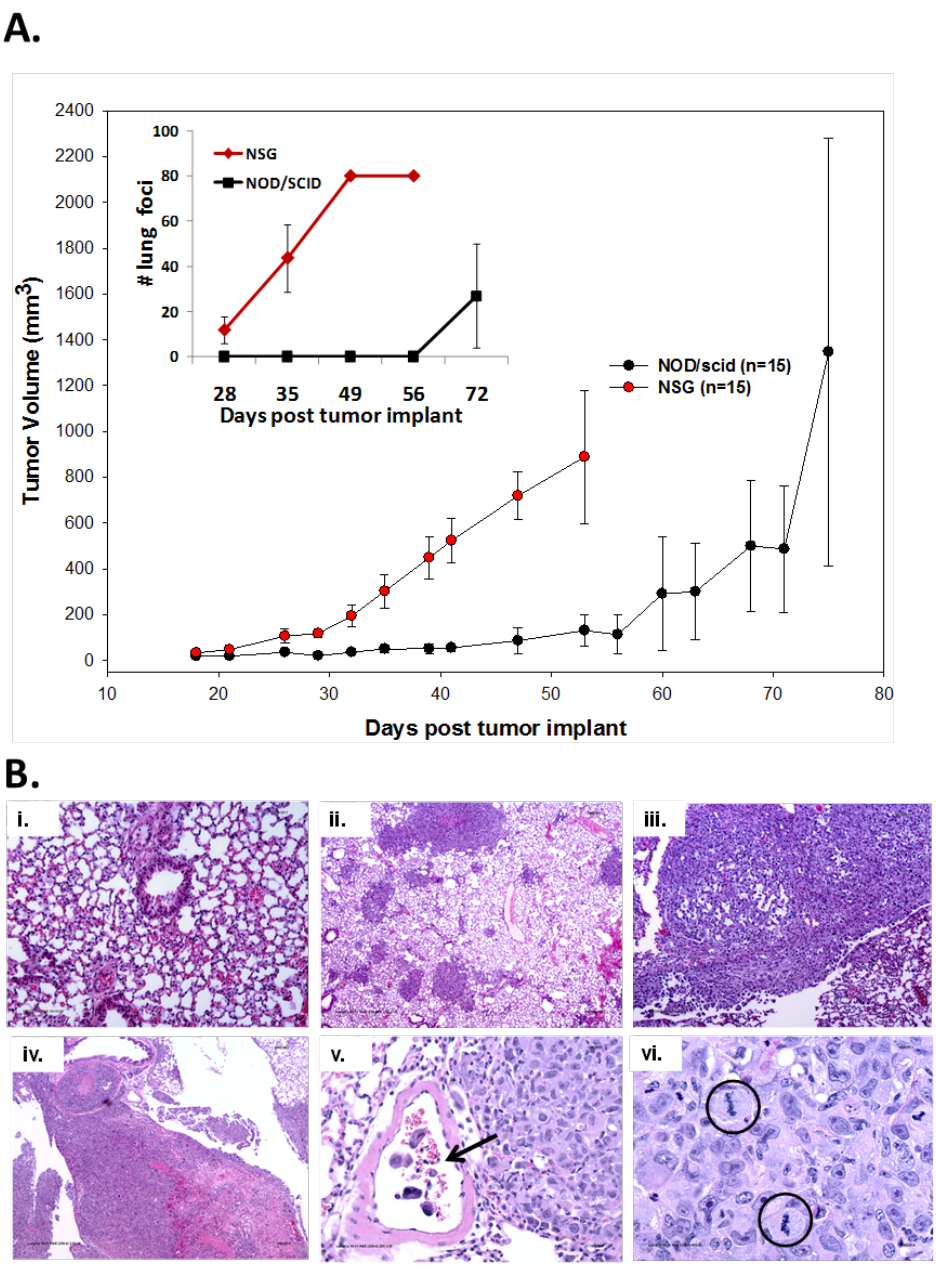

Figure 29. TMD231 tumor and metastasis is increased in NSG mice compared to NOD/Scid mice. NOD/scid and NSG mice were implanted with 1x10^6 TMD231 cells into the mammary fat pad and allowed to grow. Tumor growth in the mammary fat pad was monitored via caliper over time. Mice were sacrificed throughout the study to evaluate the formation of lung metastases. (A) Tumors had increased growth kinetics in the NSG

mice compared to NOD/scid mice. Additionally, there were increased lung metastases with foci detected as early as 28 days post implant. Metastases were not detected in NOD/scid mice until 72 days post implant. (B) Histology using H&E staining confirmed metastases in the lungs of NSG mice implanted with TMD231 cells in the mammary fat pad. Normal mouse lung (i) compared to multiple metastatic foci (ii) in the lungs. Metastatic foci were numerable (>50 small to moderate foci to too numerous to count). Many of the foci were large and coalescing into one another (iii). Tumor emboli were observed in some mice blocking blood flow within in the lungs (iv). Circulating tumor cells were also observed within the blood vessels of the lungs (v). Mitotic index was high with about 4+ mitotic figures per high power field (vi).

In the development of the *in vivo* animal model to study human breast cancers, we discovered it was necessary to develop a more sensitive and accurate measure of early tumor burden especially since the TMD231 are very aggressive growing cells *in vivo*. We were looking for a non-invasive, easily measureable, and highly sensitive manner in which to determine early tumor burden. Once the mammary fat pad tumors become palpable, we determined that the treatment window is very short and can prevent the use of full treatment schemas. Before this model optimization was conducted, it routinely took nearly two weeks of tumor growth before most tumors would be measurable using a caliper. The endpoint of the studies was reached when the primary tumors reached ~1000mm^3 tumor volume which took about 6-8 weeks when 1x10^6 TMD231 cells were implanted into the mammary fat pad. Since the study time frame was typically about 8 weeks, there was not much time remaining for drug treatments. At the initiation of treatment, our objective was to start with a reasonable tumor volume so that the tumor to body size ratio of the mice was comparable to the tumor to body size ratio we might find in clinical situations (topic presented by Dr. Susan Clare, "Delivery of nanovectors in vivo by hitching a ride with the Immune System" at Drug Delivery and Cancer: Challenges and New Directions for Cancer Therapy, Purdue University, 2011). In collaboration with Dr. Helmut Hanenberg, we designed a lentiviral vector construct that expressed the E2-Crimson fluorescent protein (Figure 30A). The E2-Crimson fluorescent protein had excitation and emission spectra that best matched the laser/filter set of the *in vivo* fluorescent imaging machine, the Optix MX3 (Figure 30C) (ART Technologies). The TMD231 cells were transduced with the E2-Crimson

lentiviral sup and became known as TMD231-CR. The TMD231-CR cells were evaluated using flow cytometry and TMD231 parental cells were used as a control. The TMD231-CR cells were >80% positive for the E2-Crimson fluorescent protein and this allowed us to maintain the original population of TMD231 cells and not select for a subpopulation which could have different cellular and molecular responses to treatment (Figure 30B).

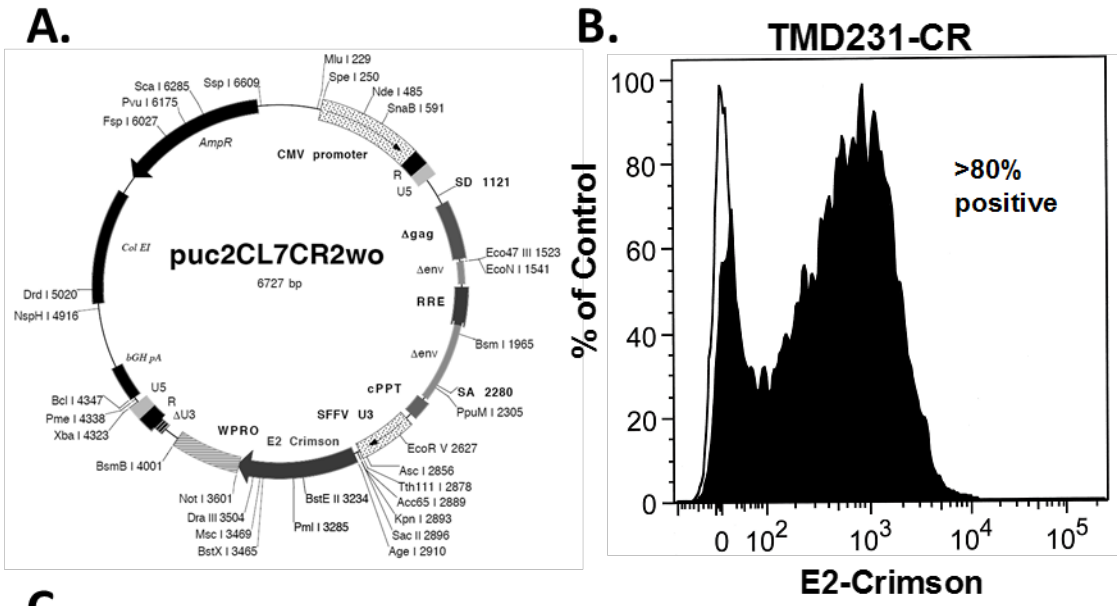

C.

Fluorescent protein	Excitation (nm)	Emission (nm)
E2-Crimson	611	646

Figure 30. TMD231 cells stably express the E2-Crimson fluorescent protein. (A) E2-Crimson fluorescent protein was expressed in the puc2CL7CR2wo lentiviral vector under a SFFV promoter. (B) TMD231 cells were transduced with the E2-Crimson lentivirus. Transduction efficiency was determined using flow cytometry with about 80% positive cells (TMD231-CR). (C) The excitation and emission spectra was 611/646nm.

Since the TMD231-CR was transduced with a lentiviral vector, which can integrate at random into the genome, we wanted to test the cellular sensitivity of the TMD231-CR cells to our drug treatments using methylene blue proliferation assays. The TMD231-CR cells had similar sensitivity as the parental TMD231 cells (Figure 31). In the TMD231-CR cells, the IC_{50} value was 22.7μM±1.1 for Nutlin-3a, 7μM±0.3 for carboplatin, and 1.1μM±0.1 for the combination treatments (Figure 31B) compared to 19±3μM for Nutlin-3a, 6.3±1.9μM for carboplatin, and 0.7±0.5μM for combination treatments in TMD231 cells (Figure 31A).

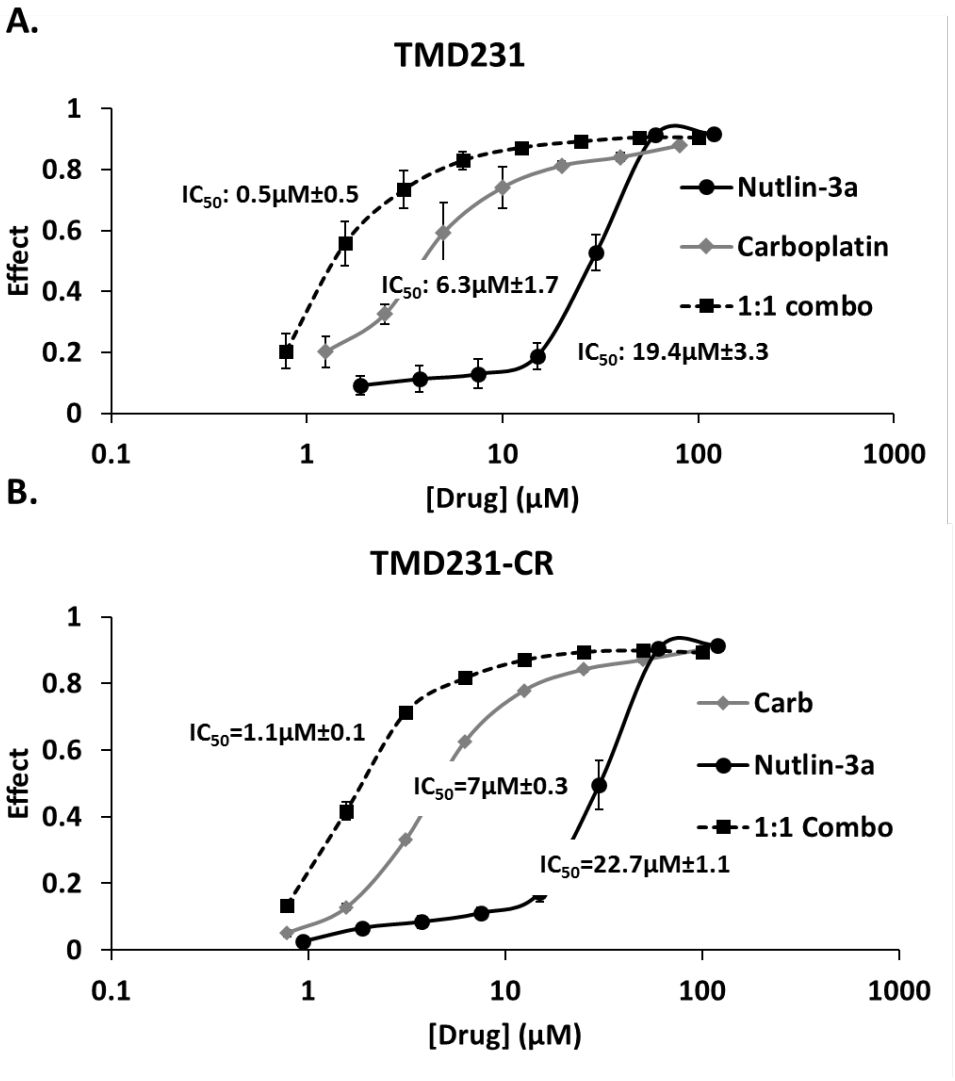

Figure 31. Combination treatment has similar enhanced potency in TMD231-CR cells when compared to TMD231 cells. TMD231-CR cells were treated with increasing concentrations of Nutlin-3a, carboplatin, or 1:1 concomitant combination treatment and allowed to grow for 5 days. Cell proliferation was determined using methylene blue staining. (A) Combination treatment had an increased potency in TMD231 cells compared to Nutlin-3a and carboplatin alone treated cells. (B) Combination treatment had an increased potency in TMD231-CR cells compared to Nutlin-3a and carboplatin alone treated cells.

To validate our imaging approach, pilot studies were next conducted to optimize cell dose for early imaging assessment. As first, we established the relationship between cell number and fluorescent intensity both *in vitro* and *in vivo* was determined. We hypothesized that there would be a cell number-dependent increase in fluorescent intensity as the cell number increased. For the *in vitro* imaging experiment, parental TMD231 served as the background control for the TMD231-CR cells. PBS alone was also imaged as an additional control. Images were collected to visualize relative fluorescent signals between the groups (Figure 32A). Images were analyzed and fluorescent intensity was calculated using the OptiView software (ART Technologies). Any fluorescence collected from the appropriate TMD231 parental cells was subtracted from the TMD231-CR cells resulting in fluorescent intensity represented by 'normalized counts' (NC) units. As expected, there was a cell number-dependent increase in fluorescent intensity with an R^2=0.976 (Figure 32B).

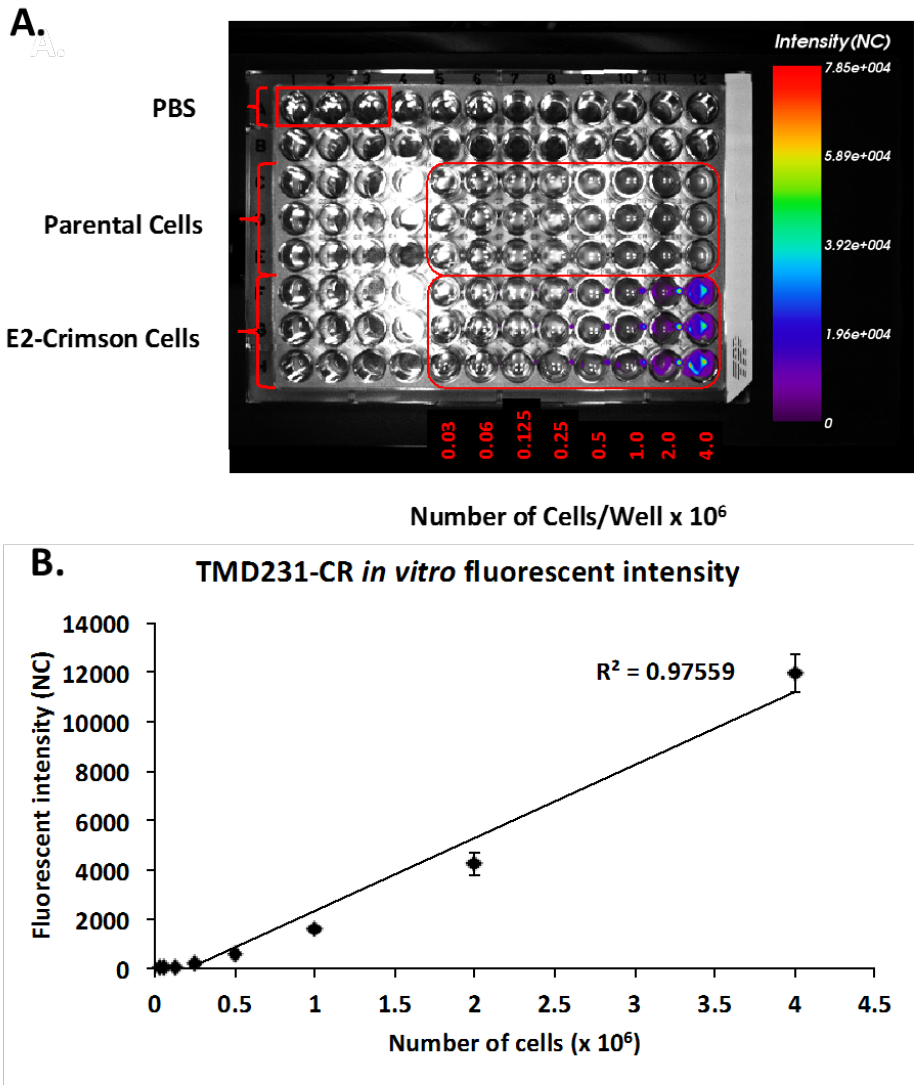

Figure 32. *In vitro* imaging of TMD231-CR cells shows a cell number-dependent increase in fluorescent intensity. (A) TMD231 and TMD231-CR cells were plated with 0.03125, 0.0625, 0.125, 0.5, 1, 2, and $4x10^6$ cells per well in triplicate and imaged *in vitro*. Parental TMD231 cells were used as a control for any auto-fluorescence. PBS was used as a control for background. (B) Graphical representation of the TMD231-CR fluorescent intensity showed that the fluorescent intensity increased in a cell number-dependent manner. The fluorescent intensity of the parental TMD231 cells was used as background and subtracted from the fluorescent intensity of TMD231-CR cells.

To further support our *in vitro* imaging data, we then tested if there were cell number-dependent increases in fluorescent intensity *in vivo*. For *in vivo* imaging, four different TMD231 and TMD231-CR cell numbers (0.125, 0.25, 0.5, and 1.0 $x10^6$) implanted into mice, and two hours following implant the mice were imaged (Figure 33A). There was a cell number-dependent increase in fluorescent intensity with R^2=0.996 (Figure 33B). The TMD231 parental cell implanted mice had minimal background fluorescence as shown in Figure 33B. All of the TMD231-CR cell numbers implanted were detected during fluorescent imaging indicating the sensitivity of the *in vivo* Optix MX3 imaging system (ART Technologies).

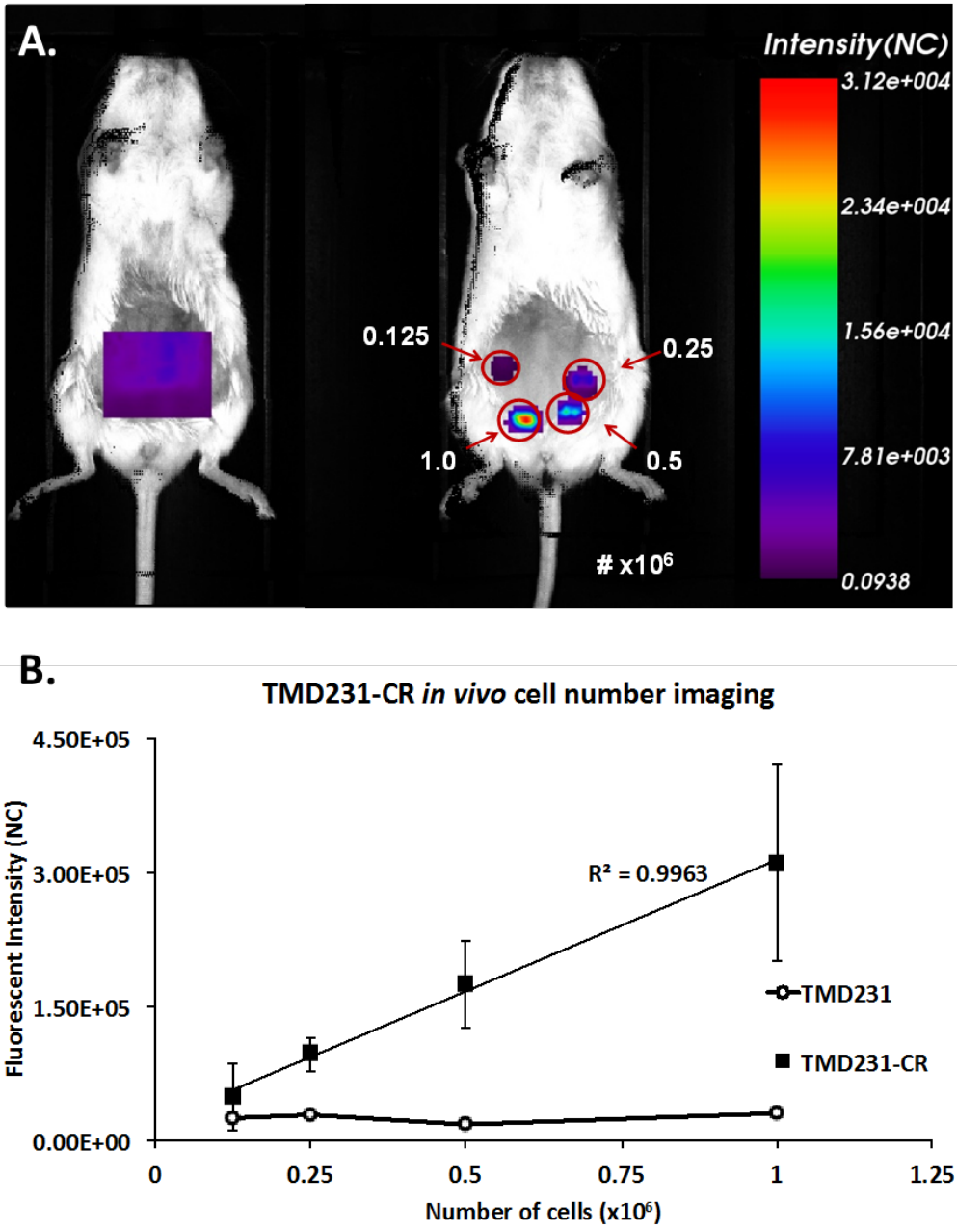

Figure 33. Fluorescent intensity increases in a cell number-dependent manner *in vivo*. (A) NSG mice were implanted with increasing cell numbers (0.125, 0.25, 0.5, and 1.0 x10^6) of TMD231 or TMD231-CR in the mammary fat pad. At 2 hours post implant, the tumor bearing mice were imaged. (B) Graphical representation of fluorescent intensities for 0.125, 0.25, 0.5, and 1.0 x10^6 cells *in vivo*.

Following the *in vitro* and *in vivo* cell number imaging experiments, we next determine if *in vivo* imaging would be a viable way to measure tumor volume. We designed a longitudinal TMD231-CR imaging study to examine tumor growth coupled with *in vivo* imaging. Starting on Day 7 post implant and every week thereafter for a total of 5 weeks, mice were imaged and primary tumor fluorescent intensity was determined. Longitudinal images were collected and a representative picture shows the same three mice throughout the course of the study (Figure 34A). Mouse No. 1 is not pictured in the Day 35 image as its tumor reached the >1000mm^3 endpoint before the last imaging date and was sacrificed. The tumor growth of the TMD231 parental and TMD231-CR tumors as measured by caliper were plotted over time, and there were similar growth rates for the two cell lines *in vivo* (Figure 34B). Additionally, fluorescent intensity was plotted as a function of tumor volume as measured via caliper showing fluorescent intensity and measured tumor volume correlated cell with R^2=0.991 (Figure 34C).

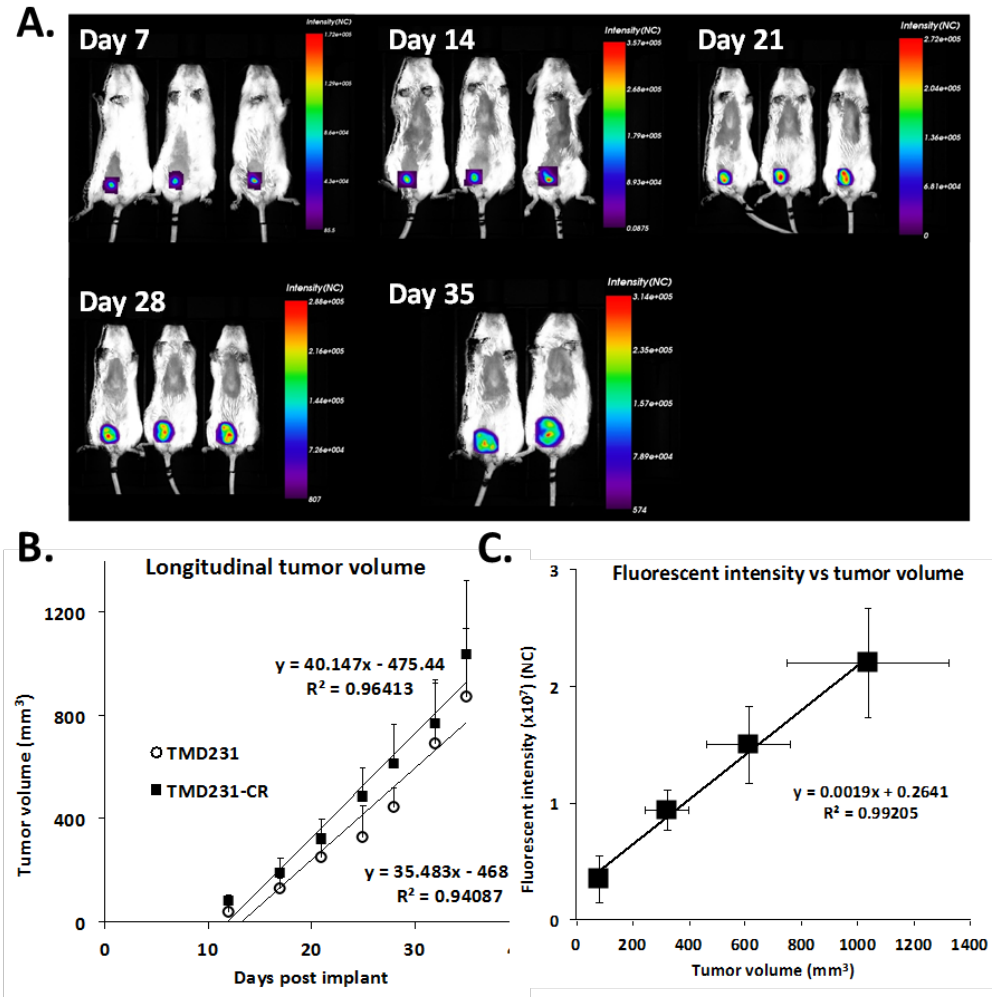

Figure 34. TMD231-CR fluorescent intensity correlates with tumor volume over time.

(A) NSG mice were implanted in the mammary fat pad with $1x10^6$ TMD231-CR cells and imaged weekly after implant for a total of 5 weeks. These are representative images of the same mice over the course of the study. (B) Tumors from TMD231 and TMD231-CR bearing mice were measured via caliper twice weekly and tumor volume was recorded throughout the study. TMD231 and TMD231-CR tumors grew at similar rates and increased over time. (C) Longitudinal images were analyzed and compared to measured tumor volume. Increased fluorescent intensity correlated with increased tumor volume over time with an R^2=0.991.

Since the TMD231-CR cell line is comprised of a transduced (80%) and non-transduced (20%) cells (Figure 30B), we wanted to ensure that the cell line maintained the levels of the fluorescent protein following implant in the mice. At the termination of the longitudinal imaging study, two mice bearing tumors from TMD231 parental and TMD231-CR cells were excised from sacrificed mice and examined using flow cytometry for E2-Crimson levels. Following flow cytometry, the two TMD231-CR tumors from mouse numbers 207317-1 and 207317-2 maintained E2-Crimson fluorescence with >75% positive for the fluorescent protein compared to >80% from initial flow cytometry analysis of the TMD231-CR cell line (Figure 30 and 35). The percentage of transduced cells did not significantly change following passage *in vivo* and the mean fluorescence intensity of the population was stably maintained over the course of a long-term animal study, which would be useful for longitudinal imaging studies.

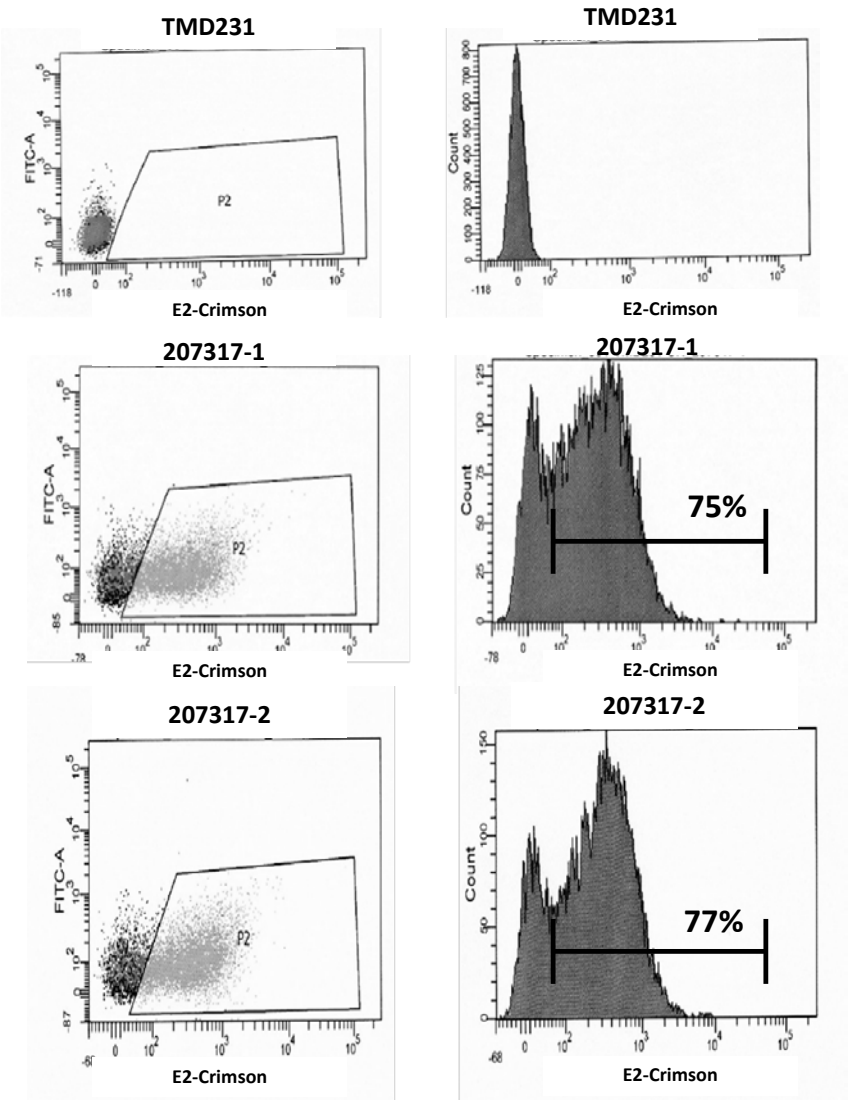

Figure 35. TMD231-CR tumors stably express E2-Crimson over time *in vivo*. NSG mice were implanted with 1x10^6 TMD231 or TMD231-CR cells into the mammary fat pad and allowed to grow. At the completion of the study, tumors were excised from TMD231 and TMD231-CR bearing mice, dissociated, and grown in culture. These cells were then analyzed using flow cytometry to evaluate E2-Crimson levels. Tumors from TMD231-CR mice (203317-1 and 207317-2) maintained the E2-Crimson fluorescent protein with only small losses compared to 80% positivity (Figure 30B).

Based on our pilot *in vitro* and *in vivo* imaging data, we concluded that fluorescent imaging was a sensitive measure of early tumor burden. We developed a standardized protocol for all subsequent dose finding studies and combination drug studies. We incorporated *in vivo* imaging as a measure of early tumor burden. Primary tumor was easily visualized with positive fluorescent intensity (Figure 36A). After analysis, each mouse received a fluorescent intensity value that was used to randomize the mice into different treatment groups. Each treatment group received an equal average amount of E2-Crimson fluorescent intensity as measured by fluorescent intensity of each mouse (Figure 36B). Using fluorescent imaging allowed mice to be randomized into treatment groups at a very early time with small tumor burden. If caliper measurements had been used for the randomization, this would not have been possible until at least days 18-21 post implant of TMD231 cells. At this time point, the tumors have entered a phase of exponential growth and due to the highly aggressive nature of this cell line, expand very quickly leaving the treatment window relatively small. Thus, our standard protocol for all subsequent animal studies was to image mice on Day 7 post implantation of TMD231-CR cells followed by randomization into treatment groups. An acclimation period following imaging and randomization was included and drug treatments began shortly thereafter, on Day 10.

A.

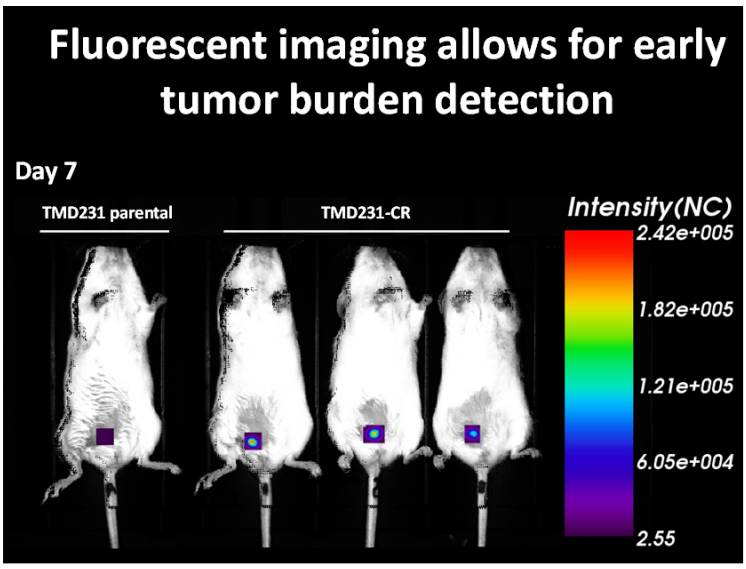

B.

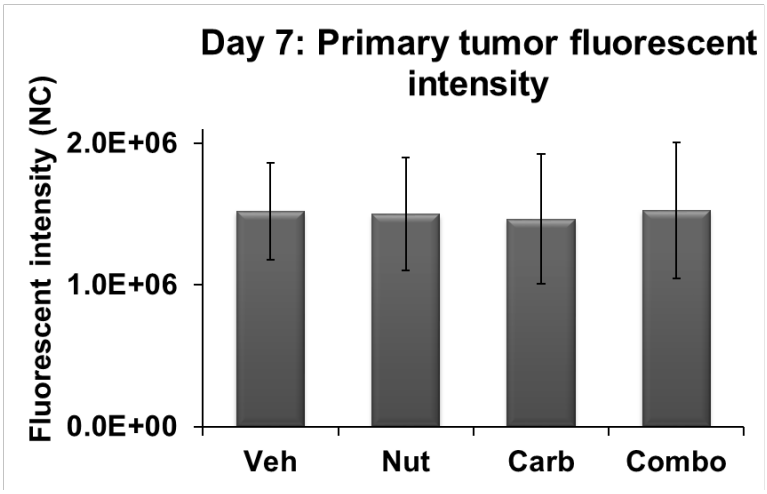

Figure 36. Fluorescent imaging allows for sensitive detection of early tumor burden. NSG mice were implanted with $1x10^6$ TMD231 or TMD231-CR cells into the mammary fat pad on Day 0. (A) The primary tumor region of TMD231 and TMD231-CR bearing NSG mice were imaged on Day 7 post implant. (B) Non-palpable tumors were imaged using fluorescent imaging. Fluorescent intensity was determined for each mouse after imaging and used to randomize the mice into treatment groups (Veh, Carb, Nut, and Combo). Each treatment group received equal amounts of tumor as determined by fluorescent imaging.

C. **Discussion and Future Directions**

Fluorescent imaging provided a sensitive measure of early tumor burden *in vivo*, which would allow drug treatment to begin at an early time point in tumor development allowing for a larger treatment window to be used. The TMD231 cells were transduced with the E2-Crimson fluorescent protein with a lentiviral vector allowing for stable levels of the protein over time. Flow cytometry confirmed that there was >80% TMD231 cells positive for E2-Crimson. A series of *in vitro* and *in vivo* experiments validated the use of TMD231-CR cells for the use in future animal studies as a measurement of non-palpable early tumor burden which is immeasurable with a caliper. The TMD231-CR cells were plated in increasing cell number on 96-well plates and imaged *in vitro* in the optical imaging machine, Optix MX3. There was a cell-dependent increase in fluorescent intensity in the TMD231-CR cells. To test the sensitivity of *in vivo* imaging, NSG mice were implanted with 0.125, 0.25, 0.5, and $1.0x10^6$ TMD231-CR cells in the mammary fat pad and imaged two hours post implant. Fluorescent intensities were collected from all cell numbers and indicated cell number-dependent increases in fluorescent intensity when plotted graphically. Additionally, we wanted to correlate fluorescent intensity with tumor volume over time. We designed a longitudinal study to collect weekly imaging data and plotted the fluorescent intensities as compared to tumor volumes as measured by caliper. There were increases in fluorescent intensity as a function of increasing tumor volume. Taken together, these data suggest that fluorescent imaging is a sensitive measure of early tumor burden since fluorescent intensity is cell number dependent *in vitro* and *in vivo* and over time, tumor size-dependent *in vivo*. Fluorescent

imaging allowed for a non-invasive and relatively quick measure of non-palpable tumor burden allowing for a sufficient therapeutic window of time. Since the laser within the imaging apparatus excited the fluorescent protein expressed within the tumor, there was no need for an injected substrate as compared to bioluminescent imaging. Blood flow can greatly influence the movement of a substrate to the target tissues for bioluminescent imaging. Also, fluorescent imaging was relatively quick with scan times <5 minutes as compared to bioluminescent imaging (>20 minute scans). The length of time while under anesthesia and away from the animal room can add increased stress to the mice. We wanted to reduce the amount of stress that was exposed to the treatment mice for future studies since tumor burden not only increases the overall stress on the animal but coupled with the increased animal handling associated with the treatment dosing as well as effects from the drug treatments themselves. All of these factors contribute to the overall health of the mice and we wanted to decrease as much stress as possible. It is clear from numerous studies in the laboratory that a "stress threshold" exists and once this threshold is surpassed, the impact of therapy can no longer be assessed accurately.

The use of fluorescent imaging could also be used to detect metastases. However, in our system, the use of fluorescent imaging of E2-Crimson with the Optix MX3 did not prove to be sensitive enough to measure lung metastases at the depth required in the whole animal. One study suggested that fluorescent imaging of GFP was sensitive enough to measure as small as 50 cells *in vivo*; however, the design of that experiment utilized a microscope connected directly to the camera [153]. In other studies

windows were created in the skin to allow for imaging directly into the body cavity [152]. This method would be quite invasive and would not be conducive for long-term studies. The use of NIR proteins allows for increased sensitivity of fluorescence measurement since there are fewer signals lost to surrounding tissues [152]. Additionally, the use of NIR fluorescent proteins would lead to imaging with increased depth capacities allowing for deeper tissues to be examined [152]. The use of NIR fluorescent proteins could allow for metastases to be detected within the lungs and other secondary tissues. More sensitive imaging modalities could be explored and validated in the future to measure primary tumor growth and metastases *in vivo*.

Chapter 4. Aim 4: Determination of efficacy of combination carboplatin and Nutlin-3a treatment *in vivo*

A. Background and Rationale

Carboplatin is currently being investigated in numerous clinical trials specifically treated metastatic TNBC: NCT01881230, NCT00691379, and NCT01281150 (clinicaltrials.gov). Nutlin-3a is a pre-clinical tool being used to study the effects of modulating Mdm2 signaling. As described previously, Nutlin-3a is a small molecule inhibitor that was designed to bind into the hydrophobic pocket of Mdm2 and inhibit the binding of p53 [40]. In later studies, it was also discovered that Nutlin-3a also inhibiting the binding of p73, E2F1 and Hif-1α from Mdm2 [62,65,66]. These four binding partners of Mdm2 all have a conserved domain in which binds into the hydrophobic pocket of Mdm2 [62]. Due to the multi-functional role Mdm2 plays in several signaling pathways, we wanted to examine the combined effects of Nutlin-3a and standard of care chemotherapeutic, carboplatin, *in vivo*. Our *in vitro* results indicate a strong synergistic interaction when Nutlin-3a and carboplatin are used in a 1:1 ratio in cell proliferation with enhanced cell death and apoptosis (see Chapter 1). Mdm2 also plays an important role in DNA damage by antagonizing Nbs1 which is involved in DNA repair and thus increased Mdm2 leads to increased genomic instability by delaying DNA repair [35]. We also observed increased levels of Mdm2 in the chromatin fraction isolated from cells treated with combination carboplatin and Nutlin-3a (see Chapter 2). Taken these data together, we wanted to design *in vivo* efficacy studies utilizing NSG mice implanted with

TMD231-CR cells in the mammary fat pad. The mice were randomized based on validated *in vivo* imaging studies as previously described (see Chapter 3).

Before moving into combination efficacy studies, we next determined the dose of carboplatin that would inhibit ~50% of primary tumor growth in the carboplatin dose finding study. This dose of carboplatin would later be combined with Nutlin-3a, and therefore we did not want to completely abolish the primary tumor growth with carboplatin alone. Our primary goals in the combination efficacy studies were to determine the effects of combination treatment compared to each single drug on primary tumor growth and metastasis to the lung. Additionally, we needed to determine the drug dosing schema in which we had efficacy while balancing the stress on the animals as well as normal tissue toxicity. Dosing was further optimized between combination study 1 and combination study 2 in which changes to the dose of carboplatin was reduced as well as the time between drug dosing was lengthened to reduce stress on the animals. The effects of drug treatment on probability of survival were examined in combination study 2. We also examined the toxicity of the combination drug treatment with expanded toxicity examinations with each subsequent combination study by utilizing a number of toxicity measures including health of bone marrow, effects on blood cells, effects on other tissues, as well as body weights throughout the studies. Since the bone marrow is one of the most sensitive measures of normal tissue toxicity, we elected to evaluate possible effects of therapy in detail [110]. The mice received Uniprim® (TD.06596, Harlan Laboratories) which is a specialty rodent diet that have 275 ppm trimethoprim and 1,365 ppm of the sulfonamide sulfadiazine to

help reduce the risk of infection. When the mice are taken to imaging, they are removed from their sterile environment and could be exposed to circulating pathogens. The NSG mice are particularly susceptible due to their compromised immune system. The mice received additional supportive care at the beginning of drug dosing by receiving water soaked Uniprim® chow which helped to maintain or restore losses in body weights after the start of drug treatment. The combination studies evolved from study to study taking the data and applying necessary changes to improve each subsequent animal study to increase knowledge and understanding.

We also completed a small pharmacodynamic study to see if we could validate protein target modulation *in vivo*. Mice were implanted with the TMD231-CR cells and once the tumors reached about 500mm^3, the mice were treated with an aggressive dosing regimen and then sacrificed shortly thereafter to study the effects of drug treatment on protein levels within the tumor. We also took a portion of the primary tumors and examined the levels of human VEGF to see the effects of Nutlin-3a treatment on the primary tumor.

B. ***In vivo* combination drug efficacy studies**

Our overall experimental goal was to investigate the therapeutic potential of modulating the Mdm2 signaling network via Nutlin-3a in combination with carboplatin and to determine the molecular targets active in our system. Therefore, we next conducted complete carboplatin dose-finding studies to determine the appropriate dose of carboplatin that would inhibit ~50% tumor growth. The results from the carboplatin dose finding study would help design future efficacy combination studies conducted in combination with Nutlin-3a. The Nutlin-3a dose used for *in vivo* studies was selected based on other *in vivo* dose-finding studies already completed in the laboratory in human brain cancer models and was set at 200 mg/kg (Figure 37). The maximal Nutlin-3a plasma concentration (C_{max}) was measured to be 35μM, which was higher than the IC_{50} value of 19.4μM±3.3 determined for Nutlin-3a *in vitro* in the TMD231 cells (Figure 6). The t_{max} or time to reach maximal plasma concentrations was 1 hour while the half-life ($t_{½}$) was calculated to be 5.5 hours. The apparent oral clearance (Cl/F) was calculated to measure the rate of clearance of the drug when given orally. Extensive pharmacokinetic studies were completed by Zhang and colleagues, which examined the distribution of Nutlin-3a in mice [154]. In those studies, they showed that Nutlin-3a had high bioavailability and was well distributed from plasma to the tissues including the lungs indicating that Nutlin-3a should be present in the lungs in our model [154]. Figure 38 shows the carboplatin dose finding study schema.

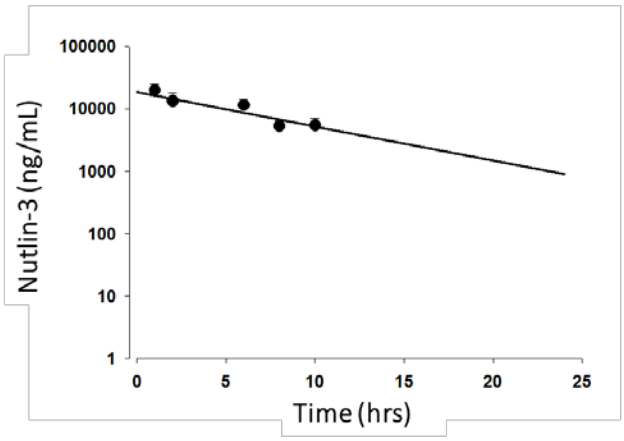

Nutlin-3 parameters	
C_{max}	20,417 ng/mL (35 µM)
t_{max}	1 hour
$t_{½}$	5.5 hours
Cl/F	0.25 mL/min

Figure 37. Pharmacokinetics of Nutlin-3a in NSG mice. (A) Mice received 100 mg/kg Nutlin-3a p.o. and plasma samples collected and processed from 1-24 hours for quantification (n= 3 mice per time point). Quantification of the compounds was determined using liquid-liquid extraction followed by HPLC-MS/MS (API 4000). Data are represented as the mean ± SD. For quantification of Nutlin-3a, the line illustrates the line of best fit (using the last four points). (B) Summary of Nutlin-3a PK parameters. The maximal Nutlin-3a plasma concentration (C_{max}) was measured to be 35µM. The t_{max} or time to reach maximal plasma concentrations was 1 hour while the half-life ($t_{½}$) was calculated to be 5.5 hours. The apparent oral clearance (Cl/F) was calculated to measure the rate of clearance of the drug when given orally.

Figure 38. Carboplatin dose finding study design

Objective: Determine the dose of carboplatin needed to inhibit ~50% tumor growth to later be combined with Nutlin-3a treatment in combination efficacy studies

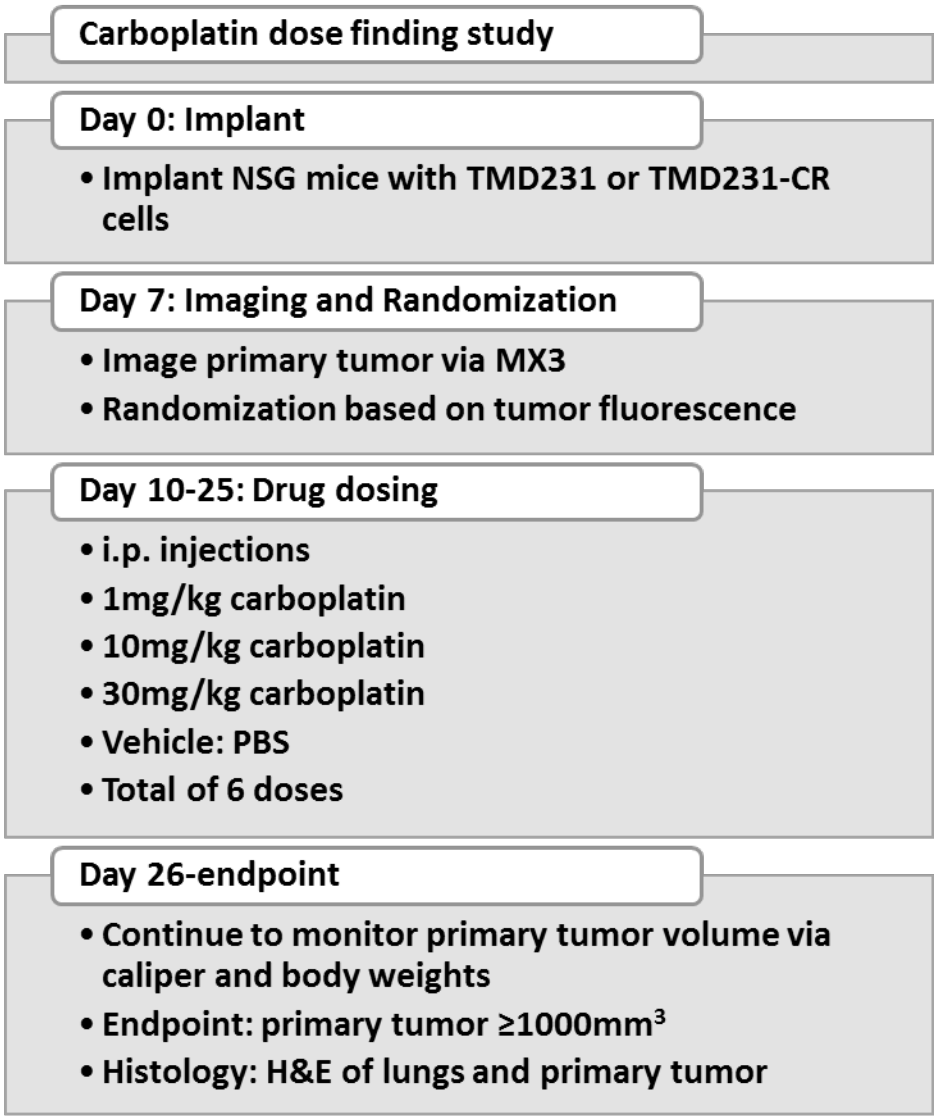

The carboplatin dose-finding study showed that carboplatin inhibited primary tumor growth in a dose-dependent manner compared to vehicle-treated mice. (Figure 39A). At 3mg/kg and 30mg/kg carboplatin, the growth of primary tumors was significantly inhibited compared to Vehicle treated mice (Two-Way ANOVA, $p<0.001$, n=8-9). Additionally, mice were sacrificed when the primary tumor reached ≥1000mm^3, and carboplatin treatment increased the probability of survival at this endpoint (Figure 39B). Based on the carboplatin dose-finding studies, we elected to treat mice with 25mg/kg carboplatin in combination efficacy studies.

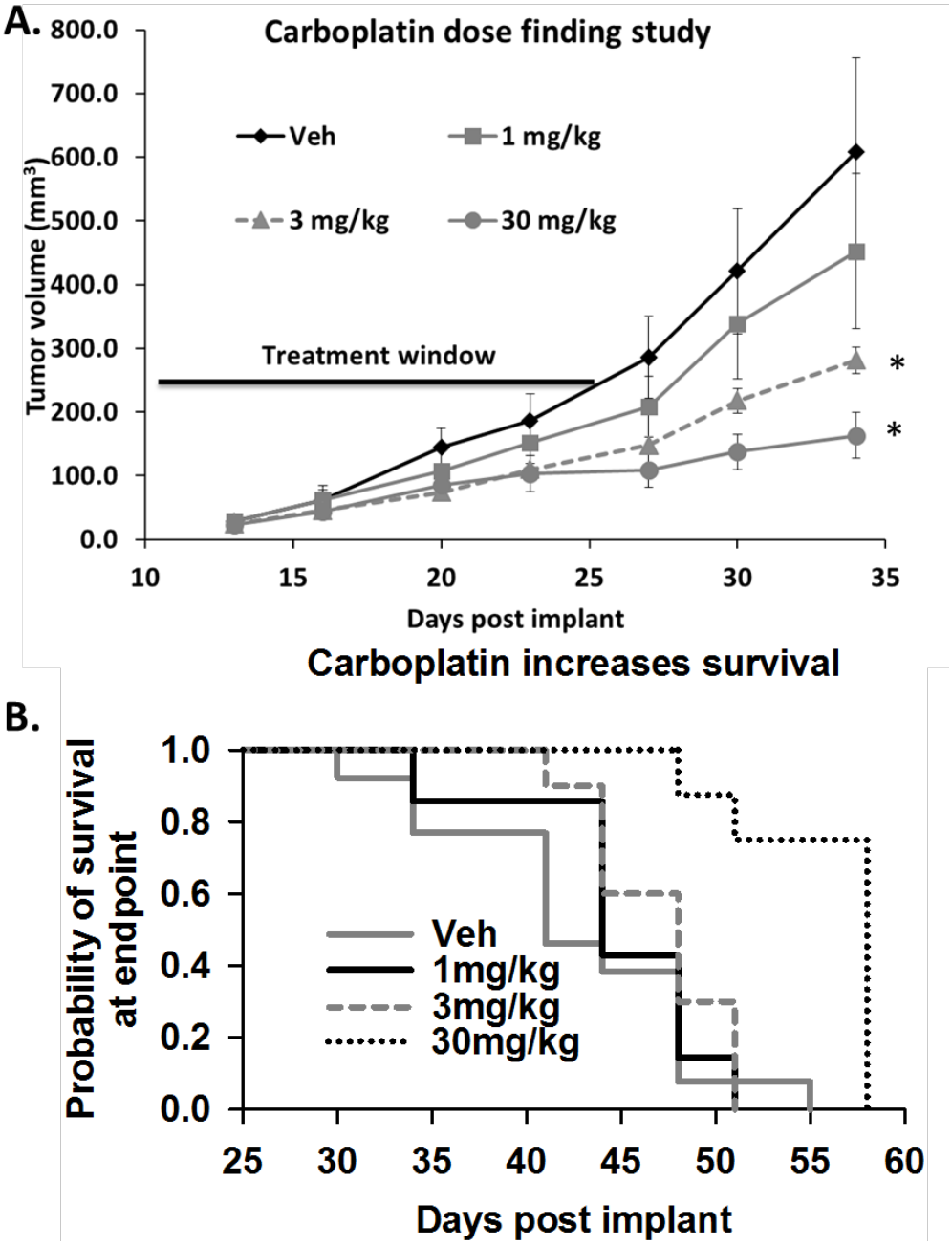

Figure 39. Carboplatin inhibits tumor growth and increases survival in a dose-dependent manner. NSG mice were implanted with 1x10^6 TMD231 as a background control for imaging or TMD231-CR cells into the mammary fat pad and allowed to grow. On Day 7, mice were imaged and randomized into treatment groups (Vehicle, 1mg/kg, 3mg/kg, and 30mg/kg carboplatin). Mice started drug treatment on Day 12 post implant

and were dosed i.p. MWF for 2 weeks for a total of 6 doses. Primary tumor growth was evaluated twice weekly via caliper measurements. (A) Tumor growth was inhibited in a carboplatin dose-dependent manner. The 3mg/kg and 30mg/kg carboplatin treatments significantly inhibited tumor growth when compared to Vehicle treated mice (Two-Way ANOVA, *$p<0.001$ as compared to Vehicle treated, n=8-9, mean±SEM). (B) Carboplatin increased probability of survival at endpoint in a dose-dependent manner. Mice were sacrificed when primary tumors reached 1000mm^3.

As we began to design the first combination animal study, our objectives were to evaluate the effects of the combination Nutlin-3a and carboplatin treatment on primary tumor growth and metastasis to the lung as well as evaluate *in vivo* imaging following drug treatment. Figure 40 illustrates the overall study design. The combination treatment significantly inhibited primary tumor growth compared to Vehicle- and single Nutlin-3a- and carboplatin-treated mice over the course of the entire study (Two-Way ANOVA, $p<0.001$, n=7-9, ±SEM) (Figure 41A). There was no difference between Vehicle- and Nutlin-3a-treated mice. Carboplatin alone inhibited tumor growth, however, the combination of carboplatin and Nutlin-3a further decreased primary tumor growth (Figure 41A). During this initial phase of developing a rational dosing regimen, mice were monitored daily for signs of therapy-induced stress and toxicity. The dosing schema in study one began with dosing three times weekly, but was subsequently altered to twice weekly dosing due to increased stress on the mice (decreased appetite, lack of grooming, and 10% body weight loss). These adjustments were made during the first combination study and continued in subsequent studies. When the first primary tumors reached ≥1000mm^3, all of the mice were sacrificed, which was about a week after the completion of drug treatment in combination study 1. As a secondary measure of tumor size, following necropsy, the primary tumors were excised from mice and weighed. The average weight tumors from the combination treated mice were significantly smaller than tumors from Vehicle and single Nutlin-3a and carboplatin treated mice (One-Way ANOVA, $p<0.001$, n=7-9, ±SEM) (Figure 41B). A pictorial view of excised tumors from treated mice visually showed primary tumors from combination

treated mice were smaller in size compared to tumors from Vehicle and single Nutlin-3a and carboplatin treated mice (Figure 41C).

Figure 40. Combination animal study 1 design

Objective: Evaluate the effects of combination Nutlin-3a and carboplatin treatment on primary and secondary tumor growth and evaluate primary tumor response to treatment via optical imaging

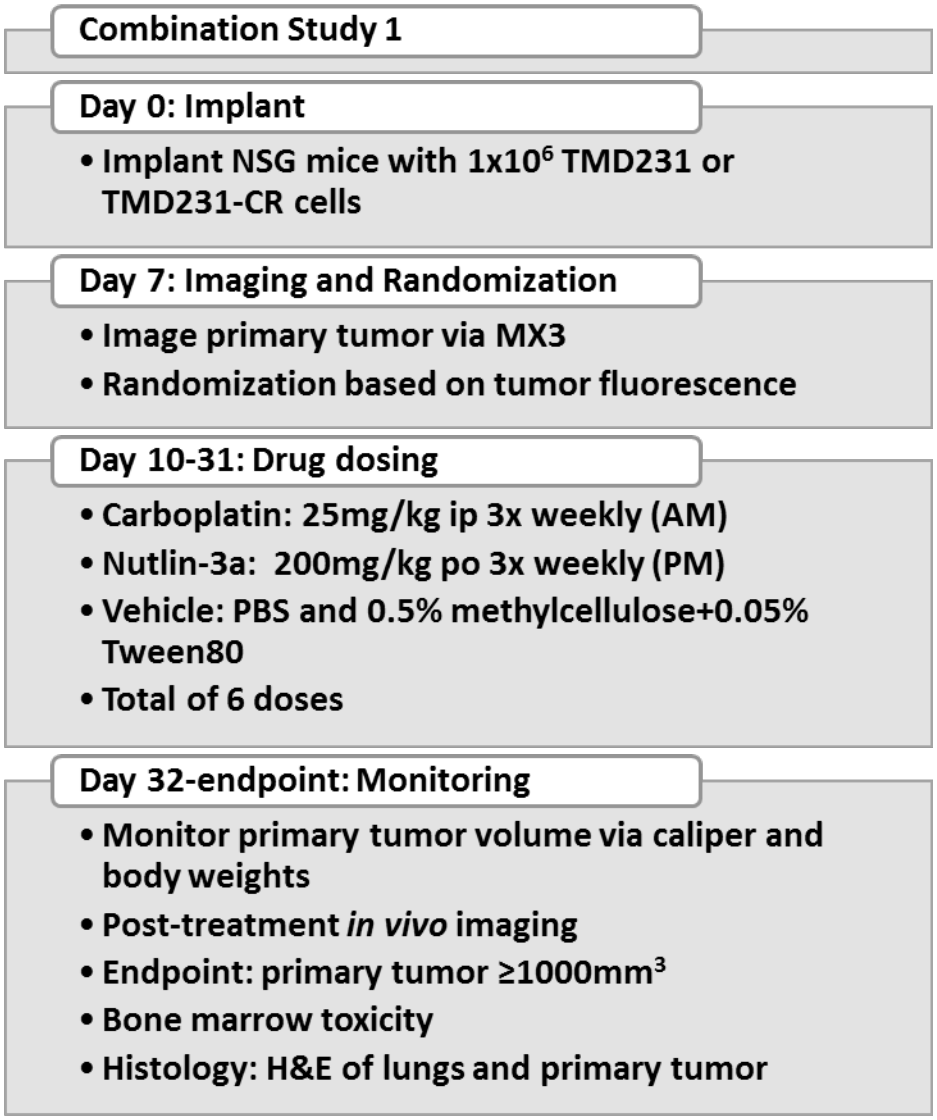

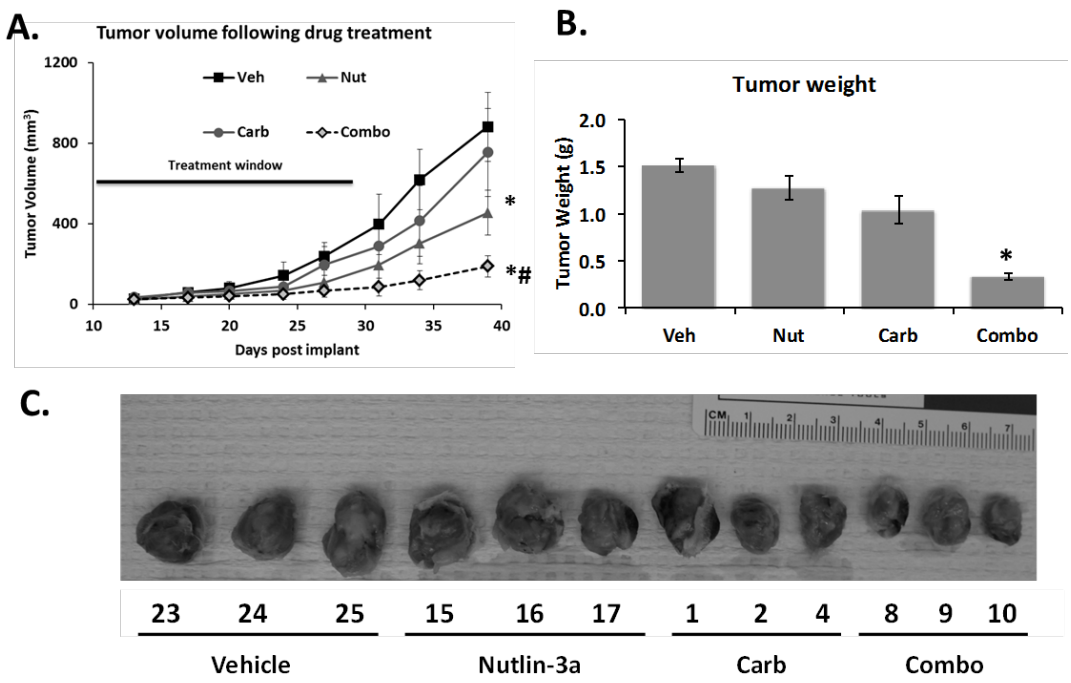

Figure 41. Combination treatment significantly inhibits primary tumor growth *in vivo*. NSG mice were implanted with $1x10^6$ TMD231 as a background control for imaging or TMD231-CR cells into the mammary fat pad on Day 0. Mice were imaged on Day 7 post implant and randomized into treatment groups using fluorescent intensity. Mice were dosed with Veh (PBS and 0.5% methylcellulose+0.05% Tween80), 25mg/kg carboplatin i.p., 200mg/kg p.o., or 25mg/kg carboplatin i.p. + 200mg/kg p.o. three times weekly for total of 6 doses. Primary tumor volume was evaluated using caliper measurements throughout the study. (A) Carboplatin alone, Nutlin-3a alone, and combination all significantly inhibited primary tumor growth compared to Vehicle treated mice with the combination treatment significantly inhibiting tumor growth when compared to both single drug treatments (Two-Way ANOVA, *p<0.001 as compared to Vehicle, # p<0.001 as compared to Nut and Carb alone, n=7-9, ±SEM). (B) At study completion, mice were sacrificed and primary tumors were excised and weighed. Primary tumor weight was

significantly reduced in combination treated mice compared to Vehicle and single drug treated groups (One-Way ANOVA, *p<0.001, n=7-9, ±SEM). (C) Representative pictures of tumors from each treatment group.

Throughout the study, we evaluated the mice for overt toxicity to drug treatments. During the study, the mice did not lose more than 10% body weight overall (Figure 42A). The first drop in body weight occurred during the first week of drug treatment. The mice were supplemented with water soaked Uniprim® food which helped the mice recover lost body weight. All subsequent animal studies used water soaked Uniprim® food as supportive care. As an additional measure of drug toxicity, bone marrow cellularity was determined. There was a decrease in total bone marrow cell numbers from mice treated with the combination treatment compared to the Vehicle and single drug treated mice (Figure 42B) (One-Way ANOVA, $p<0.001$, n=7-9, ±SD). While there were decreases in total bone marrow cell counts in the combination treated mice, this loss did not result in blast crisis (Figure 42B). Since the mice were sacrificed only 7 days following the completion of drug treatment, this presumably did not allow for an adequate recovery period of the bone marrow cells in response to carboplatin. Subsequent animal studies incorporated a revised study design that allowed us to evaluate potential toxicity to the bone marrow following an increased recovery period; in this study design, total bone marrow cell counts returned to normal levels (Figure 49).

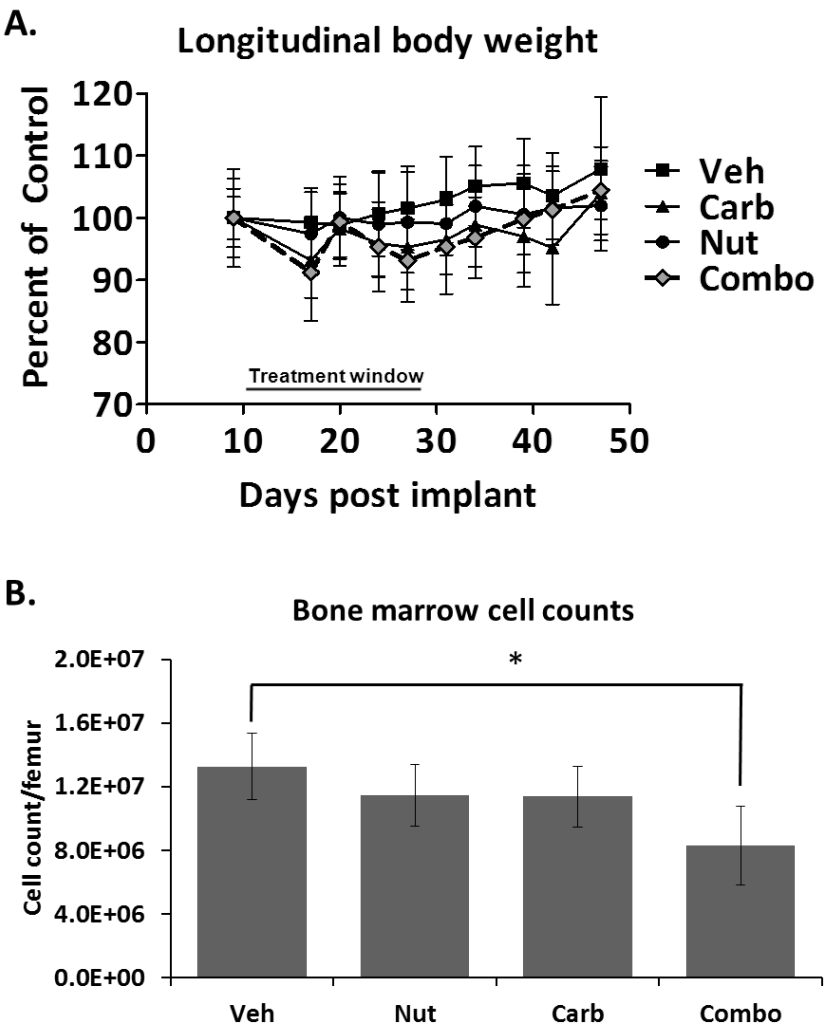

Figure 42. Drug treatment is well tolerated with minimal toxicity. (A) Body weight did not significantly change throughout study. Body weights of mice were evaluated throughout the study as a measure of overall mouse health. After the first week of drug treatment, mice were given water soaked Uniprim® food as supportive care after which body weights improved. (B) Total bone marrow cell counts were determined from excised femurs of treated mice. Bone marrow cell counts were significantly reduced in the combination treated mice compared to Vehicle treated mice (One-Way ANOVA, *$p<0.001$, n=7-9, ±SD).

Since the combination treatment inhibited primary tumor growth, we also examined the effects of combination treatment on metastatic lesions in the lung. Representative pictures of H&E slides of lungs were taken and combination mice had smaller sized and less numbered lung metastases (Figure 43A). The human tumor cells in the lungs appear purple in color due to the Haematoxylin dye, which stains basophilic structures in the cells like DNA, RNA, and endoplasmic reticulum (The Histology Guide, University of Leeds). Eosin stains acidophilic parts of the cells, which includes the cytoplasm. Due to the large and aneuploid structures of the tumor cells, they appear more purple in color compared to the much smaller diploid mouse cells in the lungs, which appear more pink in color. The Vehicle-treated mice had very large metastases that coalesced into one another forming large areas of tumor cells in the lungs. The carboplatin and Nutlin-3a alone treated mice had lower numbers and smaller metastases compared to the Vehicle-treated mice. A blinded pathologist scored the H&E slides of lung tissues with a scoring system based on Grade 1-5 (Figure 43D). The traditional scoring by pathologist showed that the combination treated mice had significantly smaller Grade metastatic lesions compared to Vehicle- and single drug-treated mice (One-Way ANOVA, $p<0.05$, $n=5$, $\pm$SD). As a secondary measure of metastases, H&E stained slides were also scanned using the Aperio ScanScope system (Leica Biosystems) and analyzed using ImageScope software (Leica Biosystems). Positive staining can be collected digitally allowing for a non-biased measure of pathological staining. Following ImageScope analysis for positivity, it was confirmed that lungs from combination treated mice had less lung metastases compared to Vehicle- and single-

drug treated mice (One-Way ANOVA, $p<0.05$, $n=5$, ±SD) (Figure 43C). While the combination-treated mice had less lung metastases, the study design does not answer the question if the combination treatment inhibits the metastatic process or simply inhibits primary tumor growth, which would result in less metastatic cells entering the blood stream, and therefore less cells able to metastasize to the lungs. To answer this question, mice would need to be implanted with TMD231 cells and tumors allowed to grow until ~3 weeks post implant where metastases in the lungs have been visualized. At that point, the mice could be randomized based on tumor volume and treatment would begin. This way, the mice already have metastases present in the lungs. Following treatment, smaller lung metastases would indicate that the drug treatment inhibited tumor growth in the lungs. The disadvantage to this metastasis model would be the large size of the primary tumors. Metastasis begins around 21 days post implant, which does not leave a large treatment window due to the size of the primary tumor. The primary tumor would likely need to be resected so that they lung metastases could form and become large enough to visualize any differences in number and size following drug treatment. This study design would be similar to what is observed in the clinic in which women with breast cancer may have surgery to remove the tumor and then treated systemically for any metastatic sites.

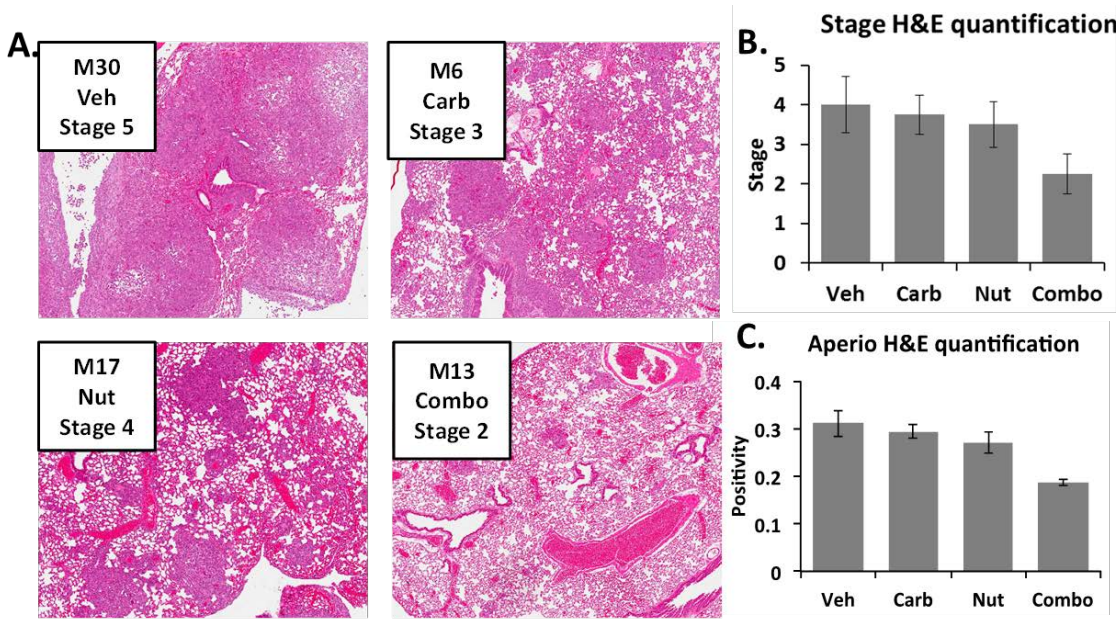

D.

Stage description	Stage
Small number of mets and composed of under 25 cells	1
Mets from small(25 to 100 cells) to moderate (100 to 500) cells	2
Mets from small(5 to 40 cells) to very large (600 to 1200) cells	3
Mets from small(10 to 40 cells) to very large(600 to 2500) cells	4
Numerous mets per lung lobe and coalescing into large diffuse tumor balls. Unable to count	5

Figure 43. Combination treatment inhibits tumor growth in secondary sites. Following sacrifice, lungs were excised and fixed in 10% buffered formalin. Lungs were paraffin blocked, sections were cut, and stained for H&E. (A) Pictorial representation of primary tumor H&E staining of the lungs. Combination-treated mice had the smallest tumor Stage bearing the smallest number and size of lung metastases compared to the Vehicle- and single drug-treated mice (4X magnification). (B) Mice were scored by stage by a blinded pathologist. Stage parameters were determined in the table (D). The combination mice had significantly smaller lung metastases as determined by Grade compared to all other groups (One-Way ANOVA, *$p<0.05$, $n=5$, ±SD). Additionally, slides

were scanned using Aperio ImageScope system and analyzed for digital positivity of staining. (C) Combination-treated mice had a significant reduction in positivity compared to other treatment groups which confirmed traditional histology quantification (One-Way ANOVA, *$p<0.05$, $n=5$, ±SD).

To better understand the effects of drug treatment on cell proliferation within tumors at the time of mouse sacrifice, excised tumors were stained for Ki67. Representative pictures of tumors from Vehicle, Nulin-3a alone, carboplatin alone, and combination-treated mice showed that combination treated mice had less Ki67 staining (Brown) compared to the other groups (Figure 44A). ImageScope analysis confirmed that there was significantly less Ki67 staining in combination treated mice compared to Vehicle treated mice (One-Way ANOVA, $p<0.05$, $n=4$, ±SD) (Figure 44B). There was a downward trend in Ki67 staining in tumors from Nutlin-3a and carboplatin alone treated mice.

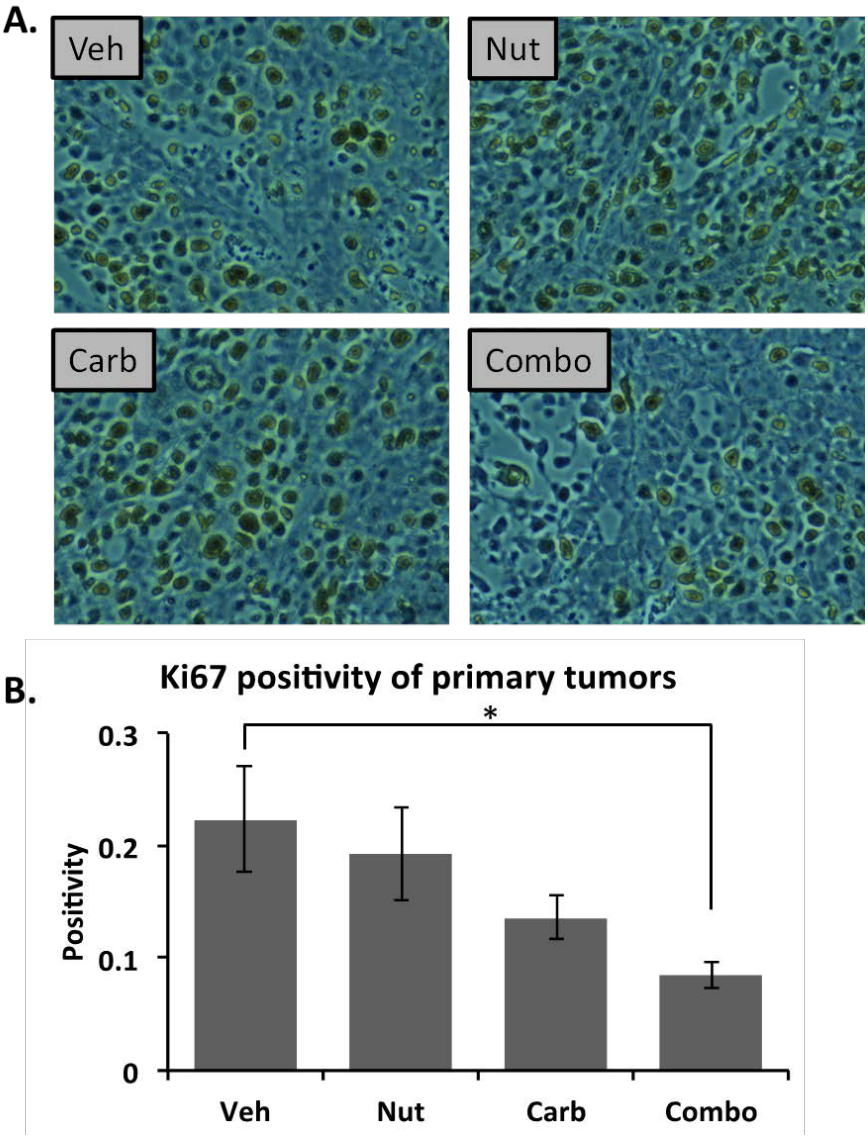

Figure 44. Cellular proliferation is decreased in combination treated mice. Slides were also cut for Ki67 staining. (A) Pictorial representation of primary tumor Ki67 staining (brown stain) showed less staining in combination treated mice compared to Vehicle treated mouse tumors (40X magnification). (B) Graphical representation showed a significant reduction in Ki67 staining in combination treated mice compared to Vehicle treated mice (One-Way ANOVA, *$p<0.05$, $n=4$, ±SD). There was a downward trend in Ki67 staining in the Nutlin-3a and carboplatin alone treated mice.

In our second objective, we evaluated the primary tumor response to drug treatment using optical imaging. Mice were imaged on Day 7 as baseline fluorescent intensity analysis for randomization. The fluorescent intensity was highly variable after the drug treatment and did not yield statistical significance (Figure 45). There were downward trends in the combination treatment compared to Vehicle treated mice; however, there was no difference between combination and carboplatin alone treated mice. The measured tumor volume via caliper and tumor weights showed that the combination treated mice had significantly smaller tumors compared to the Vehicle- and single drug-treated mice and this was confirmed by tumor weight measurements taken at the end of the study. Our data indicate that fluorescence imaging in this model system does not provide an accurate measure of tumor volume following drug treatment and was also not sensitive enough to pick up fluorescence from metastatic lung foci. As the tumors grew larger, some developed necrotic cores and dead cells. And it is highly probable that due to tissue attenuation effects and remaining E2-Crimson protein in dying and/or necrotic cells was the reason for lack of correlation between imaging results and other measures of tumor growth. In discussions with the Indiana Institute for Biomedical Imaging Sciences, we also believe that the machine could not accurately detect fluorescence at the depth required to obtain accurate measure of response to treatment. If the depth of signal was variable between mice, this could have added to the overall variability of fluorescent intensity values. Additionally, imaging is an added stressor to mice already highly stressed following tumor implant and drug

treatment. In future studies, we elected to only use the *in vivo* imaging as a measure of early tumor burden in the mice.

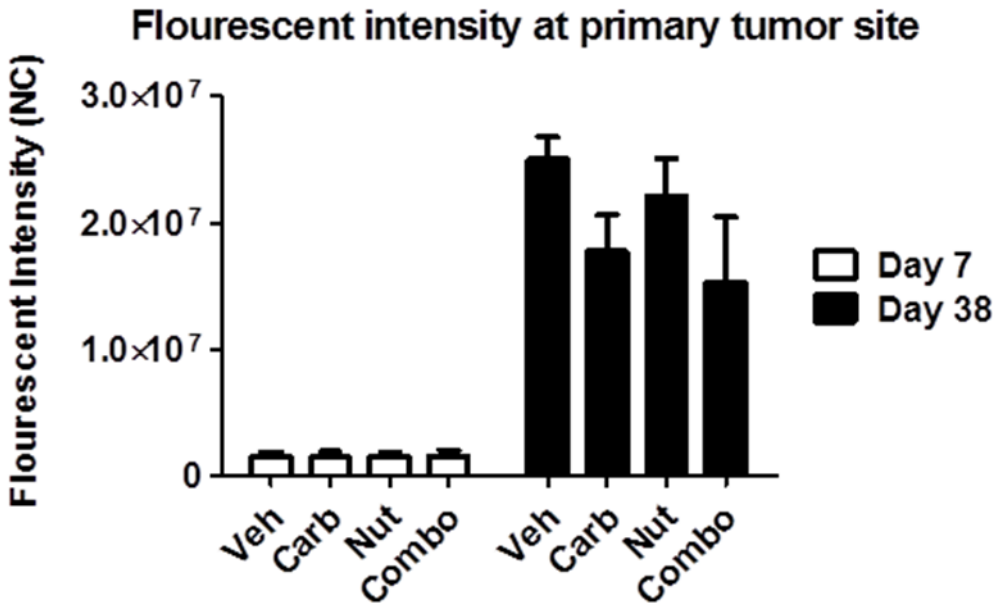

Figure 45. Fluorescent intensity is highly variable after drug treatment and does not correlate with other measurements of tumor growth. NSG mice were implanted with $1x10^6$ TMD231 and TMD231-CR cells into the mammary fat pad on Day 0. Mice were imaged on Day 7 and randomized into treatment groups. Mice were dosed with Vehicle (PBS and 0.5% methylcellulose+0.05% Tween80), 25mg/kg carboplatin i.p., 200mg/kg Nutlin-3a p.o., or 25mg/kg carboplatin+ 200mg/kg Nutlin-3a combination. Mice were allowed a week recovery period following the completion of drug treatment, and then the mice were imaged. Following imaging analysis on Day 38, there was a downward trend in fluorescent intensity for the combination mice compared to Vehicle and single drug treated mice. However, the fluorescent intensity was highly variable and did not denote significant differences (n=7-9, ±SEM).

Based on positive data from the first combination animal study, we next designed an *in vivo* experiment that would repeat and also expand upon the combination animal study design to answer additional experimental questions (Figure 46, see schema of study design). Combination study 2 was designed in a similar fashion to the first combination study. There were groups of mice that were designed to validate the first study with mice sacrificed when the first tumors reached ≥1000mm^3. There were also groups of mice that were used to study the effects of the drug treatment on the probability to survive to the endpoint of 800mm^3 tumor volume. We also wanted to further evaluate bone-marrow toxicity following drug treatment. Slight changes were made to the dosing schema with the carboplatin dose being reduced from 25mg/kg to 20mg/kg due to decreased body weights in the carboplatin and combination treated mice in Combination Study 1. Mice were dosed twice weekly to reduce stress for a total of 8 doses. Mice were given supportive care with the addition of water soaked Uniprim® food, which helped to increase food uptake in the mice. Histology with H&E staining of the lungs was also repeated to confirm the first combination study.

Figure 46. Combination animal study 2 design

Objective: Confirm results of combination study 1, adjust dosing schema, evaluate the effects of combination treatment on survival, and examine bone marrow toxicity

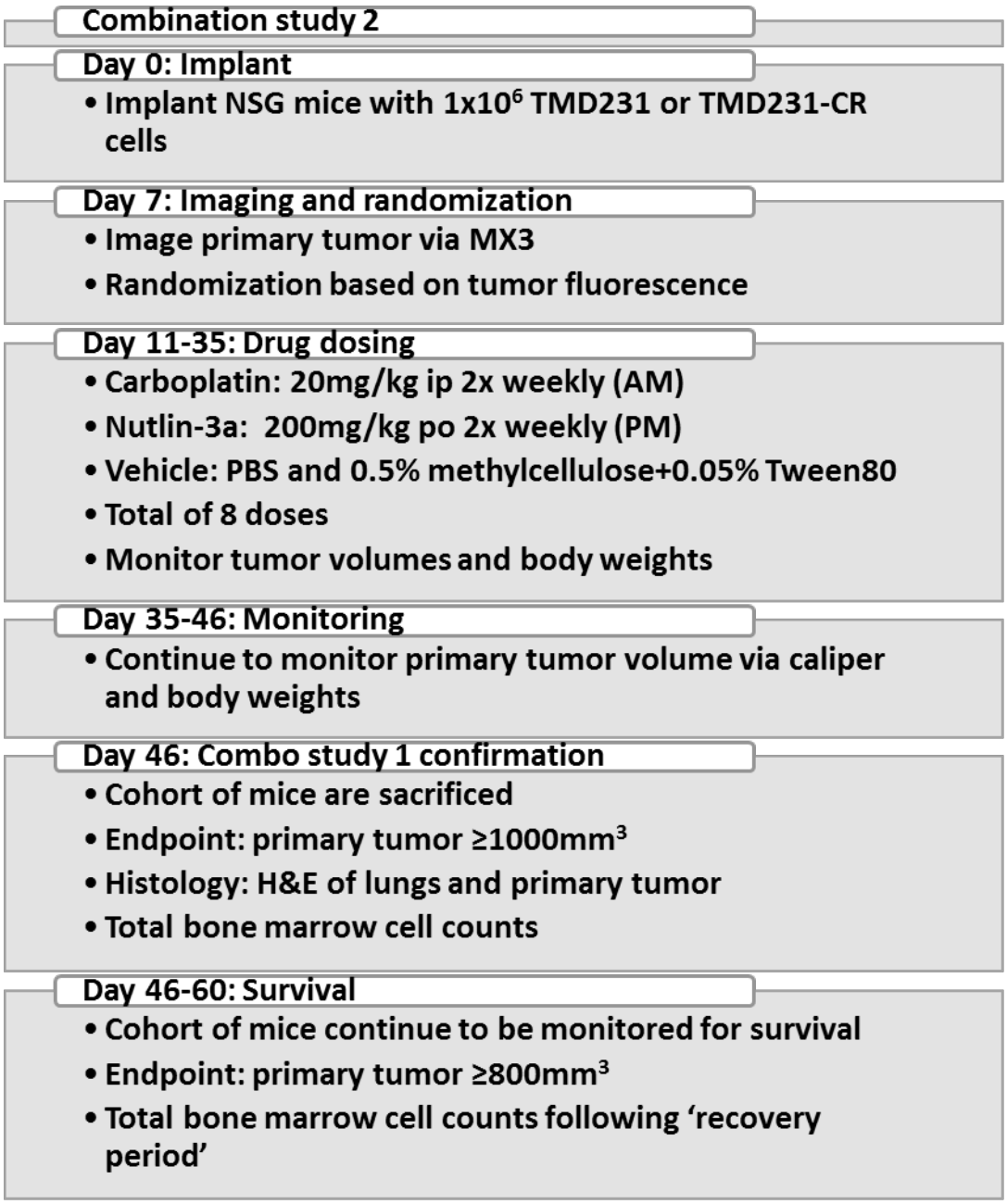

Similar to the first combination study, the combination treated mice had significantly smaller primary tumors compared to Vehicle- and both single drug-treated (Two-Way ANOVA, $p<0.05$, n=12, ±SEM) (Figure 47A). The group of mice used to confirm the first combination study was sacrificed on Day 41, which was 5 days after the completion of drug treatment. During necropsy, the primary tumors, lungs, and femurs were excised for further analysis. Primary tumor weight was significantly reduced in combination treated mice compared to Vehicle and single carboplatin and Nutlin-3a treated mice (Figure 47B) (Student's T-test, $*p<0.05$, n=3-4, ±SEM). Histology was used to examine primary tumors and lungs for H&E staining. Bone-marrow cellularity was also evaluated from excised femur bones (Figure 49). Since the sample size was small in the repeat study mice group coupled with innate variability in animal studies, the histology data from H&E stained lungs did not show significant differences between the treatment groups (data not shown).

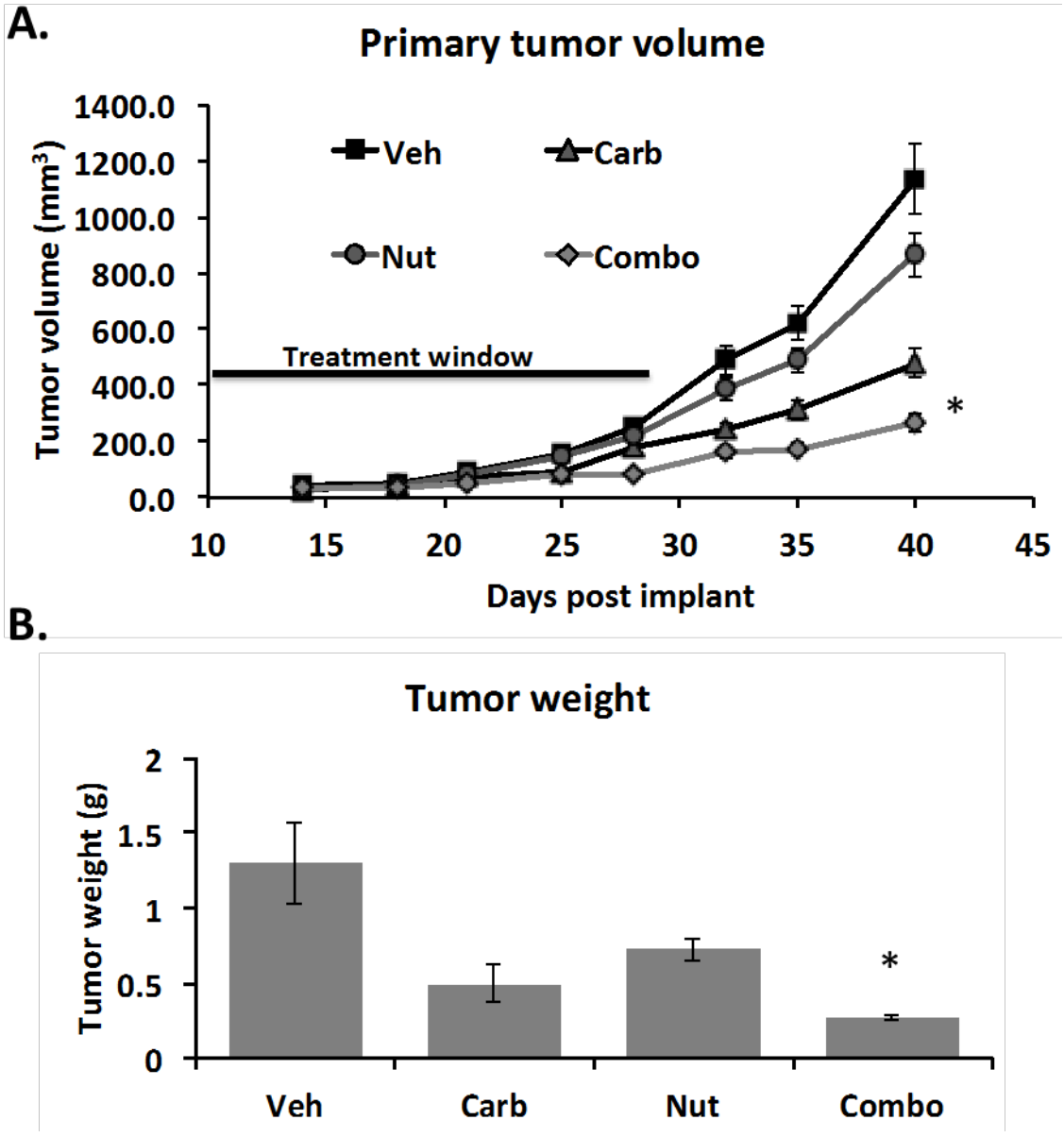

Figure 47. Combination treatment significantly inhibits primary tumor growth *in vivo*. NSG mice were implanted with 1x10^6 TMD231 or TMD231-CR cells into the mammary fat pad on Day 0. Mice were imaged on Day 7 post implant and randomized into treatment groups. Mice were dosed with Veh (PBS and 0.5% methylcellulose+0.05% Twenn80), 20mg/kg carboplatin i.p., 200mg/kg p.o., or 20mg/kg carboplatin i.p. + 200mg/kg p.o. two times weekly for total of 8 doses. Primary tumor volume was

evaluated using caliper measurements throughout the study. (A) The combination treated mice had significantly smaller tumors compared to Vehicle and both single drug treated groups (Two-Way ANOVA, $p<0.05$, $n=12$, ±SEM). (B) At study completion, mice were sacrificed and primary tumors were excised and weighed. Primary tumor weight was significantly reduced in combination treated mice compared to Vehicle and single drug treated groups (Student's T-test, $*p<0.05$, $n=3-4$).

To better understand the effect of combination drug treatment on probability of survival, a second group of mice from different treatment groups were examined for survival. The endpoint for survival mice was set as the time point when the primary tumor reached 800mm^3. The combination treated mice a significant probability of survival at the time point at which the tumors reached 800mm^3 compared to Vehicle and single drug treated mice (Figure 48A). Kaplan-Meier analysis using SigmaPlot showed that the survival time for Vehicle was 39.3±0.6 days, Nutlin-3a was 39±1 days, carboplatin was 47.5±1.8 days, and combination was 54.3±1.5 days (Figure 48B).

A.

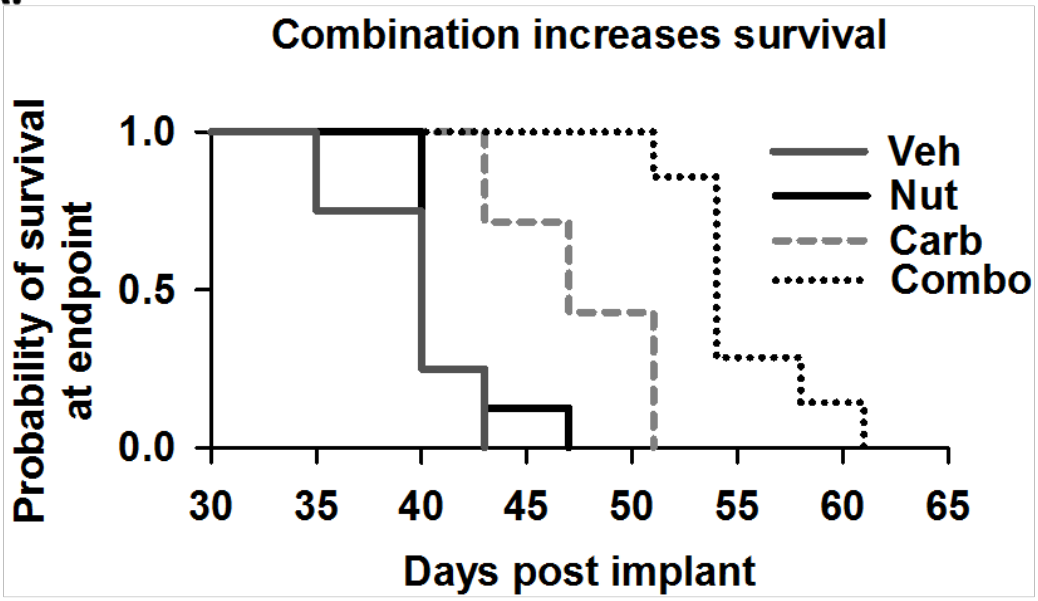

B.

Treatment Group	Survival (days)
Vehicle	39.3±0.6
Nutlin-3a	39±1
Carboplatin	47.5±1.8
Combination	54.3±1.5

Figure 48. Combination treatment increases probability of survival. Groups of mice were studied for probability of survival with the survival endpoint determined when the primary tumor reached 800mm^3. (A) Following Kaplan-Meier analysis (SigmaPlot), the combination treated mice had a significantly increased probability of survival compared to Vehicle and single drug treated mice (n=7-8, $p<0.05$). (B) Survival for Vehicle was 39.3±0.6 days, Nutlin-3a was 39±1 days, carboplatin was 47.5±1.8 days, and combination was 54.3±1.5 days.

When the mice reached the tumor volume endpoint, the mice were sacrificed and femurs were collected for total bone marrow cell counts. Measurements of bone-marrow cellularity are a sensitive measure of tissue toxicity, which is important since one of the side effects of carboplatin is myelosuppression[155]. In the group of mice examined for survival, the mice were not sacrificed until a later time point, which resulted in about a 2-weeks recovery period following the end of drug treatment. The total bone marrow cell counts were compared between the groups used to confirm combination study 1 which were harvested 5 days following the completion of drug treatment and the group in study 2 used to examine survival which were harvested after a two week recovery period following the completion of drug treatment. There was a significant reduction in total bone marrow cell counts in the combination treated mice compared to Vehicle treated mice in the group that only received a 5 day recovery period (Two-Way ANOVA, # $p<0.05$, n=4, ±SD) (Figure 49). However, the significant reduction in total bone marrow cell counts returned to normal levels in groups of mice used to examine survival after a two-week recovery period (Two-Way ANOVA, *$p<0.05$, n=3, ±SD) (Figure 49). Thus, bone-marrow toxicity in the combination treated mice is reversible and not a long lasting effect; bone-marrow cell counts returned to normal levels within 2 weeks following the completion of drug treatment.

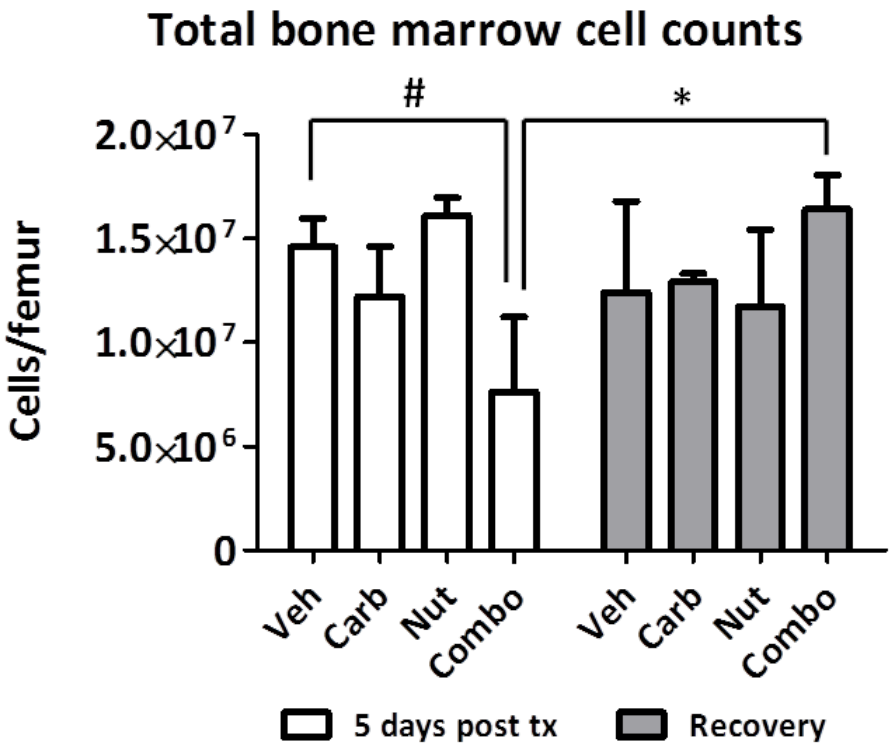

Figure 49. Total bone marrow cell counts recover to normal levels following recovery period after treatment. A group of mice were sacrificed 5 days after the end of treatment and bone marrow cell counts were determined as described in the Materials and Methods. The combination treated mice had a significantly reduced number of bone marrow cells compared to Vehicle treated mice (Two-Way ANOVA, # $p<0.05$, n=4, ±SD). However, after a two-week recovery period, the levels of total bone marrow cell counts came back to normal levels in the combination treated mice (Two-Way ANOVA, *$p<0.05$, n=3, ±SD).

Breast cancers can metastasize to many tissue compartments including brain and bone. Since we already had processed femurs of mice for bone-marrow cellularity measurements, we next determined if there were any metastatic tumor cells present in the bone marrow compartment. Since the tumor cells are marked with the E2-Crimson fluorescent protein, detection of tumor cells could be readily determined by flow cytometry experiments. TMD231 parental cells were first used to set the gates for fluorescent protein negative cells (Figure 50A). TMD231-CR cells were used as a positive marker for the presence of the E2-Crimson fluorescent protein (Figure 50B). Additionally, we isolated bone marrow from a normal NSG mouse (WT BM) that was untreated and non-implanted (Figure 50C). We also used normal NSG bone marrow spiked with two different ratios of the TMD231-CR cells (1:1 WT:231-CR and 9:1 WT:231-CR) as a positive marker for E2-Crimson cells present in mouse bone marrow. In the samples containing the mixtures of the bone marrow and TMD231-CR cells, flow cytometry showed E2-Crimson cell number-dependent increases in positive cells in the wild-type bone marrow (Figure 50D-E). Bone marrow cells from Vehicle- and Nutlin-3a-treated groups were evaluated for the presence of TMD231-CR cells. Following flow cytometry analysis, there were no TMD231-CR cells present in isolated bone marrow (Figure 50F-G). A tabular summary of the data can be found in Figure 50H. At the time of these analyses, there were 3 Vehicle and 3 Nutlin-3a treated mice that were sacrificed on the same day so we elected to examine the bone marrow of these mice for the presence of E2-Crimson expressing tumor cells. The carboplatin and combination treated mice were much more variable in the time to reach the endpoint. We expected

the most tumor cells to be present in the Vehicle and Nutlin-3a treatment groups since their tumors were the largest and had significantly more lung metastases than the other two treatment groups. Since we did not detect any tumor cells in the bone marrow isolated from Vehicle or Nutlin-3a treated mice, we did not evaluate this in the other treatment groups.

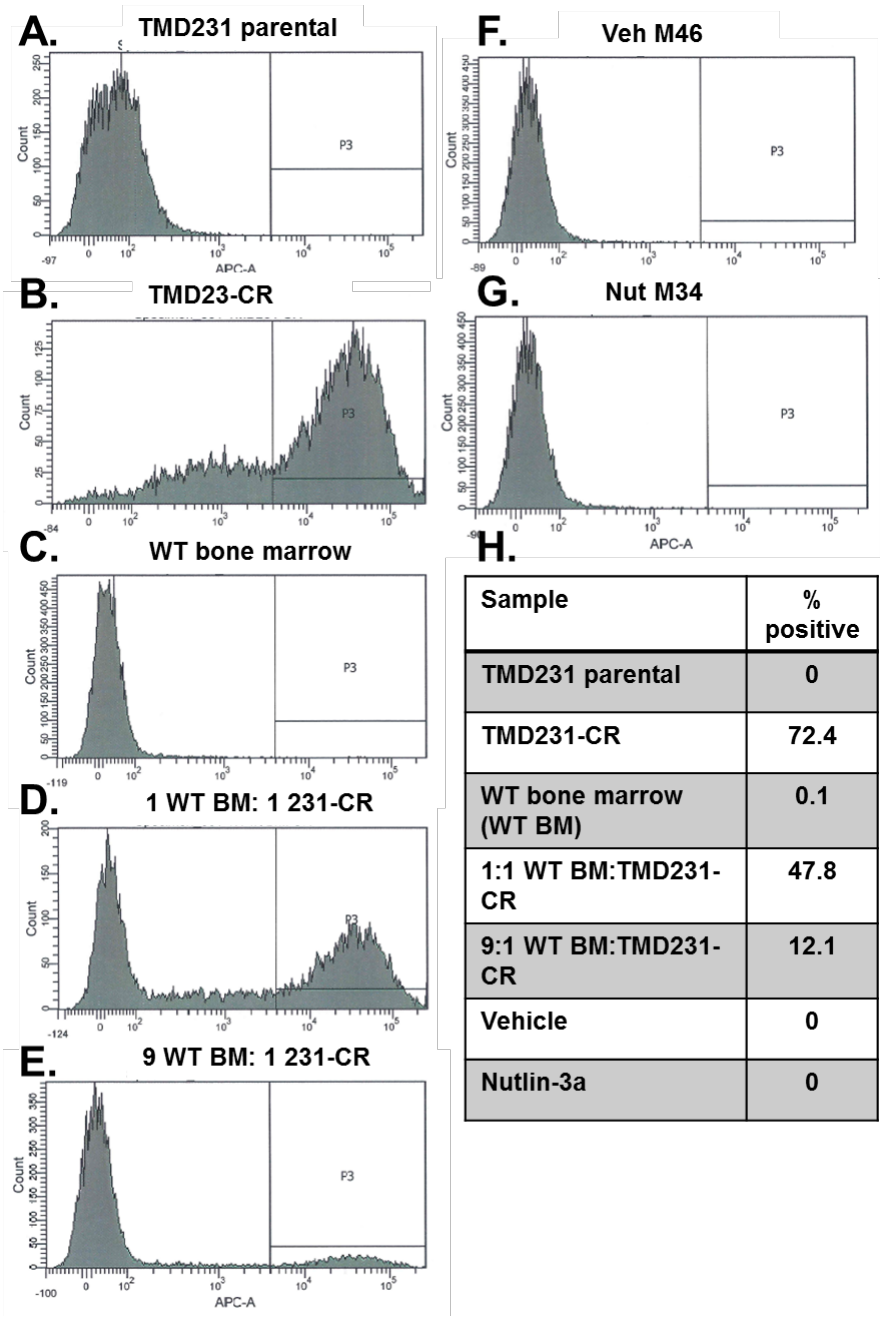

H.

Sample	% positive
TMD231 parental	0
TMD231-CR	72.4
WT bone marrow (WT BM)	0.1
1:1 WT BM:TMD231-CR	47.8
9:1 WT BM:TMD231-CR	12.1
Vehicle	0
Nutlin-3a	0

Figure 50. Tumor cells are not present in isolated bone marrow. Bone marrow cells were prepared by crushing excised femur bones with mortar and pestle. Crushed bones were passed through a 70µm cell strainer, and red blood cells were lysed with RBC lysis buffer. Isolated cells were washed with PBS and the presence of TMD231-CR tumor cells were assessed using flow cytometry. (A-C) TMD231 parental, TMD231-CR, and bone

marrow cells from a wild-type mouse were used as controls for flow cytometry. (D-E) wild-type bone marrow was spiked with two different ratios of TMD231-CR cells (1:1 WT:231-CR and 9:1 WT:231-CR) as controls. Bone marrow from three mice from Vehicle and Nutlin-3a treated groups were evaluated for the presence of TMD231-CR cells. (F-G) Representative plots of Vehicle- and Nutlin-3a-treated mice show that there were no TMD231-CR cells present in isolated bone marrow. (H) Table shows numerical values of cells positive for the Crimson fluorescent protein.

In combination study 3, we made further adjustments to the study design. Our objectives were to confirm combination study 1 with histology and added further assessments of carboplatin and Nutlin-3a combination treatment on toxicity by further examining bone marrow health and secondary tissues. During the time of combination study 2 and combination study 3, the motherboard of the Optix MX3 was damaged. Therefore, we were unable to image the mice on Day 7 for randomization purposes. We elected to randomize the mice based on body weights on Day 7 so that drug treatment could begin on Day 10 as in other studies. Following necropsy, lungs, primary tumors, livers, spleens and femurs were collected. We performed H&E staining of the lungs, primary tumors, livers, spleens, and femurs. We repeated bone marrow cellularity and also evaluated the effects of the drug treatments on complete blood counts (CBCs) and progenitor assays. An outline of combination study 3 can be found in Figure 51.

Figure 51. Combination animal study 3 design

Objective: confirm combination study 1 and assess combination Nutlin-3a and carboplatin toxicity evaluating bone marrow health and tissues

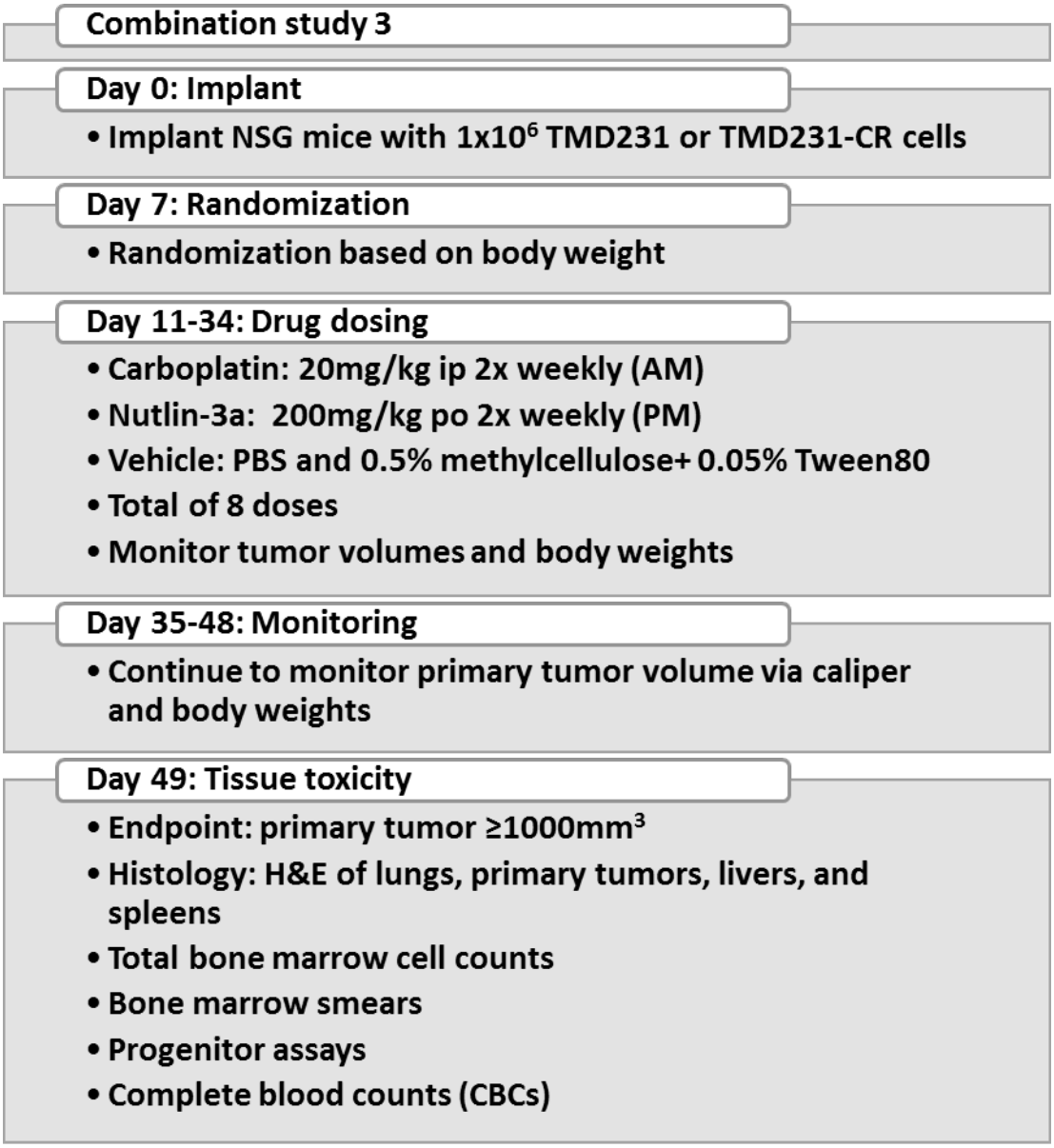

As in combination studies 1 and 2, the combination treatment significantly inhibited primary tumor growth when compared to Vehicle and single drug treated mice (Figure 52A) (Two-Way ANOVA, $p<0.05$, n=8, ±SEM). At study completion, mice were sacrificed, and the primary tumors were excised and weighed. The average primary tumor weight was significantly reduced in the combination treated mice compared to Vehicle and single drug-treated groups (Figure 52B) (Student's T-test, $p<0.05$, n=7-8, mean±SEM). These results add further support to the combination treatment efficacy on primary tumor volume.

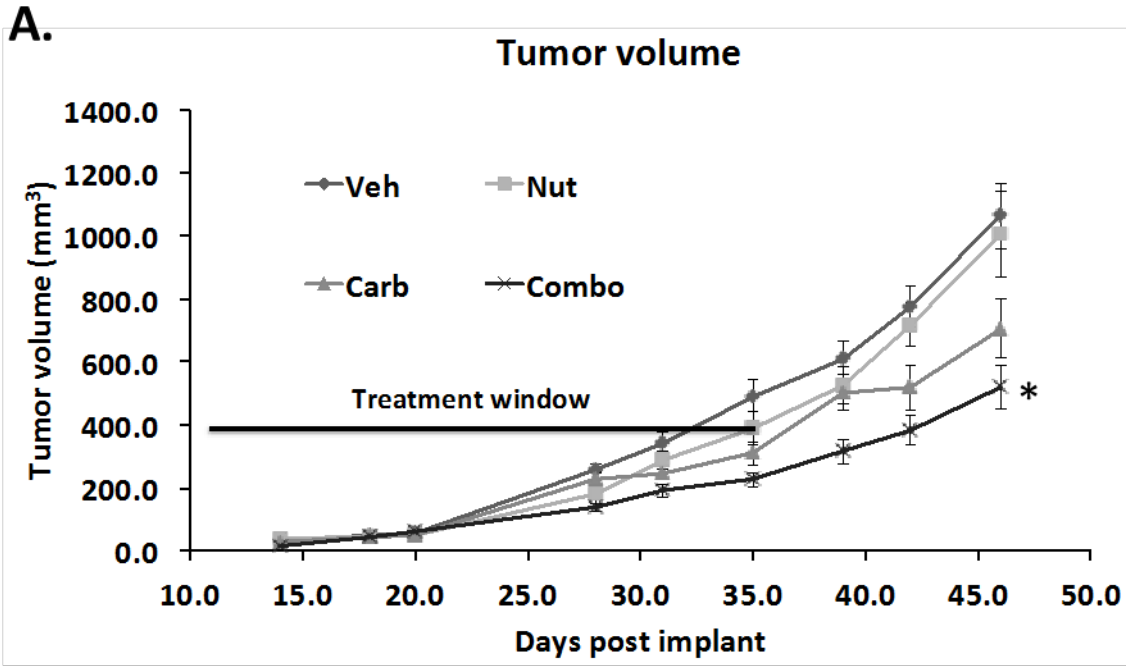

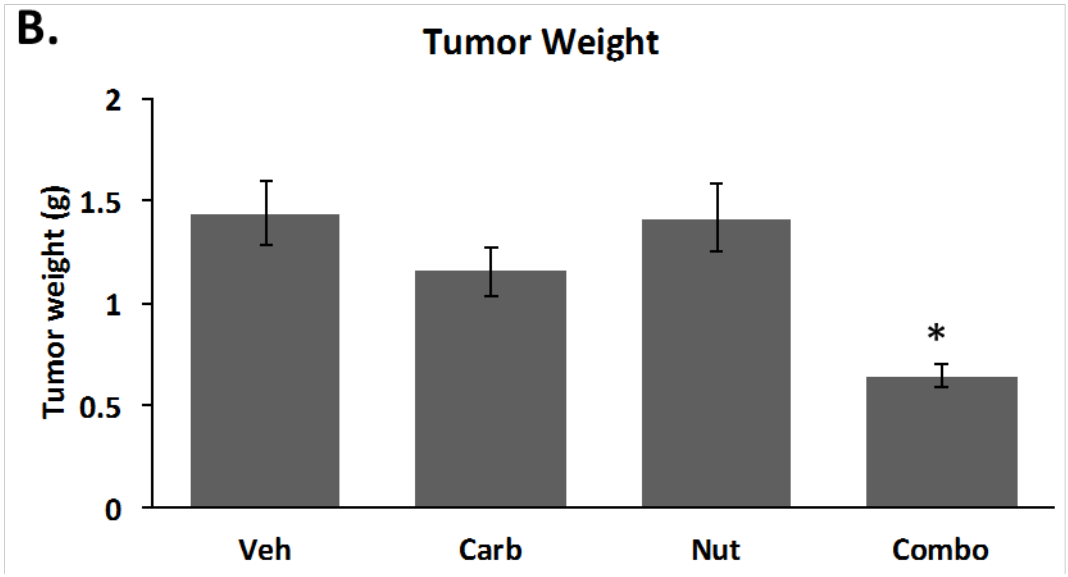

Figure 52. Combination treatment significantly inhibits primary tumor growth *in vivo*. NSG mice were implanted with 1x10^6 TMD231 or TMD231-CR cells into the mammary fat pad on Day 0. Mice were imaged on Day 7 post implant and randomized into treatment groups. Mice were dosed with Veh (PBS and 0.5% methylcellulose+0.05% Tween80), 20mg/kg carboplatin i.p., 200mg/kg p.o., or 20mg/kg carboplatin i.p. +

200mg/kg p.o. three times weekly for total of 8 doses. Primary tumor volume was evaluated using caliper measurements throughout the study. (A) The combination treated mice had significantly smaller tumors compared to Vehicle and both single drug treated groups (Two-Way ANOVA, *$p<0.05$ as compared other treatment groups, n=12, ±SEM). (B) At study completion, mice were sacrificed and primary tumors were excised and weighed. Primary tumor weight was significantly reduced in combination treated mice compared to Vehicle and single drug treated groups (Student's T-test, *$p<0.05$, n=7-8, mean±SEM).

To better understand the effects of combination carboplatin and Nulin-3a on bone marrow health, bone marrow cellularity was evaluated. At the time of sacrifice, the mice had about a two-week recovery period following the completion of drug treatment. There were no differences in bone marrow cellularity between all of the treatment groups, which confirmed results from combination study 2 that bone marrow returns to normal following a recovery period (n=8±SD) (Figure 53A). However, there was a measurable difference in frequency of hematopoietic progenitor cells in the carboplatin alone and combination treated mice compared to Vehicle treated mice (One-Way ANOVA, $p<0.05$, n=3, mean±SD) (Figure 53B).

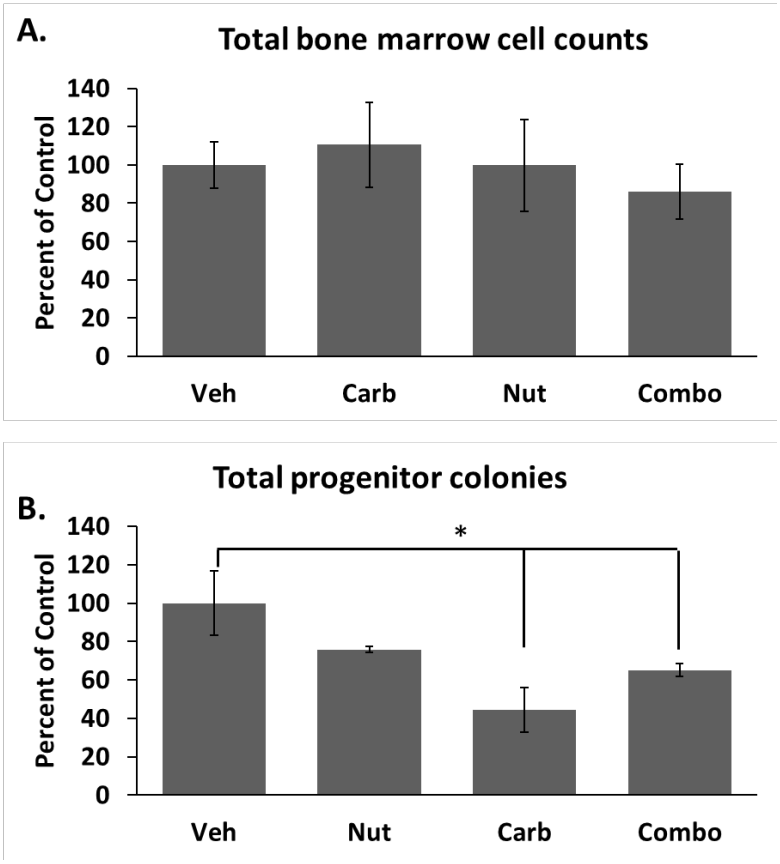

Figure 53. ***In vivo*** **administration of carboplatin and Nutlin-3a does not affect overall bone marrow cellularity but causes a decrease in the frequency of hematopoietic progenitor cells.** Tumor-bearing mice were treated with vehicle control (Veh), carboplatin (Carb), Nutlin-3a (Nut) or combination carboplatin and Nutlin-3a (Combo). After a 2-week recovery period, mice were sacrificed and femurs harvested. (A) Bone marrow cells were isolated and cellularity determined per femur (n=8, mean ± SD). (B) The number of hematopoietic progenitor cells was determined using a colony forming unit (CFU) assay. Bone marrow cells were plated in triplicate at $2x10^4$ per dish in MethoCult GF M3434 and allowed to grow for 2 weeks. Carboplatin and combination treated mice formed less progenitor colonies compared to Vehicle treated mice (One-Way ANOVA, *$p<0.05$, n=3, ±SD).

Additionally, just before sacrifice, an aliquot of peripheral blood was collected from each mouse to examine complete blood counts (CBCs). Peripheral blood was analyzed via hemavet for red blood cells, thrombocytes, and white blood cells. There were significant reductions in red blood cells, thrombocytes, and white blood cells in the combination treated mice compared to Vehicle treated mice (One-Way ANOVA, $p<0.05$, n=7-8, mean±SD) (Figure 54). While there were significant decreases in peripheral blood cells, these levels of toxicity were acceptable since decreased counts did not appear to affect overall health of the mice nor body weights. We also looked at bone marrow histology with bone marrow smears. There were no overt signs of toxicity in bone marrow smears from all treatment groups and also there was no detection of tumor cells, which confirmed our flow cytometry results from combination study 2 (Figure 55). In addition myeloid hyperplasia was noted by the pathologist to be present in all treatment groups with no notable differences between treatment groups (Figure 55).

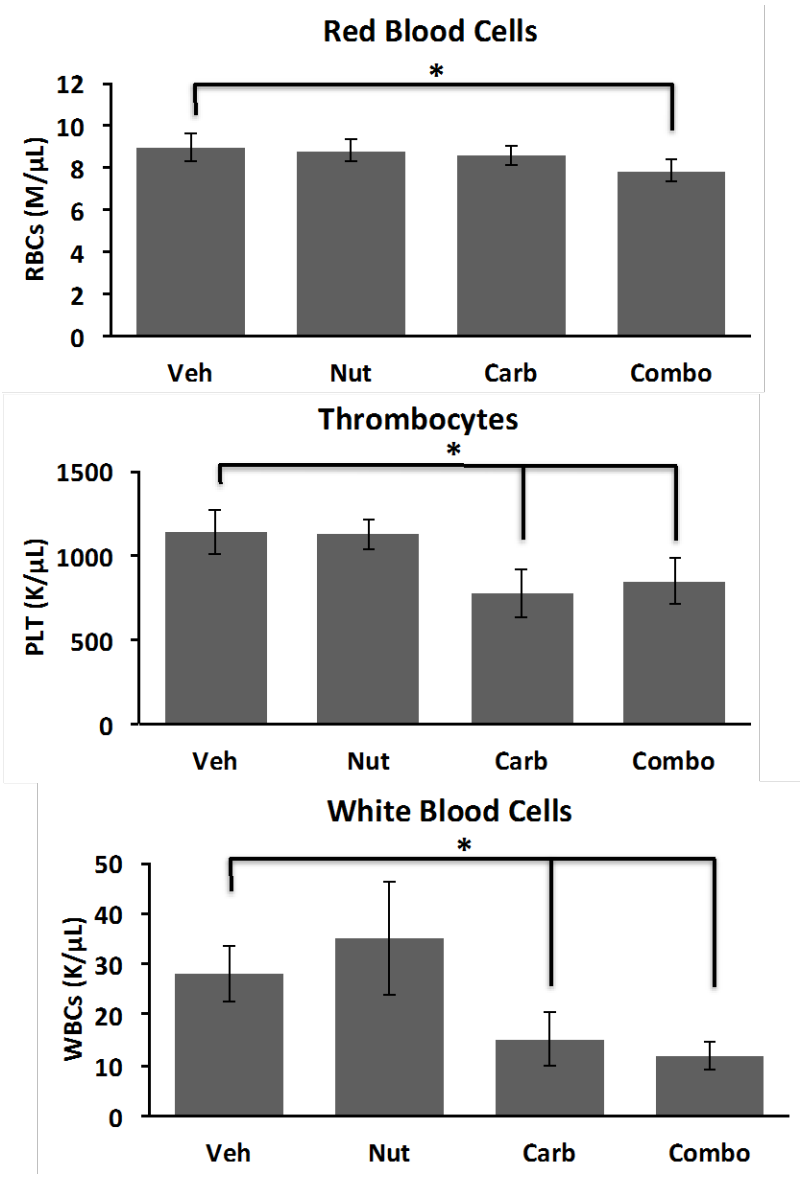

Figure 54. *In vivo* administration of carboplatin and Nutlin-3a leads to decreases in red blood cells, thrombocytes, and white blood cells. Tumor-bearing mice were treated with vehicle control (Veh), carboplatin (Carb), Nutlin-3a (Nut) or combination carboplatin and Nutlin-3a (Combo). After a 2-week recovery period, an aliquot of peripheral blood was analyzed via hemavet for red blood cells, thrombocytes, and white blood cells. The combination treatment led to decreased red blood cells, thrombocytes, and white blood cells (One-Way ANOVA, *$p<0.05$, n=7-8, mean±SD).

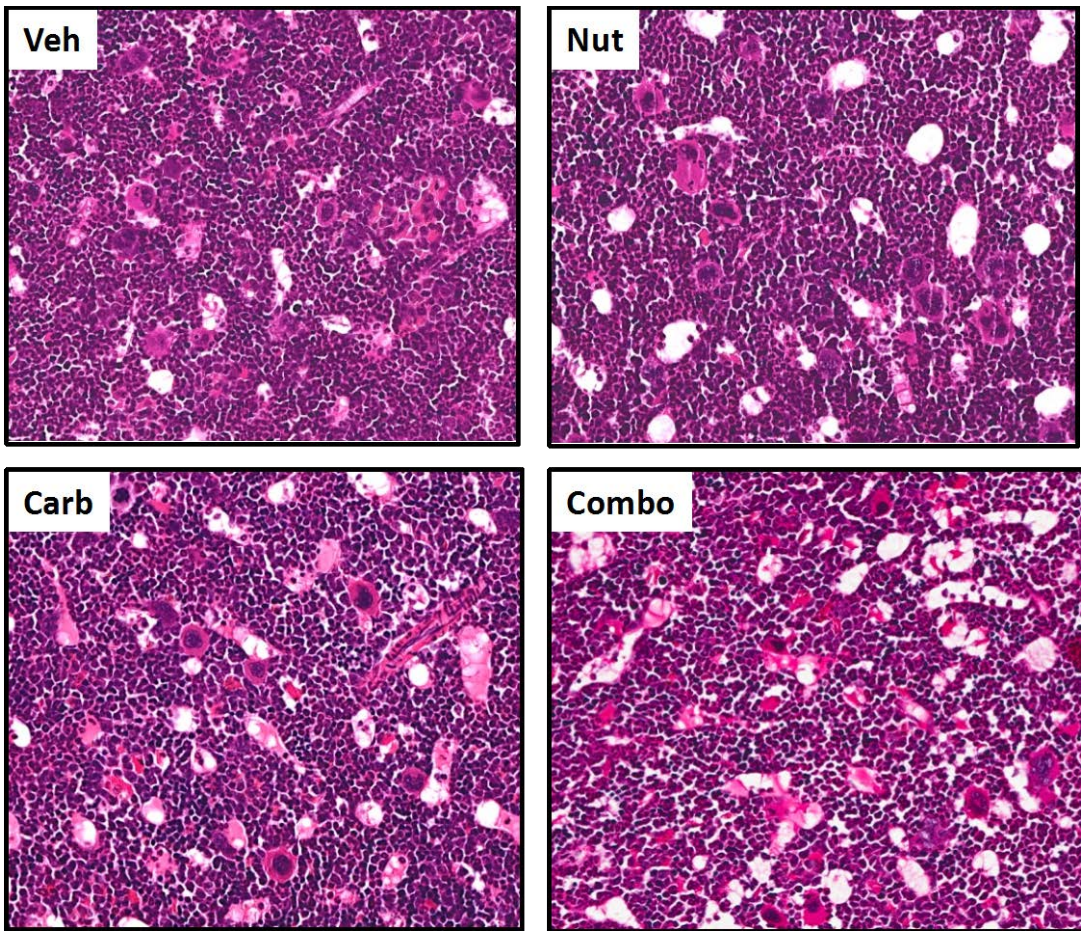

Figure 55. Myeloid hyperplasia is evident in bone smears from all treatment groups but no changes are observed in overall bone marrow composition following treatment. Femur bones were excised during necropsy. Bones were fixed in 10% buffered formalin and decalcified with Decal®. Bones were set in paraffin blocks, sectioned, and stained with H&E. There were no overt signs of toxicity in bone marrow smears from all treatment groups. There was myeloid hyperplasia present in all treatment groups.

To examine other tissue toxicity to combination drug treatment, we evaluated the liver and spleen of treated mice. Spleens from all treatment groups exhibited increased myeloid stem cells in the spleens while only some of the livers from the same mice exhibited extramedullary hematopoiesis (EMH) in livers (Table 2). Three mice exhibited focal lesions in the livers, which did not correlate to the treatment groups indicating that the metastasis to the liver was a random event. Two mice from the carboplatin-treated group had one focal lesion in the liver while one Nutlin-3a treated mouse exhibited 2 focal lesions in the liver (Table 2). Despite exhibiting extramedullary hematopoiesis, the spleens and livers from all treatment groups appeared normal with no regions of necrosis or inflammation.

Treatment Group	Mouse No.	Liver	Spleen
Carb	M3	0	severe EMH
Carb	M7	1 focal lesion	severe EMH
Carb	M8	1 focal lesion	EMH
Combo	M13	0	EMH
Combo	M15	0	EMH
Combo	M16	0	EMH
Nut	M18	2 focal lesions	severe EMH
Nut	M21	EMH	EMH
Nut	M23	EMH	EMH
Veh	M27	EMH	EMH
Veh	M29	EMH	EMH
Veh	M31	EMH	EMH

Table 2. All spleens and some livers exhibit extramedullary hematopoiesis (EMH) with few focal lesions. Spleens and livers were collected from sacrificed mice. Tissues were embedded, sectioned, and examined using H&E staining. All spleens collected from each of the treatment groups exhibited increased myeloid stem cells in the spleens while only some of the livers collected from the same mice exhibited extramedullary hematopoiesis (EMH) in livers. Three mice exhibited focal lesions in the livers, which did not correlate to the treatment groups.

A pharmacodynamic study was conducted to begin to understand what the combination treatment may modulate at the molecular level *in vivo*. Based on *in vitro* results, we showed that the combination treatment led to synergistic effects in methylene blue proliferation assays. We also observed increases in Mdm2 protein levels in Nutlin-3a- and combination-treated TMD231 cells when examined with Western blot. It has been shown in the literature that Nutlin-3a inhibits the binding of Mdm2 to Hif-1α which led to decreased VEGF [62]. With decreased levels of VEGF, the tumor cells would have limited angiogenesis capabilities. Based on these data, we determined the *in vivo* pharmacodynamic effects of the combination treatment on tumors by examining the effect of drug treatment on human VEGF levels and target protein modulation in primary tumors following a short treatment schema. Complete study design is outlined in Figure 56.

Figure 56. Pharmacodynamic study design

Objective: Examine the pharmacodynamic effects of combination Nutlin-3a and carboplatin treatment at the site of primary tumors following short-term drug treatment

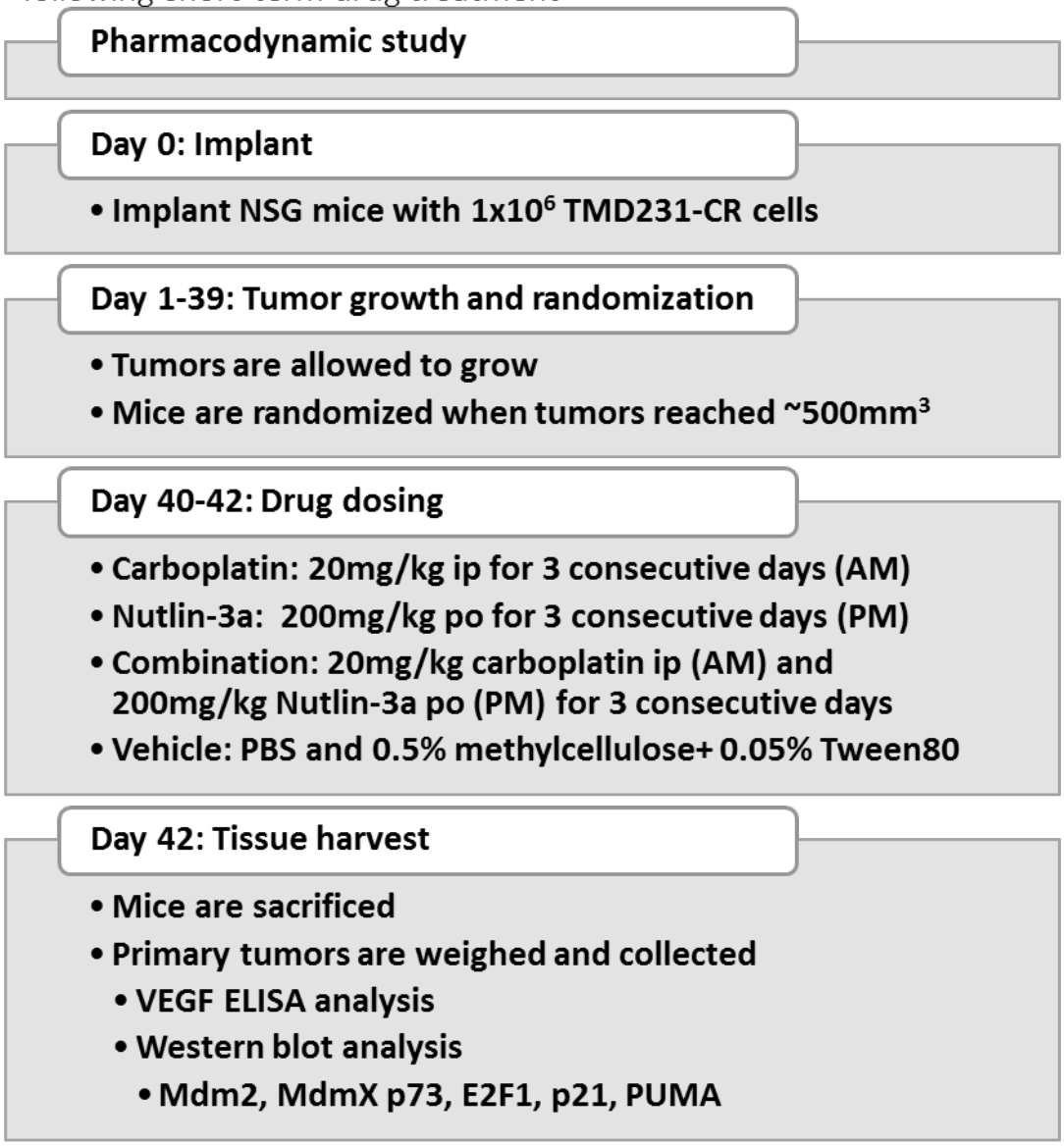

NSG mice were implanted with TMD231-CR cells and allowed to grow. Once the tumors reached ~500mm^3 as measured by caliper, the mice were randomized into treatment groups so that each group received equivalent tumor sizes. The mice were dosed for 3 consecutive days and sacrificed 2 hours following the completion of drug treatment. The tumors were excised, cut in half, and snap frozen for use in VEGF ELISA and Western blot analysis. Tumors were lysed and equal protein was loaded into the Human VEGF Quantikine ELISA Kit (R&D Systems) plate as per manufacturer's instructions. There was no difference in human VEGF levels present in any tumors between any of the treatment groups (n=5, mean±SD) (Figure 57). The Human VEGF Quantikine ELISA Kit utilizes antibodies raised against the most common form of VEGF, $VEGF_{165}$. If there were any differences in any of the other VEGF isoforms, we would not have been able to detect these differences with this particular ELISA format.

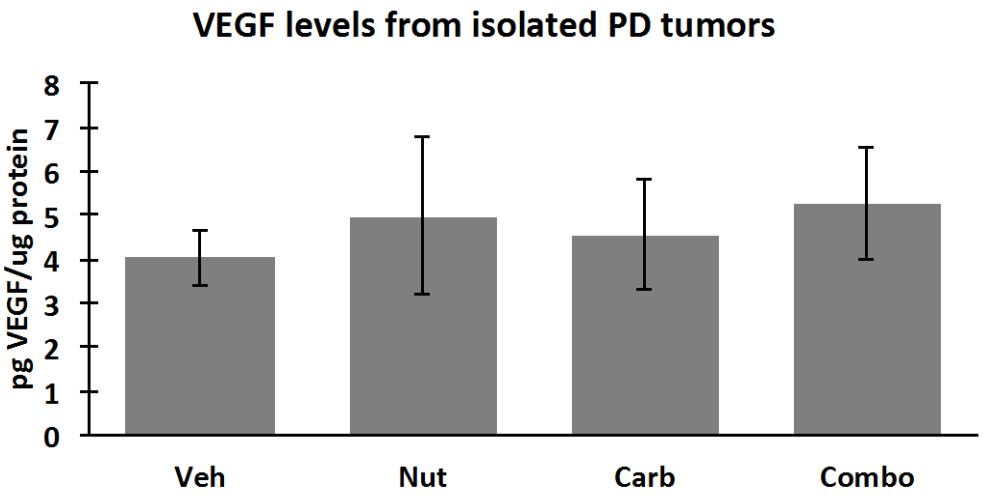

Figure 57. Human $VEGF_{165}$ levels are not altered by drug treatment *in vivo*. NSG mice were implanted with $1x10^6$ TMD231-CR cells, and when primary tumors reached approximately $500mm^3$, randomized based on tumor volume. Mice were dosed with 20mg/kg i.p. carboplatin alone in the morning, 200mg/kg Nutlin-3a p.o. alone in the afternoon, or combination for 3 consecutive days. Mice were sacrificed 2 hours following the administration of the last dose of Nutlin-3a, and primary tumors were excised and collected. Tumors were homogenized using the Tissue Tearor™ Homogenizer, and evaluated for the presence of Human VEGF using an ELISA assay. There was no difference in Human $VEGF_{165}$ present in tumors between any of the treatment groups (n=5, ±SD).

The other half of the primary tumors collected at the completion of the pharmacodynamic experiment was used to evaluate the effects of carboplatin and Nutlin-3a drug treatment *in vivo*. There were increases in Mdm2 protein levels in mice treated with Nutlin-3a alone while the increases in Mdm2 following combination treatment were not as robust (Figure 58). This result was similar to what we observed with *in vitro* experiments (Figure 17). There was a significant increase in MdmX, E2F1, and p21 levels in the combination treated mice compared to Vehicle (Mouse 1, 2, and 4) treated mice (Student's T-test, $p<0.05$, n=3-4, mean±SEM) (Figure 58). Overall, there were no noticeable changes in PUMA levels when comparing the different treatment groups. This could be due to the time point at which the tumors were harvested. We may need to make alterations to the dosing schema to gain a better understanding in PUMA levels. In the future, time-course experiments could be done to better elucidate the signaling mechanisms that are operative *in vivo* following short-term drug treatment. Immunohistochemistry staining for Mdm2 localization (nuclear versus cytoplasmic) will be used in the future to better understand the mechanism *in vivo*.

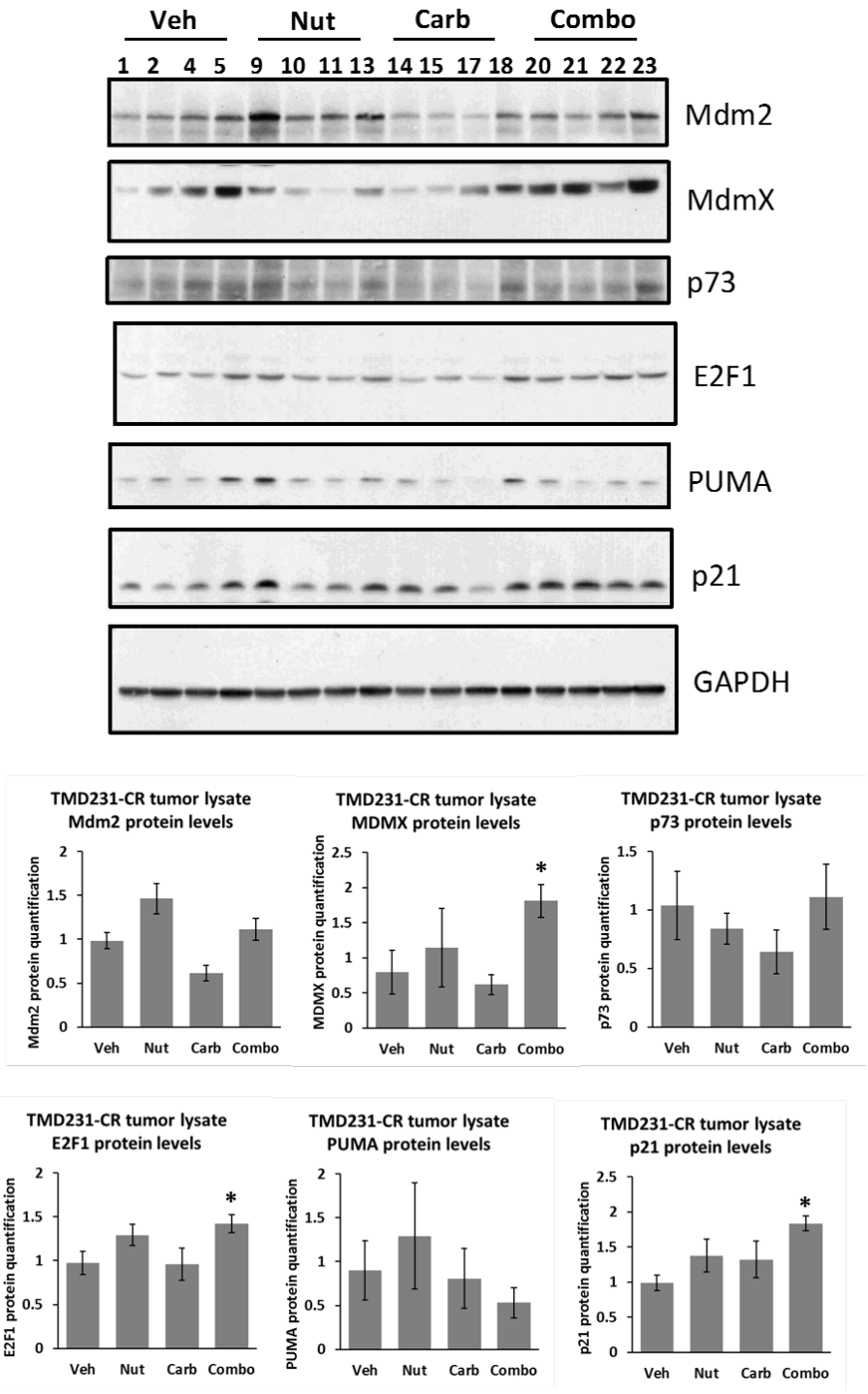

Figure 58. Combination treatment significantly increases MdmX, E2F1, and p21 protein levels *in vivo*. NSG mice were implanted with 1x10^6 TMD231-CR cells, and when primary tumors reached approximately 500mm^3, randomized into treatment groups based on

tumor volume. Mice were dosed with Vehicle (PBS and 0.5% methylcellulose+0.05% Tween80) (Veh), 20mg/kg i.p. carboplatin alone (Carb) in the morning, 200mg/kg Nutlin-3a p.o. alone (Nut) in the afternoon, or combination (Combo) for 3 consecutive days. Mice were sacrificed 2 hours following the last administration of Nutlin-3a and primary tumors were excised and collected. Tumors were homogenized using the Tissue Tearor™ Homogenizer and evaluated for changes in target protein levels by Western blot. There was a noticeable increase in Mdm2 protein levels the combination-treated mice however it was not as high as that observed in the Nutlin-3a-treated mice, which was similar to that of the *in vitro* data (Figure 17). There was a significant increase in E2F1 and MdmX levels in the combination treated mice compared to Vehicle (Mouse 1, 2, and 4) and carboplatin-treated mice (Student's T-test, $p<0.05$, n=3-4, ±SEM). There was a significant increase p21 levels in the combination treated mice compared to Vehicle (Mouse 1, 2, and 4) treated mice (Student's t-test, $p<0.05$, n=4, ±SEM).

C. **Discussion and Future Directions**

To summarize combination study 1, combination drug dosing schema was tested for feasibility, efficacy, and overall tolerability in mice. The combination treatment significantly inhibited primary tumor growth that was confirmed following post-necropsy tumor weights when compared to tumor growth and weights of Vehicle- and single drug-treated mice. The number of metastases in the lungs in the combination-treated mice was significantly reduced compared to Vehicle- and single drug-treated mice. The decreased lung metastases was confirmed with traditional pathologist scoring by hand as well as using measuring positivity of staining utilizing the Aperio ImageScope (Leica Biosystems) software analysis. The use of the automated image quantification increased speed of tissue analysis, decreased the cost of analysis and reduced any bias in analyzing tissue samples [156]. The use of *in vivo* imaging was best used as a sensitive way to measure non-palpable tumors when the goal was to randomize mice at an early tumor burden.

Overall in combination study 2, we further optimized the drug dosing schema by reducing the dose of carboplatin to 20mg/kg from 25mg/kg and lengthened the time between doses to decrease stress and drug induced toxicity on the animals. This dosing optimization is very important *in vivo* when trying to reduce toxicity in the animals. Studies examining the optimization of the dosing schema using a second generation Nutlin-3a derivative, RG7388, concluded that a 50mg/kg weekly dose was equivalent in efficacy to 10mg/kg daily dosing in an osteosarcoma model while reducing toxicity [149]. Further drug dosing optimization could be completed in future studies to improve upon

efficacy while decreasing tissue toxicity. We determined that the combination treatment increased the probability of survival when compared to Vehicle and single carboplatin and Nutlin-3a treatment. The combination treatment significantly decreased total bone marrow cells immediately following drug treatment. However, after a recovery period of about 2 weeks, the levels of total bone marrow cells in combination treated mice come back up to normal levels. Additionally, while breast cancer cells can metastasize to bone, we did not detect any TMD231-CR present in isolated bone marrow cells from any of the treatment groups.

Combination study 3 continued to validate the previous two studies as well as further expand on examining toxicity at the bone marrow as well as other tissues. As in the previous combination studies, the combination treatment significantly decreased primary tumor volume when compared to Vehicle and single carboplatin and Nutlin-3a treated mice. The mice were sacrificed after a 2-week recovery period after the completion of drug treatment. Bone marrow cellularity analysis indicated that there was no difference in the combination treated-mice compared to the Vehicle- and single-drug treated mice which further confirms that there is not a long lasting effect of drug treatment on total bone-marrow cell counts. Additionally, we used clonogenic progenitor assays to examine the effects of drug treatment on the progenitor cells from isolated bone marrow of treated mice. There was a significant reduction in number of progenitor cells in the combination-treated mice compared to the Vehicle- and single drug treated-mice. We also examined the effects of drug treatment on peripheral blood counts by completing CBC analysis. We saw a significant reduction in red blood cells in

combination treated mice compared to Vehicle and single drug treated mice. Also, there were significant reduction in white blood cells and platelets in the carboplatin and combination treated mice compared to the Vehicle and Nutlin-3a alone treated mice. While there were reductions in peripheral blood cell counts and progenitor assays, overall there did not seem to be any overt toxicity as a result of these changes. We also used histology to examine the effects of drug treatment on bone marrow using bone marrow smears, as well as spleens and livers of treated mice. Based on bone marrow smears, there was no overt toxicity present with all groups presenting with myeloid hyperplasia. The presence of tumor cells in the bone marrow was not detected during analysis. The livers and spleens of the mice did not appear to be different between treatment groups after analysis with H&E staining. There was extramedullary hyperplasia (EMH) present in all spleens from the all of the treatment groups. There was EMH present in some of the livers as well as a few mice that presented with focal lesions in the livers. The presence of the focal lesions did not correlate to the drug treatment groups and seems to be at random. There were no signs of overt tissue toxicity in the livers and spleens of mice with no areas of necrosis or abnormal cellular phenotypes.

Combination therapies are common in treating cancer as the multi-targeted approach has been beneficial in improving treatments and patient outcomes. Finding new therapeutic targets is of great interest. Our studies show an improved outcome following the combination of Nutlin-3a and carboplatin. Additional therapeutic targets could be examined in our model system. One study showed in TNBC cells harboring mutant p53, that inhibition of Chk1 in combination with DNA damage led to a bypass of

Chk1-mediated checkpoint signaling and increased apoptosis in a patient xenograft model [157]. In our system, Chk1 inhibitors could be added to potentially increased efficacy and lead to further tumor inhibition. Additionally, the TMD231 cells are very invasive as shown by *in vitro* cell invasion assays and the presence of *in vivo* lung metastases. Price and colleagues showed that in the parental MDA-MB-231 cells, activity of EGFR led to increased migration through Phosphatidylinositol 3'-Kinase (PI3K) and Phospholipase C- (PLC) dependent signaling [158]. In these studies, it was shown that epidermal growth factor (EGF), which is the substrate for EFGR, led to increased cell migration while not affecting cell proliferation in the MDA-MB-231 cells [158]. The migratory nature of the cells towards EGF was inhibited by the treatment of the cells with EGFR tyrosine kinase inhibitors, AG1478 and PD153035, the PI3K inhibitor, wortmannin, MEK inhibitor, PD098059, as well as the PLC inhibitor, U73122 [158]. Following flow cytometry experiments of TMD231 cells, we observed that a high percentage of cells (>95%) express EGFR (data not shown), which could help drive distant migration *in vivo*. Additionally, Ferraro and colleagues showed *in vitro* and *in vivo* model of TNBC that inhibition of EGFR using certain combinations of EGFR antibodies led to downregulation of the EGFR, inhibited EGFR recycling, and migration *in vitro* as well as inhibition of tumorigenic growth *in vivo* [159]. While EGFR antagonists have not been highly successful in clinical trials, the authors propose that the use of combinations of EGFR antibodies in which there is no epitope overlap may lead increased efficacy compared to those antibody combinations where the epitope of EGFR overlaps between

the two antibodies [159]. These treatment strategies could be integrated into our model system to further inhibit the tumorigenicity of TNBCs.

The pharmacodynamic study was designed to better understand the combination treatment effects on protein levels *in vivo*. The pharmacodynamic study showed no difference in human $VEGF_{165}$ levels following VEGF ELISA analysis. Further analysis would need to be completed to examine the other isoforms of VEGF since the VEGF ELISA utilized only looked at the presence of the most prevalent VEGF isoform, $VEGF_{165}$. Western analysis from PD tumor lysates showed significant increases in E2F1, MdmX, and p21 compared to Vehicle treated mice *in vivo* following combination treatment. These *in vivo* results were different from *in vitro* results as the combination treatment led to decreases in MdmX following combination treatment *in vitro*. It has been in our experience that modulation of targets may differ between *in vitro* and *in vivo* settings since there are difference in tumor microenvironment with the lack of stromal cells in many *in vitro* settings as well as differences in oxygen content available to the tumor cells, which is especially true *in vivo*. Stromal cells may offer support to growing tumor cells by excreting growth factors [160]. Often in tumors *in vivo*, the cells must adapt to surviving in hypoxic conditions due to decreased and/or abnormal blood flow to the tumor. *In vitro*, the cells typically are grown in 5% oxygen, which is much higher than found in tumor settings [161,162]. These differences in microenvironment may lead to different signaling pathways to be altered in tumor cells especially following drug treatment. Further studies will need to be conducted to identify and validate biomarkers of efficacy following drug treatment *in viv*o. We observed increasing trends

of Mdm2 in the Nutlin-3a and combination treated mice compared to Vehicle, which is similar to *in vitro* results, and we did not observe increases in PUMA levels across the treatment groups. We may need to alter the dosing schema for the pharmacodynamic study, possibly increasing the length of treatment to visualize the modulation of other molecular markers. We essentially took a snapshot in time when the tumors were harvested. We may have missed or not reached maximal protein levels of Mdm2 and PUMA in our system. Additionally, PUMA may not be playing a large role in our system due to other factors that inhibit PUMA signaling including antagonization by the EGFR receptor [143]. Experiments would need to be completed to examine if EGFR is playing a role in our system. Further experiments would need to be conducted to better understand how the drug treatments affect signaling molecules that could be potential biomarkers of treatment effect *in vivo*.

Overall the combination drug treatment was well tolerated in mice with minimal toxicity and high efficacy at inhibiting the primary tumor growth and metastasis in the lung. Preliminary pharmacodynamic studies show some evidence of target modulation following drug treatment. Further studies will need to be conducted to increase our understanding of the signaling mechanism *in vivo*. Similar studies could be completed with MdmX especially since it has been shown that MdmX has similar functions at inhibiting DNA repair by binding to Nbs1 [99]. It would be especially interesting since we saw increased Mdm2 levels *in vitro* following the combination treatment but did not observe significant increases in Mdm2 *in vivo* compared to Vehicle control mice. The opposite was true with MdmX levels in the tumors from combination treated-mice. *In*

vivo, MdmX levels were increased in the combination treated mice while there were no increases in MdmX levels in the *in vitro* experiments. Further experiments are being conducted to examine all seven-mouse tumors from the Vehicle and combination treated mice to see if there is a more robust effect when all samples are examined. We also plan on completing immunohistochemistry of tumor samples to look at Mdm2 levels and cellular localization. The tumor samples from the PD study mice were completely lysed and there could be sub-compartments of the tumors that differentially express molecular targets. Possibly, there are significant changes in Mdm2 and MdmX levels in subsections of the tumors and following complete lysis, the signal was diluted to the point where differences were hard to visualize. Immunohistochemistry could provide increased understanding of protein level changes within the tumor. Additionally, it would be interesting to note the location of Mdm2 and MdmX within the cell to see if we indeed observe increased Mdm2 and MdmX in the nucleus. We could also conduct chromatin association assays from tumors to examine the levels of Mdm2 and MdmX found at the chromatin *in vivo*. We also have the lung tissues from the PD study mice, which we could use to examine the effects of drug treatment on molecular target levels in metastatic site *in vivo*. The mice were not treated until Day 40 post implant allowing for metastases to be present in the lungs. The lungs could be lysed and target modulation could be examined by Western blot. Additionally, the lungs could be examined by immunohistochemistry staining to examine molecular target levels within the metastases from whole tissue slices. The use of combined Mdm2 inhibition through Nutlin-3a and DNA damaging-carboplatin shows a potential therapeutic benefit in TNBC

with reductions in primary tumor volume, reduced lung metastases, increased survival, and no notable long lasting toxicity. Further studies will need to be conducted to better understand the signaling mechanism, but potential molecular targets that could be tracked as markers of treatment response included MdmX, p21, and E2F1 *in vivo* in this *in vivo* model of TNBC.

Chapter 5. Modulation Of The Mdm2 Signaling Axis Sensitizes Triple-Negative Breast Cancer Cells To Carboplatin Summary

In closing, this thesis showed the combined use of the PPI, Nutlin-3a, to inhibit Mdm2 and DNA damaging drug, carboplatin, led to decreased cell proliferation and increased apoptosis *in vitro* as well as decreased tumor growth and metastasis and increased survival *in vivo*. Nutlin-3a led to the potentiation of carboplatin-mediated DNA damage *in vitro* and *in vivo* allowing for several signaling pathways to be activated including p73-mediated apoptosis and delayed DNA damage response due to Mdm2 antagonization of Nbs1 *in vitro* (Figure 59). The overall objective of this thesis was to evaluate the therapeutic potential of a new combination therapy to treat TNBC independent of wild-type p53. Based on front-line therapies currently being tested in clinical trials for TNBC, the platinum agent, carboplatin was selected for study. Novel drug targets need to be elucidated to improve treatment modalities especially in treating aggressive cancers like TNBC. Mdm2 is an unexplored target in breast cancers, and histological studies have indicated that more than half of breast cancer biopsies contain high levels of Mdm2. In this thesis, the potentiation of carboplatin-mediated DNA damage in the context of blocking some aspects of Mdm2 function was investigated. Pharmacodynamic studies were designed to gain insight into and validate molecular mechanisms that based on the literature could be operative following treatment. In our correlative PD studies, we also sought to identify targets that could potentially serve as biomarkers of treatment response and efficacy for future clinical

trials of TNBC. A humanized breast-to-lung model was optimized in NSG mice and can be used in the future to further screen and validate novel combination therapies. Further studies will need to be conducted to expand and build upon our knowledge to further validate key molecular targets and operative signaling pathways present in our model system. Additionally we plan on using primary patient xenograft models with the PDX breast cancer models from Jackson Laboratories. There are several PDX models that feature TNBC with mutant p53. These primary patient tumors have been characterized with gene levels, copy number variation, and histology data. These primary patient samples will allow for us to examine the effects of dual Nutlin-3a and carboplatin treatment in more clinically relevant models. The data presented in this thesis indicate that Mdm2 represents a valid therapeutic target in TNBC and is worthy of further exploration at the cellular and molecular levels. In closing, the *in vitro* and *in vivo* results provide solid confirmation that modulation of Mdm2 in the context of platinum-based cytotoxic therapy is a valid approach for improving treatment of TNBC.

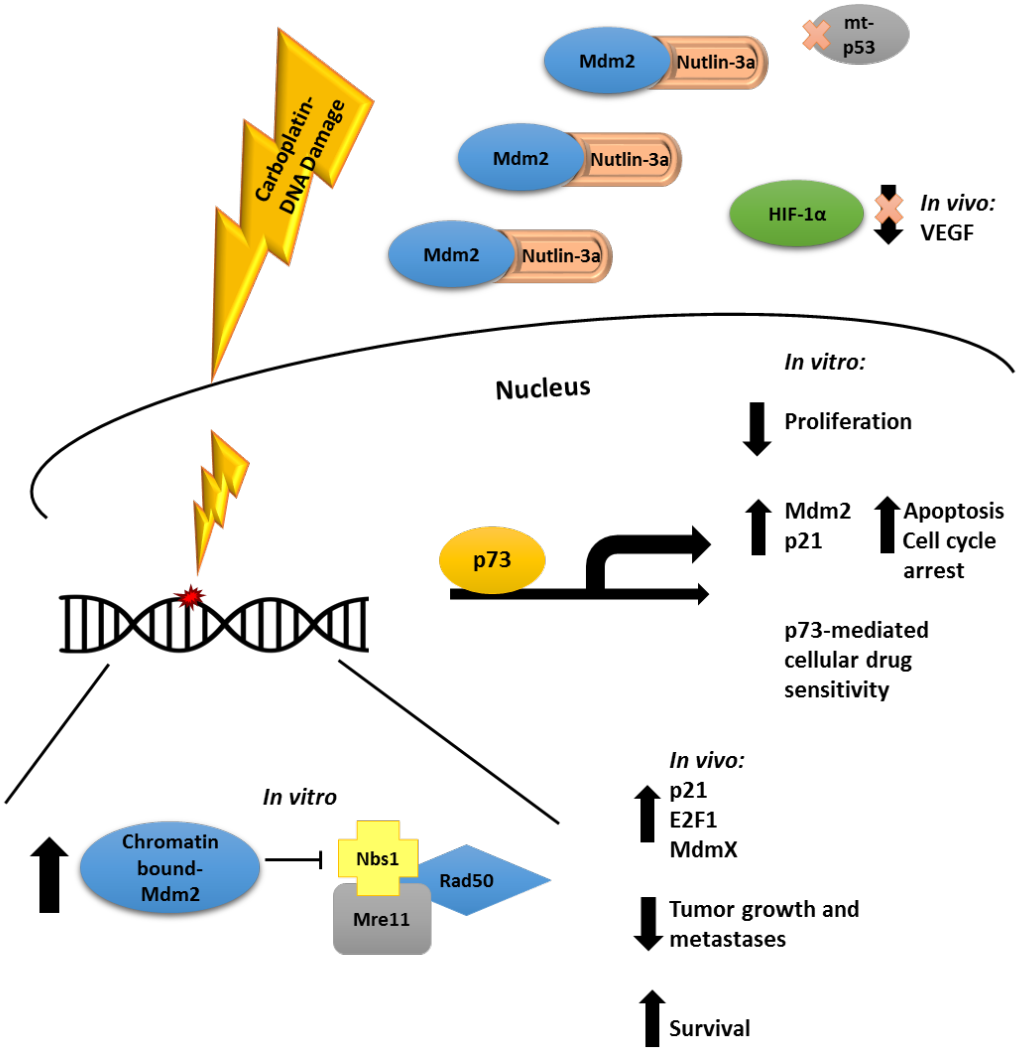

Figure 59. Mdm2 as a therapeutic target and potential molecular markers for TNBC using Nutlin-3a and carboplatin in combination. Nutlin-3a was designed as a small molecular inhibitor that bound into the hydrophobic pocket of Mdm2 inhibiting the binding of p53. It was later shown that Nutlin-3a also inhibited the binding of E2F1, p73 and Hif-1α to Mdm2. In recent years, the use of platinum drugs has gained popularity in the treatment of breast cancers. Carboplatin causes DNA damage by causing intra and interstrand crosslinks in the DNA ultimately leading to cell death. In our model system of TNBC with mutant p53, we sought to understand the molecular targets being

modulated *in vitro* and *in vivo*. *In vitro*, we observed increased p21 and Mdm2 protein levels following drug treatment. There were concentration-dependent increases in p21 following single Nutlin-3a treatment. Nutlin-3a alone and combination treatment led to increased Mdm2 levels following Western blot. We also observed increased Mdm2 associated with the chromatin following combination treatment than each single drug alone. We hypothesized that increased levels of Mdm2 at the chromatin led to increased binding of Mdm2 to Nbs1, which in turn led to decreased DNA repair and was supported by Bouska and colleagues [35]. Additionally, following siRNA-mediated knockdown of p73, we observed p73-dependent cellular sensitivity to carboplatin drug treatment. Following a PD study *in vivo*, we observed changes in MdmX, p21, and E2F1 protein levels in combination treated mice compared to Vehicle and single drug treated mice. We did not observe significant changes in $VEGF_{165}$ levels between treatment groups.

REFERENCES

1 Hanahan, D. & Weinberg, R. A. Hallmarks of cancer: the next generation. *Cell* **144**, 646-674, doi:10.1016/j.cell.2011.02.013 (2011).

2 Blackwood, M. A. & Weber, B. L. BRCA1 and BRCA2: from molecular genetics to clinical medicine. *J Clin Oncol* **16**, 1969-1977 (1998).

3 O'Shaughnessy, J. Extending survival with chemotherapy in metastatic breast cancer. *Oncologist* **10 Suppl 3**, 20-29, doi:10.1634/theoncologist.10-90003-20 (2005).

4 Altekruse SF, K. C., Krapcho M, Neyman N, Aminou R, Waldron W, Ruhl J, Howlader N, Tatalovich Z, Cho H, Mariotto A, Eisner MP, Lewis DR, Cronin K, Chen HS, Feuer EJ, Stinchcomb DG, Edwards BK (eds). *SEER Cancer Statistics Review*, <http://seer.cancer.gov/statfacts/html/breast.html> (1975-2007).

5 Schnitt, S. J. Classification and prognosis of invasive breast cancer: from morphology to molecular taxonomy. *Modern pathology : an official journal of the United States and Canadian Academy of Pathology, Inc* **23 Suppl 2**, S60-64, doi:10.1038/modpathol.2010.33 (2010).

6 Creighton, C. J. The molecular profile of luminal B breast cancer. *Biologics : targets & therapy* **6**, 289-297, doi:10.2147/BTT.S29923 (2012).

7 Chuang, H. C., Kapuriya, N., Kulp, S. K., Chen, C. S. & Shapiro, C. L. Differential anti-proliferative activities of poly(ADP-ribose) polymerase (PARP) inhibitors in triple-negative breast cancer cells. *Breast Cancer Res Treat* **134**, 649-659, doi:10.1007/s10549-012-2106-5 (2012).

8 Dent, R. *et al.* Triple-negative breast cancer: clinical features and patterns of recurrence. *Clin Cancer Res* **13**, 4429-4434, doi:10.1158/1078-0432.CCR-06-3045 (2007).

9 Ashworth, A. A synthetic lethal therapeutic approach: poly(ADP) ribose polymerase inhibitors for the treatment of cancers deficient in DNA double-strand break repair. *J Clin Oncol* **26**, 3785-3790, doi:10.1200/JCO.2008.16.0812 (2008).

10 Mehta, R. S. Dose-dense and/or metronomic schedules of specific chemotherapies consolidate the chemosensitivity of triple-negative breast cancer: a step toward reversing triple-negative paradox. *J Clin Oncol* **26**, 3286-3288; author reply 3288, doi:10.1200/JCO.2008.17.1116 (2008).

11 Villarreal-Garza, C. *et al.* Platinum-based chemotherapy in triple-negative advanced breast cancer. *Breast Cancer Res Treat* **146**, 567-572, doi:10.1007/s10549-014-3033-4 (2014).

12 Hurley, J. *et al.* The use of neoadjuvant platinum-based chemotherapy in locally advanced breast cancer that is triple negative: retrospective analysis of 144 patients. *Breast Cancer Res Treat* **138**, 783-794, doi:10.1007/s10549-013-2497-y (2013).

13 Arun, B. *et al.* Response to neoadjuvant systemic therapy for breast cancer in BRCA mutation carriers and noncarriers: a single-institution experience. *J Clin Oncol* **29**, 3739-3746, doi:10.1200/JCO.2011.35.2682 (2011).

14 Fuertes, M. A., Castilla, J., Alonso, C. & Perez, J. M. Cisplatin biochemical mechanism of action: from cytotoxicity to induction of cell death through interconnections between apoptotic and necrotic pathways. *Current medicinal chemistry* **10**, 257-266 (2003).

15 Lokich, J. & Anderson, N. Carboplatin versus cisplatin in solid tumors: an analysis of the literature. *Ann Oncol* **9**, 13-21 (1998).

16 Kim, J. B., Stein, R. & O'Hare, M. J. Three-dimensional in vitro tissue culture models of breast cancer-- a review. *Breast Cancer Res Treat* **85**, 281-291, doi:10.1023/B:BREA.0000025418.88785.2b (2004).

17 Helbig, G. *et al.* NF-kappaB promotes breast cancer cell migration and metastasis by inducing the expression of the chemokine receptor CXCR4. *J Biol Chem* **278**, 21631-21638, doi:10.1074/jbc.M300609200M300609200 [pii] (2003).

18 Vantyghem, S. A. *et al.* A new model for lymphatic metastasis: development of a variant of the MDA-MB-468 human breast cancer cell line that aggressively metastasizes to lymph nodes. *Clinical & experimental metastasis* **22**, 351-361, doi:10.1007/s10585-005-0745-1 (2005).

19 Junk, D. J. *et al.* Different mutant/wild-type p53 combinations cause a spectrum of increased invasive potential in nonmalignant immortalized human mammary epithelial cells. *Neoplasia* **10**, 450-461 (2008).

20 Bamford, S. *et al.* The COSMIC (Catalogue of Somatic Mutations in Cancer) database and website. *Br J Cancer* **91**, 355-358, doi:10.1038/sj.bjc.6601894 (2004).

21 Kelland, L. R. Of mice and men: values and liabilities of the athymic nude mouse model in anticancer drug development. *European journal of cancer* **40**, 827-836, doi:10.1016/j.ejca.2003.11.028 (2004).

22 Shultz, L. D. *et al.* Multiple defects in innate and adaptive immunologic function in NOD/LtSz-scid mice. *J Immunol* **154**, 180-191 (1995).

23 Shultz, L. D. *et al.* Human lymphoid and myeloid cell development in NOD/LtSz-scid IL2R gamma null mice engrafted with mobilized human hemopoietic stem cells. *J Immunol* **174**, 6477-6489, doi:174/10/6477 [pii] (2005).

24 Cheon, D. J. & Orsulic, S. Mouse models of cancer. *Annual review of pathology* **6**, 95-119, doi:10.1146/annurev.pathol.3.121806.154244 (2011).

25 Klerk, C. P. *et al.* Validity of bioluminescence measurements for noninvasive in vivo imaging of tumor load in small animals. *BioTechniques* **43**, 7-13, 30 (2007).

26 Shcherbakova, D. M. & Verkhusha, V. V. Near-infrared fluorescent proteins for multicolor in vivo imaging. *Nature methods* **10**, 751-754, doi:10.1038/nmeth.2521 (2013).

27 Strack, R. L. *et al.* A rapidly maturing far-red derivative of DsRed-Express2 for whole-cell labeling. *Biochemistry* **48**, 8279-8281, doi:10.1021/bi900870u (2009).

28 Shaner, N. C. *et al.* Improved monomeric red, orange and yellow fluorescent proteins derived from Discosoma sp. red fluorescent protein. *Nature biotechnology* **22**, 1567-1572, doi:10.1038/nbt1037 (2004).

29 Cahilly-Snyder, L., Yang-Feng, T., Francke, U. & George, D. L. Molecular analysis and chromosomal mapping of amplified genes isolated from a transformed mouse 3T3 cell line. *Somat Cell Mol Genet* **13**, 235-244 (1987).

30 Fakharzadeh, S. S., Trusko, S. P. & George, D. L. Tumorigenic potential associated with enhanced expression of a gene that is amplified in a mouse tumor cell line. *EMBO J* **10**, 1565-1569 (1991).

31 Jones, S. N., Roe, A. E., Donehower, L. A. & Bradley, A. Rescue of embryonic lethality in Mdm2-deficient mice by absence of p53. *Nature* **378**, 206-208, doi:10.1038/378206a0 (1995).

32 Montes de Oca Luna, R., Wagner, D. S. & Lozano, G. Rescue of early embryonic lethality in mdm2-deficient mice by deletion of p53. *Nature* **378**, 203-206, doi:10.1038/378203a0 (1995).

33 Oliner, J. D., Kinzler, K. W., Meltzer, P. S., George, D. L. & Vogelstein, B. Amplification of a gene encoding a p53-associated protein in human sarcomas. *Nature* **358**, 80-83, doi:10.1038/358080a0 (1992).

34 Leach, F. S. *et al.* p53 Mutation and MDM2 amplification in human soft tissue sarcomas. *Cancer Res* **53**, 2231-2234 (1993).

35 Bouska, A., Lushnikova, T., Plaza, S. & Eischen, C. M. Mdm2 promotes genetic instability and transformation independent of p53. *Mol Cell Biol* **28**, 4862-4874, doi:MCB.01584-07 [pii]10.1128/MCB.01584-07 (2008).

36 Rayburn, E., Zhang, R., He, J. & Wang, H. MDM2 and human malignancies: expression, clinical pathology, prognostic markers, and implications for chemotherapy. *Curr Cancer Drug Targets* **5**, 27-41 (2005).

37 Chen, X. *et al.* MDM2 promotes invasion and metastasis in invasive ductal breast carcinoma by inducing matrix metalloproteinase-9. *PloS one* **8**, e78794, doi:10.1371/journal.pone.0078794 (2013).

38 Araki, S. *et al.* TGF-beta1-induced expression of human Mdm2 correlates with late-stage metastatic breast cancer. *J Clin Invest* **120**, 290-302, doi:39194 [pii]10.1172/JCI39194 (2010).

39 Cheng, T. H. & Cohen, S. N. Human MDM2 isoforms translated differentially on constitutive versus p53-regulated transcripts have distinct functions in the p53/MDM2 and TSG101/MDM2 feedback control loops. *Mol Cell Biol* **27**, 111-119, doi:10.1128/MCB.00235-06 (2007).

40 Vassilev, L. T. *et al.* In vivo activation of the p53 pathway by small-molecule antagonists of MDM2. *Science* **303**, 844-848, doi:10.1126/science.10924721092472 [pii] (2004).

41 Kussie, P. H. *et al.* Structure of the MDM2 oncoprotein bound to the p53 tumor suppressor transactivation domain. *Science* **274**, 948-953 (1996).

42 Meek, D. W. & Knippschild, U. Posttranslational modification of MDM2. *Mol Cancer Res* **1**, 1017-1026 (2003).

43 Mayo, L. D. & Donner, D. B. A phosphatidylinositol 3-kinase/Akt pathway promotes translocation of Mdm2 from the cytoplasm to the nucleus. *Proc Natl Acad Sci U S A* **98**, 11598-11603, doi:10.1073/pnas.181181198 (2001).

44 Zhou, B. P. *et al.* HER-2/neu induces p53 ubiquitination via Akt-mediated MDM2 phosphorylation. *Nature cell biology* **3**, 973-982, doi:10.1038/ncb1101-973 (2001).

45 Fang, S., Jensen, J. P., Ludwig, R. L., Vousden, K. H. & Weissman, A. M. Mdm2 is a RING finger-dependent ubiquitin protein ligase for itself and p53. *J Biol Chem* **275**, 8945-8951 (2000).

46 Honda, R. & Yasuda, H. Activity of MDM2, a ubiquitin ligase, toward p53 or itself is dependent on the RING finger domain of the ligase. *Oncogene* **19**, 1473-1476, doi:10.1038/sj.onc.1203464 (2000).

47 Lai, Z. *et al.* Human mdm2 mediates multiple mono-ubiquitination of p53 by a mechanism requiring enzyme isomerization. *J Biol Chem* **276**, 31357-31367, doi:10.1074/jbc.M011517200 (2001).

48 Grossman, S. R. *et al.* Polyubiquitination of p53 by a ubiquitin ligase activity of p300. *Science* **300**, 342-344, doi:10.1126/science.1080386 (2003).

49 Meek, D. W. & Hupp, T. R. The regulation of MDM2 by multisite phosphorylation--opportunities for molecular-based intervention to target tumours? *Seminars in cancer biology* **20**, 19-28, doi:10.1016/j.semcancer.2009.10.005 (2010).

50 Iwakuma, T. & Lozano, G. MDM2, an introduction. *Mol Cancer Res* **1**, 993-1000 (2003).

51 Sionov, R. V. *et al.* c-Abl neutralizes the inhibitory effect of Mdm2 on p53. *J Biol Chem* **274**, 8371-8374 (1999).

52 Goldberg, Z. *et al.* Tyrosine phosphorylation of Mdm2 by c-Abl: implications for p53 regulation. *EMBO J* **21**, 3715-3727, doi:10.1093/emboj/cdf384 (2002).

53 Dias, S. S., Milne, D. M. & Meek, D. W. c-Abl phosphorylates Hdm2 at tyrosine 276 in response to DNA damage and regulates interaction with ARF. *Oncogene* **25**, 6666-6671, doi:10.1038/sj.onc.1209671 (2006).

54 Haupt, Y., Maya, R., Kazaz, A. & Oren, M. Mdm2 promotes the rapid degradation of p53. *Nature* **387**, 296-299, doi:10.1038/387296a0 (1997).

55 Maya, R. *et al.* ATM-dependent phosphorylation of Mdm2 on serine 395: role in p53 activation by DNA damage. *Genes & development* **15**, 1067-1077, doi:10.1101/gad.886901 (2001).

56 Khosravi, R. *et al.* Rapid ATM-dependent phosphorylation of MDM2 precedes p53 accumulation in response to DNA damage. *Proc Natl Acad Sci U S A* **96**, 14973-14977 (1999).

57 de Toledo, S. M., Azzam, E. I., Dahlberg, W. K., Gooding, T. B. & Little, J. B. ATM complexes with HDM2 and promotes its rapid phosphorylation in a p53-independent manner in normal and tumor human cells exposed to ionizing radiation. *Oncogene* **19**, 6185-6193, doi:10.1038/sj.onc.1204020 (2000).

58 Barak, Y., Juven, T., Haffner, R. & Oren, M. mdm2 expression is induced by wild type p53 activity. *EMBO J* **12**, 461-468 (1993).

59 Balint, E., Bates, S. & Vousden, K. H. Mdm2 binds p73 alpha without targeting degradation. *Oncogene* **18**, 3923-3929, doi:10.1038/sj.onc.1202781 (1999).

60 Dobbelstein, M., Wienzek, S., Konig, C. & Roth, J. Inactivation of the p53-homologue p73 by the mdm2-oncoprotein. *Oncogene* **18**, 2101-2106, doi:10.1038/sj.onc.1202512 (1999).

61 Zeng, X. *et al.* MDM2 suppresses p73 function without promoting p73 degradation. *Mol Cell Biol* **19**, 3257-3266 (1999).

62 LaRusch, G. A. *et al.* Nutlin3 blocks vascular endothelial growth factor induction by preventing the interaction between hypoxia inducible factor 1alpha and Hdm2. *Cancer Res* **67**, 450-454, doi:67/2/450 [pii]10.1158/0008-5472.CAN-06-2710 (2007).

63 Yang, H. Y. *et al.* Roles for negative cell regulator 14-3-3sigma in control of MDM2 activities. *Oncogene* **26**, 7355-7362, doi:10.1038/sj.onc.1210540 (2007).

64 Vercoutter-Edouart, A. S. *et al.* Proteomic analysis reveals that 14-3-3sigma is down-regulated in human breast cancer cells. *Cancer Res* **61**, 76-80 (2001).

65 Ambrosini, G. *et al.* Mouse double minute antagonist Nutlin-3a enhances chemotherapy-induced apoptosis in cancer cells with mutant p53 by activating E2F1. *Oncogene* **26**, 3473-3481, doi:1210136 [pii]10.1038/sj.onc.1210136 (2007).

66 Lau, L. M., Nugent, J. K., Zhao, X. & Irwin, M. S. HDM2 antagonist Nutlin-3 disrupts p73-HDM2 binding and enhances p73 function. *Oncogene* **27**, 997-1003, doi:1210707 [pii]10.1038/sj.onc.1210707 (2008).

67 Walerych, D., Napoli, M., Collavin, L. & Del Sal, G. The rebel angel: mutant p53 as the driving oncogene in breast cancer. *Carcinogenesis* **33**, 2007-2017, doi:10.1093/carcin/bgs232 (2012).

68 Shah, S. P. *et al.* The clonal and mutational evolution spectrum of primary triple-negative breast cancers. *Nature* **486**, 395-399, doi:10.1038/nature10933 (2012).

69 Soussi, T. & Beroud, C. Assessing TP53 status in human tumours to evaluate clinical outcome. *Nat Rev Cancer* **1**, 233-240, doi:10.1038/35106009 (2001).

70 Dotsch, V., Bernassola, F., Coutandin, D., Candi, E. & Melino, G. p63 and p73, the Ancestors of p53. *Cold Spring Harb Perspect Biol*, doi:cshperspect.a004887 [pii]10.1101/cshperspect.a004887 (2010).

71 Xu, J. *et al.* Gain of function of mutant p53 by coaggregation with multiple tumor suppressors. *Nature chemical biology* **7**, 285-295, doi:10.1038/nchembio.546 (2011).

72 Zawacka-Pankau, J., Kostecka, A., Sznarkowska, A., Hedstrom, E. & Kawiak, A. p73 tumor suppressor protein: a close relative of p53 not only in structure but also in anti-cancer approach? *Cell Cycle* **9**, 720-728, doi:10668 [pii] (2010).

73 Wang, P. *et al.* p53 domains: structure, oligomerization, and transformation. *Mol Cell Biol* **14**, 5182-5191 (1994).

74 Joerger, A. C. *et al.* Structural evolution of p53, p63, and p73: implication for heterotetramer formation. *Proc Natl Acad Sci U S A* **106**, 17705-17710, doi:10.1073/pnas.0905867106 (2009).

75 Rossi, M. *et al.* The ubiquitin-protein ligase Itch regulates p73 stability. *EMBO J* **24**, 836-848, doi:7600444 [pii]10.1038/sj.emboj.7600444 (2005).

76 Levy, D., Reuven, N. & Shaul, Y. A regulatory circuit controlling Itch-mediated p73 degradation by Runx. *J Biol Chem* **283**, 27462-27468, doi:10.1074/jbc.M803941200 (2008).

77 Strano, S. *et al.* The transcriptional coactivator Yes-associated protein drives p73 gene-target specificity in response to DNA Damage. *Molecular cell* **18**, 447-459, doi:10.1016/j.molcel.2005.04.008 (2005).

78 Jost, C. A., Marin, M. C. & Kaelin, W. G., Jr. p73 is a simian [correction of human] p53-related protein that can induce apoptosis. *Nature* **389**, 191-194, doi:10.1038/38298 (1997).

79 Melino, G. *et al.* p73 Induces apoptosis via PUMA transactivation and Bax mitochondrial translocation. *J Biol Chem* **279**, 8076-8083, doi:10.1074/jbc.M307469200M307469200 [pii] (2004).

80 Murray-Zmijewski, F., Lane, D. P. & Bourdon, J. C. p53/p63/p73 isoforms: an orchestra of isoforms to harmonise cell differentiation and response to stress. *Cell Death Differ* **13**, 962-972, doi:4401914 [pii]10.1038/sj.cdd.4401914 (2006).

81 Melino, G., Lu, X., Gasco, M., Crook, T. & Knight, R. A. Functional regulation of p73 and p63: development and cancer. *Trends in biochemical sciences* **28**, 663-670, doi:10.1016/j.tibs.2003.10.004 (2003).

82 Zhu, J., Jiang, J., Zhou, W. & Chen, X. The potential tumor suppressor p73 differentially regulates cellular p53 target genes. *Cancer Res* **58**, 5061-5065 (1998).

83 Tamura, R. E. *et al.* GADD45 proteins: central players in tumorigenesis. *Current molecular medicine* **12**, 634-651 (2012).

84 Wagner, G. Ending the prolonged life of cancer cells. *Nature chemical biology* **1**, 8-9, doi:10.1038/nchembio0605-8 (2005).

85 Yuan, Z. M. *et al.* p73 is regulated by tyrosine kinase c-Abl in the apoptotic response to DNA damage. *Nature* **399**, 814-817, doi:10.1038/21704 (1999).

86 Gong, J. G. *et al.* The tyrosine kinase c-Abl regulates p73 in apoptotic response to cisplatin-induced DNA damage. *Nature* **399**, 806-809, doi:10.1038/21690 (1999).

87 Agami, R., Blandino, G., Oren, M. & Shaul, Y. Interaction of c-Abl and p73alpha and their collaboration to induce apoptosis. *Nature* **399**, 809-813, doi:10.1038/21697 (1999).

88 Tophkhane, C. *et al.* p53 inactivation upregulates p73 expression through E2F-1 mediated transcription. *PloS one* **7**, e43564, doi:10.1371/journal.pone.0043564 (2012).

89 Urist, M., Tanaka, T., Poyurovsky, M. V. & Prives, C. p73 induction after DNA damage is regulated by checkpoint kinases Chk1 and Chk2. *Genes & development* **18**, 3041-3054, doi:10.1101/gad.1221004 (2004).

90 Abbas, T. & Dutta, A. p21 in cancer: intricate networks and multiple activities. *Nat Rev Cancer* **9**, 400-414, doi:10.1038/nrc2657 (2009).

91 La Thangue, N. B. The yin and yang of E2F-1: balancing life and death. *Nature cell biology* **5**, 587-589, doi:10.1038/ncb0703-587 (2003).

92 Loughran, O. & La Thangue, N. B. Apoptotic and growth-promoting activity of E2F modulated by MDM2. *Mol Cell Biol* **20**, 2186-2197 (2000).

93 Yamasaki, L. *et al.* Tumor induction and tissue atrophy in mice lacking E2F-1. *Cell* **85**, 537-548 (1996).

94 Hicklin, D. J. & Ellis, L. M. Role of the vascular endothelial growth factor pathway in tumor growth and angiogenesis. *J Clin Oncol* **23**, 1011-1027, doi:10.1200/JCO.2005.06.081 (2005).

95 Lehman, J. A. & Mayo, L. D. Integration of DNA damage and repair with murine double-minute 2 (mdm2) in tumorigenesis. *International journal of molecular sciences* **13**, 16373-16386, doi:10.3390/ijms131216373 (2012).

96 Borst, P., Rottenberg, S. & Jonkers, J. How do real tumors become resistant to cisplatin? *Cell Cycle* **7**, 1353-1359 (2008).

97 Jung, Y. S., Qian, Y. & Chen, X. DNA polymerase eta is targeted by Mdm2 for polyubiquitination and proteasomal degradation in response to ultraviolet irradiation. *DNA Repair (Amst)* **11**, 177-184, doi:10.1016/j.dnarep.2011.10.017 (2012).

98 Gilkes, D. M. *et al.* Regulation of MDMX expression by mitogenic signaling. *Mol Cell Biol* **28**, 1999-2010, doi:10.1128/MCB.01633-07 (2008).

99 Carrillo, A. M., Bouska, A., Arrate, M. P. & Eischen, C. M. Mdmx promotes genomic instability independent of p53 and Mdm2. *Oncogene* **0**, doi:10.1038/onc.2014.27 (2014).

100 Lim, L. Y., Vidnovic, N., Ellisen, L. W. & Leong, C. O. Mutant p53 mediates survival of breast cancer cells. *Br J Cancer* **101**, 1606-1612, doi:6605335 [pii]10.1038/sj.bjc.6605335 (2009).

101 Adorno, M. *et al.* A Mutant-p53/Smad complex opposes p63 to empower TGFbeta-induced metastasis. *Cell* **137**, 87-98, doi:10.1016/j.cell.2009.01.039 (2009).

102 Oliver, M. H., Harrison, N. K., Bishop, J. E., Cole, P. J. & Laurent, G. J. A rapid and convenient assay for counting cells cultured in microwell plates: application for assessment of growth factors. *J Cell Sci* **92 (Pt 3)**, 513-518 (1989).

103 Hanenberg, H. *et al.* Colocalization of retrovirus and target cells on specific fibronectin fragments increases genetic transduction of mammalian cells. *Nat Med* **2**, 876-882 (1996).

104 Leurs, C. *et al.* Comparison of three retroviral vector systems for transduction of nonobese diabetic/severe combined immunodeficiency mice repopulating human CD34+ cord blood cells. *Human gene therapy* **14**, 509-519, doi:10.1089/104303403764539305 (2003).

105 Braden, W. A. *et al.* Distinct action of the retinoblastoma pathway on the DNA replication machinery defines specific roles for cyclin-dependent kinase complexes in prereplication complex assembly and S-phase progression. *Mol Cell Biol* **26**, 7667-7681, doi:10.1128/MCB.00045-06 (2006).

106 Alt, J. R., Greiner, T. C., Cleveland, J. L. & Eischen, C. M. Mdm2 haplo-insufficiency profoundly inhibits Myc-induced lymphomagenesis. *EMBO J* **22**, 1442-1450, doi:10.1093/emboj/cdg133 (2003).

107 Laird, P. W. *et al.* Simplified mammalian DNA isolation procedure. *Nucleic Acids Res* **19**, 4293 (1991).

108 Chou, T. C. & Talalay, P. Quantitative analysis of dose-effect relationships: the combined effects of multiple drugs or enzyme inhibitors. *Advances in enzyme regulation* **22**, 27-55 (1984).

109 Tallarida, R. J. Quantitative methods for assessing drug synergism. *Genes & cancer* **2**, 1003-1008, doi:10.1177/1947601912440575 (2011).

110 Cai, S. *et al.* Humanized bone marrow mouse model as a preclinical tool to assess therapy-mediated hematotoxicity. *Clin Cancer Res* **17**, 2195-2206, doi:10.1158/1078-0432.CCR-10-1959 (2011).

111 Ali, A. *et al.* Differential regulation of the REGgamma-proteasome pathway by p53/TGF-beta signalling and mutant p53 in cancer cells. *Nature communications* **4**, 2667, doi:10.1038/ncomms3667 (2013).

112 Muller, P. A. *et al.* Mutant p53 drives invasion by promoting integrin recycling. *Cell* **139**, 1327-1341, doi:10.1016/j.cell.2009.11.026 (2009).

113 Lapenna, S. & Giordano, A. Cell cycle kinases as therapeutic targets for cancer. *Nature reviews. Drug discovery* **8**, 547-566, doi:10.1038/nrd2907 (2009).

114 Schmid, I., Krall, W. J., Uittenbogaart, C. H., Braun, J. & Giorgi, J. V. Dead cell discrimination with 7-amino-actinomycin D in combination with dual color immunofluorescence in single laser flow cytometry. *Cytometry* **13**, 204-208, doi:10.1002/cyto.990130216 (1992).

115 Malumbres, M. & Barbacid, M. To cycle or not to cycle: a critical decision in cancer. *Nat Rev Cancer* **1**, 222-231, doi:10.1038/35106065 (2001).

116 Storchova, Z. & Pellman, D. From polyploidy to aneuploidy, genome instability and cancer. *Nature reviews. Molecular cell biology* **5**, 45-54, doi:10.1038/nrm1276 (2004).

117 Lu, X., Lu, X. & Kang, Y. Organ-specific enhancement of metastasis by spontaneous ploidy duplication and cell size enlargement. *Cell research* **20**, 1012-1022, doi:10.1038/cr.2010.93 (2010).

118 Coulson, P. B., Thornthwaite, J. T., Woolley, T. W., Sugarbaker, E. V. & Seckinger, D. Prognostic indicators including DNA histogram type, receptor content, and staging related to human breast cancer patient survival. *Cancer Res* **44**, 4187-4196 (1984).

119 Kallioniemi, O. P. *et al.* Improving the prognostic value of DNA flow cytometry in breast cancer by combining DNA index and S-phase fraction. A proposed classification of DNA histograms in breast cancer. *Cancer* **62**, 2183-2190 (1988).

120 Wang, S., Zhang, H., Cheng, L., Evans, C. & Pan, C. X. Analysis of the cytotoxic activity of carboplatin and gemcitabine combination. *Anticancer research* **30**, 4573-4578 (2010).

121 Grallert, B. & Boye, E. The multiple facets of the intra-S checkpoint. *Cell Cycle* **7**, 2315-2320 (2008).

122 Telli, M. Optimizing chemotherapy in triple-negative breast cancer: the role of platinum. *American Society of Clinical Oncology educational book / ASCO. American Society of Clinical Oncology. Meeting*, e37-42, doi:10.14694/EdBook_AM.2014.34.e37 (2014).

123 Smith, M. L. Mdm2 sensitizes MCF7 breast cancer cells to cisplatin or carboplatin. *Breast Cancer Res Treat* **58**, 99-105 (1999).

124 Jin, Y., Lee, H., Zeng, S. X., Dai, M. S. & Lu, H. MDM2 promotes p21waf1/cip1 proteasomal turnover independently of ubiquitylation. *EMBO J* **22**, 6365-6377, doi:10.1093/emboj/cdg600 (2003).

125 Efeyan, A. *et al.* Induction of p53-dependent senescence by the MDM2 antagonist nutlin-3a in mouse cells of fibroblast origin. *Cancer Res* **67**, 7350-7357, doi:10.1158/0008-5472.CAN-07-0200 (2007).

126 Korotchkina, L. G., Demidenko, Z. N., Gudkov, A. V. & Blagosklonny, M. V. Cellular quiescence caused by the Mdm2 inhibitor nutlin-3A. *Cell Cycle* **8**, 3777-3781 (2009).

127 Castedo, M. *et al.* Cell death by mitotic catastrophe: a molecular definition. *Oncogene* **23**, 2825-2837, doi:10.1038/sj.onc.1207528 (2004).

128 Jyoti, S., Khan, S., Afzal, M. & Siddique, Y. H. Micronucleus investigation in human buccal epithelial cells of gutkha users. *Advanced biomedical research* **1**, 35, doi:10.4103/2277-9175.100128 (2012).

129 Nersesyan, A., Kundi, M., Atefie, K., Schulte-Hermann, R. & Knasmuller, S. Effect of staining procedures on the results of micronucleus assays with exfoliated oral mucosa cells. *Cancer epidemiology, biomarkers & prevention : a publication of the American Association for Cancer Research, cosponsored by the American Society of Preventive Oncology* **15**, 1835-1840, doi:10.1158/1055-9965.EPI-06-0248 (2006).

130 Wang, X. Q., Ongkeko, W. M., Lau, A. W., Leung, K. M. & Poon, R. Y. A possible role of p73 on the modulation of p53 level through MDM2. *Cancer Res* **61**, 1598-1603 (2001).

131 Biswas, A. K. & Johnson, D. G. Transcriptional and nontranscriptional functions of E2F1 in response to DNA damage. *Cancer Res* **72**, 13-17, doi:10.1158/0008-5472.CAN-11-2196 (2012).

132 Irwin, M. *et al.* Role for the p53 homologue p73 in E2F-1-induced apoptosis. *Nature* **407**, 645-648, doi:10.1038/35036614 (2000).

133 Lee, C. W. & La Thangue, N. B. Promoter specificity and stability control of the p53-related protein p73. *Oncogene* **18**, 4171-4181, doi:10.1038/sj.onc.1202793 (1999).

134 Boutros, M. & Ahringer, J. The art and design of genetic screens: RNA interference. *Nat Rev Genet* **9**, 554-566, doi:10.1038/nrg2364 (2008).

135 Kawai, H. *et al.* DNA damage-induced MDMX degradation is mediated by MDM2. *J Biol Chem* **278**, 45946-45953, doi:10.1074/jbc.M308295200 (2003).

136 Pan, Y. & Chen, J. MDM2 promotes ubiquitination and degradation of MDMX. *Mol Cell Biol* **23**, 5113-5121 (2003).

137 Pereg, Y. *et al.* Phosphorylation of Hdmx mediates its Hdm2- and ATM-dependent degradation in response to DNA damage. *Proc Natl Acad Sci U S A* **102**, 5056-5061, doi:10.1073/pnas.0408595102 (2005).

138 Wakatsuki, T., Schwab, B., Thompson, N. C. & Elson, E. L. Effects of cytochalasin D and latrunculin B on mechanical properties of cells. *J Cell Sci* **114**, 1025-1036 (2001).

139 Lissy, N. A., Davis, P. K., Irwin, M., Kaelin, W. G. & Dowdy, S. F. A common E2F-1 and p73 pathway mediates cell death induced by TCR activation. *Nature* **407**, 642-645, doi:10.1038/35036608 (2000).

140 Grob, T. J. *et al.* Human delta Np73 regulates a dominant negative feedback loop for TAp73 and p53. *Cell Death Differ* **8**, 1213-1223, doi:10.1038/sj.cdd.4400962 (2001).

141 Nakagawa, T. *et al.* Autoinhibitory regulation of p73 by Delta Np73 to modulate cell survival and death through a p73-specific target element within the Delta Np73 promoter. *Mol Cell Biol* **22**, 2575-2585 (2002).

142 Demory, M. L. *et al.* Epidermal growth factor receptor translocation to the mitochondria: regulation and effect. *J Biol Chem* **284**, 36592-36604, doi:10.1074/jbc.M109.000760 (2009).

143 Zhu, H., Cao, X., Ali-Osman, F., Keir, S. & Lo, H. W. EGFR and EGFRvIII interact with PUMA to inhibit mitochondrial translocalization of PUMA and PUMA-mediated apoptosis independent of EGFR kinase activity. *Cancer Lett* **294**, 101-110, doi:10.1016/j.canlet.2010.01.028 (2010).

144 Basu, S., Totty, N. F., Irwin, M. S., Sudol, M. & Downward, J. Akt phosphorylates the Yes-associated protein, YAP, to induce interaction with 14-3-3 and attenuation of p73-mediated apoptosis. *Molecular cell* **11**, 11-23 (2003).

145 Hirai, H. *et al.* MK-2206, an allosteric Akt inhibitor, enhances antitumor efficacy by standard chemotherapeutic agents or molecular targeted drugs in vitro and in vivo. *Mol Cancer Ther* **9**, 1956-1967, doi:10.1158/1535-7163.MCT-09-1012 (2010).

146 Wasylyk, C. & Wasylyk, B. Defect in the p53-Mdm2 autoregulatory loop resulting from inactivation of TAF(II)250 in cell cycle mutant tsBN462 cells. *Mol Cell Biol* **20**, 5554-5570 (2000).

147 Gu, L., Findley, H. W. & Zhou, M. MDM2 induces NF-kappaB/p65 expression transcriptionally through Sp1-binding sites: a novel, p53-independent role of

MDM2 in doxorubicin resistance in acute lymphoblastic leukemia. *Blood* **99**, 3367-3375 (2002).

148 Iancu-Rubin, C. *et al.* Activation of p53 by the MDM2 inhibitor RG7112 impairs thrombopoiesis. *Experimental hematology* **42**, 137-145 e135, doi:10.1016/j.exphem.2013.11.012 (2014).

149 Higgins, B. *et al.* Preclinical optimization of MDM2 antagonist scheduling for cancer treatment by using a model-based approach. *Clin Cancer Res* **20**, 3742-3752, doi:10.1158/1078-0432.CCR-14-0460 (2014).

150 Vivier, E., Tomasello, E., Baratin, M., Walzer, T. & Ugolini, S. Functions of natural killer cells. *Nature immunology* **9**, 503-510, doi:10.1038/ni1582 (2008).

151 Kitamura, D. *How the immune system recognizes self and nonself : immunoreceptors and their signaling*. (Springer, 2008).

152 Choy, G., Choyke, P. & Libutti, S. K. Current advances in molecular imaging: noninvasive in vivo bioluminescent and fluorescent optical imaging in cancer research. *Molecular imaging* **2**, 303-312 (2003).

153 Yang, M. *et al.* Whole-body optical imaging of green fluorescent protein-expressing tumors and metastases. *Proc Natl Acad Sci U S A* **97**, 1206-1211 (2000).

154 Zhang, F. *et al.* Whole-body physiologically based pharmacokinetic model for nutlin-3a in mice after intravenous and oral administration. *Drug Metab Dispos* **39**, 15-21, doi:dmd.110.035915 [pii]10.1124/dmd.110.035915 (2011).

155 Schmitt, A. *et al.* Factors for hematopoietic toxicity of carboplatin: refining the targeting of carboplatin systemic exposure. *J Clin Oncol* **28**, 4568-4574, doi:10.1200/JCO.2010.29.3597 (2010).

156 Rizzardi, A. E. *et al.* Quantitative comparison of immunohistochemical staining measured by digital image analysis versus pathologist visual scoring. *Diagnostic pathology* **7**, 42, doi:10.1186/1746-1596-7-42 (2012).

157 Ma, C. X. *et al.* Targeting Chk1 in p53-deficient triple-negative breast cancer is therapeutically beneficial in human-in-mouse tumor models. *J Clin Invest* **122**, 1541-1552, doi:10.1172/JCI58765 (2012).

158 Price, J. T., Tiganis, T., Agarwal, A., Djakiew, D. & Thompson, E. W. Epidermal growth factor promotes MDA-MB-231 breast cancer cell migration through a phosphatidylinositol 3'-kinase and phospholipase C-dependent mechanism. *Cancer Res* **59**, 5475-5478 (1999).

159 Ferraro, D. A. *et al.* Inhibition of triple-negative breast cancer models by combinations of antibodies to EGFR. *Proc Natl Acad Sci U S A* **110**, 1815-1820, doi:10.1073/pnas.1220763110 (2013).

160 Mao, Y., Keller, E. T., Garfield, D. H., Shen, K. & Wang, J. Stromal cells in tumor microenvironment and breast cancer. *Cancer metastasis reviews* **32**, 303-315, doi:10.1007/s10555-012-9415-3 (2013).

161 Brown, J. M. & Wilson, W. R. Exploiting tumour hypoxia in cancer treatment. *Nat Rev Cancer* **4**, 437-447, doi:10.1038/nrc1367 (2004).

162 Hockel, M. & Vaupel, P. Biological consequences of tumor hypoxia. *Seminars in oncology* **28**, 36-41 (2001).

CURRICULUM VITAE

Eva Y. Tonsing-Carter

EDUCATION

2009–2014 Doctor of Philosophy, Department of Pharmacology and Toxicology, Indiana University, Indianapolis, IN

2004–2008 Bachelor of Science, Biology, Concentration in Molecular Cell Biology, Magna cum laude, Saint Mary's College, Notre Dame, IN

PEER REVIEWED PUBLICATIONS

E. Tonsing-Carter, A.L. Sinn, J. Silver, K.M. Peterson, B.J. Bailey, C.M. Eischen, H. Wang, H.S. Shannon, J. Ding, S. Cai, A.A. Sprouse, P.R. Territo, G.E. Sandusky, L.D. Mayo, J. Li, C.B. Marchal, H. Hanenberg, and K.E. Pollok. *Potentiation of carboplatin-mediated DNA damage by the MDM2 modulator Nutlin-3a in a humanized orthotopic breast-to-lung metastatic model.* In preparation.

Harlan E. Shannon*, E. Tonsing-Carter*, B.J. Bailey, A.L. Sinn, T.K. Spragins, H. Wang, J. Ding, S. Cai, P.R. Territo, H. Hanenberg, and K.E. Pollok. *Front-line therapy for metastatic MYC-N amplified neuroblastoma is augmented by the Mdm2 Antagonist RG7112. In preparation.* *both contributed equally

H. Wang, S. Cai, B.J. Bailey, M.R. Saadatzadeh, E. Tonsing-Carter, J. Ding, T.M. Georgiadis, T.Z. Gunter, E.C. Long, R.E. Mindo, K.R. Gordon, S.E. Sen, W. Cai, J.A. Eitel, D.L. Waning, L.R. Bringman, C.D. Wells, M.E. Murray, J. Sarkaria, L.M. Gelbert, D.R. Jones, A. Cohen-Gadol, L.D. Mayo, H.E. Shannon, and K.E. Pollok. *Mdm2 Antagonist Decreases Glioblastoma Resistance to Temozolomide, Downregulates DNA repair, and Increases Survival of Mice with Human Intracranial Xenografts.* Submitted.

Invited Book Chapters

H. Wang, S. Cai, E. Tonsing-Carter, and K.E. Pollok. (2011) *Therapeutic Modulation of DNA-damage and –repair mechanisms in blood cells.* Chapter in DNA Repair, InTech Publishers. October 2011.

GRANTS AND FELLOWSHIPS

Fellowships:

2012-2013 DeVault Fellowship- Indiana University Simon Cancer Center Cancer Biology Training Program (Competitive renewal)

2011-2012 Indiana University Simon Cancer Center Biology Training Program Fellowship

2009-2011 Indiana University School of Medicine Fellowship

HONORS AND AWARDS

2014 Paradise Travel Award, R. R. Paradise Memorial Fund, Department of Pharmacology and Toxicology, 2014 AACR Annual Meeting, San Diego, CA

2013 IUSM Graduate Student Travel Award, 2014 AACR Annual Meeting, San Diego, CA

2013 IUSCC Travel Grant, Experimental and Molecular Therapeutics Session Minisymposia Oral Presentation, Abstract #4639, 2013 AACR Annual Meeting, Washington DC

2012-2013 DeVault Fellowship- Indiana University Simon Cancer Center Cancer Biology Training Program (see Grants and Fellowships)

2012 Indiana University Simon Cancer Center Cancer Research Day Honorable Mention Award for Graduate Student in Basic Science Poster Competition

2011-2012 Indiana University Simon Cancer Center Cancer Biology Training Award

2009-2011 Indiana University School of Medicine Fellowship

2004-2008 Saint Mary's College Presidential Scholarship

2004-2008 Saint Mary's College Honor's List

OTHER APPOINTMENTS AND PROFESSIONAL CONSULTANTSHIPS

2013 Student Mentor, IU Simon Cancer Center Summer Research Program (SRP), Indiana University School of Medicine, Indianapolis, IN

2013 Molecular Mechanism in Action (MMIA), Career Session Expert (Pre-doctoral Student), Wells Center for Pediatric Research, Indianapolis, IN

2012 Student Mentor, Herman B Wells Center for Pediatric Research Summer Internship Program, Indianapolis, IN

2012 Student Mentor, Biomedical Research Exploration Internship, Indianapolis, IN

2012 Molecular Mechanism in Action (MMIA), Career Session Expert (Pre-doctoral Student), Wells Center for Pediatric Research, Indianapolis, IN

2011 Student Mentor, 2011 IUSCC Summer Research Program, Indiana University School of Medicine, Indianapolis, IN

LABORATORY EXPERIENCE

2011-2014 Indiana University School of Medicine, Indianapolis, IN,
Department of Pharmacology and Toxicology
Supervisor: Karen Pollok, Ph.D.
PhD Candidate
Characterizing the modulation of MDM2 signaling and its signaling role in vivo in a humanized breast cancer model using small molecule inhibitor Nutlin-3a in combination with carboplatin.

2010 Indiana University School of Medicine, Indianapolis, IN
Department of Pharmacology and Toxicology
Supervisor: Karen Pollok, Ph.D.
Rotation Student
Examined small molecule analogs of Nutlin-3a in a pilot drug discovery project.

2010 Indiana University School of Medicine, Indianapolis, IN
Department of Pharmacology and Toxicology
Supervisor: Jian-Ting Zhang, Ph.D.
Rotation Student
Characterized protein expression of eIF3i and its function in chemoresistance in a colon cancer model.

2009 Indiana University School of Medicine, Indianapolis, IN
Department of Pharmacology and Toxicology
Supervisor: Kai-Ming Chou, Ph.D.
Rotation Student
Characterized cellular mechanisms of polymerase σ in relation to DNA repair and chemoresistance in Xeroderma pigmentosum cells.

2007-2008 Saint Mary's College, Notre Dame, IN
Department of Biology
Supervisor: Kara Eberly, Ph.D.
Researcher
Examined the genetic profile of superantigen genes in Streptococcus pyogenes samples collected from patients with Streptococcal pharyngitis or strep throat.

2006 Saint Mary's College, Notre Dame, IN
Department of Biology

Supervisor: Kara Eberly, Ph.D.
Laboratory Assistant
Helped coordinate microbiology lab course as well as prepared materials for lab experiments.

UNIVERSITY SERVICE

2010-2013 Ambassador to prospective students visiting Indiana University School of Medicine. Activities include Building Guide, Poster Presentations, accompaniment to dinners and lunches.

INVITED TALKS AND SEMINARS

2014 IUSCC Cancer Research Day, Modulation of MDM2 in context of DNA damage enhances cell death in a metastatic breast-to-lung xenograft model, Indianapolis, IN (Poster)

2014 AACR Annual Meeting, Modulation of MDM2 in context of DNA damage enhances cell death in a metastatic breast-to-lung xenograft model. Abstract #1680, San Diego, CA (Poster)

2013 Department of Pharmacology and Toxicology Student Seminar Series, Blockade of MDM2-mediated Signaling in Context of DNA Damage Increases E2F1 Expression and Enhances Cell Death in Triple Negative Breast Cancer Cells, Indianapolis, IN (Seminar)

2013 IUSCC Seminar for Travel Awardees, Blockade of MDM2-mediated Signaling in Context of DNA Damage Increases E2F1 Expression and Enhances Cell Death in Triple-negative Breast Cancer Cells. Indianapolis, IN (Seminar)

2013 IUSCC Cancer Research Day, Blockade of MDM2-mediated Signaling in Context of DNA Damage Increases E2F1 Expression and Enhances Cell Death in Triple-negative Breast Cancer Cells. Indianapolis, IN (Poster)

2013 Department of Pharmacology and Toxicology Student Seminar Series, Modulation of DNA damage and repair by the Mdm2 signaling network. Indianapolis, IN (Seminar)

2013 Cancer Biology Research Club, Modulation of DNA damage and repair by the Mdm2 signaling network. Indianapolis, IN (Seminar)

2013 AACR Annual Meeting, Experimental and Molecular Therapeutics Session Minisymposia Oral Presentation, Blockade of MDM2-mediated Signaling in Context of DNA Damage Increases E2F1 Expression and Enhances Cell Death in Triple-negative Breast Cancer Cells Abstract #4639, Washington DC (Seminar)

2012 IUSCC Cancer Research Day, Real-time in vivo imaging for sensitive detection of primary and metastatic disease in a human breast–to–lung orthotopic model, Indianapolis, IN (Poster)

2012 AACR Annual Meeting, Real-time in vivo imaging for sensitive detection of primary and metastatic disease in a human breast–to–lung orthotopic model. Abstract #1409, Chicago, IL (Poster)

2012 Department of Pharmacology and Toxicology Student Seminar Series, Modulation of carboplatin-mediated DNA damage in a human breast-to-lung metastatic model. Indianapolis, IN (Seminar)

2011 IUPUI Imaging Symposium, Real-time in vivo imaging for sensitive detection of primary and metastatic disease in a human breast–to–lung orthotopic model. Indianapolis, IN (Poster)

2011 Department of Pharmacology and Toxicology Student Seminar Series, Therapeutic modulation of MDM2-mediated signaling in metastatic breast cancer and melanoma. Indianapolis, IN (Seminar)

ATTENDED TALKS AND SEMINARS

2014 IUSCC Cancer Research Day, Indianapolis, IN

2014 AACR 2014 Annual Meeting, San Diego, CA

2013 IUSCC Cancer Research Day, Indianapolis, IN

2013 AACR 2013 Annual Meeting, Washington DC

2012 IUSCC Cancer Research Day, Indianapolis, IN

2012 AACR 2012 Annual Meeting, Chicago, IL

2011 IUPUI Imaging Symposium, Indianapolis, IN

2011 Purdue University Center for Cancer Research Drug Delivery and Cancer: Challenges and New Directions for Cancer Therapy, West Lafayette, IN

2011 Indiana CTSI Third Annual Meeting, Indianapolis, IN

2011 Amelia Project Giving Wings to Research, Indianapolis, IN

2010 Metastatic Breast Cancer Network National Meeting, Indianapolis, IN

2009-2014 Department of Pharmacology and Toxicology Seminar Series

2009-2014 Department of Pharmacology and Toxicology Student Seminar Series

2009-2014 IUSCC Combined Seminar Series

ABSTRACTS

2014 IUSCC Cancer Research Day, Modulation of MDM2 in context of DNA damage enhances cell death in a metastatic breast-to-lung xenograft model, Indianapolis, IN

2013 2014 AACR, Modulation of MDM2 in context of DNA damage enhances cell death in a metastatic breast-to-lung xenograft model, Abstract #1680, San Diego, CA

2013 IUSCC Cancer Research Day, Blockade of MDM2-mediated signaling in context of DNA damage increases E2F1 expression and enhances cell death in triple-negative breast cancer cells, Indianapolis, IN

2013 AACR, Blockade of MDM2-mediated signaling in context of DNA damage increases E2F1 expression and enhances cell death in triple-negative breast cancer cells, Abstract #4639, Washington D.C.

2012 IUSCC Cancer Research Day, Real-time in vivo imaging for sensitive detection of primary and metastatic disease in a human breast–to–lung orthotopic model, Indianapolis, IN

2012 IUPUI Research Day, Real-time in vivo imaging for sensitive detection of primary and metastatic disease in a human breast–to–lung orthotopic model, Indianapolis, IN

2012 AACR, Real-time in vivo imaging for sensitive detection of primary and metastatic disease in a human breast–to–lung orthotopic model. Abstract #1409, Chicago, IL

2011 IUPUI Imaging Symposium, Real-time in vivo imaging for sensitive detection of primary and metastatic disease in a human breast–to–lung orthotopic model. Indianapolis, IN

LICENSURE AND CERTIFICATION

2011 Participant, “Grant Writers’ Seminar & Workshops: Getting Started as a Successful Grant Write & Academician,” Continuing Medical Education, Indiana University School of Medicine

2010 Participant, Molecular Biology Workshop, Indiana School of Medicine

2010 Collaborative Institutional Training Initiative (CITI) RCR Module

PROFESSIONAL ORGANIZATIONS

2014	Student Member, American Society for Clinical Pharmacology and Therapeutics (ASCPT)
2011-2014	Junior Member, Association for Women in Science
2011-2014	Associate Member, American Association for Cancer Research
2010-2014	Sponsored Member, American Association for the Advancement of Science